

COMSAT
Technical Review

Volume 9 Number 2A, Fall 1979

Advisory Board Joseph V. Charyk
William W. Hagerty
John V. Harrington
B. I. Edelson
Sidney Metzger

Editorial Board Pier L. Bargellini, Chairman
S. J. Campanella
William L. Cook
C. Dorian
H. W. Flieger
Jorge C. Fuenzalida
William J. Getsinger
R. W. Kreutel
Akos G. Revesz
George R. Welti

Editorial Staff Daniel N. Crampton
MANAGING EDITOR
Margaret B. Jacocks
Elizabeth Christie
Pearl Coleman
TECHNICAL EDITORS
Edgar Bolen
PRODUCTION
Vicki A. Araujo
CIRCULATION

COMSAT TECHNICAL REVIEW is published twice a year by Communications Satellite Corporation (COMSAT). Subscriptions, which include the two issues published within a calendar year, are: one year, \$7 U.S.; two years, \$12; three years, \$15; single copies, \$5; article reprints, \$1. Make checks payable to COMSAT and address to Treasurer's Office, Communications Satellite Corporation, 950 L'Enfant Plaza, S.W., Washington, D.C. 20024, U.S.A.

© COMMUNICATIONS SATELLITE CORPORATION 1980

COMSAT TECHNICAL REVIEW

Volume 9 Number 2, Fall 1979

PART A (TDMA)

- v FOREWORD P. L. Bargellini
- 293 THE INTELSAT TDMA FIELD TRIAL S. J. Campanella, R. J. Colby, B. A. Pontano, H. Suyderhoud, AND M. Onufry
- 341 OPEN-LOOP TDMA FRAME ACQUISITION AND SYNCHRONIZATION S. J. Campanella AND K. Hodson
- 387 TECHNIQUES FOR TDMA SYSTEM MONITORING D. J. Schaefer
- 413 TDMA MODEM DESIGN CRITERIA C. J. Wolejsza AND D. Chakraborty
- 465 OPTIMUM FILTERING FOR QPSK IN BANDWIDTH-LIMITED NON-LINEAR SATELLITE CHANNELS M. E. Jones AND M. R. Wachs
- 509 TRANSLATIONS OF ABSTRACTS
FRENCH 509 SPANISH 513

PART B

- 517 FSK BURST RECEIVER FOR DATA COLLECTION SYSTEMS K. H. Greene AND R. F. Hefele
- 549 SMALL EARTH TERMINALS AT 12/14 GHz J. Kaiser, I. Veenstra, E. Ackermann, AND F. Seidel
- 604 PERIODIC BANDPASS CHARACTERISTIC OF MICROSTRIP MEANDER LINE Y. S. Lee AND R. C. Trushel
- 617 12-GHZ 10-W AMPLIFIER USING GaAs IMPATT DIODES S. Chou
- 629 RAIN DEPOLARIZATION MEASUREMENTS AT 4 GHz D. J. Kennedy
- 669 A MODEL FOR PACKET SWITCHING NODE INCLUDING PACKET RETRANSMISSION EFFECTS A. Kaul
- 689 CTR NOTES
THE EFFECT OF BUFFER ACCESS TIME ON HDLC PERFORMANCE A. Kaul 689
INTELLIGIBLE CROSSTALK BETWEEN LARGE FDM-FM CARRIERS AMPLIFIED BY KLYSTRONS C. B. Cotner AND A. J. Barnes 705
NOTE ON CRYPTOSYSTEMS L. N. Lee 717
FREQUENCY REUSE LIMITS FOR THE GEOSTATIONARY ORBIT G. R. Welti 723
- 731 TRANSLATIONS OF ABSTRACTS
FRENCH 731 SPANISH 735

Foreword

PIER L. BARGELLINI

In presenting this special issue of *COMSAT Technical Review* dedicated to TDMA, and covering in particular the 1979 INTELSAT TDMA Field Trial over the Atlantic Ocean region, it seems appropriate to recall that multiple access, *i.e.*, the capability of establishing simultaneous links via a single spacecraft among many pairs of earth stations, is a fundamental advantage of satellite communications systems.

In the early days of satellite communications it was recognized that separation of the accesses could occur in the physical domains of frequency, time, polarization and space. In addition, suitable signal encoding procedures were proposed to provide further separation of the accesses within the above-mentioned domains.

The selection of a specific method of multiple access depends on analyses directed toward the optimum utilization of the power and bandwidth available on a spacecraft in the sense of maximizing the number of accesses without incurring excessive signal impairments resulting from the imperfections of the transmission channel. Most objectionable among these are amplitude and phase nonlinearities of the power amplifiers which generate intermodulation noise and cross-talk when several accesses are simultaneously present.

While Frequency Domain (Division) Multiple Access (FDMA) and

Pier L. Bargellini is Senior Scientist at COMSAT Laboratories

Time Domain (Division) Multiple Access (TDMA) have been major contenders in commercial satellite communications, the ultimate potential of TDMA had been predicted since the middle 1960's. However, the economies of the then predominant analog voice and video transmission and the extensive experience of frequency modulation and frequency division multiplexing in ground-based communications systems led to the choice of FDMA in the INTELSAT system and in most domestic satellite systems of various countries. This choice occurred in spite of the chief drawback of FDMA, which is the great loss of communications capacity when a transponder is shared by several accesses.

Not surprisingly, the outstanding success and rapid growth of communications satellites, with substantial investments in the space and earth segments, tended to justify resistance to changes and resulted in a "freezing" of the technology at the operational level. However the increase of communications capacity from one generation of satellites to another, and the forecast of heavier future traffic, led technologists to reconsider the potential advantages of TDMA. Continued work at COMSAT Laboratories and elsewhere, including a number of field trials by INTELSAT and others, culminating with those reported in this issue, confirmed the practicality of TDMA, and led to a better understanding of some of its operational aspects. In the meantime, reduced complexity of implementation and advances in solid state technology are making lower-cost TDMA equipment available for earth station use.

The expansion of digital communications with its many advantages, and the development of multiple-beam communications satellites capable of providing onboard signal regeneration and switching, in addition to amplification, will undoubtedly stimulate the widespread introduction of TDMA.

It is hoped that this special issue will help to accelerate this process with substantial ultimate benefits to all users of satellite communications.

Index: time-division multiple access, field test, INTELSAT

The INTELSAT TDMA field trial

S. J. CAMPANELLA, R. J. COLBY, B. A. PONTANO,
H. SUYDERHOUD, AND M. ONUFRY

(Manuscript received July 27, 1979)

Abstract

INTELSAT conducted a field trial of TDMA terminals equipped for digital speech interpolation in the Atlantic Ocean Region, principally to test and evaluate TDMA equipment in the typical earth station environment and to assess the quality of live traffic service. Participating countries included France, the Federal Republic of Germany, Italy, the U.S., and the U.K. Equipments were developed by two different teams of manufacturers in accordance with INTELSAT specifications. This paper reports on the organization of the field trial, details the earth and space segment parameters, and presents the results of the tests performed. The operational experience gained and the subsequent suggestions for modifications and improvements to current TDMA equipment specifications are discussed.

Introduction

Satellites have been used primarily to connect sources and destinations with diverse traffic requirements. To simplify the interface with surface communications networks, satellite systems have traditionally

This paper is based upon work performed under the sponsorship of the International Telecommunications Satellite Organization (INTELSAT).

operated in the FDM/FM/FDMA mode, which is efficient for single-carrier-per-transponder operation but less efficient in multicarrier operation.

In TDMA, nonoverlapping carrier bursts are transmitted through the full bandwidth of the satellite repeater so that many signals can share a common repeater. Such a technique offers several advantages over multicarrier FDMA because it provides a significant increase in capacity and operational flexibility. It also provides compatibility with evolving digital terrestrial networks.

COMSAT began investigations in this area in 1964; in 1966 the first TDMA field trials were conducted with three earth terminals via the INTELSAT I (Early Bird) satellite [1]. These tests showed that burst synchronization to accuracies within a few nanoseconds could be achieved. Since that time many TDMA systems have been developed and operated; the knowledge gained from them was incorporated in an INTELSAT prototype performance specification. This paper concerns a TDMA field test which was designed to test and evaluate TDMA terminals based on this specification. Following authorization by the INTELSAT Board of Governors, five INTELSAT Signatories participated in the field trial: France, the Federal Republic of Germany (F.R.G.), Italy, the U.S., and the U.K. France and the Federal Republic of Germany used TDMA terminals built by a French/German consortium consisting of SEL, Siemens, and AEG-Telefunken in the Federal Republic of Germany, and SAT, Thomson CSF, and CIT in France. Italy and the U.S. used terminals built by a team of companies consisting of NEC (Japan), DCC (U.S.), and SIT Siemens (Italy). The U.K., a later participant in the field trial, utilized a laboratory model terminal constructed within the British Post Office, with some units fabricated by Cambridge Consultants and Marconi.

The principal objective of the field trials was to demonstrate the TDMA system as a practical part of the future INTELSAT network having the required characteristics of transmission quality, reliability, and stability. In particular, the field trial was intended to determine whether TDMA terminals constructed to INTELSAT performance specifications would function compatibly in a scenario representative of operational use. This objective was met by operating equipments constructed by different teams of companies.

Tests of a new transmission system monitor (TSM) for observing the burst emissions of individual stations and several experiments to investigate open-loop synchronization methods [2] were also per-

formed, but since they were not strictly part of the field trial, these experiments are not described in this paper.

Terminal equipment

The TDMA field trial terminals carried traffic in discrete bursts of preassigned length and position in a repeated 750- μ s TDMA frame. Burst length and position could be varied to accommodate changing patterns of traffic flow. QPSK modulation was employed at a bit rate of 60.032 Mbit/s, but the equipment could be converted to operate at twice this rate. The traffic capacity that can be achieved in an INTELSAT IV-A 40-MHz transponder channel using conventional PCM is 935 voice channels less approximately 3 channels per access. With digital speech interpolation (DSI), this capacity is doubled. The basic hardware units of a typical terminal consisted of a codec to differentially encode the PSK transmission, a rate expansion multiplexer for transmit burst generation, a rate compression demultiplexer for receive burst decomposition, a QPSK burst modem, and a system control unit that provided synchronization, acquisition, and housekeeping functions. The principal features of the equipment described in the INTELSAT TDMA System Specification are summarized in the following.

The system incorporated a reference burst, emitted by a station designated as the primary reference station, which contains only the information needed by all other stations to locate their bursts relative to the reference burst. First and second standby reference stations were designated to replace the primary reference station in the event of its failure. The reference burst nominally consisted of 30 symbols for carrier and bit timing recovery, 10 symbols for the unique word and 3 symbols for a station identity code. A superframe of 2^{17} frames was indicated by a change in the unique word transmission pattern.

Data bursts located at assigned positions in the frame carried the normal traffic for each station. The reference station's data burst could be assigned anywhere in the frame. Each data burst consisted of a preamble having the same structure as a reference burst plus two symbols for a control signaling channel, two for teletype order wire, and 24 for two voice order wires. The data part of the burst, which consisted of a succession of contiguous 24-symbol slots carrying sets of six PCM samples for each voice channel, could also provide for transmission of direct digital data streams and bulk-encoded 60-channel FDM supergroups. A digital energy dispersal pattern was added to the

data and voice order wire parts of the bursts to reduce the peak power spectrum density for information containing fixed bit patterns.

Two acquisition modes were defined for the system, initial and fast reentry. Initial acquisition, which occurred when the local station had been out of service for more than five minutes or the sync unique word had not been detected for more than three seconds, was performed within a window of 2^{12} frames assigned in the superframe. The initial acquisition signal level was set at 25 dB below normal to avoid interfering with traffic of other stations. When the initial acquisition signal appeared correctly located in the target burst slot, it was replaced by a normal power burst consisting of the preamble only; subsequently, following fine position corrections, the traffic data portion of the burst was added.

Burst position was defined in increments of four bits measured relative to the last symbol of the unique word. The positions of all bursts in normal operation remained positioned within plus or minus one symbol with respect to the nominal position. If the burst position deviated by more than plus or minus four symbols, the station initiated a fast reentry process by transmitting the preamble only. Fast reentry was included to recover quickly from short-term outages of five minutes or less.

The speech interpolation equipment, designed to interface at the analog voice channel level, provided a CEPT [3] digital format for transmission. Both point-to-point and multidestination modes were available. A digital TASI design was used, incorporating an overload mode of operation in which additional channels were made available by appropriating the least significant bit of normal channels. This feature virtually eliminated speech clipping at a DSI gain of two to one. DSI was implemented in 60-channel modules, and as many as four modules could be used at each terminal. The freeze-out fraction averaged over one minute was continually monitored, and an alarm was provided at freeze-out values adjusted between 0.005 and 0.5 percent. During the peak busy hour loads, channel assignments were made within 300 ms for 99.9 percent of the time; once an assignment is made, no chopping can occur. In normal operation at a DSI gain of 2:1 without overload channels invoked, the system would yield a freeze-out ratio of 0.5 percent; with the overload channels invoked, the ratio would drop to 0.05 percent. Assignment messages for DSI channel control were carried in a 48-bit block at the beginning of the DSI burst, and the traffic signals were carried in contiguous groups of 48 bits in the DSI burst.

The French and German terminals were essentially similar; the French terminal was fully redundant while the German terminal was a laboratory model without redundant units. Both terminals contained a maintenance and monitoring center to initiate switchover to redundant units, to detect all status changes of TDMA units, to indicate alarms, and to localize units which initiate alarms.

The U.S. and Italian terminals were also very similar. Although designed to eventually incorporate fully redundant implementation, they were nonredundant during the field trial.

The U.K. terminal, designed by the British Post Office, consisted of an integrated TDMA system test set and a TDMA terminal for field trial purposes. As a test set, it transmitted and received both continuous and burst mode signals, provided signal conditions at the receiver representative of those of a real system, provided for measurement of IF and baseband distortions and effects, and was capable of utilizing an empty transponder or occupying part of a predefined TDMA transponder format by incorporating synchronization capability.

Earth terminal characteristics

The earth stations were Pleumeur Bodou (PB), France; Raisting (RA), Federal Republic of Germany; Goonhilly (GH), U.K.; Lario (LA), Italy; and Andover (AN), U.S. Typical earth station parameters used to establish the operating points in the system are listed in Table 1. The high-power amplifier (HPA) backoff values, which correspond to a nominal e.i.r.p. of 85 dBW at beam center, determine the amount of spectrum spreading due to HPA nonlinearity.

TABLE 1. EARTH STATION PARAMETERS

Earth Station	Transmit Antenna Gain (dB)	Feed Losses (dB)	Effective ^a Gain (dB)	Saturated Power (dBW)	HPA ^b Output Backoff	G/T (dB/K)
PB	63	1.0 (max)	62	37	13.0	40.8
RA	63	1.6	61.4	35.3	10.2	42.5
GH	62.5	3.2	59.3	39	12.3	41.9
LA	64	2.4	61.6	34.8	11.8	41.1
AN	62.7	1.7	61	41.1	17.1	43.4

^a At the output of the HPA.

^b Based on the nominal e.i.r.p. of 85 dBW.

The overall channel transmission characteristic from transmitter to receiver should typically be an $x/\sin x$ compensated raised cosine to

achieve the best compromise between minimum intersymbol interference and maximum out-of-band rejection. In the INTELSAT TDMA specification, this filtering is accomplished on the modem transmit side. The transmission amplitude and phase masks for the filter are shown in Figure 1. The amplitude mask encompasses a range of $x/\sin x$ compensated raised cosine filters from 20 percent (inner bound) to 27 percent (outer bound) and represents a roll-off characteristic which is too severe, resulting in less than optimum operation in a nonlinear channel.

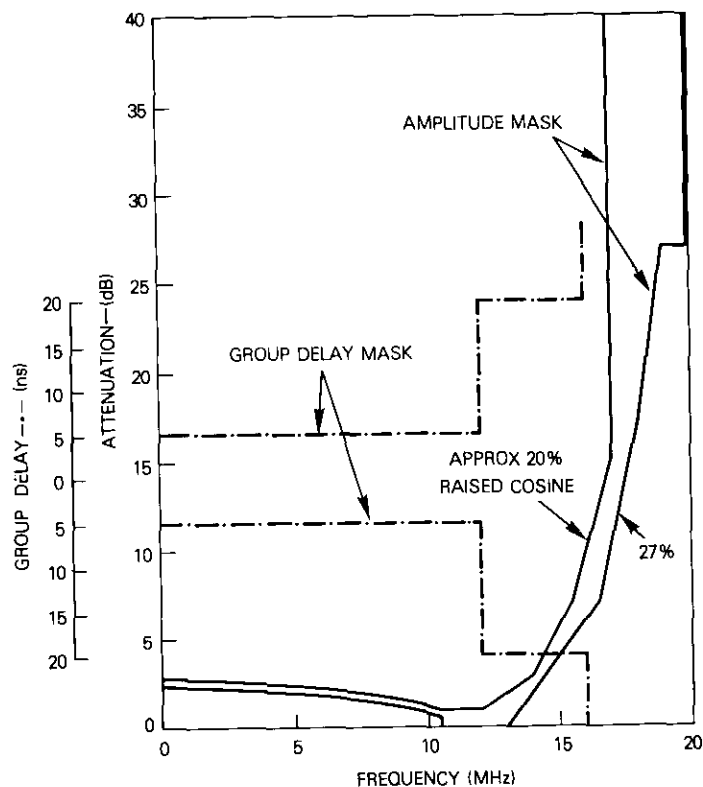


Figure 1. *Transmit Channel Filter Amplitude and Group Delay Response Masks*

The receive filter specification is intended to reduce noise and down-link adjacent channel interference without introducing significant ad-

ditional intersymbol interference. Essentially, the receiver filter design is more relaxed in terms of out-of-band rejection than the transmit filter design.

The modem must exhibit a bit-error rate (BER) of less than 10^{-4} for a bit energy to noise density ratio (E_b/N_o) of 10.6 dB for all symbols after the 40th in the burst. This includes the modem implementation margin, the degradation due to the filters and variations in the frequency of the received carrier from burst to burst. For an E_b/N_o of 14.6 dB, the BER will be less than 10^{-6} for symbols 41 to 72 and less than 10^{-7} averaged in any 300-symbol slot in the data part of the burst. A unique word error rate (UWER) of less than 10^{-6} will result at an E_b/N_o of 10.6 dB.

The transmit frequency of the earth station must not deviate more than 2 kHz from the nominal value due to instabilities and adjustment inaccuracies. The receive carrier frequency deviation is considered to consist of two components. One, common to all bursts, is due to the combination of satellite translation frequency instability and down-path Doppler and may reach ± 45 kHz. The other, which may vary from burst to burst, is due to transmit chain instabilities and up-path Doppler and may reach ± 5 kHz.

Satellite and transmission path characteristics

During the independent station tests, transponder no. 8 on INTELSAT IV-A (F-2) was used to support the TDMA bursts. Values of the parameters used to determine transmission performance are listed in Table 2 for each of the earth stations. Of particular interest are the expected E_b/N_o values at the earth stations under clear sky conditions. These values, which range from 18.3 to 19.7 dB, assume a traveling wave tube amplifier (TWTA) input backoff of 2.5 dB.

Figure 2 shows the measured prelaunch transmission amplitude and phase characteristics of transponder no. 8 of INTELSAT IV-A (F-2) at saturation. These characteristics differed little from those at the backoff used in the field trial. The amplitude and group delay variations encountered over the bandwidth of the TDMA channel defined in Figure 1 are quite small and easily eliminated by earth terminal equalization.

The end-to-end transmission path was equalized by loopback transmission at each earth station. In general, equalization is performed on the transmit side to compensate for unwanted amplitude and phase

TABLE 2. RF PERFORMANCE SUMMARY FOR INTELSAT IV-A (F-2), TRANSPONDER 8

Parameter	Earth Station				
	AN	GH	PB	RA	LR
ψ_s (dBW/m ²)	-75.4	-75.6	-75.6	-75.5	-75.6
G/T (dB/K)	-14.6	-14.4	-14.4	-14.5	-14.4
e.i.r.p. (dBW)	24.8	24.8	24.8	24.7	24.7
Input Backoff (dB)	2.5	2.5	2.5	2.5	2.5
6-GHz Path Loss (dB)	200.3	200.2	200.2	200.4	200.3
4-GHz Path Loss (dB)	196.5	196.4	196.4	196.5	196.5
Station G/T (dB/K)	43.2	41.9	40.8	42.5	41.1
Elevation Angle (deg)	24.5	28.2	28.7	22.6	24.9
Estimated Clear Sky E_b/N_o (dB·Hz)	19.7	19.0	18.3	19.3	18.5

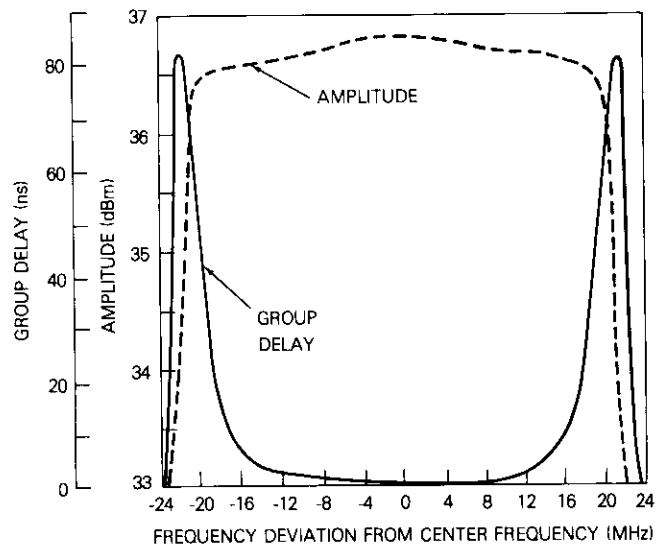


Figure 2. Measured Prelaunch Transponder Amplitude and Phase Characteristics

variations caused by any filters that follow the modem and for the up-converter and HPA, hence ensuring that the modem filter characteristics dominate the transmitted signal phase and amplitude spectrum. The receive side was separately equalized to compensate for the satellite

transponder, the LNA, the down-converter, and the receive filter before the modem. In each case, the equalization should result in linear amplitude and ripple distortion components not exceeding 0.03 dB/MHz and 0.4 dB peak-to-peak, respectively, and linear, parabolic, and ripple group delay components not exceeding 0.10 ns/MHz, 0.01 ns/MHz², and 1.5 ns peak-to-peak, respectively, over a ± 15 -MHz band about the center frequency. The above procedure minimized differences in the signals transmitted from each earth station and ensured compatibility among all earth stations.

Summary of the test plan

The field trial test plan was divided into three parts: Part I. Independent Station Tests, Part II. System Tests, and Part III. Live Traffic Tests. Part I was intended to test all individual subsystems of the TDMA terminals to determine their correspondence to the INTELSAT system specifications up to the point at which the respective terminals were known to perform properly on a loop basis through the satellite. The tests included modem back-to-back performance and calibration; earth station performance and calibration in the up- and down-converter, RF earth station, and satellite loops; TDMA terminal performance and calibration, in which the terminals were tested through both an earth station RF and satellite loop; and terrestrial interface module (TIM) tests, in which the DSI transmit interface modules were tested in back-to-back and satellite loop configurations.

Part II was intended to test the interworking protocols of the TDMA system and the DSI modules. The tests included initial acquisition, fast reentry acquisition, steady-state synchronization, reference station replacement, and nonreference station synchronization unique word loss protocol timing for global beam operation. The DSI portion of these tests included DSI operation control and performance tests, and were intended to qualify the terminals for the live traffic tests.

Part III of the field trial consisted of carefully monitored live traffic testing of TDMA/DSI performance. During this test, all the DSI channels, except for a few which were reserved for testing, were loaded with live traffic derived in parallel from normal FDMA channels carried over the normal operational INTELSAT facilities. The channels reserved for testing carried circuits over which customer calls were placed by a special call routing facility. Telephone operators in France, Italy, and the U.S. called back the customers and interviewed them to determine

the quality of service. Both percentage difficulty and mean opinion scores were determined and appropriate questions asked to probe cause of the difficulty.

Live traffic tests were performed at DSI gains (or channel multiplication ratios) of 2, 2.2, and 2.4 using parallel live traffic loading, and at a DSI gain of 2 using a controlled artificially devised loading to simulate operation in the busy period.

Transmission system monitor

Experiments were also performed with the TDMA system monitor (TSM) [4] installed at the Andover, Maine, earth station, which performed real-time measurements of TDMA data bursts. The received data power, relative transmit burst position, and down-link frequency were measured for individual TDMA bursts and their received BER was estimated.

Open-loop synchronization and acquisition

Two experiments were performed to gather data on the performance of open-loop acquisition and synchronization. These experiments, not strictly part of the field trial, were performed on a noninterfering basis. Four of the TDMA field trial participants, France, Italy, the U.K., and the U.S., generated data which were collected at Pleumeur Bodou, France, for subsequent analysis.

The first experiment compared the predicted and measured relative satellite range from Pleumeur Bodou. The predicted range was calculated by determining zero-, first-, and second-order coefficients for zero-, first-, and second-order polynomial extrapolation functions. The coefficients were derived from range samples taken at intervals which could be varied under operator control. The experiment was designed to demonstrate optimum coefficient refreshment rates needed to maintain TDMA terminal data burst synchronization within the limits needed for operation for each order of extrapolation.

The second experiment demonstrated open-loop acquisition and synchronization by using a linear solution for actual satellite location to compute the TDMA data burst timing phase for the Goonhilly terminal. Goonhilly measured and recorded the difference between the timing phase determined by a conventional closed-loop burst synchronizer and the open-loop timing phase.

Test results

Independent station tests

The independent station and TDMA system tests were designed not only to prepare for the live traffic subjective evaluation tests, but also to yield performance data for the subsequent operational TDMA specification. Accordingly, a very large amount of data was obtained during the field trial and only a summary is presented here.

The overall performance of a digital satellite system is critically influenced by the choice of channel characteristic and the manner in which that characteristic is shared between transmitter and receiver. The form of channel filtering chosen for the INTELSAT field trial concentrated a rather severe roll-off characteristic at the transmitter and thus tended to show a proportionately greater degree of sensitivity to nonlinearity than more gentle roll-off filters [5].

BER as a function of E_b/N_o

Figure 3 shows BER versus E_b/N_o for modem back-to-back tests in the continuous mode, including the theoretical performance curve and the INTELSAT modem performance specification. It can be seen that all equipments fall within the specification and that the mean of the spread is approximately 1.9 dB from theoretical in the region of interest between 10^{-6} and 10^{-8} . Figure 4 shows the spread of in-station HPA loopback BER versus E_b/N_o continuous mode performance curves, as well as the mean back-to-back performance of the modems (dashed curve). It can be seen that there is an additional degradation of approximately 0.5 dB. Figure 5, which shows the spread of continuous mode performance curves for the satellite loopback mode, indicates that there is an additional degradation of approximately 2.5 to 3 dB compared to the HPA loopback mode and that the total degradation from theoretical lies between 4.7 and 5.7 dB.

Burst mode BER versus E_b/N_o performance data reported by some of the stations are compared with the continuous mode data for the satellite loopback mode in Figure 6. It can be seen that the burst mode data differ only slightly from the continuous mode data, with the former showing more flare at the low error rates. Figure 7 shows BER variation as a function of symbol position after the carrier and bit timing recovery period for a typical earth station. The wide variations in the upper curve during the unique word period and slightly thereafter, due to the fixed unique word pattern and a consequent stationary

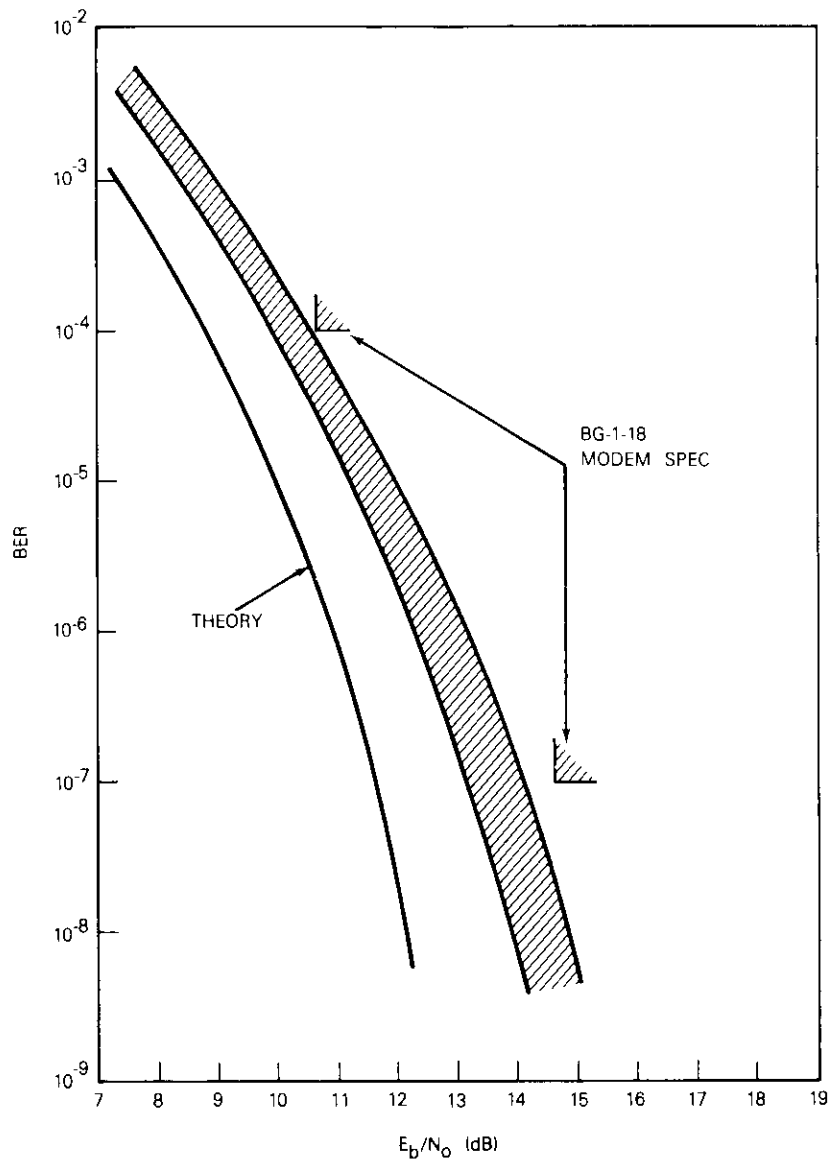


Figure 3. BER as a Function of E_b/N_0 ; Spread of Modem Performances

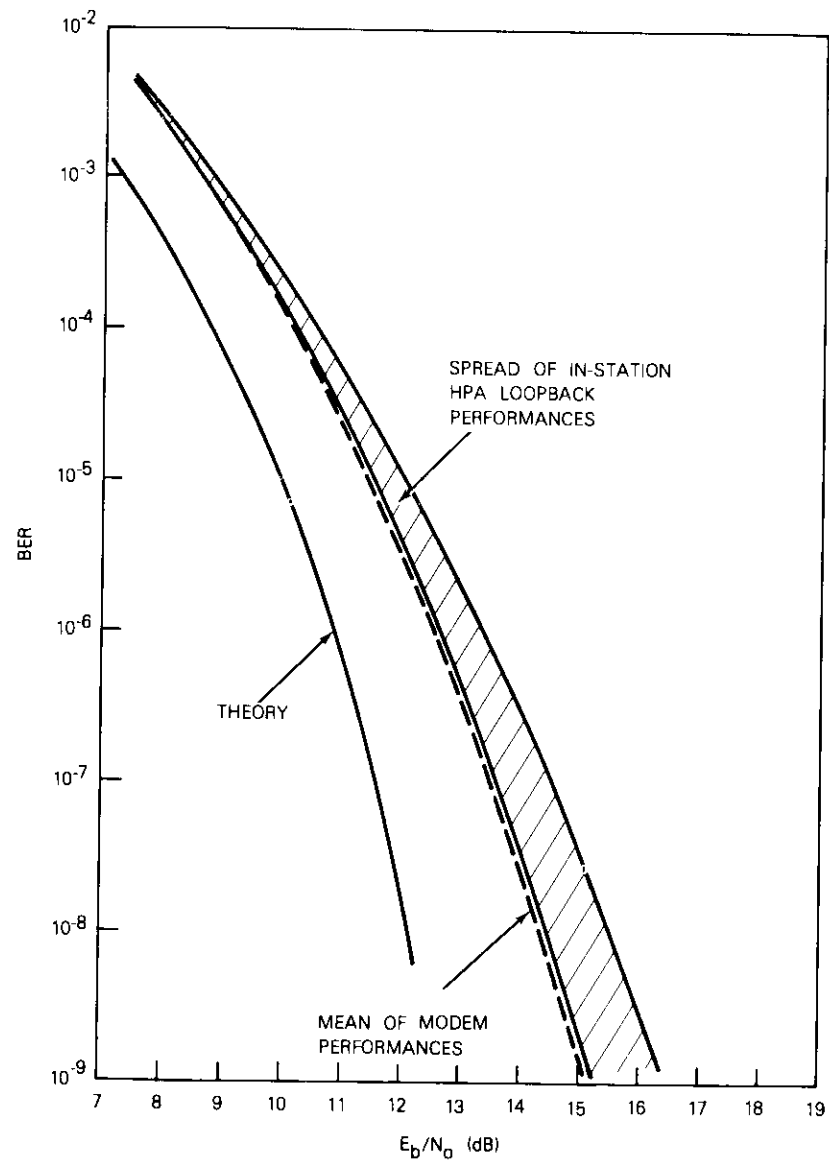


Figure 4. BER as a Function of E_b/N_0 in the HPA Loopback Mode

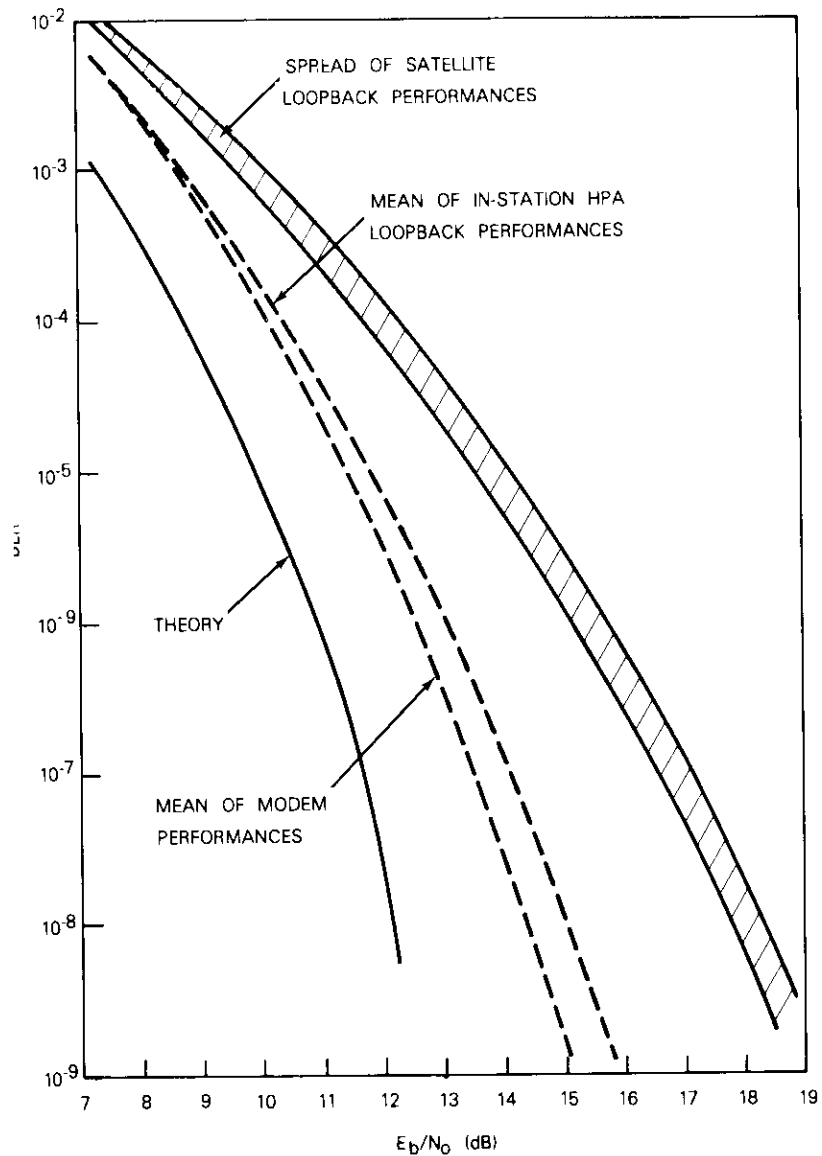


Figure 5. BER as a Function of Receive E_b/N_0 in the Continuous Mode

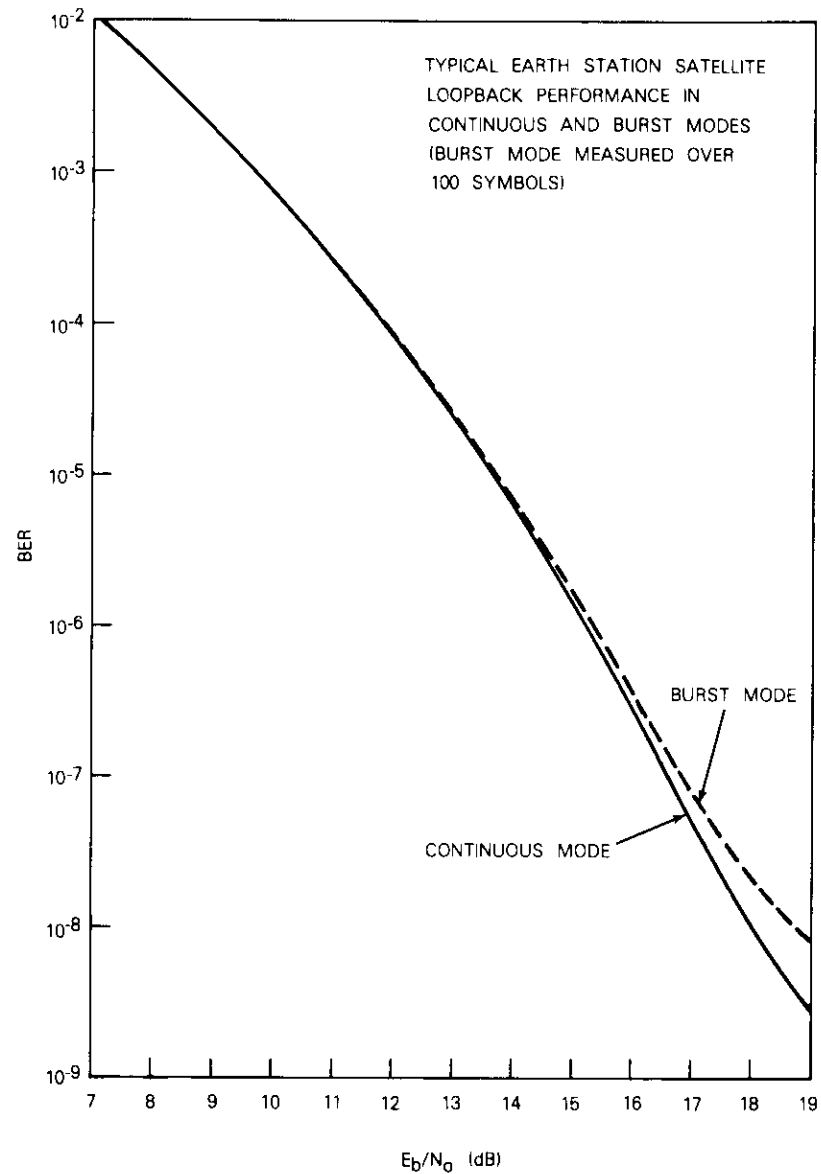


Figure 6. BER as a Function of Receive E_b/N_0 in the Satellite Loop Mode

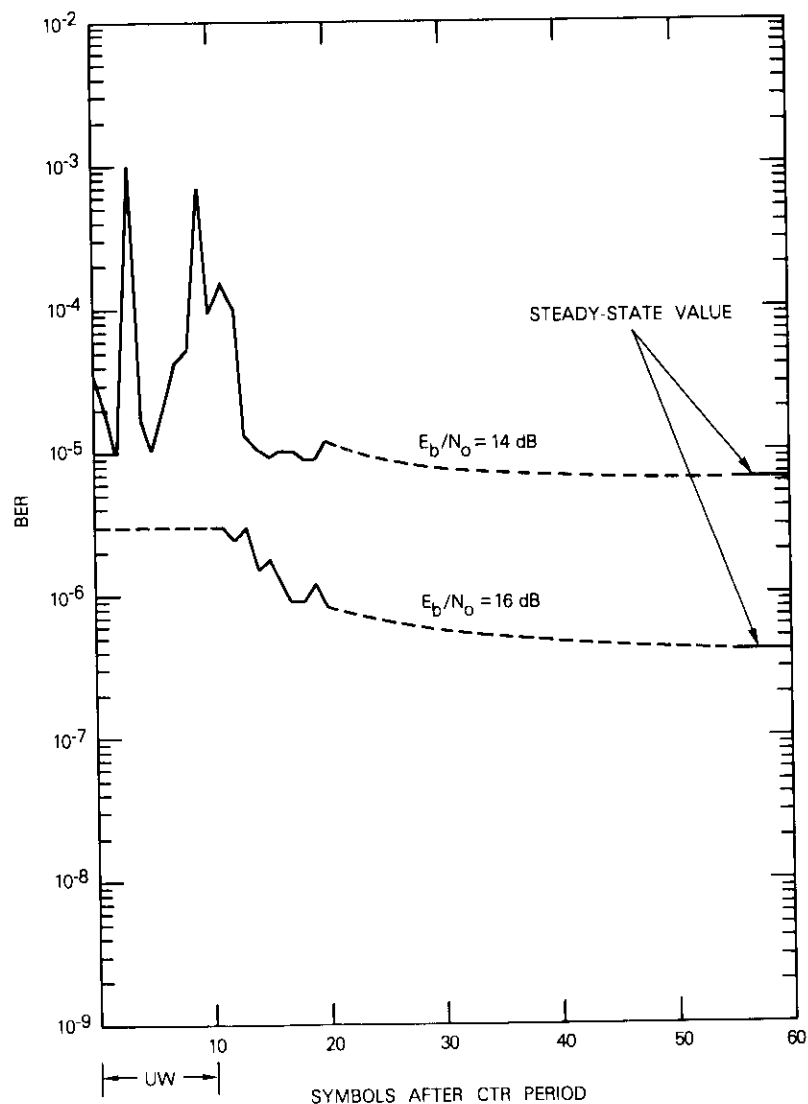


Figure 7. BER as a Function of Symbol Position

intersymbol interference pattern, must be averaged to obtain the appropriate BER. This averaging has been performed for the lower

curve. Both curves exhibited a gradual transient approach to a steady-state value which is reached after a symbol count of approximately 55.

BER as a function of e.i.r.p.

To assess the impact of earth station e.i.r.p. (and hence satellite TWTA operating point) on received BER, stations were required to vary e.i.r.p. while observing the BER. Varying e.i.r.p. has several effects:

- Initially, if it is assumed that e.i.r.p. is reduced from a value at, or close to, saturation, a rapid reduction of the distortion introduced by the satellite TWTA is observed.
- The noise suppression and intersymbol intermodulation (non-linear intersymbol interference) effects vary.
- There may be a significant change in the distortion introduced by the earth station HPA, if the e.i.r.p. necessary to saturate the satellite causes the earth station HPA to operate nonlinearly. This is especially the case when the HPA used is common to other carriers.

A typical result for BER as a function of earth station e.i.r.p. in the continuous mode is shown in Figure 8. The curve was obtained without additional noise at the receiver, and the minimum is an indicator of the optimum satellite operating point. As previously noted, a variation in earth station e.i.r.p. results in changes in satellite operating point, distortion, receiver carrier-to-noise ratio, and, to a lesser extent, earth station HPA operating point. The e.i.r.p. vs BER curve shows the tradeoffs between increasing distortion due to the satellite operating point moving closer to saturation, and the improved carrier-to-noise ratio in the receiver accompanying the move toward saturation. Because of the soft limiting characteristic of the satellite TWTA power transfer curve, the degradation due to distortion may increase at a faster rate than the improvement in receive E_b/N_o .

With the channel filtering arrangements used in the field trial, the transmission link tends to be distortion limited rather than power limited, and causes the optimum BER performance to occur before the TWTA is saturated. This is generally characteristic of the sharper roll-off transmit side filter. Table 3 lists the estimated optimum e.i.r.p. for the various earth stations, together with the resulting BER experienced in the field trial.

Error distribution

Bit error distribution data in the form of error-free intervals were

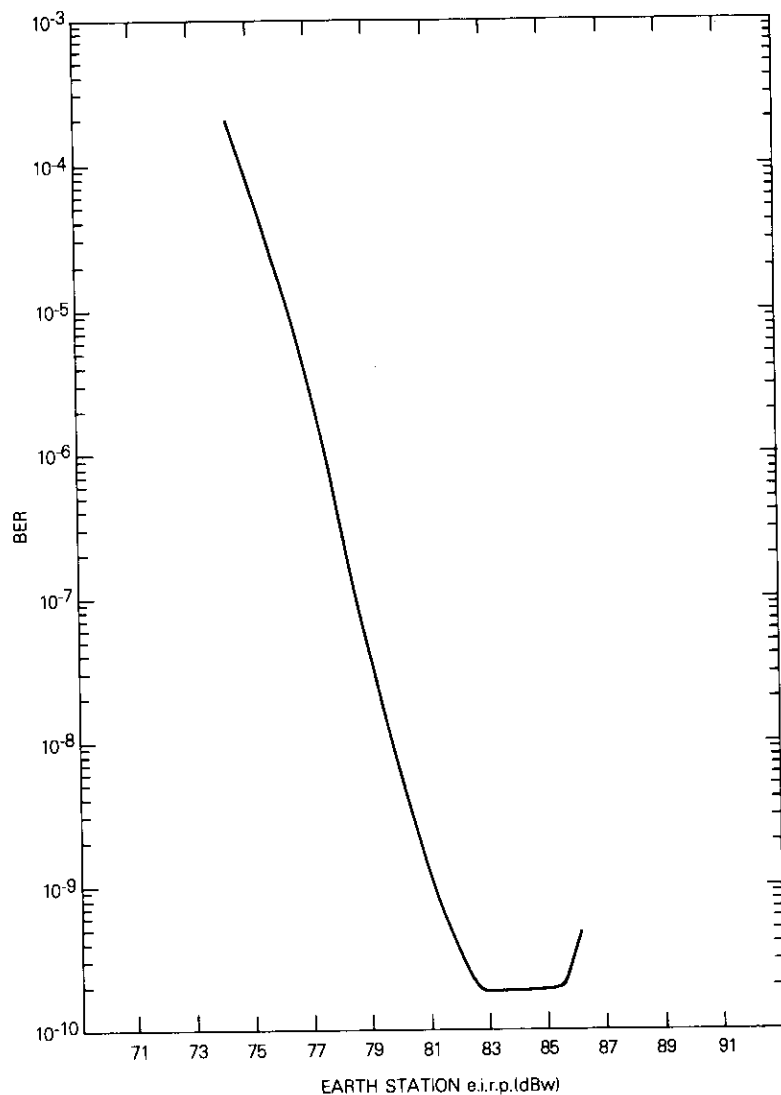


Figure 8. BER as a Function of Earth Station e.i.r.p. in the Continuous Mode

collected for the back-to-back, RF loop, and satellite loop at Pleumeur Bodou. The data collection apparatus counted the number of occur-

TABLE 3. ESTIMATED OPTIMUM EARTH STATION OPERATING POINT

Station	e.i.r.p.	BER	HPA
AN	84.5	3×10^{-9}	Common
LR	85.0	7×10^{-9}	Separate
GH	85.0	2×10^{-8}	Separate
PB	83.5	2×10^{-9}	Common
RA	84.5	2×10^{-10}	Separate

rences of error-free intervals x for the range $x = 0$ and for the set of ranges $2^r \leq x < 2^{r+1}$ which give the ranges $1 \leq x < 2$, $2 \leq x < 4$, $4 \leq x < 8$, The results for the satellite loop data at a BER of 10^{-4} corresponding to an $E_b/N_o = 11.8$ dB and an earth station e.i.r.p. of 83 dBW are shown in Figure 9. The total number of bits in the measurement period was 10^8 .

The number of occurrences in the interval $0 \leq x < 1$ is 2076, which is the number of contiguous errors. This information alone does not reveal the grouping of the errors, but the remainder of the distribution gives some indication. For an error rate of 10^{-4} , if all the errors were double errors, then the mean error-free distance and hence the peak of the distribution would be 20,000. Figure 9 indicates that this is very nearly the case and thus double errors appear to predominate. This was expected because of differential encoding which inherently tends to generate double bit errors.

Conclusions from the independent station tests

Bit-error rate measurements were reported in both continuous and burst modes for back-to-back, long RF loop, and satellite loop operation. The independent station tests demonstrated that the transmission performance of the different TDMA terminals conformed to the BG-1-18 (Rev. 2) specification and was adequate for TDMA operation, even though these terminals were used with standard A earth stations primarily designed for FDMA earth station operation.

Analysis of the observations of BER versus earth station e.i.r.p. showed that the optimum satellite operating point was achieved at about the same value of e.i.r.p. for all earth stations, even though Andover and Pleumeur-Bodou operated with multicarrier HPAs. The operating point of the earth station HPA did not prove critical, probably because the HPAs were backed off to operate in the linear region.

The predominant feature of the link which limits the BER performance

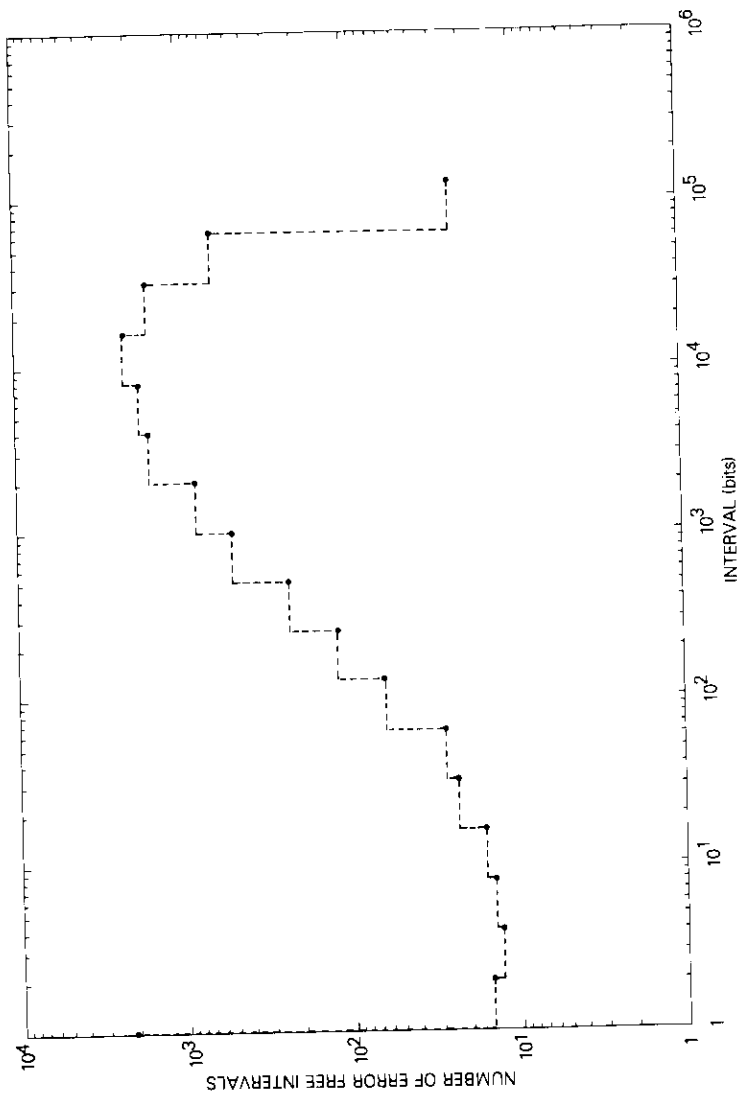


Figure 9. Distribution of Error-Free Intervals for the Satellite Loop Taken at Pleumeur-Bodou

in the satellite loop with tight channel filtering appears to be the operating point of the satellite TWTA. In the TDMA field trial this point was selected to be 2.5-dB input backoff from saturation. It is believed that this backoff resulted in near-optimum performance, considering the tradeoff among down-link power, TWTA nonlinear distortion, and filter characteristics.

TDMA system tests

The system control protocols contained in the INTELSAT TDMA specification are concerned with obtaining and maintaining the correct relationship among the bursts in the TDMA frame. To establish the necessary common time base for the various stations to transmit traffic bursts, a reference burst is also transmitted by one of these stations. Many of the system control protocols are necessitated by the replacement of a faulty reference burst (reference replacement), while another group is concerned with the initial placement (initial acquisition) of the burst of a station joining a working frame, or for rapidly rejoining a working frame after a short outage (fast reentry).

The TDMA system tests were designed to thoroughly exercise the operation of protocols among the stations in the INTELSAT TDMA field trial. Concurrently with these tests, the protocols were examined for their accuracy, adequacy, and complexity. The test results contain much important information concerning the operation of TDMA system control.

Initial acquisition test

Initial acquisition is the technique of obtaining a burst position estimate used for entering the working TDMA frame. This is accomplished by transmitting a low-level signal, either in bursts of CW or modulated by a pseudo-random sequence. Both methods allow a timing estimate without undue disturbance of the existing (working) TDMA bursts. The test showed that acquisition could be achieved without significant disturbance to working bursts already in the frame, even at an error rate of 10^{-3} .

Fast reentry protocol

The fast reentry protocol is included in the system control specification to permit rapid recovery from short-term outages. To predict the timing of the burst following the short-term outage, the terminal

must make a prediction based on the rate of change of burst timing prior to the outage. This limits to 5 minutes the interval following the outage when fast reentry may be attempted. Fast reentry uses a full power blast, which is shortened to include only the preamble, allowing greatly increased guard times to accommodate the uncertainties of the local burst timing prediction. This test uncovered serious ambiguities and omissions within this protocol which will be discussed later.

Steady-state synchronization test

The steady-state synchronization protocols are concerned with the maintenance of the burst timing within the TDMA frame. The stations were required to measure the position of their bursts relative to the reference burst, and to introduce corrections in order to remain within ± 3 symbols of their nominal position.

The required response to a ± 4 -symbol shift in the relative reference burst position is not clear from the specification; this led to different interpretations by the various manufacturers of field trial terminals. However, corrections of burst position up to ± 3 symbols were demonstrated.

Reference station replacement protocols

The reference station in this prototype INTELSAT TDMA system establishes the time base upon which all burst timing is performed. Therefore, the loss of a reference station cannot be tolerated for more than a short period. To replace a failed reference station, a complicated protocol is evoked which is based on observations by the primary, first standby, and second standby reference stations.

The specification contains several ambiguities and omissions in describing this protocol. This led to several interpretations of the requirements by the various manufacturers, and subsequent difficulty was experienced in the interworking of the protocol. Therefore, only one reliable reference configuration could be demonstrated. The main ambiguity centered on the necessity to transmit sync loss messages continuously or intermittently.

DSI systems test data

The DSI equipment used in the field trial is a computer-based system and is fundamentally difficult to test. However, a number of tests were devised and included in the TDMA test plan, and the results of the more important tests have been provided by Andover (AN), Lario (LR), and

Pleumeur Bodou (PB). To obtain these results, a TDMA/DSI network was established with these three stations to assess various multidestination and multimanufacturer effects. An outline of the test is given below, followed by a brief discussion of the results:

a. Start of DSI: To enter the DSI mode, an exchange of messages takes place in the TDMA control signaling channel (CSC). This procedure was tested many times and operated satisfactorily.

b. Stop of DSI: Stop of DSI is initiated by a manual command on the TTY or when an excessive error rate has been detected on the assignment channel. It is also achieved by an exchange of messages.

The procedure was conducted successfully between the participants; however, in rare cases, it did not work with Andover. In such cases, after a BER alarm on the Andover assignment channel in PB, the stop procedure was initiated and was not successful: PB would go into the bypass mode while Andover stayed in DSI. Printouts in PB indicated that Andover did not answer the request to stop from PB.

System test result conclusions

The TDMA/DSI system tests were designed to thoroughly exercise operation of the system protocols. It was discovered that the specification contains ambiguities and omissions and was unnecessarily complicated. The system tests showed that the manufacturers interpreted some areas of the specification in slightly different ways. Some modifications were made by participants, resulting in a working TDMA system which adequately supported the live traffic tests.

The protocols in future specifications should be considerably simplified. Furthermore, great care should be exercised to ensure that the various protocols do not conflict, since many of the problems experienced in the field trials resulted from such conflicts.

Live traffic tests

A principal objective of the TDMA/DSI Field Trial was to evaluate the INTELSAT TDMA/DSI system's subjective performance in an operational environment relative to that of a conventional FDM/FM system. The required subjective assessment data were obtained by customer interviewing.

The countries participating in the live traffic tests were France, Italy, and the U.S. Three test conditions were used for the TDMA/DSI system,

and data were collected at both ends of two links, France/U.S. and Italy/U.S.

A DSI gain of two was established as test condition 1, since it represents the specified TDMA/DSI operating condition. The increased DSI gain of 2.4 in test condition 2 was selected to obtain an indication of the robustness of the TDMA/DSI system, and test condition 3 provided a controlled, artificially devised, heavy load which simulated busy hour traffic. The DSI loading for test conditions 1 and 2 was provided by live traffic. Subjective assessment data were collected from the reference FDM/FDMA system throughout the entire test interval from September 5 to December 15.

The subjective measures used were mean opinion score (MOS) and percent difficulty (%D). The MOS is an average score resulting from users' opinions of the circuit: "excellent," "good," "fair," or "poor." The mean opinion score is calculated by weighting excellent = 4, good = 3, fair = 2, and poor = 1. Both France and the U.S. used this MOS method. The second measure, %D, is simply the percent of the users indicating that they had difficulty using the circuit.

Confidence intervals were computed for both MOS and %D. When a customer reported difficulty, additional probing was done in an attempt to determine the cause. The probing questions were selected to identify difficulties that might be related to TDMA/DSI operation as well as other typical difficulties encountered in telephone service.

Discussion of French results

The results in terms of MOS and %D are summarized in Table 4. Under test condition 1, representing normal TDMA/DSI operation at a DSI gain of 2, the performance was slightly lower than that experienced for FDM/FDMA circuits. This is seen in both MOS and %D scores. The MOS was very high and the %D unusually low for the FDM/FDMA results observed; no explanation has been found. In the TDMA/DSI case similar behavior was encountered. Performance decreased

TABLE 4. SUMMARY OF FRENCH TEST DATA

	No. of Interviews	MOS	%D
Test Condition 1	338	3.12	18.0
Test Condition 2	179	3.04	25.1
Test Condition 3	157	3.11	21.0
Reference FDM/FDMA	349	3.20	9.4

slightly under test condition 2, where the DSI gain was increased to 2.4. Performance remained unchanged for test condition 3, where the system was continuously subjected to the maximum busy hour load at a DSI gain of 2.

The circuit quality distributions are given in Figure 10 for all test conditions. One observation is the almost identical distributions for

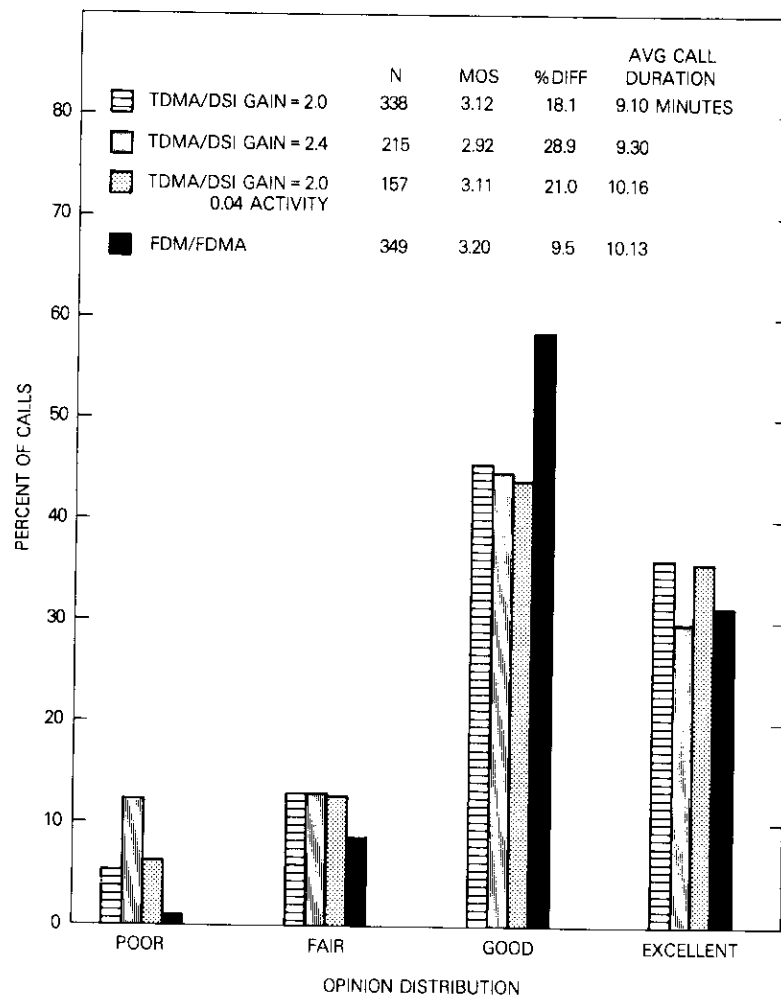


Figure 10. Circuit Quality Distributions for French Respondents

test conditions 1 and 3. From this it appears that the average performance of the TDMA/DSI circuits during the maximum busy hour differed little from that experienced under live traffic conditions.

Reasons for difficulty distributions are shown in Figure 11. Low volume is the leading cause of difficulty in all test conditions, with other major contributors including "noisy/hum," "fading," "other," and in one case "crosstalk." One very important observation is the striking difference between the distributions for FDMA and TDMA/DSI. The frequency of occurrence of difficulties on the FDM/FDMA circuits was lower than that for one or more TDMA/DSI test conditions in the categories of "low volume," "noise/hum," "fading," and "other." Except for "other," these categories are not associated with TDMA/DSI. The implication is that the observed differences between TDMA/DSI system, viz, "chopping," "front-end clipping" and "voice distortion," show very little change as a function of TDMA/DSI test condition. One additional item of importance is that, given that a difficulty occurred, the distribution of the reasons for difficulty is independent of the test condition. This implies that causes of difficulty are not likely to be due to TDMA/DSI related problems.

Discussion of Italian results

This section presents the subjective test data collected in Italy for test conditions 1, 2, and 3. The numerical results should not be compared directly to the French and the U.S. results because the Italian results use a 5-point rather than a 4-point opinion scale. Furthermore, it should be noted that in test condition 3 the DSI was operated in the bypass mode.

The results are summarized in Table 5, and the details of the opinion scores are shown in Figure 12. The distribution of the reasons for difficulty is given in Figure 13.

TABLE 5. SUMMARY OF ITALIAN TEST DATA

	No. of Interviews	Mean Opinion Score
TDMA/DSI I Gain = 2.0	165	3.03
TDMA/DSI II Gain = 2.4	222	3.05
TDMA/DSI III Gain = 1.0	158	3.18
FDM/FDMA	157	3.01

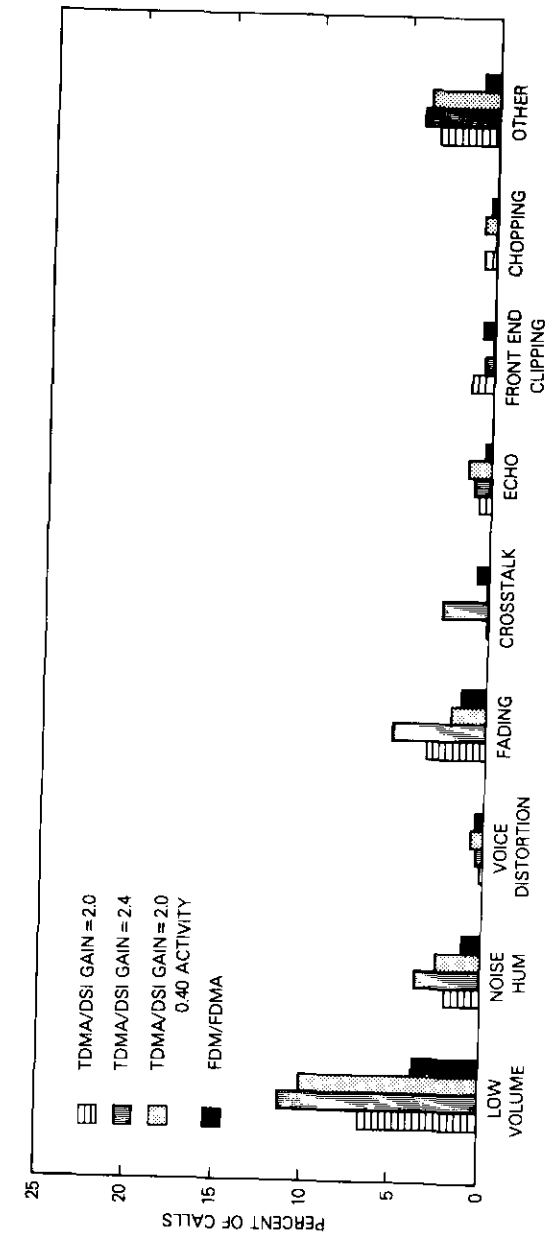


Figure 11. Reasons for Difficulty for French Respondents

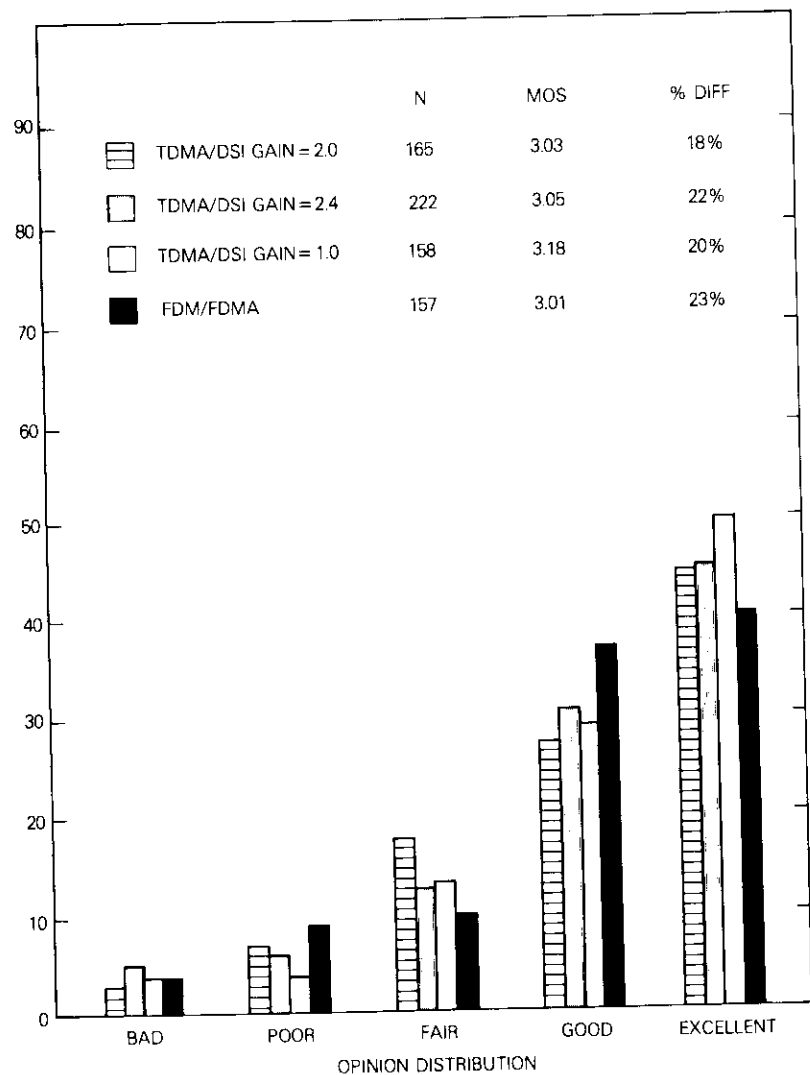


Figure 12. Circuit Quality Distributions for Italian Respondents

The results show that the MOS slightly exceeds 3.0 for TDMA/DSI conditions 1 and 2 and approaches 3.18 for TDMA/DSI condition 3 (bypass); the final mean opinion score, 3.01, is indicated for the FDM/FDMA system. In all three test conditions the TDMA/DSI system

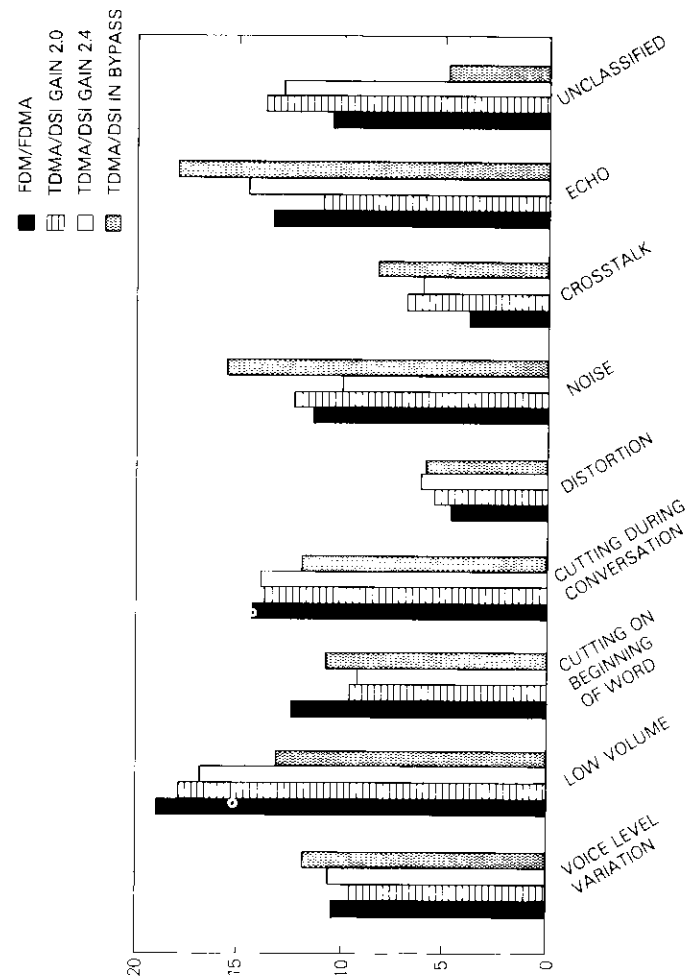


Figure 13. Reasons for Difficulty for Italian Respondents

percent difficulty score stabilized at a slightly lower value than the FDM/FDMA system score of 23 percent. The distributions of the reasons for difficulty show only small differences between TDMA/DSI and FDM/FDMA. In terms of the mean opinion score, the distributions for TDMA/DSI and FDM/FDMA are very similar and no difference was perceived between the two systems.

Discussion of U.S. results

The subjective test data were collected in the U.S. with the extensive cooperation of AT&T Long Lines. A "double blind" experiment was conducted in that an outside firm interviewed the customers. Neither the interviewing company nor the customers had knowledge of the test conditions.

Three operating conditions were used for the TDMA/DSI system. In test conditions 1 and 2, bridged live traffic was used to load the DSI system, and the DSI gains were 2.0 and 2.4, respectively. In test condition 3, for the France/U.S. link, simulated 40-percent speech activity was used for loading and the DSI gain was 2.0. During test condition 3, the channels in the Italy/U.S. link were operated in the DSI bypass mode, and consequently were not interpolated.

Analysis was performed for test conditions 1, 2, 3, and FDM/FDMA, respectively. Table 6 summarizes the U.S. data. The opinion distributions for the France to U.S. and Italy to U.S. paths are shown in Figures 14 and 15, respectively.

TABLE 6. SUMMARY OF U.S. TEST DATA

Test Condition	Total No. of Interviews			Total No. of Interviews		
	Total No. of Interviews	MOS	% Diff.	Total No. of Interviews	MOS	% Diff.
1 TDMA/DSI	671	2.86	32.2	281	2.71	33.1
FDM/FDMA	559	2.91	25.8	387	2.87	28.9
2 TDMA/DSI	325	2.72	34.5	112	2.59	40.2
FDM/FDMA	362	2.89	29.3	375	2.69	34.7
3 TDMA/DSI	144	2.66 ^a	36.8 ^a	55	2.70 ^b	40.0 ^b
FDM/FDMA	202	2.84	31.7	72	2.72	25.0

^a DSI gain = 2.0 with simulated 40-percent speech activity.

^b DSI gain = 1.0, i.e., bypass.

A detailed statistical analysis of the data shows that customers were unable to perceive any substantial differences between TDMA/DSI and

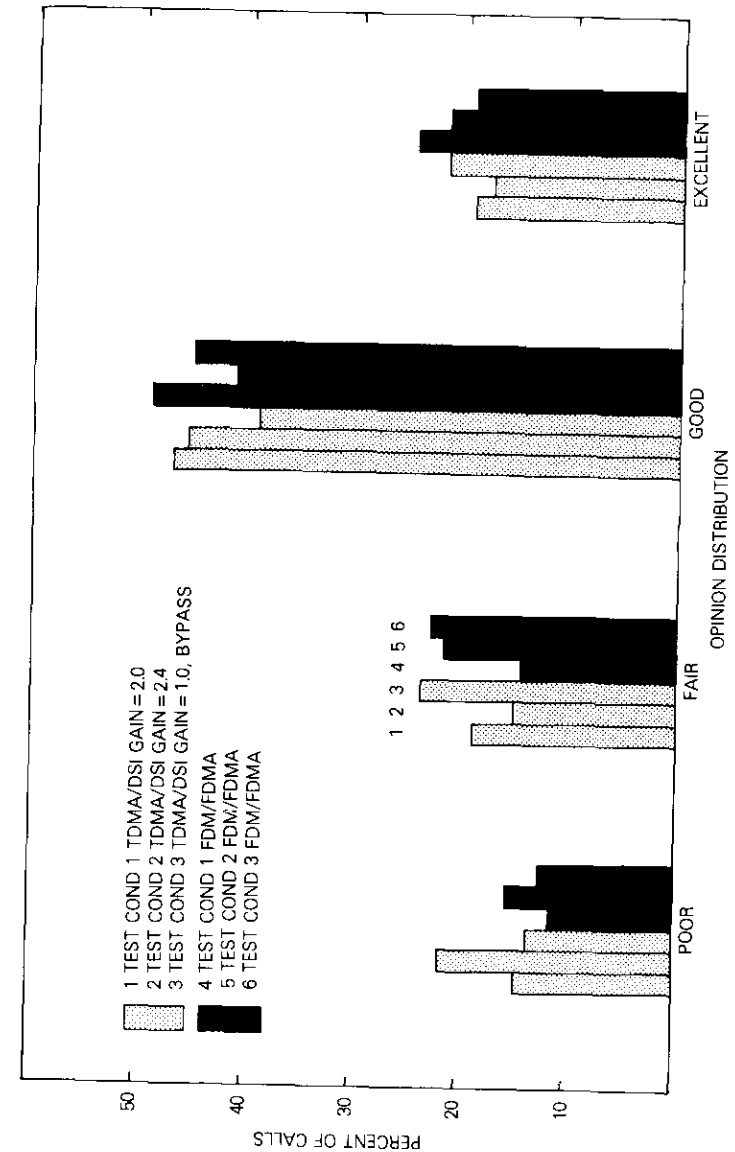


Figure 14. Circuit Quality Distribution for U.S. Respondents on France-to-U.S. Link

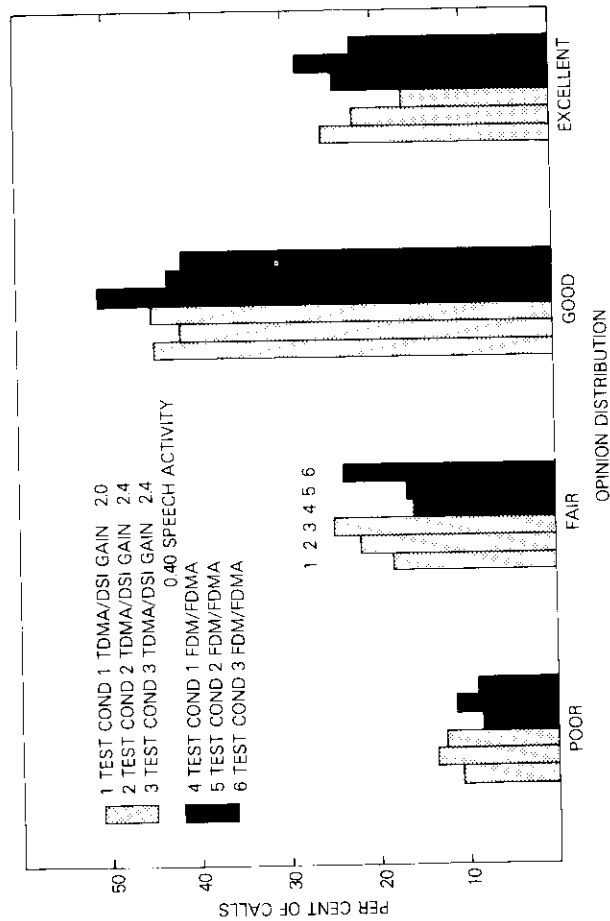


Figure 15. Circuit Quality Distribution for U.S. Respondents on Italy-to-U.S. Link

FDMA transmission. However, the observed results generally do show slightly lower mean opinion scores and higher percent difficulty with TDMA/DSI than with FDM/FDMA transmission.

Distributions of the causes of difficulty are given in Figures 16 and 17. The leading causes of difficulty are echo, low volume, and static and crackling. Although echo and low volume are unrelated to TDMA/DSI operation, echo caused substantially more difficulty with TDMA/DSI than with FDM/FDMA transmission. In addition, difficulty due to causes unrelated to TDMA/DSI operation occurred slightly more often with TDMA/DSI. Reasons for this observed difference are not known.

The TDMA/DSI system is operationally quite robust under heavy loading conditions. After allowances are made for degradation in the reference FDM/FDMA circuits between test conditions 1 and 3, and for differences in occurrence of difficulties unrelated to TDMA/DSI operation, the remaining difference between test conditions 1 and 3 becomes inconsequential. This demonstrates that, under the continuous busy hour load simulated by test condition 3, customer response is essentially the same as that under the fluctuating traffic load represented by test condition 1.

Summary of live traffic tests

Table 7 summarizes the results of the live traffic tests drawn from the three sets of data provided by France, Italy, and the U.S. The MOS and %D values are listed for each test condition, transmission path, and interviewed customer location for TDMA/DSI circuits.

The results for test conditions 1 and 2, for DSI gains of 2.0 and 2.4, respectively, with bridged live traffic loading, show that the increase in DSI gain caused only a slight degradation in performance for call-backs to U.S. and French customers. This is believed to be inconsequential. The degradation in changing from a DSI gain of 2.0 to 2.4 was slightly more pronounced for the call-backs to U.S. customers on the circuits to Italy than on the circuits to France. On the other hand, the call-backs to Italian customers appear to indicate a small improvement in performance in changing DSI gain from 2.0 to 2.4.

The results for condition 3 between France and the U.S. are for simulated activity loading of the DSI circuits using an activity of 40 percent and a DSI gain of 2.0. This test condition represents full-time operation of the circuits at a load attained typically at the peak busy hour. The results for call-backs to the U.S. customers showed slightly

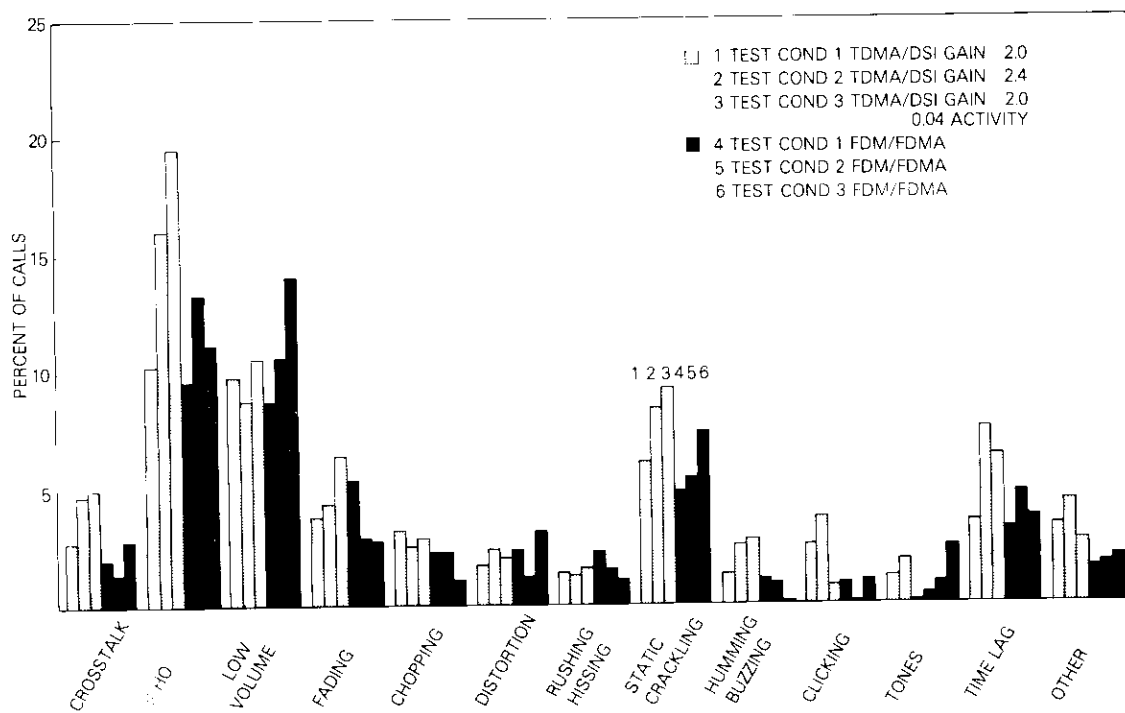


Figure 16. Reasons for Difficulty for U.S. Respondents on France-to-U.S. Link

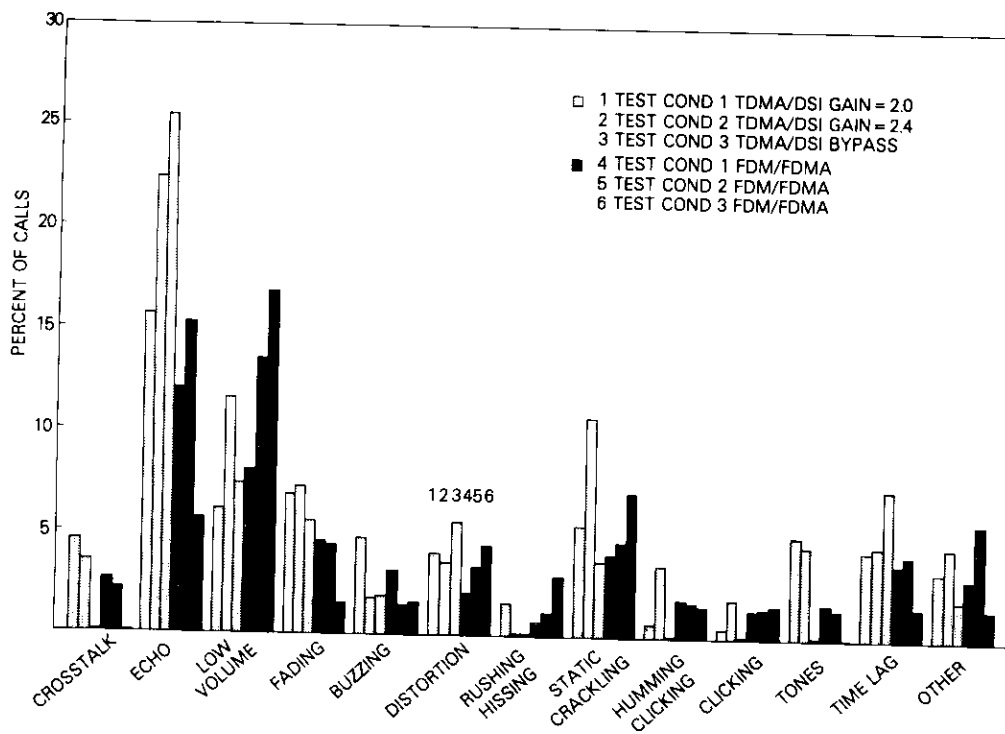


Figure 17. Reasons for Difficulty for U.S. Respondents on Italy-to-U.S. Link

TABLE 7. SUMMARY OF LIVE-TRAFFIC TEST RESULTS FOR TDMA / DSI CIRCUITS

Test Condition	DSI Gain	Link	Interviewed Customer Location	MOS	%D
1	2.0	FR/US	US	2.86	32.2
			FR	3.12	18.0
2	2.4	FR/US	US	2.72	34.5
			FR	3.04	25.1
3	2.0 ^a	FR/US	US	2.66	36.8
			FR	3.11	21.0
1	2.0	IT/US	US	2.71	33.1
			IT ^b	3.03	17.6
2	2.4	IT/US	US	2.59	40.2
			IT ^b	3.05	22.0
3	1.0 ^c	IT/US	US	2.70	40.0
			IT ^b	3.18	20.3

^a Simulated 40-percent speech activity.

^b DSI bypass mode.

^c Italian results were ranked on a 5-point rather than a 4-point rate.

decreased quality compared with conditions 1 and 2, whereas the results for call-backs to France showed a slightly increased quality compared with condition 2 but decreased compared with condition 1.

The results for condition 3 between Italy and the U.S. were taken for DSI in the bypassed condition and hence represent the performance of the TDMA circuits without DSI processing. For the call-backs to both U.S. and Italian customers, the quality was essentially the same as for condition 1, indicating that the use of the DSI processing did not appear to change the quality of the circuits.

During the data collection period, difficulties, particularly on the terrestrial extension of the TDMA/DSI circuits, occurred frequently and were reported to the telephone administrations involved for correction. Such factors are believed to have had an impact on the call-back results.

The causes of difficulty on the TDMA/DSI circuits have the same kind of distributions as those on the FDMA/FDM circuits. The principal causes of difficulty are echo, noise, and low volume, which appear to be unrelated to the features of TDMA/DSI equipment operation.

The general conclusion from the live traffic tests is that there were no differences of significant consequence between FDMA/FDM and TDMA/DSI circuit performance. Considerable variability in perform-

ance was frequently experienced which tended to mask the results and could account for many of the observed differences.

Tests to examine the performance of the TDMA/DSI circuits under DSI gain conditions of 2.2 and 2.4 and under conditions of high activity indicated that the DSI equipment is very robust and can withstand such enhanced loading conditions without significant degradation.

Operational experience gained during the field trial

The participating INTELSAT Signatories were asked to evaluate the operational performance of TDMA/DSI equipment based upon the experience gained during the field trial. The responses were divided into five main areas:

- a. earth station equalization,
- b. earth station interface considerations,
- c. TDMA terminal operation and maintenance,
- d. TDMA acquisition and synchronization,
- e. DSI equipment performance.

Earth station equalization

Each participant was requested to evaluate the method and suitability of amplitude and group delay equalization which was employed during the field trials. Adequate amplitude and group delay equalization was achieved by all participants using the methods recommended by INTELSAT, which call for specific amplitude and group delay characteristics. In all cases, the result of equalization was checked only in loop back. One participant indicated the need for re-equalization every two or three months to maintain the amplitude and group delay responses within the prescribed limits. However, the influence of these variations on BER was reported as slight.

Earth station interface considerations

Three participants used a separate HPA for TDMA transmission operating with output backoffs in the range of 10 to 13 dB. These values were held constant throughout the field trial, and resulted in no particular difficulties.

One of the participants on various occasions operated with a combination of FDM, SCPC, TV, and TDMA through a single HPA. The output backoff of the HPA was about 8 dB for FDM, SCPC, and TDMA without TV, and was about 6 dB with TV. The maximum level of

intermodulation was 21 dBW/4 kHz and 30 dBW/4 kHz without and with TV, respectively.

The other participant operated the TDMA carrier with and without TV using a common HPA. Measurements showed no degradation to either FM, SCPC, or TV carriers sharing the HPA. The HPA backoff was not held constant during the test. The output backoff was about 10.8 dB for TDMA alone, but for both TV and TDMA the output backoff was about 8.9 dB.

TDMA terminal operation and maintenance

All participants indicated that the observed BER remained relatively constant from day to day with the exception of the expected variations due to atmospheric conditions and antenna pointing. Two participants indicated high variation in the sync unique word loss rate depending on sync burst source. Although the cause was not identified, both participants reported satisfactory synchronization.

All participants indicated that their terminals synchronized properly over long periods of time. Modem synchronization for most participants was reliable and did not require periodic realignment. No cycle skipping problems were observed at nominal operating points. For one of the participants employing a laboratory modem, realignment was required about once a week.

Functions which were identified by one or more participants as requiring increased reliability were as follows:

- a. data multiplexer,
- b. scrambler,
- c. preamble transmitter,
- d. computer memories and associated software,
- e. order wire BER measurement,
- f. reference station replacement,
- g. DSI system control.

There was also evidence of connector, thermal, and software problems from time to time. All participants felt that the terminals performed satisfactorily for experimental use, although the reliability could be significantly improved by simplifying the system design.

Preoperational tests

The participants considered the following preoperational tests necessary for ensuring reliable terminal operation:

- a. check of the amplitude and group delay response,

- b. BER in burst mode (to be derived from information carried in the traffic burst),
- c. initial acquisition procedure,
- d. reference station replacement, if applicable.

It was felt that the system algorithms (*e.g.*, initial acquisition, rapid reentry, and reference replacement) need to be thoroughly tested. These tests cannot be performed without risk to operational traffic, and procedures should be designed which allow reasonable in-station tests prior to accessing the operational transponder.

TDMA acquisition and synchronization

The participants were requested to comment on the specific method of acquisition, synchronization and reference station replacement and, in particular, on the acceptability of the protocols. They were also requested to indicate their opinions concerning the specified method of maintaining burst position and the ease with which changes in traffic could be accommodated from an operator's viewpoint.

The method of acquisition worked well in the global beam configuration. However, two participants indicated that the acquisition demodulator was sensitive to the level of the received carrier.

The participants indicated that synchronization was reliable. One participant indicated that his terminal synchronization subsystem used a phase-locked loop to synchronize the transmit local clock to ensure the position of the burst to within ± 1 symbol. The remaining corrections were due only to clock instability and the variation of the Doppler effect. The phase-locked loop might not be necessary if the clock long-term stability is better than 10^{-7} .

It was generally concluded that the method of reference station replacement was not sufficiently reliable, primarily due to ambiguities in the reference station replacement protocols.

DSI equipment operation and maintenance

For the participants operating DSI equipment, the assignment technique appeared to operate reliably over long periods of time. Some participants indicated that their terminals were often forced out of DSI operation due to a perceived high error rate in the assignment message channel. This anomalous behavior remains unexplained.

It was the general opinion that DSI bypass operation could be eliminated since the complexity involved in providing this facility is large and the benefits derived are small.

Conclusions from the operational experience

The TDMA/DSI terminals functioned sufficiently well to validate the TDMA system concept embodied in the INTELSAT standard. However, problems encountered with the terminals indicated that they would be unsuitable for use in the operational environment. All but one of the terminals were nonredundant and two were lab models. Some problems were due to implementation imperfections, which can be avoided in the future. Others resulted from ambiguities and omissions in the specifications which gave rise to slight incompatibilities between the terminals. Still others were due to the complexity of the protocols employed. It was concluded that, for terminals to withstand the rigors of the operational environment, extensive revisions to the specification would be necessary to enhance simplicity, reliability and economy. Further, it was felt that building terminals to a common specification may not, by itself, ensure operational compatibility and that pre-commissioning testing may therefore be necessary.

Modifications, improvements and new concepts arising from experience in the field trial

It is now generally accepted that the INTELSAT prototype TDMA/DSI specification is too complex for an operational TDMA specification and that a new specification should be considerably simplified. In the time since the prototype specification was produced, much work has been expended on alternative TDMA control techniques, and this, together with the experience gained during the INTELSAT TDMA field trial, has suggested a mixture of modifications and improvements to the basic concept together with various new concepts which should be considered.

Transmission performance

AMPLITUDE AND GROUP DELAY EQUALIZATION FOR TDMA NETWORKS

Imperfect amplitude and group delay equalization on the earth station up-link preceding the transponder TWTA operating at, or near, saturation can impair the link BER rate more than if the channel were linear. The impairment can be avoided by operating the HPA in a linear region where it is possible to equalize for the up-link before the HPA. When nonlinearity in the earth station's HPA becomes significant, it is generally impossible to equalize the TDMA up-link to compensate for

imperfect satellite input filters by introducing equalization before the earth station HPA. Consequently, in this case post-HPA equalizers or well-equalized input satellite multiplex filters are strongly recommended. Any earth station up-link imperfection occurring before the HPA must be equalized before the HPA. The down-link (including the satellite output multiplex filter) can be separately equalized at the receiving earth stations.

MODEM FILTER CHARACTERISTICS

The BER performance of QPSK modulated carriers over a satellite link (with nonlinear earth station and satellite amplifiers) is strongly influenced by the modem transmit and receive filter characteristics. It has been found that it is possible to significantly improve overall performance by modifying the specified filter characteristics.

Various filter pair candidates have been identified by laboratory simulation and/or computer simulation. Filter pairs will be selected to minimize the carrier-to-noise ratio required for a given BER while satisfying the INTELSAT out-of-band emission limits at specified HPA backoffs (output backoffs typically of about 6 dB for 6-GHz earth stations).

The results obtained show that performance can be improved by increasing the bandwidth of the modem transmit filter by a small amount (about 10 to 15 percent). Moreover, the modem receive filter (not currently specified by INTELSAT) must be selected to minimize the combined effects of noise, intersymbol interference, and dual-path effects.

Laboratory hardware simulation involving an earth station HPA and an INTELSAT transponder simulator will help to identify the most desirable transmit and receive filter characteristics.

IMPACT OF BURST-TO-BURST AMPLITUDE VARIATIONS

The amplitude of the receive TDMA bursts could have burst-to-burst variations due to fading of up-path signals caused by rain attenuation. Bursts accessing the same transponder originate from widely separated earth stations, and will experience different amounts of fade.

The amplitude variation among bursts is expected to be worse in the 14/11-GHz and 14/4-GHz paths. The effect of interference from a large amplitude burst preceding a faded burst should be minimized. In particular, it is important to either provide sufficient dynamic range within the demodulator to accommodate the faded burst or to provide a fast-acting AGC system prior to the demodulator.

CYCLE SKIPPING

Cycle skipping in modems occurs at poor signal-to-noise ratios in both the demodulator's carrier and clock recovery loops and rarely occurs at the normal clear weather error rates ($<10^{-6}$). Under high-noise conditions, the output phase of the recovery loop will occasionally advance or fall back by one full cycle or multiples of one full cycle. These events may be short or they may extend over many symbols. In a differentially encoded system, carrier skips are not as damaging as clock skips, which may destroy frame burst timing.

In coherent systems which employ ambiguity resolution by using the unique word, a carrier skip will result in destruction of the subsequent part of the burst since the ambiguity resolution will be lost. There is currently no specification which encompasses these events, and it is conceivable that a modem could pass normal BER tests at low signal-to-noise ratios and still be unacceptable. A cycle skip can occur anywhere in the burst, and the effect on the burst can be destruction of the timing of all subsequent data. A specification for cycle skipping is needed which accommodates either coherent or differentially coherent detection.

System control

System control in a TDMA network refers to the techniques used for obtaining and maintaining the correct time relationship among the bursts in the TDMA frame. The technique chosen must be capable of allowing a station to enter the frame without causing a disturbance to stations already operating in that frame. The chosen technique must be capable of maintaining the burst positions so that time overlap (and consequent interference) is avoided. Finally, the chosen system must be compatible with operation in the spot beam environment of INTELSAT V and follow-on satellites.

The system control method adopted for the TDMA Field Trial was described earlier and provides for reference burst control, initial acquisition, and burst position control.

POSSIBLE IMPROVEMENTS TO THE EXISTING SYSTEM CONTROL CONCEPT

It is felt that the fast reentry protocol should be eliminated. The existing procedure does not seem to offer a significant return for the cost and complexity that it imposes on the terminal. This is especially true when the very limited practical use of this protocol is considered.

Therefore consideration is being given to the elimination of this procedure.

SOME ALTERNATIVE SYSTEM CONTROL METHODS

The multiple reference burst method uses several references per TDMA frame. The advantage of this method is that, because of its inherent redundancy, no sophisticated reference replacement protocol is required. When it is used in a spot beam environment, cooperating stations may be required to maintain synchronization among the multiple reference bursts. A number of different approaches are possible and further study is necessary.

The highly reliable reference station would be a special facility installed at an earth station to generate a reference burst for all stations in a TDMA network. In the INTELSAT system there would seem to be substantial advantages of introducing the concept of highly reliable reference stations. The major advantage of such a scheme lies in the simplification of terminal design and an attendant cost reduction. This scheme could be compatible with future spacecraft which may have onboard reference facilities. This approach lowers the TDMA terminal costs and provides a common specification for TDMA terminal synchronization for the foreseeable future.

Open-loop acquisition and synchronization promises to be a reliable system which may significantly reduce the cost and complexity of the TDMA terminals by eliminating the need for closed-loop acquisition and synchronization protocols. It requires satellite ranging data from at least three geographically well-separated stations to accurately determine the satellite position. A method for disseminating the open-loop control information to the TDMA terminals is required. Less precise burst position control requires less ranging accuracy and consequently can be accomplished with simpler ranging techniques.

Open-loop acquisition and synchronization may be particularly attractive for spot beam TDMA operation where a transmitting station cannot monitor its own burst position. This method does not require any separate protocol for acquisitions.

DSI system

There exists no fundamental problem in the operational use of the existing DSI system other than corrections of the various ambiguities and omissions contained in the specification. However, based on the considerable experience gained from the TDMA field trial, it is possible

to suggest modifications which promise a reduction in complexity and cost. There are also modifications necessary to ensure that the DSI unit is entirely compatible with future INTELSAT satellites and the terrestrial network.

DSI SERVICE MESSAGES CONSIDERATIONS

The service messages of the DSI system are concerned with the operation and maintenance of the system and are transmitted in the CSC of the TDMA equipment. There does not seem to be a justification for an auxiliary unit (such as DSI) to pass service messages in the CSC. This necessitates a multiplexing arrangement and imposes additional complexity in the TDMA terminal.

If DSI service messages are required, they could be transmitted as part of the DSI subburst. This would enable the DSI units to become fully autonomous and simplify TDMA CSC design. It would also facilitate the location of the DSI remotely from the TDMA terminal if desired. The disadvantage is that the overhead in the DSI subburst would be increased, but such an increase would be small.

ASSIGNMENT MESSAGE CONSIDERATIONS

In the existing system a disconnect message is sent before a new assignment's connect message. There may be no need to use a special message to break the previous connection before the new connection is established, since this could be achieved by the new assignment message. The present assignment channel uses 24 bits per TDMA frame. This is transmitted as 48 bits using a rate 1/2 Hagelbarger encoder and represents one message. The following modifications should be considered:

- a. If the disconnect message is eliminated then the connect/disconnect code (2 bits) can be eliminated also.
- b. The station identification code (6 bits) in the assignment message would not be needed for point-to-point operation. It may not be needed for multipoint operation since the sequence of the bursts identifies the origin. If retained it should be error protected.

Under peak-calling conditions there will be times when several channels become active simultaneously and thus several assignment messages will be generated simultaneously. Since only one message can be transmitted at a time, there may be a delay in establishing the channel. This delay must be minimized to avoid clipping of the start of the talk spurt.

An alternate solution which eliminates the congestion problem is to send an activity map which associates all the active terrestrial channels with their corresponding satellite channels. This alternative should be studied.

Conclusions

The experiments demonstrated that the transmission performance of the different TDMA terminals conformed to the INTELSAT prototype TDMA/DSI specification and was adequate for operational purposes even though the terminals were used at Standard A INTELSAT earth stations primarily designed for FDMA operation. The TDMA system tests which were designed to thoroughly exercise the protocols concerned with obtaining and maintaining the correct relationship among the bursts in the TDMA system frame showed that the manufacturers interpreted some areas of the specification in slightly different ways. Certain modifications were introduced by the participants, resulting in a working TDMA/DSI system which adequately supported the live traffic tests. All participants concluded that future TDMA/DSI system specifications should be much less complex and contain considerably simplified protocols.

The live traffic tests were considered a most important part of the evaluation of this TDMA/DSI system. France, Italy, and the U.S. participated in a customer call back/subjective evaluation experiment using DSI gains of 2.0 and 2.4, and a controlled heavy overload at a DSI gain of 2 (simulating busy hour traffic). The customers were unable to perceive a substantial difference between the TDMA/DSI and FDM/FDMA transmissions. The DSI gain of 2.4 produced a negligible difference in the circuit performance scores, as did operation in the simulated busy hour, which demonstrated the robust nature of the DSI technique. Participants in the field trial analyzed the results and provided appropriate conclusions. In addition, information on possible new concepts intended to improve the performance and/or reduce the cost of future TDMA systems was obtained.

The TDMA field trial confirmed that TDMA terminals constructed in accordance with the INTELSAT prototype system specification and constructed by different teams of companies for the most part functioned compatibly. The live traffic tests indicated that the customers were unable to perceive any substantial difference between the TDMA/DSI and FDMA/FDM transmissions.

Acknowledgment

While it is impossible to recognize individual contributions, the support of the International Telecommunications Satellite Organization (INTELSAT) is acknowledged and, in particular, the dedicated collaboration to the 1979 Atlantic TDMA Field Trial of the Signatories for France, Germany, Italy, the United Kingdom and the United States.

References

- [1] T. Sekimoto and J. G. Puente, "A Satellite Time-Division Multiple-Access Experiment," *IEEE Transactions on Communications Technology*, COM-16, No. 4, August 1968, pp. 581-588.
- [2] S. J. Campanella and K. Hodson, "Open-Loop Frame Acquisition and Synchronization for TDMA," *COMSAT Technical Review*, Vol. 9, No. 2, Fall 1979.
- [3] C.C.I.T.T. Recommendation G-712 Fifth Plenary Assembly, Document No. 54-E.
- [4] D. Schaefer, "TDMA System Monitoring," *COMSAT Technical Review*, Vol. 9, No. 2, Fall 1979.
- [5] M. Jones and M. Wachs, "Optimum Filtering for QPSK in Bandwidth-Limited Nonlinear Satellite Channels," *COMSAT Technical Review*, Vol. 9, No. 2, Fall 1979.



S. J. Campanella received a B.S.E.E. from the Catholic University of America, an M.S.E.E. from the University of Maryland, and a Ph.D. in electrical engineering from the Catholic University of America. Before joining COMSAT, he was Manager of the Electronics Research Center at Melpar, Inc. and prior to Melpar, Inc. was an Electronic Scientist at the Naval Research Lab engaged in sonar signal processing.

He is presently Director of the Communications Laboratory of COMSAT Laboratories. He has most recently been responsible for the technical direction of the INTELSAT TDMA field trials in the Atlantic Coast Region and for an intensive effort to develop a new low cost TDMA concept.

Dr. Campanella is a Member of AIAA, Sigma Xi, Phi Eta Sigma, and a Fellow of the IEEE and AAAS. He is also a Member of the Board of Directors of EASCON.

Roger J. Colby received an honors degree in electrical and electronic engineering from Lanchester Polytechnic, England, in 1971. Mr. Colby is with the British Post Office, Satellite Systems Division, where he was an executive engineer at the BPO Laboratories at Goonhilly Earth Station from 1971 to 1978. He was responsible for a team researching digital communications for satellites and participated extensively in CEPT and ESA studies concerning the TDMA aspects of the European OTS and ECS satellites. Currently, Mr. Colby is an INTELSAT nominee from the United Kingdom assigned to the Communications Processing Laboratory at COMSAT. In this capacity he is involved with the INTELSAT TDMA field trial and has become team leader of COMSAT's support for the revised INTELSAT TDMA/DSI specifications. Mr. Colby is currently completing a part time study with the British Open University for a Ph.D. in hybrid digital modulations.



Benjamin A. Pontano received a B.S.E.E. degree from Carnegie Institute of Technology in 1965 and the M.S.E.E. and Ph.D. degrees from Pennsylvania State University in 1967 and 1970. From 1969 to 1973 Dr. Pontano was Manager of the Laboratory Simulation Branch at COMSAT Laboratories. From 1973 to 1974, he was Director of Communications Engineering at Fairchild Space and Electronics Company. He joined INTELSAT in 1974, where he is presently Section Chief of Engineering.

Dr. Pontano is active in C.C.I.R. Study Group IV and the Aerospace and Electronics Systems Group of the IEEE. He is a member of Sigma Xi.



Henri G. Suyderhoud received the Ingenieur degree from Delft Technological University in the Netherlands in 1955, and an M.S. degree in applied mathematical statistics from Rutgers, New Brunswick, in 1966. He is currently Manager of the Signal Processing Department of the Communications Processing Laboratory where he is responsible for signal processing research and development using both digital and analog techniques as well as the development of subjective evaluation techniques to assess transmission quality. His experience includes

development of echo cancellers and speech processing and encoding techniques for achieving transmission economy. Prior to joining COMSAT, Mr. Suyderhoud worked for 11 years at Bell Telephone Laboratories in the fields of exchange area and toll transmission engineering, echo control, and picture phone. He is a senior member of IEEE and the American Statistical Association.

Michael Onufry received a B.S. degree from Pennsylvania State University in 1962 and performed graduate work at both Northeastern University and George Washington University. He is currently Assistant Manager of the Signal Processing Department in the Communications Processing Laboratory. His work includes computer simulation and the design and supervision of the implementation of various digital speech and signal processing devices including echo cancellers, echo suppressors, digital speech interpolation equipment, and ranging equipment. He has been active in planning and implementing international field trials in the INTELSAT network and is responsible for subjectively assessing various speech processing devices. Since 1977, Mr. Onufry has been the COMSAT Representative on C.C.I.T.T. Study Group XV. Mr. Onufry is a member of IEEE.



Index: time-division multiple-access burst acquisition, synchronization open-loop control, closed-loop control

Open-loop TDMA frame acquisition and synchronization

S. J. CAMPANELLA AND K. HODSON

(Manuscript received July 23, 1979)

Abstract

Control of TDMA burst position can be accomplished by either closed-loop or open-loop techniques. The closed-loop method used in most of the TDMA systems thus far is convenient only when a station can see its own traffic burst return from the satellite. Also, scanning at low power is required for acquisition. Open-loop control provides a means of controlling TDMA burst position without the need of a station seeing its own traffic burst return; it avoids scanning at low power, and can be used for acquisition only or for both acquisition and synchronization. This paper discusses methods for determining range to the satellite for open-loop control and presents the results of experiments performed during the recent INTELSAT TDMA Field Trial. Departures of satellite position from nominal were observed at Andover, Pleumeur Bodou and Lario and used to calculate burst position corrections for the earth station at Goonhilly.

Introduction

Concepts of open-loop frame acquisition and synchronization for a time-division multiple-access (TDMA) system which may be employed by INTELSAT during the INTELSAT V series of satellites are presented. As opposed to closed-loop control, which implies control of the traffic burst transmission epoch by observation of its position in the frame,

This paper is based upon work performed under the sponsorship of the International Telecommunications Satellite Organization (INTELSAT).

open-loop control in a TDMA system implies control of the traffic burst transmission epoch by calculation in terms of the distance assumed between the satellite and an earth station. Also described in this paper are experiments performed during the 1978 TDMA Field Trial [1] to investigate certain aspects of the open-loop technique, and to gain some operational experience which could be applied to a future TDMA system. Alternative methods of operating an open-loop system and their features in terms of burst position accuracy, simplicity of operation, degree of computational complexity, and network topology are presented. It should be noted that open-loop experiments have also been performed under the CENSAR Project System [2] and that a simple form of open-loop control is used in the MARISAT for ship-to-shore TDMA telegraphy [3].

TDMA frame acquisition and synchronization

General

In a TDMA system [4], [5], earth stations access a given satellite transponder sequentially in time so that each station, during the time dedicated to its own traffic, uses the entire power and bandwidth available. With this method of sharing a satellite among several stations, each station must transmit traffic in bursts so that no overlap of bursts occurs at the satellite. Acquisition refers to the process of initially positioning a traffic burst in a frame, and synchronization refers to maintaining the burst position within a specified level of precision.

In an open-loop system, acquisition is initiated by informing a station entering the network of the time shift which it must introduce between the TDMA frame arriving from the satellite and the frame established within its terminal equipment. In the acquisition phase, a station may transmit a short burst consisting of the preamble and unique word in the time slot assigned for its traffic burst or in a special time slot set aside in the frame for acquisition purposes. Access to this acquisition time slot may be on a time-shared basis. A network control monitor may observe the actual location of this short burst and if this location is correct inform the acquiring station that it is cleared to start transmitting traffic. The monitoring station may also send corrections to the entering stations to refine their burst positions. Alternatively, if there is sufficient confidence in predicting the TDMA frame occurrence and traffic burst location, a station may simply enter the frame with its full traffic burst. Synchronization, which consists of continued correc-

tion of the timing of the station's TDMA frame to compensate for satellite position drift, requires means for continuous, accurate tracking of satellite motion. Open-loop control can be used for both acquisition and synchronization, or for acquisition only, with synchronization accomplished by closed-loop control which may involve feedback from a monitoring station.

To avoid unnecessarily long gaps between the end of one burst and the beginning of the next, the data burst at the satellite must not vary in position by more than a specified amount. The space allowed for variation is called guard time. In the first INTELSAT TDMA system specification* the variation allowed is ± 3 symbols.† Such precision of burst positioning enhances the accuracy of the process by which receiving stations detect the unique word pattern contained within the burst, and hence enables all of the bits within the burst to be correctly interpreted. A receiving station can open a "window" in which it expects to receive the appropriate unique word. Gating of the unique word detector during this window greatly reduces the probability of a false unique word detection. Open-loop control systems may require an increase in the guard time due to uncertainty in determining satellite location.

Requirements for synchronization to a reference burst

In a TDMA system, either closed- or open-loop controlled, the task of a local station (*i.e.*, one that carries traffic and has no network control functions) is to synchronize its traffic burst to the appropriate position in the TDMA frame. The station observes the reference burst coming from the satellite and adjusts its own transmit frame periodicity and timing so that its traffic burst falls in the assigned time slot in the TDMA frame occurring in the satellite. To accomplish this, the start of the transmit side TDMA frame must be shifted in time relative to the reference burst by an amount determined by the distance to the satellite and the frame period. Only if the distance between the satellite and an earth station is a precise integer multiple of the TDMA frame period (which is highly unlikely) will the time shift be zero.

Calculation of the time shift needed to achieve the assigned position

*This specification is the one commonly referred to as BG-1-18 (Rev.2) and should not be confused with the new specification which is currently being prepared.

†A symbol period is about 33 ns in a 60-Mbit/s TDMA system and 17 ns in a 120-Mbit/s system with QPSK modulation.

in the satellite is illustrated in the time/space graph of Figure 1. The upper time line is at the satellite and shows the sequence of reference bursts, designated by *R*, and assigned occurrence indices *n*, *n* + 1, The time interval between the reference bursts, *T_F*, is the TDMA frame period. An earth station *N* is assigned a transmit burst epoch in the frame beginning at time τ_N after the initiation of the reference burst

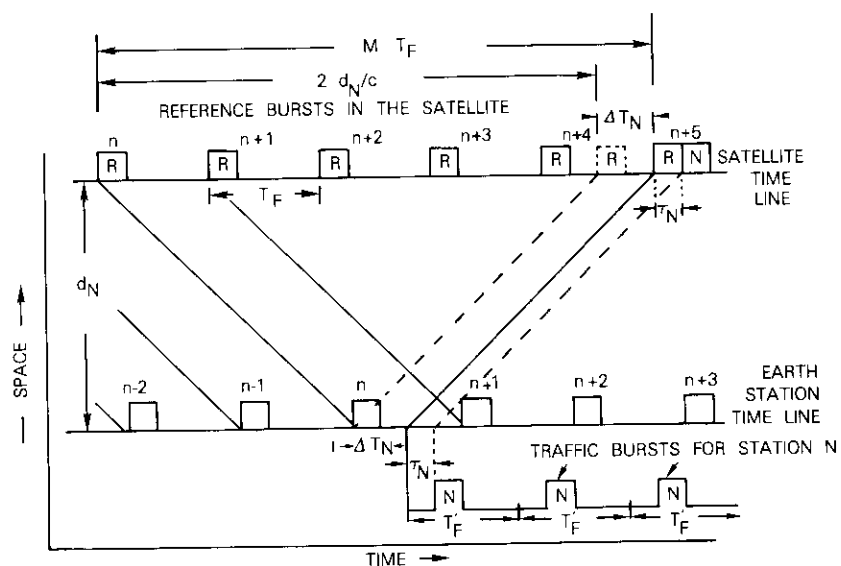


Figure 1. Time/Space Graph for TDMA Frame Synchronization

and lasting for some assigned period. Because the earth station is at a distance d_N from the satellite, there is a time shift between the TDMA frame established in the satellite by the reference burst and the frame returned to the satellite via the earth station transmission. This time shift must be zero; therefore, the TDMA frame at the earth station must be retarded by an amount ΔT_N , which is the time difference between the periodic reference burst function in the satellite and that returned via the earth station with no compensation. This is illustrated by the position of the dotted reference burst in Figure 1. As shown in Figure 1, ΔT_N is the minimum amount by which the propagation delay from the satellite to the earth station and back falls short of an integer multiple of TDMA frame periods, MT_F . Thus,

$$\Delta T_N = MT_F - 2 \frac{d_N}{c} \quad (1)$$

where *M* is an integer such that ΔT_N assumes the minimum positive value.* Equation (1) permits determination of ΔT_N in terms of d_N and is a key relation in achieving open-loop control of burst position. Conversely, it permits determination of changes in d_N from changes in ΔT_N . Finally, it may be used to observe changes in satellite position from closed-loop TDMA terminals to be used for implementing open-loop control at other terminals.

For transmission bursts generated at earth stations to properly coincide in the satellite, the earth local TDMA frame at the earth station must be retarded by ΔT_N relative to the received reference burst. The relationship between the retarded frame at the earth station and the frame at the satellite is illustrated in Figure 2, where the indices correspond to the occurrences of events relative to the reference burst at the satellite and are retarded at the earth station by ΔT_N .† In the example shown, the value of ΔT_N equals eight time index intervals and

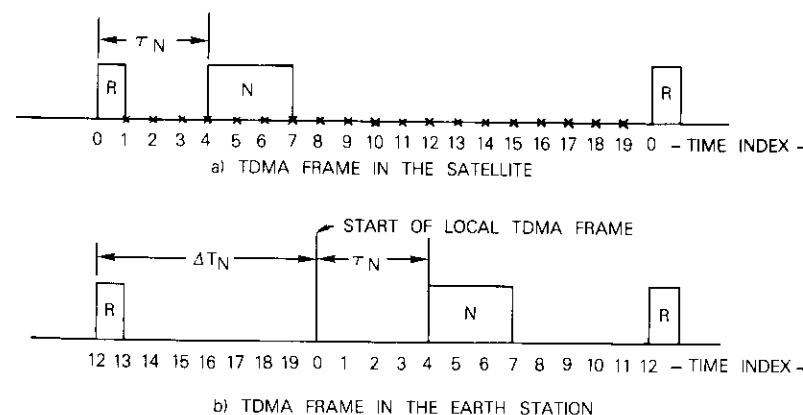


Figure 2. Relationship Between Earth Station and Satellite TDMA Frames

*A useful alternate form of this expression is $\Delta T_N = T_F - \text{MOD}(2d_N/c, T_F)$.

†The value used at an earth station may be increased by multiples of T_F without invalidating the proper time shift. This may be done to prevent passage of the time retardation value through zero and to avoid attendant implementation problems.

the start of the TDMA frame is correspondingly retarded at the earth station. All apertures for transmitted traffic bursts are assigned to appropriate indices in the shifted TDMA frame.

It should be recognized that actually a satellite in geostationary orbit is subject to small motions due to imperfections in the orbit. (An east/west drift of $\pm 0.1^\circ$, north/south drift of $\pm 0.1^\circ$, and eccentricity of 0.001 are expected for INTELSAT V.) Thus, distance d_N is not constant and typically can vary by as much as 166 km, which is equivalent to 550 μs . The round trip propagation time variation is twice this value. Therefore, if the TDMA frame period is long compared to this variation, no ambiguity problems should result.

The distance variation also introduces Doppler on the TDMA frame frequency; corrections to d_N must be made sufficiently often so that transmit burst position does not exceed a specified tolerance variation. The typical tolerance is ± 3 symbols, but it may be increased in systems designed for open-loop control. For a satellite with the parameters given above, the worst-case velocity is 20.5 km/hr, resulting in a worst-case time rate of change of 40 ns/s. Thus, maintaining a 60-Msymbol/s TDMA burst position with a precision of 1 symbol requires a minimum update rate of once every 416 ms for d_N . Typically in TDMA systems using closed-loop synchronization, corrections are made at a maximum rate corresponding to a single-hop propagation time (*i.e.*, once every 250 ms). Clearly, the above estimates would be reduced by invoking tighter tolerance on satellite position keeping. For example, if the north/south angle drift were reduced to $\pm 0.1^\circ$, the round trip propagation delay variation would be reduced to 0.6 ms.

Global beam TDMA

In a TDMA system configured to operate within a global or a regional beam which contains all corresponding stations, each station can receive the entire frame from the satellite and directly see its position as well as those of all other stations relative to the reference burst. This enables any station to observe deviations from its assigned position and to apply a correction to its transmit burst timing to achieve the correct position. Corrections are made by increasing or decreasing the time elapsed between reception of the reference burst and transmission of the traffic burst; thus, they permit ΔT_N to be adjusted to the value needed to achieve the proper position at the satellite. Corrections are usually made by shifting the transmit burst occurrence in steps of one symbol period. An alternate means of making the correction is by

varying the controlling clock rate. This method is generally referred to as closed-loop synchronization and is typical of current TDMA systems. Provided that the period between corrections is greater than the round trip propagation time between the earth station and the satellite, an accurate, simple, and stable method of position control is achieved.

Spot beam TDMA

TDMA will be extensively used with spot beam antennas [6] because the spot beams allow frequency reuse. Global beams will remain in use for services such as SPADE [7], SCPC, and TV and for applications in which large numbers of small stations will require diverse interconnection.

The major difference between TDMA operation through a spot beam [8] and a global beam is that in the former case a station can no longer receive its own data burst; therefore, it cannot directly derive an error signal for synchronization. The reference burst which defines the time base and enables remote stations to decode the received burst is also invisible to the transmitting stations for the spot beam synchronization method as currently conceived. Nevertheless, the traffic bursts must maintain a strict timing relationship with the reference burst during normal operation and must be able to enter an established TDMA frame without introducing interference during acquisition.

Most solutions proposed for spot beam TDMA burst position control depend on a remote station which observes timing error relative to the reference frame burst and signals back corrections to the transmitting station. The acquiring station transmits specially coded and identifiable low-level signals. These signals permit a remote station to provide coarse timing information that enables the acquiring station to position its burst in the assigned epoch without interfering with other traffic bursts during acquisition. Once the assigned position is achieved, the acquiring station brings its level to full power. The remote station must continue to monitor the burst throughout transmission to provide the error control signal which keeps the burst in its assigned position despite the satellite motion. Figure 3 shows the time/space graph for closed-loop spot beam system operation. Note that the synchronization burst from west beam to east beam, designated as R , is the time reference for bursts from west to east.

The reference station in the west beam sends synchronization reference bursts, R , to the satellite to establish the TDMA frame. Station

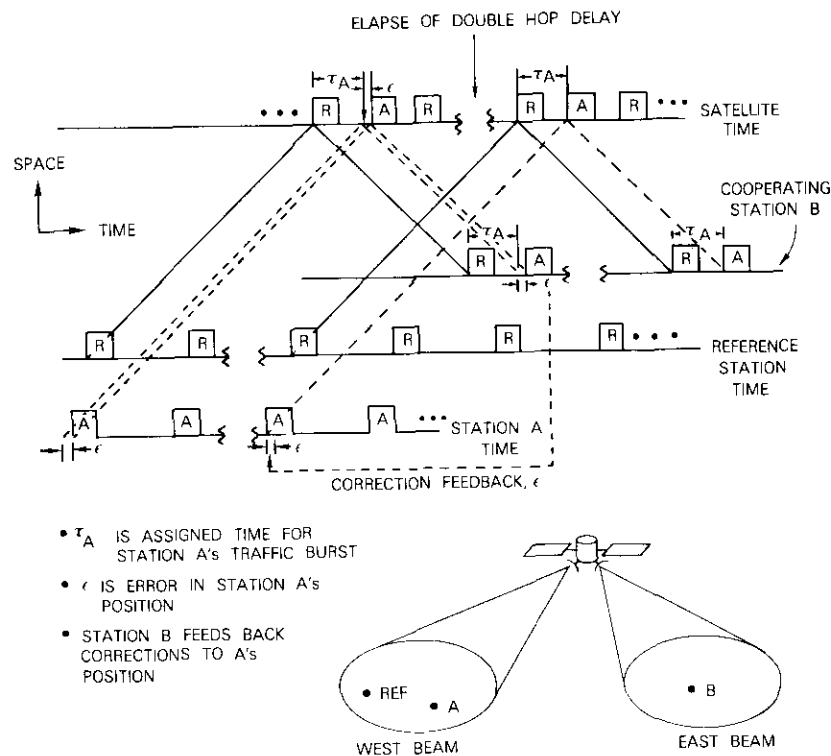


Figure 3. Time/Space Graph for Spot Beam Closed-Loop Synchronization

A in the west beam also sends its traffic burst A into the same satellite transponder. A cooperating station B in the east beam observes the time difference, ϵ , between station A's actual burst position and the assigned target position, which is assumed to be at time τ_A after the initiation of the reference burst. It sends the observed difference, ϵ , back to station A in its own traffic burst. A double-hop time lapse occurs between a correction at A and the return of the result via B's observation to A. Figure 3 shows the position of station A's traffic burst before and after a correction. Similarly, a synchronization reference burst for east/west communications would be transmitted from the east to west beam and a cooperating station in the west beam would be used to control stations in the east to west direction.

Closed-loop spot beam synchronization is not without drawbacks. Each non-reference station needs a monitoring station in the remote beam; for redundancy, two or three such stations would be preferable. It would be difficult for a monitoring station to serve more than one acquiring station at a time without confusion since such bursts would probably overlap in time. The network would be complex to administer since it would require stations to acquire in a prescribed order and it would be cumbersome from an operational viewpoint.

Open-loop acquisition and synchronization

General

With open-loop control, burst position is maintained, not by observation of timing error as with closed-loop control, but by knowledge of the satellite and earth station positions. This information enables a traffic burst position to be controlled on the basis of calculations of ΔT_N as given in equation (1) from the knowledge of the range, d_N , between the satellite and the earth station. Open-loop control may be applied only to the acquisition phase of TDMA operation or to both acquisition and synchronization. If used for acquisition only, open-loop control need only be sufficiently accurate to place a short acquisition burst near the center of an assigned epoch of the TDMA frame. In this case, the required accuracy is considerably less than that normally required for synchronization. Higher accuracy for synchronization would then be accomplished by using the conventional closed-loop synchronization method. This combination of open- and closed-loop control reduces the complexity of initial acquisition but retains the high synchronization accuracy of the closed-loop method.

Use of open-loop control for both acquisition and synchronization requires sufficient accuracy to provide the needed burst position precision for synchronization. The inherent accuracy may have to be high (e.g., ± 3 symbols of the digital transmission signal) in short frame TDMA symbols with a high number of traffic bursts, or it can be quite low ($\pm 10 \mu\text{s}$ or more) in long or very long frame TDMA systems. If high accuracy is required, then the accuracy of d_N must also be high. For example, for 30-Msymbol/s TDMA the distance accuracy must be ± 15 m to achieve the desired burst positioning within ± 3 symbols, which is equivalent to ± 100 ns; for 50 users in a 750- μs frame, this would provide an average TDMA frame burst efficiency of 98 percent. On the other hand, for a system with a 25-ms frame period servicing

50 users, a burst positioning accuracy of $\pm 10 \mu\text{s}$ with a corresponding distance accuracy of $\pm 1,500 \text{ m}$ would provide an average TDMA frame burst efficiency of 96 percent. Because of this reduced burst position accuracy, open-loop control methods become more attractive as the TDMA frame period is increased. In addition, simpler ranging methods can be used for such long frame systems.

Open-loop acquisition and synchronization control also appears attractive for spot beam operation. As explained previously, closed-loop acquisition and synchronization of TDMA terminals with spot beams is complicated because earth stations cannot see their own down-link signals. Open-loop control eliminates the need for a terminal to see its own signal and is therefore inherently attractive for spot beam use. However, the satellite position must be determined with accuracy sufficient to achieve the burst position control needed for acquisition and synchronization.

Figure 4a shows how an open-loop system would operate within a spot beam environment. It is assumed that station A is located in the west beam and station B in the east beam; the traffic burst from west to east (*i.e.*, from station A to station B) is referenced to the reference burst from east to west, *i.e.*, in an opposite manner to the closed-loop case. Open-loop corrections of ΔT_A and ΔT_B derived from satellite to earth station distances d_A and d_B are required. Because each station uses the reference burst of the opposite beam to decode the TDMA frame, the reference bursts in both directions must be coincident or separated by a known time at the satellite. This is best achieved by ensuring that one of the reference stations uses the open-loop technique to align its reference burst with the reference burst coming from the opposite beam, as shown in Figure 4b. Using the reference burst emitted by the west beam reference station, open-loop correction ΔT_R , derived from the distance between the satellite and the east beam reference station, must be applied to the reference burst emitted from the east beam reference station. Consequently, any errors introduced by the open-loop technique can disturb both the reference burst and the traffic bursts.

Determination of satellite position

From the foregoing discussion it is apparent that open-loop control requires frequent and accurate information on the distance between the satellite and each earth station. This can be obtained from knowledge of the satellite position and the geographic coordinates of

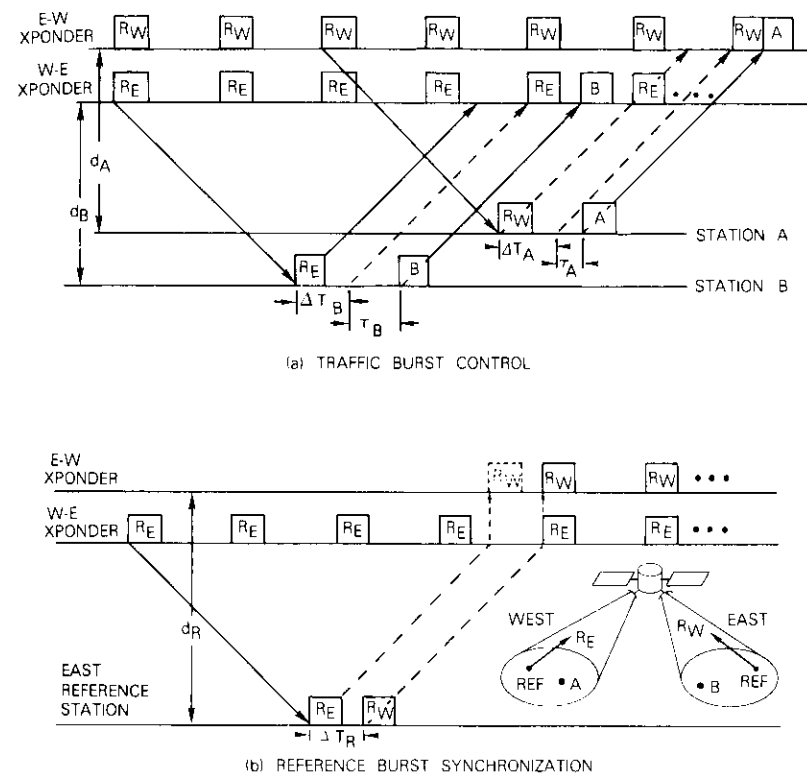


Figure 4. Open-Loop Burst Position Control in a Spot Beam System

the earth stations. Two methods for obtaining satellite position are predicted from telemetry, tracking, and command (TT&C) data and real-time satellite ranging using wideband digital open-loop synchronization (DIOS) [9] or narrowband analog global beam open-loop synchronization (AGOS) [10]. Prediction from TT&C data or AGOS ranging can be used for both global/regional beam and spot beam systems, whereas DIOS ranging can be used only in a global beam system. Prediction using TT&C data may not provide sufficient satellite position accuracy during satellite maneuvers, whereas real-time ranging using DIOS or AGOS can maintain synchronization throughout maneuvers. The range data needed for a triangulation satellite position tracking network may also be obtained by using only one ranging

station combined with observation of departures of the traffic bursts of three open-loop controlled stations from assigned frame positions. These methods are described in the following subsections.

PREDICTION USING TT&C DATA

The satellite position can be determined from the predicted ephemeris data available from the INTELSAT TT&C network. The accuracy of these data is sufficient to permit the distance between the satellite and the earth station to be determined to within ± 10 m. This is sufficient to maintain TDMA traffic burst position to a tolerance of ± 66 ns or ± 4 symbols for 60-Msymbol/s modulation, and is obviously more than sufficient in long frame systems requiring less precision. However, the TT&C network is presently configured for predicting the satellite's position to provide earth stations with an alternative source of antenna pointing data which are not needed on a real-time basis. Accordingly, several days of data smoothing are used to refine the ephemeris parameters from range and azimuth and elevation angle observations after a maneuver. During this time satellite position accuracy may not be sufficient to support open-loop control.

Satellite maneuvers occur regularly, typically every six weeks for a north-south stationkeeping maneuver and every four weeks for an east-west maneuver. Consequently, there are regular periods during which observations of the satellite's actual motion are needed.

These considerations make the presently configured TT&C network unsuitable for determining the satellite's position for open-loop acquisition and synchronization. The network could be reconfigured so that a satellite is monitored continuously by three stations with a sampling rate sufficient to provide real-time position data.

REAL-TIME RANGE MEASUREMENT

Real-time range measurements are the preferred method of determining the satellite position for an open-loop system because they are continuously available. Three geographically diverse stations can measure satellite range by either the DIOS or AGOS techniques described below. All range data must be collected at a central location and processed in real time to enable the satellite's position to be determined for all orbit conditions including maneuvers. If the central location also knows the geographic coordinates of all the earth stations, it can calculate the time corrections, ΔT_N , and disseminate them over a satellite link, which may be a sub-burst in the reference burst.

DIOS Ranging. DIOS, or digital in-band open-loop synchronization,

is a technique which uses a TDMA terminal to measure satellite range. To use DIOS, a station must be able to receive its own burst relayed via the satellite. A simple code can be inserted into the burst preamble to represent a signal with a period greater than the round trip propagation delay (240 to 280 ms). The satellite's range is obtained directly by measuring the time difference between the transmitted signal and the same received signal. DIOS is simple and accurate because, effectively, the full power and bandwidth of the satellite transponder are used for the measurement.

DIOS operation and functional implementation are shown in Figure 5. Part *a* of this figure shows the sampling of a coded clock at the instant of TDMA burst transmission. This code must have 24-bit precision to provide the 1-symbol position accuracy which is possible with 60-Msymbol/s TDMA burst transmission and a round trip propagation time of 280 ms to the satellite. The coded send times, t_s^i , are transmitted as part of the data in the station's traffic burst. When the same burst returns, its time of reception, t_r^i , is sampled and the difference, Δt_i , determined. This computation gives the round trip propagation delay in terms of the number of symbol periods; half of this number gives the distance to the satellite in terms of symbol periods. When this information is combined with similar measurements from two other geographically dispersed stations, satellite position can be determined, and, provided that the precise geographic coordinates of the earth station are known, the range to any of the stations can be calculated.

Actually, it will be shown later that a simple zero-order approximation method can be used to determine satellite departure from an established initial position in terms of a weighted sum of the departures from the three observation stations. This approximate solution can be easily implemented using a simple microprocessor.

AGOS Ranging. AGOS refers to analog global beam open-loop synchronization. Its name is derived from a ranging method intended principally for establishing open-loop synchronization of a TDMA terminal by means of a sinusoidal signal which is transmitted to and from the satellite on an FM carrier using the power and bandwidth of an INTELSAT SCPC channel. Making the sinusoid period equal to the TDMA frame period allows its use as a reference for an entire TDMA network. Changes in the range to the satellite can be accurately measured by comparing the phase of the transmitted and received signals.

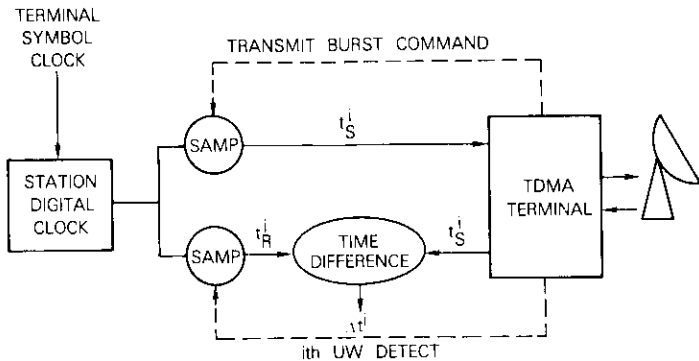
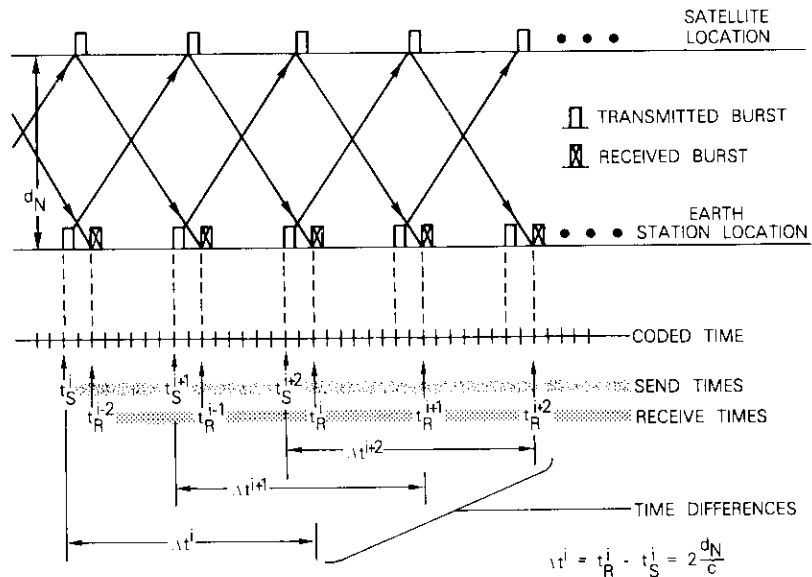


Figure 5. Digital Open-Loop Synchronization, DIOS Ranging Method

The AGOS method is illustrated in Figure 6. The sinusoidal signal is generated by a digital sine function generator driven by the TDMA terminal symbol clock. If the TDMA symbol period is 750 μs, the sinusoidal signal frequency is 1333 Hz. This signal frequency modulates

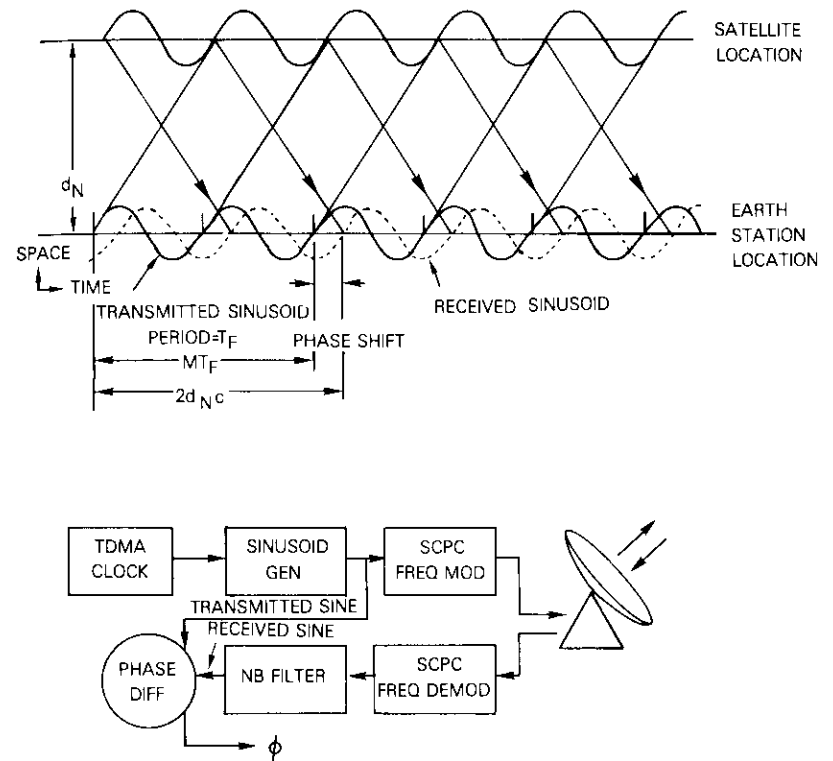


Figure 6. Analog Open-Loop Synchronization, AGOS Ranging Method

a carrier which is transmitted to the satellite transponder. The received signal, after demodulation, is passed through a very narrowband filter to increase the signal-to-noise ratio to a value high enough to allow phase measurement to the precision of a TDMA symbol period. A signal-to-noise ratio of 80 dB is needed to achieve a phase accuracy of 33 ns, which is the symbol period for 60-Mbit/s TDMA with 90-percent confidence. If it is assumed that the SCPC channel bandwidth is 38 kHz and its carrier-to-noise density ratio, C/N_0 , is 59 dB·Hz, then a 1-Hz bandwidth post-demodulation filter will yield the required 80-dB signal-to-noise ratio. The 1-second response time of this filter is sufficiently fast to accommodate the maximum rate of change of the round trip delay.

Satellite position tracking

THREE-STATION RANGING

This discussion pertains to a satellite position tracking system that uses techniques such as DIOS or AGOS to observe the range from three designated stations in real time. The geometry of the configuration is shown in Figure 7. Distances to the satellite from the ranging earth stations are designated as A , B , and C , respectively, for earth stations at locations a , b , and c . The distance from the satellite to the controlled station at location q is designated as Q . Calculation of Q from the geometry shown in Figure 7 permits determination of the appropriate time for traffic burst transmission.*

To simplify the satellite tracking process, a linear approximation method developed in Appendix A is used. This approximation is useful in analyzing the process and also in simplifying its implementation. The satellite is assumed to have a nominal location for which the nominal values of A_0 , B_0 , C_0 , and Q_0 apply. The analysis in Appendix A shows that the following zero-order approximation exists between the change from nominal for Q and the changes from nominal for A , B and C :

$$Q - Q_0 = K_{QA}(A - A_0) + K_{QB}(B - B_0) + K_{QC}(C - C_0) \quad (2)$$

This approximation will be sufficiently accurate provided that the differences between the actual and nominal positions are very small compared to the range to the satellite. In the cases of interest here, this is most certainly true.

Alternate expressions K_{QA} , K_{QB} and K_{QC} as given in general matrix form in Appendix A will now be derived. Since K_{QA} , K_{QB} and K_{QC} are the partial derivatives of Q with respect to A , B and C , respectively, the geometry related to any one of the coefficients is simplified by holding the distances from the satellite to any pair of the ranging stations constant while the distances to the third ranging station and to the controlled station are permitted to vary. The variation in the

*The solution presented here is for the propagation times and hence distances between the ranging earth stations and the satellite, and is based on the intersection of three spheres. Direct observation of these distances may not be possible in a spot-beam system. An alternate solution involving the round trip propagation times between stations in different beams based on the intersection of ellipsoids can be used instead.

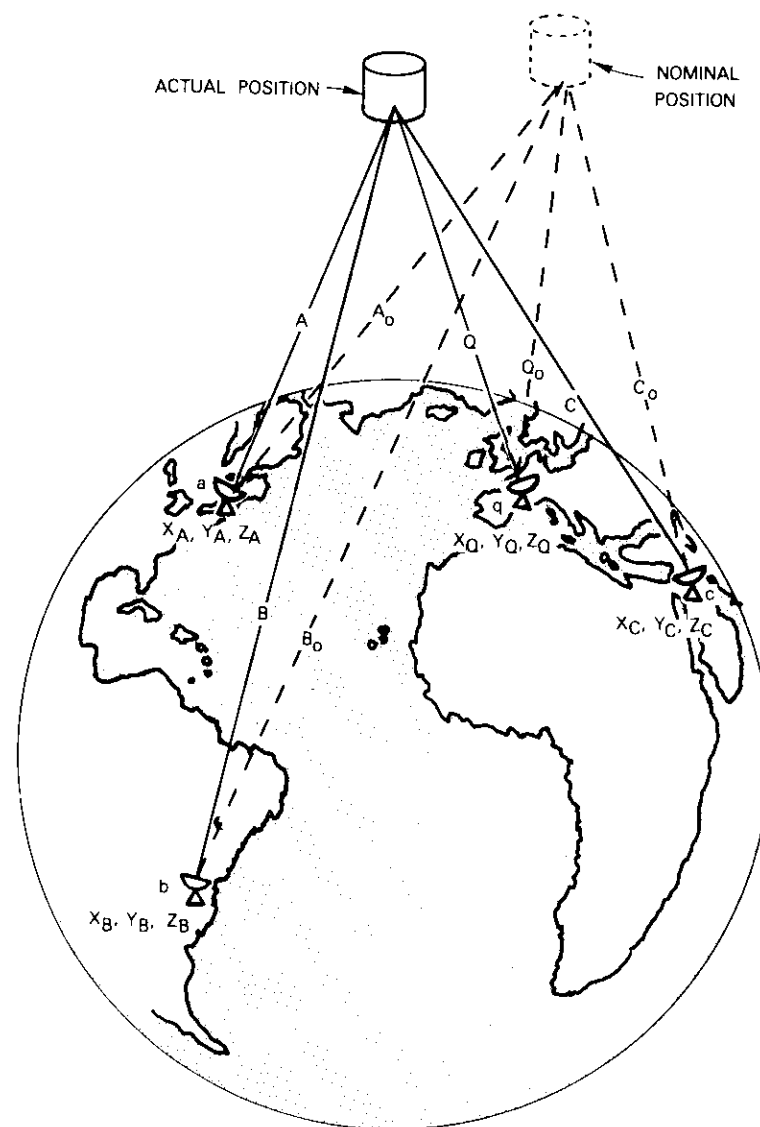


Figure 7. Geometry of Satellite and Earth Stations

distance to the controlled station is then determined for the variation in the distance to the third ranging station. This model is further

simplified without serious loss of generality by assuming that all stations lie in the same plane, as in Appendix B, where distances A and B between the satellite and ranging stations at a and b are held constant while C is permitted to vary. This analysis yields the coefficient K_{QC} , which gives the ratio of variation induced in the distance Q due to variation in the distance C :

$$K_{QC} = \frac{\delta Q}{\delta C} = \frac{C d_{oa}^c \cos \alpha_q^c}{Q d_{oc} \cos \alpha_c} \quad (3)$$

For the small departures from the nominal position expected in actual system operation the above approximation is sufficient for burst position control. This was demonstrated by experiments performed during the INTELSAT TDMA Field Trial and reported later in this paper. Definitions of the angles and distances involved are given in Figure 8. The origin is the point of intersection of the line ab joining stations at a and b , and a perpendicular to the line ab intercepting the satellite position S . Distance d_{oc} and angle α_c , measured from a normal to line ab , locate the station at c ; similarly, d_{oa}^c and α_q^c locate the controlled station at q . The superscript notation designates that the variation is due to C . Note that for stationary orbit satellites the ratio C/Q is very nearly unity and for any given station it is essentially a constant.

Coefficient K_{QC} , which expresses the amount of change imparted to the distance to Q due to change in distance C , also expresses the sensitivity of the range Q to error in observing C . For values of K_{QC} in the vicinity of unity, errors in measuring C will not have a serious impact, but for large values of K_{QC} (such as 4), the impact of error would be excessive.

Valuable insight into the magnitude of K_{QC} can be obtained by examining equation (3). First consider the ratio of d_{oa}^c/d_{oc} . If the distances from the origin to the controlled station at q and to the ranging station of c are equal, the value of K_{QC} is near unity and the error induced in Q due to error in C is about the same. However, if the distance to the controlled station is much less than that to the ranging station, K_{QC} is less than unity and the impact of observation error is considerably diminished. If the reverse is true, K_{QC} is greater than unity and the impact of observation error is magnified.

Secondly, consider the influence of α_c , the angle to the observation station. As α_c approaches values near $\pm\pi/2$, the distance term $d_{oc} \cos \alpha_c$ in the denominator of equation (2) approaches zero and the

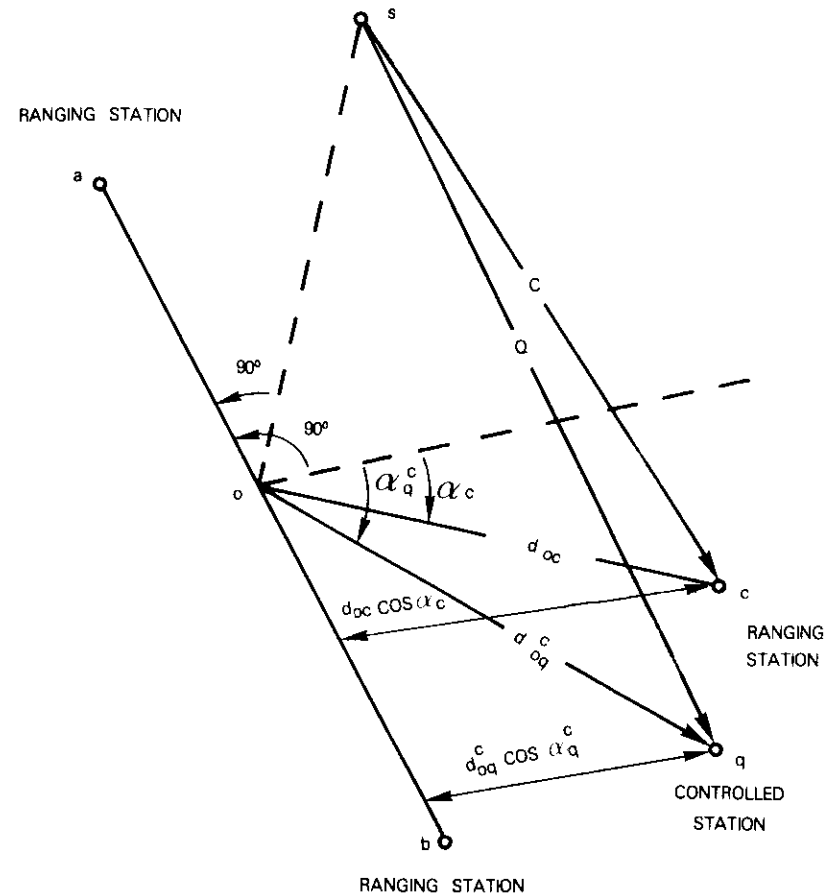


Figure 8. Geometry for Coefficient K_{QC}

value of K_{QC} becomes extremely large. This represents the condition in which all three ranging stations fall on or near the same line so that the error in the triangulation solution becomes very large. This is a condition that is to be avoided.

Thirdly, consider the influence of α_q^c , the angle to the controlled station. Its impact is represented by $\cos \alpha_q^c$, which can never be greater than unity. If α_q^c assumes the values $\pm\pi/2$, which would place the controlled station on a line connecting any pair of ranging stations, the impact of errors introduced by the ranging station reduces to zero.

This discussion pertains not only to K_{qc} but also to coefficients K_{qa} and K_{qb} . Figure 9 illustrates the geometries involved for the angles and distances in the expressions for all three coefficients, K_{qa} , K_{qb} and K_{qc} . Note that for these configurations the angles α_a , α_b , and α_c are zero and cannot be seen in the geometry.

The configuration shown in Figure 9 is for the special case of stations lying on a circle whose center is the subsatellite point, and is optimum in terms of locating ranging stations to minimize the combined influence of coefficients K_{qa} , K_{qb} , and K_{qc} on the total error induced in the calculated range to the controlled station. In general the stations should be geographically dispersed as widely as possible. Ideally the projections of the station locations on a plane normal to a line connecting to the satellite should lie on a circle whose center is at the intersection of the line and the plane. This situation can be approximated in the Atlantic, Indian, and Pacific Ocean regions by proper selection of ranging stations; a specific example for the Atlantic Ocean Region is given subsequently.

The combined behavior of K_{qa} , K_{qb} , and K_{qc} for a given geometry must be analyzed to determine the total impact of error from all three range observations. If the error from each range source is designated as σ_A , σ_B , and σ_C , respectively, and is assumed to be random, then the total squared error in the estimated range to the controlled station is

$$\sigma_q^2 = (\sigma_A K_{qa})^2 + (\sigma_B K_{qb})^2 + (\sigma_C K_{qc})^2 \quad (4)$$

From this expression, using the previously defined values for the coefficients and assigning proper error magnitudes, it is possible to calculate the resulting ranging error to all controlled stations. It will of course be necessary to correct for the spherical geometry of the earth's surface when stations become widely separated, but this will not greatly modify the results obtained from the planar geometry.

To provide insight into the behavior of the total error for 3-station ranging, a closed solution has been developed for the case shown in Figure 10, where all three ranging stations are equally spaced (120° apart) on the circumference of a circle of radius R . The satellite is located on the perpendicular to the plane of the circle, intersecting it at its center, and the controlled station and ranging stations are in the same plane with the controlled station at distance R_q and angle θ from the center. Angle θ is measured relative to a line to station C. For this special geometry, it is shown in Appendix C that the expressions for the three coefficients become

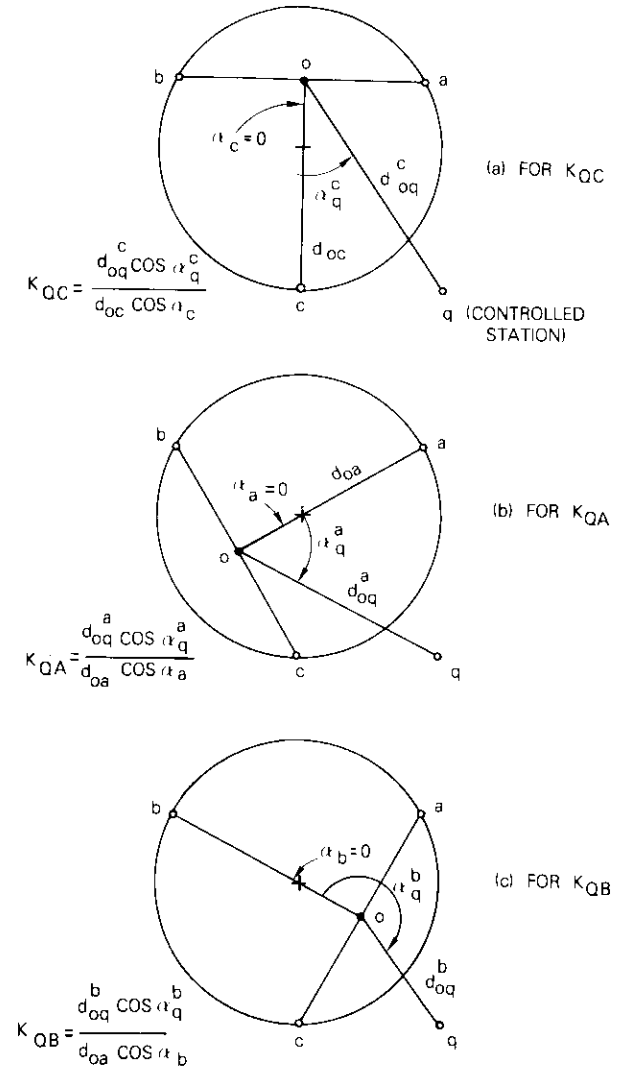


Figure 9. Geometries for the Three Linear Approximation Coefficients

$$K_{QA} = \frac{2R_q \cos(\theta - 120^\circ) + R}{3R} \quad (5a)$$

$$K_{QB} = \frac{2R_q \cos(\theta + 120^\circ) + R}{3R} \quad (5b)$$

$$K_{QC} = \frac{2R_q \cos(\theta) + R}{3R} \quad (5c)$$

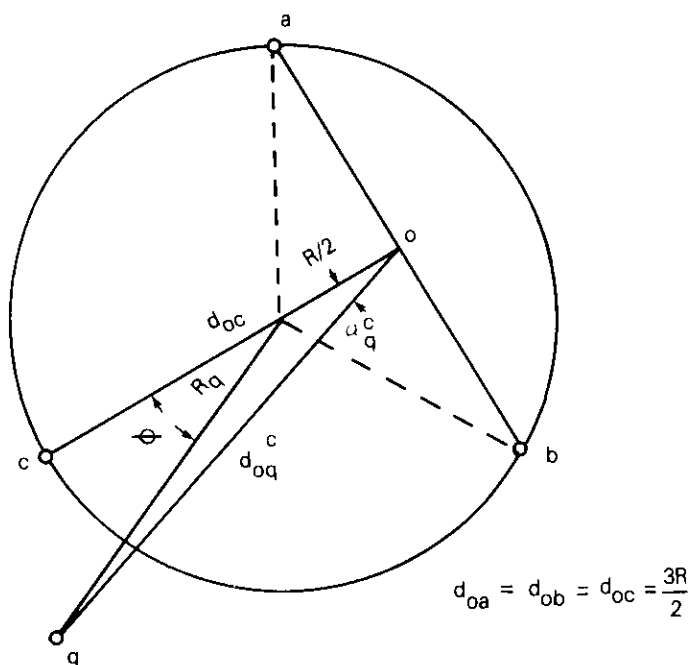


Figure 10. Equally Spaced Ranging Station Geometry

Figures 11 and 12 are graphs of the behavior of the above coefficients for $R_q = R/2$ and $R_q = R$, respectively. In both cases the values of K_{QA} , K_{QB} , and K_{QC} are given by sinusoidal functions of equal amplitudes and phases shifted by 120° . The sums of their squared values are constant, as will be further discussed below. For the condition $R_q \leq R/2$ the coefficients are always positive. For values of $R_q > R/2$, the coefficients become negative for certain angle intervals, as shown in Figure 12 for $R_q = R$. Note that the coefficient for a given ranging

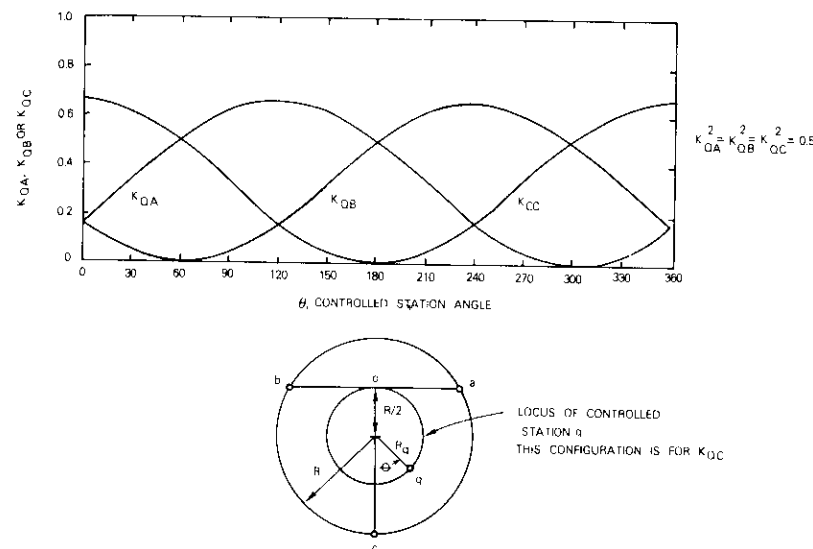


Figure 11. Coefficients K_{QA} , K_{QB} , and K_{QC} for $R_q = R/2$

station is zero when the controlled station lies on a line drawn through the two other ranging stations.

If it is assumed that all three error magnitudes have the same value σ (i.e., $\sigma = \sigma_A = \sigma_B = \sigma_C$), the total error becomes

$$\sigma_q^2 = \frac{\sigma^2}{3} \left[1 + 2 \left(\frac{R_q}{R} \right)^2 \right] \quad (6)$$

This function, plotted in Figure 13, shows that for the ranging station arrangement under consideration, the total error varies as a hyperbolic function of the ratio R_q/R with a minimum of $\sigma/\sqrt{3}$ for $R_q = 0$. As should be expected, the resulting error increases with increasing departure of the controlled station from the center of the circle, becoming σ for $R_q = R$ and doubling again to 2σ for $R_q = 2.35R$.

An arrangement approximating that described above could be achieved in the INTELSAT system by proper selection of ranging earth stations. For example, earth stations at Andover, Maine, U.S.A.; Balcarce, Argentina; and Taif, Saudi Arabia would provide control accuracy for the Atlantic Ocean Region approximating that determined in the example described above. It could be expected that most Atlantic Ocean Region stations will be contained within a circle connecting

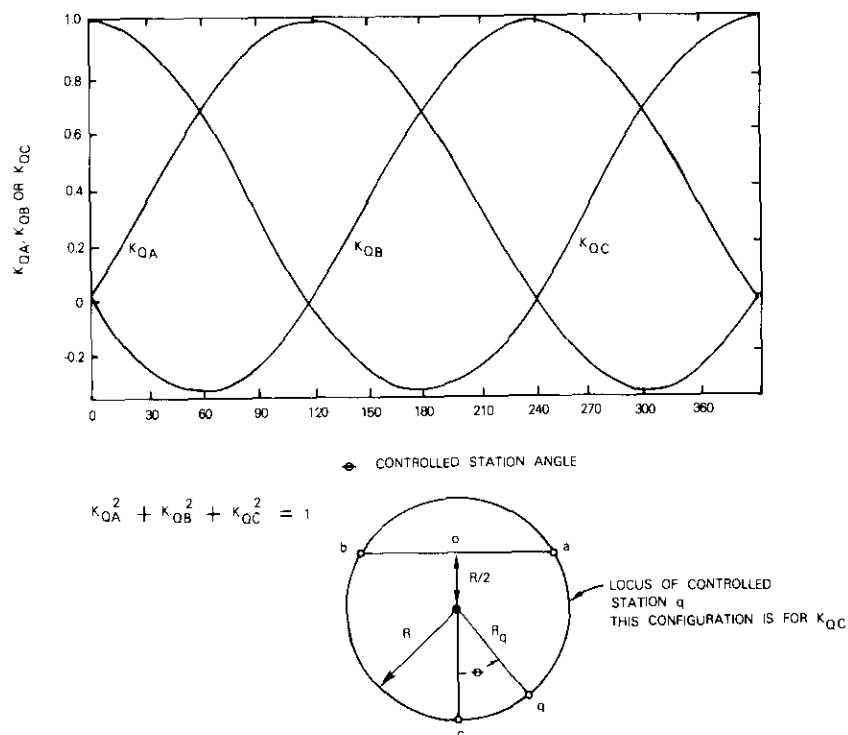


Figure 12. Coefficients K_{QA} , K_{QB} , and K_{QC} for $R_q = R$

these three stations and will experience an error magnification no greater than unity. Uncertainties contributing to the value of σ include principally TDMA timing granularity and variations in propagation delay due to atmospheric and earth station anomalies. It should be possible to achieve values of σ between one and two TDMA symbol periods. Errors in locating earth stations can be eliminated by calibration. Departure from the ideal equally spaced ranging station arrangement described above will result in increased error magnification. Values of magnification of as much as three may have to be tolerated for the worst cases.

TRAFFIC BURST DISPLACEMENT METHOD

The variation in the range between the satellite and any open-loop controlled station can also be observed by noting the displacement of

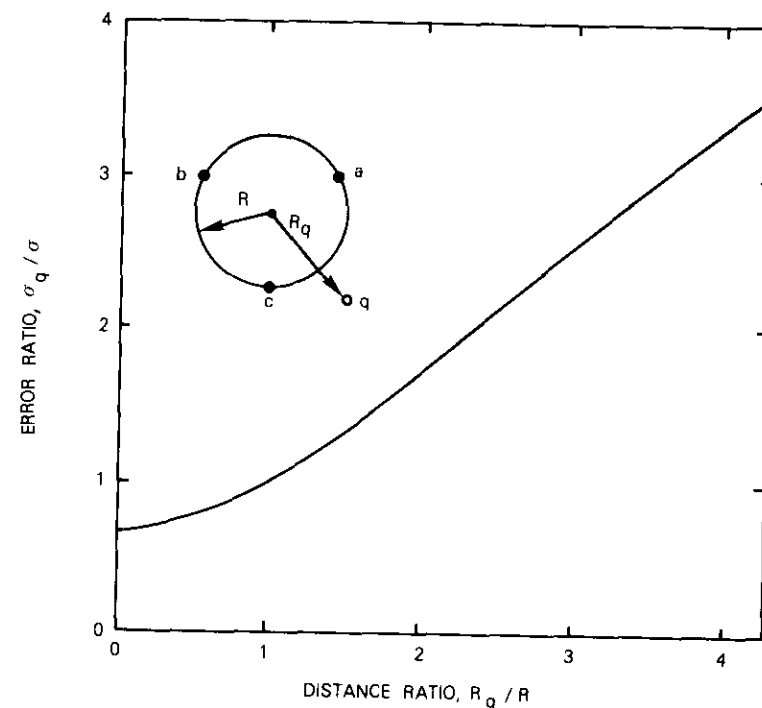


Figure 13. Total Error as a Function of the Distance Ratio R_q/R for Equally Spaced Ranging Stations

the station's traffic burst position from a target position assigned by a network controller. The mechanism of the measurement is illustrated in the time/space graph of Figure 14. Part a of this graph illustrates that due to range differences the position of a traffic burst deviates from an assigned target position by an amount $\Delta\tau_A$, which is determined by

$$\Delta\tau_A = \frac{2\Delta A}{c} \tag{7}$$

where ΔA is the difference between an assumed range to the satellite and the actual range. Equation (7) illustrates that a time displacement of a traffic burst is a direct measure of a distance displacement of the open-loop controlled station. Part b of Figure 14 illustrates how

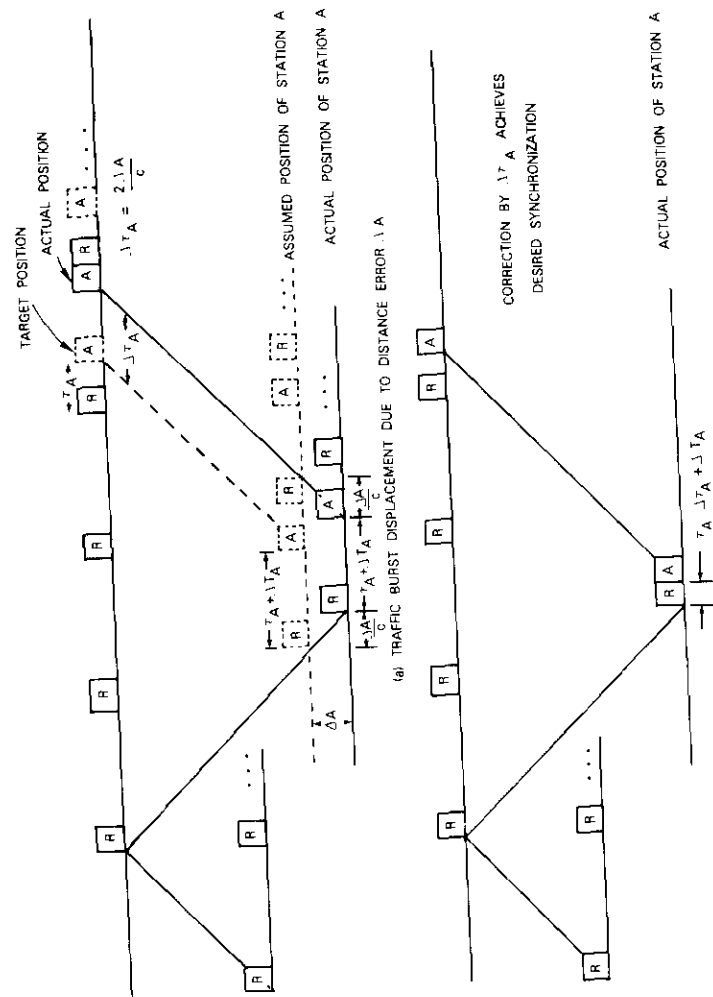


Figure 14. Relationship Between Distance Error and Traffic Burst Displacement

application of correction $\Delta \tau_A$ to the controlled station's burst position places the station's traffic burst directly on the target position.

This observation can be used to accomplish two essential operations for open-loop traffic burst control. First, it can be used to refine the accuracy of an approximate range value between the satellite and a controlled earth station. For example, if an approximate range is known with an accuracy sufficient to eliminate the TDMA frame period ambiguity (*i.e.*, one quarter of a TDMA frame period), it can be used to initially position the traffic burst preamble of an open-loop controlled station; the deviation observed from the assigned target position can be used to calculate the error and refine the range estimate to bring the traffic burst preamble onto the target.

Second, once the traffic burst preamble of the controlled station undergoes the above initial acquisition correction, any further deviations can be interpreted as measures of incremental satellite departures from the nominal position and used to generate one or more of the $A - A_0$, $B - B_0$ and $C - C_0$ corrections needed to update the positions of all other stations in the open-loop controlled network.

Satellite position measurements of sufficient accuracy to provide initial acquisition by the open-loop method could be obtained from TT&C ephemeris data or from the range and azimuth and elevation angles observed from a single earth station. The estimated accuracy of the latter method is discussed in the following. An estimate of the upper bound of the range error needed to eliminate TDMA frame period ambiguity and thus to start the initial acquisition process is obtained by substituting $\Delta \tau_A = T_f/4$ into equation (7) to give

$$\text{initial range error} \leq c T_f / 8 \quad (8)$$

Note that, as the TDMA frame period increases, the allowable initial range error needed to start the initial acquisition process also increases. This estimate applies to any method involving open-loop initial acquisition. For a TDMA frame period of $750 \mu s$, the allowable distance error is 28 km, corresponding to a one-way propagation time uncertainty of $94 \mu s$.

SINGLE STATION RANGING

Satellite position tracking can also be accomplished by measuring satellite range and elevation and azimuth angles. The geometry of Figure 15 is used to analyze the impact of angle observation accuracy on the accuracy with which a TDMA traffic burst can be positioned.

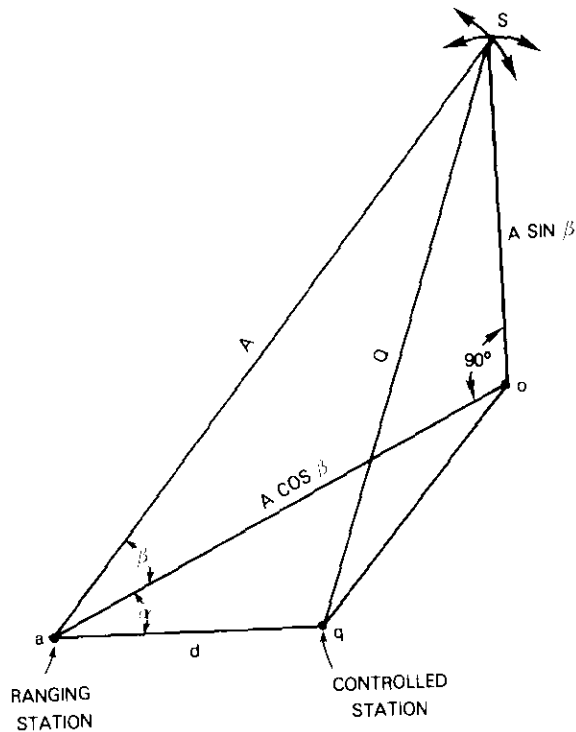


Figure 15. Single Ranging Station Geometry

It is assumed that the elevation and azimuth angles, α and β , respectively, have errors $\Delta\alpha$ and $\Delta\beta$. The controlled station is at a distance d from the ranging station and the azimuth angle is measured relative to the line through these two stations. The satellite is assumed to be at an accurately known range, R . It can be easily shown that the distance from the satellite to the controlled station is given by

$$Q^2 = A^2 + d^2 - 2Ad \cos \alpha \cos \beta \quad (9)$$

and the partial derivatives relative to angles α and β , for $A \cong Q$, are

$$\frac{\delta Q_a}{\delta \alpha} = d \cos \beta \sin \alpha \quad (10a)$$

$$\frac{\delta Q_a}{\delta \beta} = d \cos \alpha \sin \beta \quad (10b)$$

If it is assumed that random angle errors of equal variance, σ^2 , the total error is

$$\text{total range error} = d\sigma(\cos^2 \alpha \sin^2 \beta + \cos^2 \beta \sin^2 \alpha)^{1/2} \quad (11)$$

which has a maximum value $d\sigma$ or a maximum time uncertainty of $2d\sigma/c$.

This result demonstrates that, with angle measurement accuracies of $\pm 0.01^\circ$, which are considered feasible with properly equipped antennas, stations up to 100 km from the ranging station can be positioned with an accuracy of ± 116 ns, which is just sufficient for burst synchronization. For stations at greater distances from the ranging station (such as 5,000 km), the variation in burst position becomes $\pm 5.8 \mu\text{s}$. Such accuracy is sufficient to allow initial acquisition in an assigned TDMA time slot but is insufficient for burst synchronization. The accuracy needed for synchronization is currently specified as ± 3 symbol periods, which for 60-Mbit/s INTELSAT TDMA would correspond to ± 100 ns.

Experiments

General

Two experiments to demonstrate the open-loop acquisition and synchronization technique were performed in conjunction with the INTELSAT TDMA Field Trials in 1978. The participating stations were Pleumeur Bodou, France; Lario, Italy; Goonhilly, UK; and Andover, U.S.A. One was a relative range experiment and the other an open-loop acquisition and synchronization experiment for which a combination of the AGOS and DIOS techniques was used.

Range relative to Pleumeur Bodou

A TDMA terminal under open-loop control might correct its satellite propagation delay at relatively long intervals. The object of this experiment was to compare burst position determined by extrapolation of previous calculations with observed burst position and to assess the resultant difference as a function of order of extrapolation and length of extrapolation interval. Expressions for the difference terms are developed in Appendix D.

Data were obtained for extrapolation intervals of 1, 2, and 3 minutes for zero-, first- and second-order predictors. The coefficients used to refine the satellite range predictions during the extrapolation intervals were obtained by end-point analysis. Appendix D includes histograms of burst position error for the cases considered. These histograms show the percentage of time that the data burst from Pleumeur Bodou spent at each position; ϕ in each histogram corresponds to the zero error position of the Pleumeur Bodou burst.

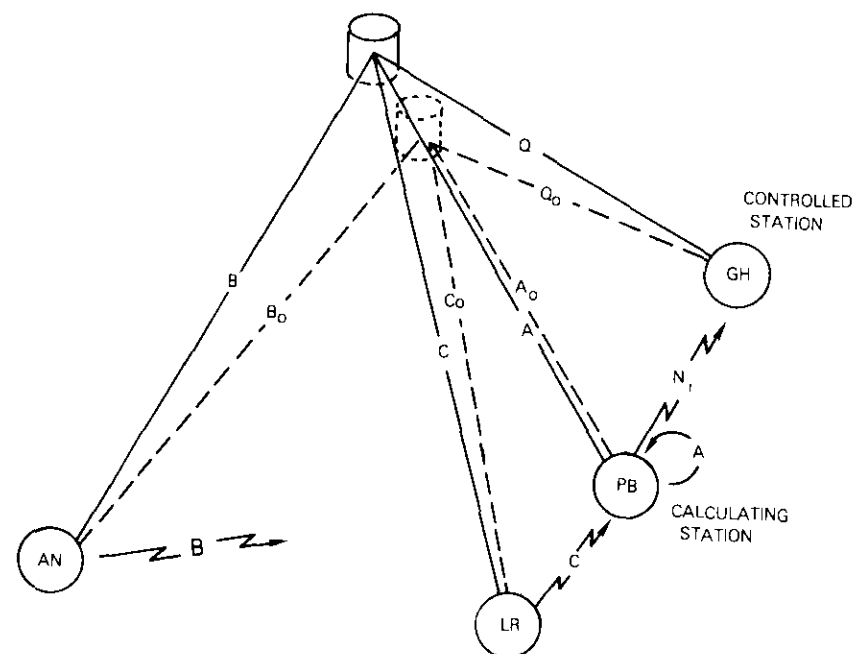
For the zero-order predictor, the burst position was maintained within ± 3 symbol periods for the 1-minute prediction interval. For the 2- and 3-minute prediction intervals, the distributions expanded asymmetrically about zero from -10 to $+1$ for both 2- and 3-minute prediction intervals. The increased spread is attributed to the inability of the zero-order predictor to keep up with the moving satellite position and the asymmetry is caused by continuous motion in one direction during the data collection interval.

The first-order predictor also maintained the burst position within ± 3 symbols for the 1-minute prediction interval. For the 2- and 3-minute intervals the position was held within a range of approximately 9 symbols, which is a little less than that observed for the zero-order case. Asymmetry was also observed, but it was not as severe as in the zero-order case.

In all cases the second-order predictions show more dispersion than the first-order predictions. This phenomenon is attributed to the dependency of the second-order coefficient on accurate measured range values. Any error incurred in the range values used to compute the second-order coefficient gives rise to an error which increases according to the square of the time into the extrapolation interval. Appendix D includes expressions which justify this statement.

DATA BURST CONTROL EXPERIMENT

This experiment involved all four participating administrations in a network shown in Figure 16. The three ranging stations, Pleumeur Bodou (PB), Andover (AN), and Lario (LR), transmitted their satellite range data to Pleumeur Bodou. Except for Pleumeur Bodou, which received range data locally from its own ranging unit, the interconnections were made by spare DS1 channels. Calculations were performed at Pleumeur Bodou to obtain N_1 , the delay between receipt of the reference burst unique word and the start of the TDMA frame in symbol periods [given by equation (A-22) of Appendix A] for Goonhilly



- $A-A_0$ = DEVIATION FROM NOMINAL AT PB
 $B-B_0$ = DEVIATION FROM NOMINAL AT AN
 $C-C_0$ = DEVIATION FROM NOMINAL AT LA
 $\phi = 22512N - 2Q$ CALCULATED BURST PHASE.

Figure 16. Geometry of Open-Loop Experiment

(GH), which acted as the controlled station in this experiment. Pleumeur Bodou relayed N_1 to Goonhilly via an SCPC channel. The participating stations were equipped as shown in Table 1.

In this experiment the minicomputer at Pleumeur Bodou was programmed to calculate N_1 for Goonhilly by means of the linear approximation solution described in Appendix A. Before the program was run, coefficients K_{QA} , K_{QB} , and K_{QC} of equation (A-17) were calculated off-line and input to the computer, together with the nominal satellite range values A_0 , B_0 , C_0 , and N_0 .

Two methods of evaluating the coefficients K_{QA} , K_{QB} , and K_{QC} are identified. First, they can be calculated from equations (A-18) to

TABLE 1. EARTH STATION EQUIPMENT

Station	Equipment
Pleumeur Bodou	DIOS Range Unit VARIAN 620/L Minicomputer Interface Circuit
Andover	DIOS and AGOS (supplied by BPO) Switchable
Lario	DIOS
Goonhilly	DIOS in Control Mode AGOS Range Unit

(A-20) of Appendix A, where the determinant elements are functions of the nominal Cartesian coordinates of the satellite and the earth station. Secondly, they can be calculated by observing satellite to earth station distances A , B , C , and Q and choosing coefficients which give a weighted sum of range difference terms ΔA , ΔB , and ΔC which matches the range difference term, ΔQ , with minimum error. For a given set of coefficients the relation between ΔA , ΔB , and ΔC and ΔQ must hold for at least one day or one cycle of the satellite movement relative to ranging and controlled stations.

The first method was used in this experiment. Coefficients were calculated using the following data:

position of PB (station A) = $48^{\circ} 47' 09''$ N $3^{\circ} 30' 49''$ W
 position of AN (station B) = $44^{\circ} 38' 00''$ N $70^{\circ} 41' 57''$ W
 position of LR (station C) = $46^{\circ} 9' 30''$ N $9^{\circ} 24' 33''$ E
 position of GH (station N) = $50^{\circ} 03' 05''$ N $5^{\circ} 10' 53''$ W
 nominal satellite position = $0^{\circ} 0' 0''$ N $325^{\circ} 25' 27''$ E
 (INTELSAT IV-A F-4)

A mean earth radius of 6,378 km and a mean geosynchronous orbit radius of 42,164 km were assumed. With this information, the coefficients were found to be

$$K_{QA} = 1.3324 \quad , \quad K_{QB} = -0.0229 \quad , \quad K_{QC} = -0.3098 \quad .$$

A nominal set of satellite range values A_0 , B_0 , C_0 and Q_0 was obtained by taking the TT&C satellite range predictions for a given time on the day on which the experiment was expected to be run. Data were fed to the computer in accordance with the TT&C predictions for

2200 GMT 21 November 1978. Rather than a whole round trip range number in TDMA symbol periods, only the remainder N_1 , after subtracting an integer multiple N_2 (N_2 is number of symbols per frame, or 22,512) was the input, together with a displacement factor to account for data burst position. Nominal satellite range values are given in Table 2.

TABLE 2. NOMINAL SATELLITE RANGE VALUES

	Station			
	A (PB)	B (AN)	C (LR)	N (GH)
Nominal Round trip Range for 2200 GMT 21 Nov. 1978 (TDMA symbols)	7792295	7778000	7883346	7799106
Remainder Term	3143	11360	4146	9954
Displacement Factor for Burst Position	2316	0	4580	0
Number Input to Computer (one-way remainder)	2730	5680	4363	4977

The displacement factor for burst position was zero for Andover and Goonhilly because Andover used AGOS ranging techniques, independent of data burst position, and Goonhilly corrected for its data burst position using a locally inserted offset.

The open-loop burst control experiment was performed on 3 and 4 December 1978 using TT&C satellite position data valid for 21 November 1978. Two maneuvers were performed on the satellite in the interim period so that data extended through and beyond a period involving maneuvers. Figure 17 is a sample of a chart recording of the open-loop controlled Goonhilly data burst position relative to the received reference station unique word for zero-order extrapolation with 3-second updates. The burst was maintained to within ± 3 symbols of nominal for the duration of the experiment (36 hours). The spikes are probably due to errors in the data communications link between Pleumeur Bodou and Goonhilly which could be corrected in an operational system. The sawtooth fluctuation is the result of the frequency offset between reference station and local station clocks interacting in the local station unique word detector. The frequency offset is caused by differences in clock frequencies and Doppler effects.

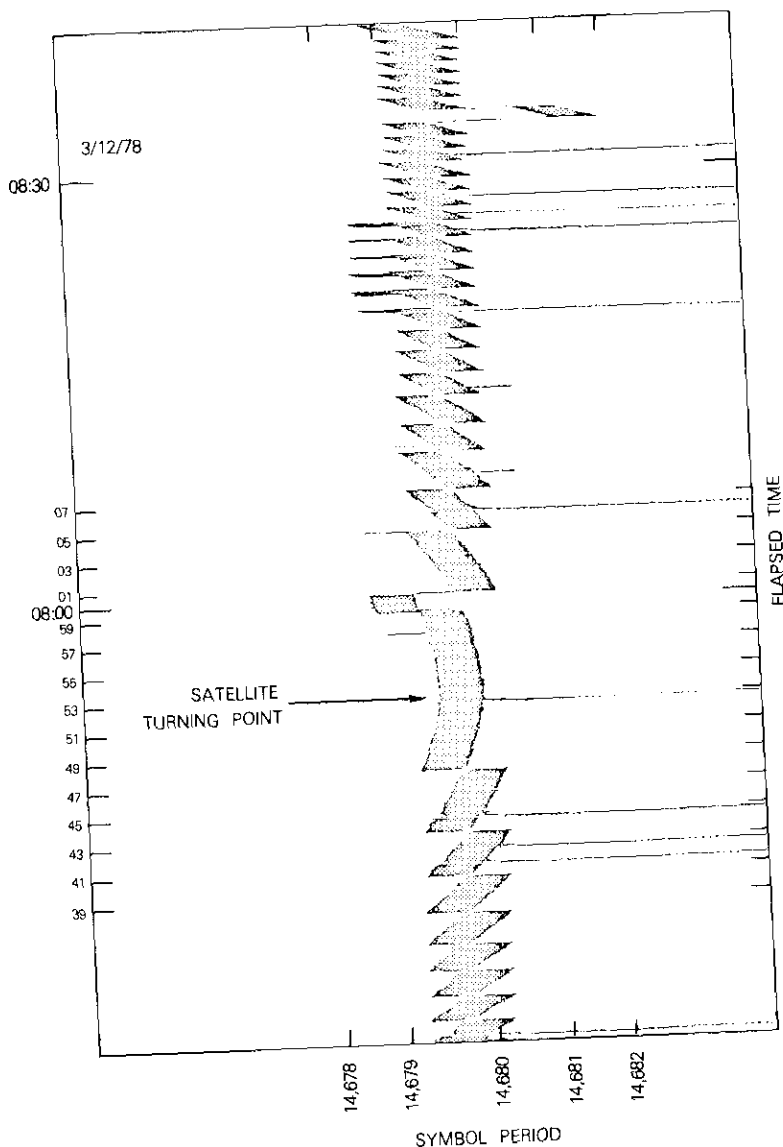


Figure 17. Open-Loop Synchronization Record Sample

Conclusions

In global beam TDMA systems, the simplification of the acquisition process appears to be the most attractive feature of open-loop control. In spot beam systems simplification of the acquisition process is also important. In addition, open-loop control eliminates the need for complicated closed-loop feedback acquisition and synchronization protocols.

Open-loop control requires a means to determine the position of the satellite. For acquisition, the satellite position accuracy need only be sufficient to place a burst in an approximate location, and a satellite position accuracy of a few kilometers is sufficient. For synchronization, the required satellite position accuracy is much greater.

TT&C stations combined with computer processing provide precise satellite orbital parameters which are sufficiently accurate to achieve both acquisition and synchronization; however, when maneuvers are executed, the position accuracy is significantly reduced and not recovered for several days.

Two other methods of position determination are digital open-loop synchronization (DIOS) and analog open-loop synchronization (AGOS). Each must be used in a triangulation arrangement to achieve unambiguous position determination and each is capable of the precision needed to accomplish both acquisition and synchronization. DIOS, which uses a TDMA terminal's traffic burst to observe the satellite range and requires that a station see its own burst transmission from the satellite, is limited to global beam operation. AGOS avoids the need for a station to see its own burst transmission by performing closed-loop ranging in an SCPC global beam channel. It is possible to use a mixed arrangement of DIOS and AGOS.

Ranging can also be accomplished by observing the displacement of a burst from any station relative to an assigned target position in the TDMA frame. Thus, the local stations of a TDMA network can be used to perform satellite position tracking needed for open-loop control.

Locations of the ranging stations can significantly influence the accuracy with which the controlled station's traffic burst is placed. In general they should be dispersed as widely as possible. In the INTELSAT system considerable flexibility exists for selecting near-optimum earth station locations.

Open-loop control in the spot beam application requires that reference bursts be established in each of the spot beams using a reference burst station in an opposite beam. This can be accomplished by using

open-loop control to properly phase the reference bursts.

Open-loop control also requires a method for disseminating the open-loop control information throughout a network. This is best accomplished by including the information as part of the reference burst. The control information can consist of the burst position coordinates of burst start time and burst duration, which are determined by a central processor. Alternatively, it can consist simply of the current satellite position coordinates in terms of departure from a nominal position; calculation of the actual burst position coordinates is then performed at each individual earth station.

Appendix A. Determination of satellite position by linear approximation method

Figure 7 is a diagram of the geographical configuration. The following parameters are defined:

- A, B, C, Q = actual satellite ranges from ranging stations a, b, and c and controlled station q normalized to TDMA symbols
- A_0, B_0, C_0, Q_0 = nominal satellite ranges from a, b, c, and q
- X_S, Y_S, Z_S = nominal earth-centered satellite coordinates
- $\Delta X, \Delta Y, \Delta Z$ = displacement coordinates relative to nominal position
- $X_A, X_B, X_C, X_Q, \dots, Z_Q$ = coordinates of a, b, c and q.

Then,

$$A_0^2 = (X_S - X_A)^2 + (Y_S - Y_A)^2 + (Z_S - Z_A)^2 \quad (\text{A-1})$$

$$B_0^2 = (X_S - X_B)^2 + (Y_S - Y_B)^2 + (Z_S - Z_B)^2 \quad (\text{A-2})$$

$$C_0^2 = (X_S - X_C)^2 + (Y_S - Y_C)^2 + (Z_S - Z_C)^2 \quad (\text{A-3})$$

$$Q_0^2 = (X_S - X_Q)^2 + (Y_S - Y_Q)^2 + (Z_S - Z_Q)^2 \quad (\text{A-4})$$

and,

$$A^2 = (X_S + \Delta X - X_A)^2 + (Y_S + \Delta Y - Y_A)^2 + (Z_S + \Delta Z - Z_A)^2 \quad (\text{A-5})$$

$$B^2 = (X_S + \Delta X - X_B)^2 + (Y_S + \Delta Y - Y_B)^2 + (Z_S + \Delta Z - Z_B)^2 \quad (\text{A-6})$$

$$C^2 = (X_S + \Delta X - X_C)^2 + (Y_S + \Delta Y - Y_C)^2 + (Z_S + \Delta Z - Z_C)^2 \quad (\text{A-7})$$

$$Q^2 = (X_S + \Delta X - X_Q)^2 + (Y_S + \Delta Y - Y_Q)^2 + (Z_S + \Delta Z - Z_Q)^2 \quad (\text{A-8})$$

Q must be determined by solving for the displacement coordinates $\Delta X, \Delta Y, \Delta Z$.

Subtracting successive pairs of equations, *i.e.*, (A-5) and (A-1), (A-6) and (A-2), (A-7) and (A-3), and (A-8) and (A-9) by using the relation $(A - A_0)(A + A_0) = A^2 - A_0^2$ gives

$$\Delta A = A - A_0 = \frac{2(X_S - X_A)\Delta X + 2(Y_S - Y_A)\Delta Y + 2(Z_S - Z_A)\Delta Z + \Delta S^2}{A + A_0} \quad (\text{A-9})$$

$$\Delta B = B - B_0 = \frac{2(X_S - X_B)\Delta X + 2(Y_S - Y_B)\Delta Y + 2(Z_S - Z_B)\Delta Z + \Delta S^2}{B + B_0} \quad (\text{A-10})$$

$$\Delta C = C - C_0 = \frac{2(X_S - X_C)\Delta X + 2(Y_S - Y_C)\Delta Y + 2(Z_S - Z_C)\Delta Z + \Delta S^2}{C + C_0} \quad (\text{A-11})$$

$$\Delta Q = Q - Q_0 = \frac{2(X_S - X_Q)\Delta X + 2(Y_S - Y_Q)\Delta Y + 2(Z_S - Z_Q)\Delta Z + \Delta S^2}{Q + Q_0} \quad (\text{A-12})$$

where $\Delta S^2 = \Delta X^2 + \Delta Y^2 + \Delta Z^2$. If ΔS^2 is neglected and $A + A_0 = 2A_0$, the above equations simplify to

$$\Delta A = K_{AX}\Delta X + K_{AY}\Delta Y + K_{AZ}\Delta Z \quad (\text{A-13})$$

$$\Delta B = K_{BX}\Delta X + K_{BY}\Delta Y + K_{BZ}\Delta Z \quad (\text{A-14})$$

$$\Delta C = K_{CX}\Delta X + K_{CY}\Delta Y + K_{CZ}\Delta Z \quad (\text{A-15})$$

$$\Delta Q = K_{QX}\Delta X + K_{QY}\Delta Y + K_{QZ}\Delta Z \quad (\text{A-16})$$

Solving for $\Delta X, \Delta Y$, and ΔZ using Cramer's rule and substituting into equation (A-16) yields

$$\Delta Q = K_{QA}\Delta A + K_{QB}\Delta B + K_{QC}\Delta C \quad (\text{A-17})$$

$$K_{QA} = \frac{\begin{vmatrix} K_{QX}K_{QY}K_{QZ} \\ K_{BX}K_{BY}K_{BZ} \\ K_{CX}K_{CY}K_{CZ} \end{vmatrix}}{D_0} \quad (\text{A-18})$$

where

$$K_{QB} = \frac{\begin{vmatrix} K_{AX}K_{AY}K_{AZ} \\ K_{QX}K_{QY}K_{QZ} \\ K_{CX}K_{CY}K_{CZ} \end{vmatrix}}{D_0} \quad (A-19)$$

$$K_{QC} = \frac{\begin{vmatrix} K_{AX}K_{AY}K_{AZ} \\ K_{BX}K_{BY}K_{BZ} \\ K_{QX}K_{QY}K_{QZ} \end{vmatrix}}{D_0} \quad (A-20)$$

and

$$D_0 = \begin{vmatrix} K_{AX} & K_{AY} & K_{AZ} \\ K_{BX} & K_{BY} & K_{BZ} \\ K_{CX} & K_{CY} & K_{CZ} \end{vmatrix}$$

Q could be obtained by substituting values of ΔX , ΔY , and ΔZ into equation (A-8), but a simpler and more direct solution is given by

$$Q = Q_0 + \Delta Q \quad (A-21)$$

where ΔQ is obtained from equation (A-17).

Finally, a displacement number N_1 can be obtained which gives the delay between receipt of a synchronization burst unique word and start of the TDMA frame in terms of TDMA symbol periods:

$$N_1 = KN_2 - \frac{2Q}{cS} \quad (A-22)$$

where N_2 = number of symbols per TDMA frame

S = TDMA symbol rate

c = velocity of light

K = positive integer chosen so that $0 < N_1 < N_2$.

Appendix B. Solution for coefficients K_{QA} , K_{QB} , and K_{QC} for planar geometry

A simplified geometric solution is possible if it is assumed that the three ranging stations and the controlled station lie on the same plane. The geometry applicable to this case is shown in Figure 8. The satellite is located at point

S and the ranging stations are at a , b , and c , respectively. To calculate the coefficient relating the change in the estimated distance to the controlled station and the change in the distance to one of the ranging stations, the satellite distances to the other two ranging stations are held constant.

Assume that \hat{a} , \hat{b} , and \hat{c} are unit vectors from the satellite to stations a , b , and c . If the ranges to a and b are fixed, then the satellite can move only in a direction perpendicular to both \hat{a} and \hat{b} , that is, in a direction given by $\hat{a} \times \hat{b}$. When the satellite moves a certain distance ΔS , the range to station c changes by a distance of ΔC . The ratio of these changes is the cosine of the angle between $\hat{a} \times \hat{b}$ and \hat{c} , that is, the sine of the angle between c and the a - b plane. Therefore,

$$\frac{\Delta C}{\Delta S} = \sin(c, ab) \quad (B-1)$$

The change in the range to another station q is given by a similar expression. Dividing one equation by the other yields

$$K_{SQ} = \frac{\Delta Q}{\Delta C} = \frac{\sin(q, ab)}{\sin(c, ab)} \quad (B-2)$$

The term $\sin(c, ab)$ can also be written as c_{ab}/C , where c_{ab} is the distance from c to the a - b plane and C is the distance from c to the satellite. The coefficient can then be written (for three stations in a plane) as

$$K_{QC} = \frac{C d_{ab}}{Q c_{ab}} = \frac{C d_{aq} \cos \alpha_q}{Q d_{ac} \cos \alpha_c} \quad (B-3)$$

Since $C \cong Q$, this can be written as

$$K_{QC} = \frac{d_{aq} \cos \alpha_q}{d_{ac} \cos \alpha_c} \quad (B-4)$$

Similarly, coefficients K_{QA} and K_{QB} are found to be

$$K_{QA} = \frac{A d_{aq} \cos \alpha_q^a}{Q d_{aa} \cos \alpha_a} \quad (B-5)$$

$$K_{QB} = \frac{B d_{bq} \cos \alpha_q^b}{Q d_{bb} \cos \alpha_b} \quad (B-6)$$

*This is true only if the sub-satellite point is on line a - b ; otherwise, there is a factor which will later cancel from the numerator and denominator.

Appendix C. K_{QA} , K_{QB} and K_{QC} for equally spaced ranging stations

The general expressions for coefficients K_{QA} , K_{QB} , and K_{QC} have been developed in Appendix B. This appendix will develop simplified and instructive expressions which result when the ranging stations lie on the circumference of a circle of radius R and are equally spaced at angular separations of 120° . Coefficient K_{QC} is developed below; the other coefficients are obtained by simple angle substitutions.

The general expression for K_{QC} developed in Appendix B, but with $Q \cong C$, is

$$K_{QC} = \frac{d_{oq} \cos \alpha_q^c}{d_{oc} \cos \alpha_c} \quad (C-1)$$

For the special case of interest, $\alpha_c = 0^\circ$ and $d_{oc} = d_{oa} = d_{ob} = 3R/2$. Also, the expressions for d_{oq}^2 and α_q^c become

$$d_{oq}^2 = R_q^2 + \frac{R^2}{4} + R_q R \cos \theta \quad (C-2)$$

$$\sin \alpha_q^c = \frac{R_q}{d_{oq}} \sin \theta \quad (C-3)$$

where θ is the angle of departure from the reference line for ranging station c defined in the text. Substituting equations (C-2) and (C-3) into (C-1) yields

$$K_{QC} = \frac{2R_q \cos \theta + R}{3R} \quad (C-4)$$

The expressions for K_{QA} and K_{QB} are obtained from equation (C-4) simply by replacing θ with $\theta - 120^\circ$ and $\theta + 120^\circ$, respectively. Thus,

$$K_{QA} = \frac{2R_q \cos (\theta - 120^\circ) + R}{3R} \quad (C-5)$$

$$K_{QB} = \frac{2R_q \cos (\theta + 120^\circ) + R}{3R} \quad (C-6)$$

From the above expressions, it is also possible to develop a simple resultant error coefficient expression for contributions from all three ranging stations by summing the squares of the three coefficients. Thus,

$$K_{QA}^2 + K_{QB}^2 + K_{QC}^2 = \frac{2(R_q/R)^2 + 1}{3} \quad (C-7)$$

This expression assumes that the errors from each ranging station are equal. If one or more is different, the coefficients will have to be appropriately weighted to obtain the resultant error.

Appendix D. Experiment to predict range relative to Pleumeur Bodou

In this experiment Pleumeur Bodou measured the number of TDMA symbols between transmission and reception of a traffic burst as seen in any one TDMA frame. If this number is N_1 , then the satellite round trip range is given by

$$A = MN_2 + N_1 \quad (D-1)$$

where M = number of frames per round trip range
 N_2 = number of symbols per frame.

The nominal satellite range is given by A_0 so that the difference between measured range and nominal range is

$$\Delta A = A - A_0 \quad (D-2)$$

Range measurements were taken every 300 ms and a set of difference terms $\{\Delta A_0, \Delta A_1, \dots, \Delta A_L\}$ was obtained. Every k th member of this set was used to determine zero-, first-, and second-order polynomial extrapolation expressions of round trip satellite displacement from nominal in the direction of Pleumeur Bodou to the satellite. These polynomial expressions are given by

$$\Delta E0(i) = \Delta A(nk) \quad (D-3)$$

$$\Delta E1(i) = \Delta E0(i) + [\Delta A(nk) - \Delta A\{(n-1)k\}] \left(\frac{i-nk}{k} \right) \quad (D-4)$$

$$\begin{aligned} \Delta E2(i) = \Delta E1(i) + [\Delta A(nk) - 2\Delta A\{(n-1)k\} \\ + \Delta A\{(n-2)k\}] \left(\frac{i-nk}{k} \right)^2 \end{aligned} \quad (D-5)$$

where $nk < i \leq (n+1)k$ and n is the prediction interval number.

Values of the polynomials generated for integer values of i predict the satellite displacement for the time elapsed since the last calculation of the

polynomial coefficients. Increments of i occur at 300-ms intervals.

Difference terms between actual and predicted values are given by

$$e0(i) = \Delta A(i) - \Delta E0(i) \tag{D-6}$$

$$e1(i) = \Delta A(i) - \Delta E1(i) \tag{D-7}$$

$$e2(i) = \Delta A(i) - \Delta E2(i) \tag{D-8}$$

Histograms of $e0(i)$, $e1(i)$, $e2(i)$ are shown in Figure D-1. Three k values, 180, 360, and 540, which correspond to extrapolation intervals of 1, 2, and 3 minutes, are each associated with three histograms corresponding to the three orders of prediction.

If the error associated with any single observation is assumed to be ϵ , then the resulting error in the end-estimated zero-, first-, and second-order coefficients of the polynomial approximations is ϵ , 2ϵ , and 4ϵ , respectively, and the resulting variances in predictions using the polynomial expressions become

$$\text{VAR}[\Delta E0(i)] = \epsilon^2$$

$$\text{VAR}[\Delta E1(i)] = \epsilon^2 + 4\epsilon^2 \left(\frac{i - nk}{k} \right)^2$$

$$\text{VAR}[\Delta E2(i)] = \epsilon^2 + 4\epsilon^2 \left(\frac{i - nk}{k} \right)^2 + 16\epsilon^2 \left(\frac{i - nk}{k} \right)^4$$

where the general expression used for estimating variance is

$$\text{VAR}[X] = \overline{(X - \bar{X})^2}$$

Note that, as the prediction increases, *i.e.*, as values of $(i - nk)/k$ increase, the contributions to variance from the high-order terms rapidly increase and dominate those of the lower order terms. Thus, second-order prediction can become inferior to first- and zero-order prediction as the prediction time increases.

References

- [1] S. J. Campanella et al., "The INTELSAT TDMA Field Trial," *COMSAT Technical Review*, Vol. 9, No. 2, Fall 1979, pp. 293-340.
- [2] P. P. Nuspl and R. Mamey, "Results of the CENSAR Synchronization and Orbit Perturbation Measurement Experiments," 4th International Conference on Digital Satellite Communications, Montreal, Canada, October 1978.

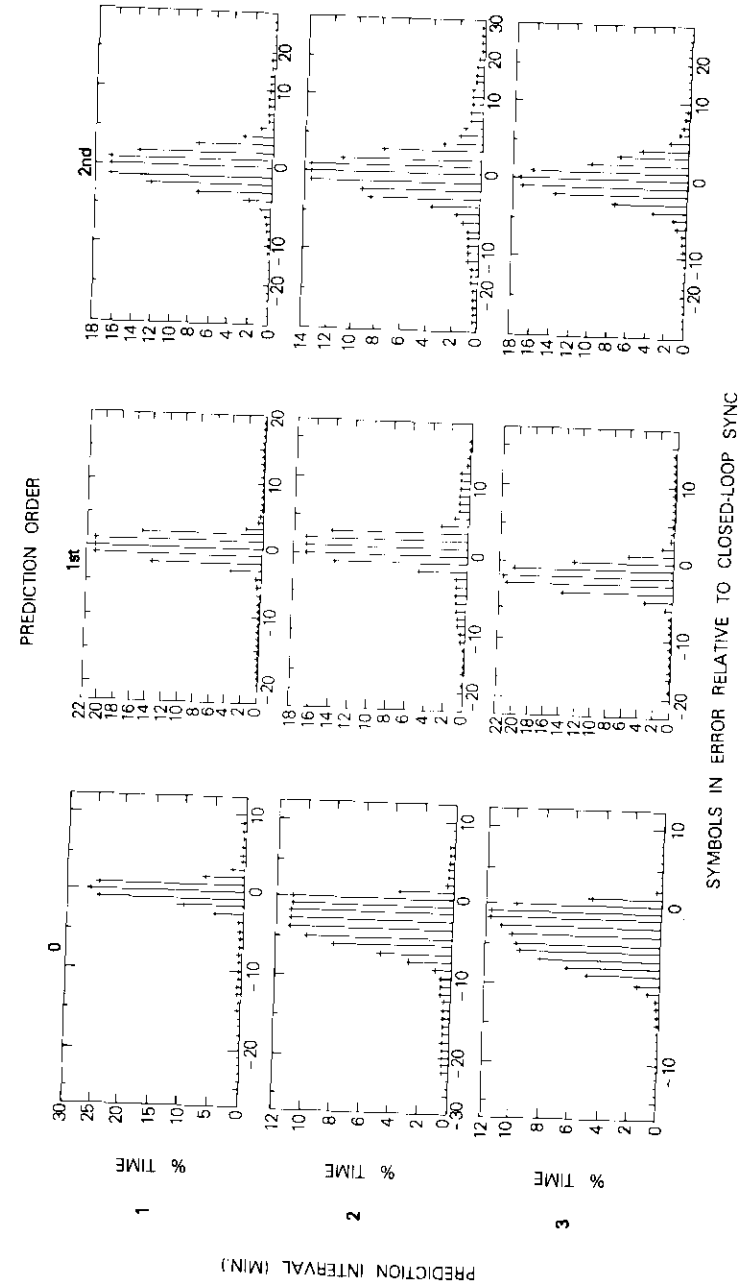


Figure D-1. Histograms of Burst Position Error

- [3] D. W. Lipke et al., "MARISAT—A Maritime Satellite Communications System," *COMSAT Technical Review*, Vol. 7, No. 2, Fall 1977, pp. 351–392.
- [4] W. G. Schmidt, "The Application of TDMA to the INTELSAT IV Satellite Series," *COMSAT Technical Review*, Vol. 3, No. 2, Fall 1973, pp. 257–276.
- [5] W. Mallet, "INTELSAT's 50 Mbit/s TDMA-2 System," 2nd International Conference on Digital Satellite Communications, Paris, France, November 1972.
- [6] D. F. DiFonzo, "Antennas—Key to Communications Satellite Growth," *Microwave Systems News*, Vol. 8, No. 6, June 1978, pp. 83–91.
- [7] E. R. Cacciamani, Jr., "The SPADE System As Applied to Data Communication and Small Earth Station Operation," *COMSAT Technical Review*, Vol. 1, No. 1, Fall 1971, pp. 171–182.
- [8] G. D. Dill, Y. Tsuji, and T. Muratani, "Application of SS-TDMA in a Channelized Satellite," International Conference on Communications, Philadelphia, Pennsylvania, 1976, Vol. 3, pp. 51-1–51-5.
- [9] J. Deal, "Open Loop Acquisition and Synchronization," Joint Automatic Control Conference, San Francisco, California, June 1974, *Proc.*, Vol. 2, pp. 1163–1169.
- [10] A. Jefferies and K. Hodson, "New Synchronization Scheme for Communications Satellite Multiple Access TDM Systems," *Electronics Letters*, Vol. 9, No. 24, November 29, 1973.



S. J. Campanella received a B.S.E.E. from the Catholic University of America, an M.S.E.E. from the University of Maryland, and a Ph.D. in electrical engineering from the Catholic University of America. Before joining COMSAT, he was Manager of the Electronics Research Center at Melpar, Inc. and prior to Melpar, Inc. was an Electronic Scientist at the Naval Research Lab engaged in sonar signal processing.

He is presently Director of the Communications Laboratory of COMSAT Laboratories. He has most recently been responsible for the technical direction of the INTELSAT TDMA field trials in the Atlantic Coast Region and for an intensive effort to develop a new low cost TDMA concept.

Dr. Campanella is a Member of AIAA, Sigma Xi, Phi Eta Sigma, and a Fellow of the IEEE and AAAS. He is also a Member of the Board of Directors of EASCON.

Kevin Hodson received a B.Sc. in electrical engineering from Imperial College, London, in 1970 and an M.Sc. from the University of Manchester Institute of Science and Technology in 1972. Prior to joining COMSAT Laboratories in January 1977 as an INTELSAT assignee, he was engaged in development work in the Space Systems Division of the British Post Office. He returned to the British Post Office in January 1979. He is a member of the IEE.



Techniques for TDMA system monitoring

D. J. SCHAEFER

(Manuscript received July 19, 1979)

Abstract

The serial nature of time-division multiple-access (TDMA) transmission through a satellite transponder makes it possible to simultaneously monitor all stations in the TDMA network. Down-link transmission from the satellite can be observed to obtain estimates of each earth terminal's overall performance without affecting network efficiency. The measurement of these performance data in real time allows a number of monitoring options ranging from simple alarm monitoring and historical network data collection to more sophisticated forms of processing suitable for real-time network control.

This examination of TDMA monitoring techniques discusses important network parameters and their measurement compatibility with normal system operation. The implementation and performance of a breadboard TDMA monitor installed at the Andover earth station in conjunction with the INTELSAT TDMA field trial are presented. Based on the experience obtained from the field trial evaluation, an operational monitor configuration is suggested as well as recommendations for implementing the individual parameter monitors. Compatibility with planned or existing INTELSAT monitoring capabilities is also discussed.

Introduction

A fully automated computer-controlled communications monitoring

This paper is based upon work performed under the sponsorship of the International Telecommunications Satellite Organization (INTELSAT).

system is being constructed to collect the necessary real-time data for INTELSAT V network control. The monitoring network, which consists of 11 systems at selected earth stations around the world, measures signal parameters of FDM/FM, FM/TV, and QPSK demand-assigned carriers. The subsystems employed in the communications monitors are intended primarily for measurement of continuous mode signals such as those encountered in FDM/FM transmission [1]. The introduction of TDMA equipment into the INTELSAT V network will require a different monitoring capability to perform real-time burst mode measurements on the TDMA transmission.

The transmission formats used in TDMA signaling are radically different from those encountered in FDM/FM transmission; therefore, a different approach has been developed for this application. The TDMA system monitor (TSM) is intended to provide the capability for performing real-time burst mode measurements of all transmissions within a selected network. The TSM data collection subsystem functions as a stand-alone system which could, in an operational monitoring system, be interfaced to the existing communications system monitoring (CSM) display and data transmission facilities via the TSM's control computer, thereby providing a fully integrated FDM/FM and TDMA monitoring capability.

Since TDMA network monitoring requirements are considerably different from those of an FDM network, a study was conducted to determine which parameters should be monitored in an operational system, as well as the technique and the degree of accuracy. The selected parameters can be classified into two general categories: those pertaining to overall network synchronization, and signal characteristics related to a particular earth station's transmission. TDMA transmissions consist of short periodic bursts of data; hence, the frame period and individual transmit burst positions were identified as essential to overall network performance. Burst power level, frequency, bit-error rate, and satellite down-link ambient noise level were selected as the most desirable parameters to monitor to ensure proper network performance. Other parameters, such as TDMA symbol clock rates, were considered but discarded since perturbation in these parameters will appear as performance variations in the set of signal parameters already defined.

To verify the applicability of the selected parameters to the TDMA monitoring requirement, a breadboard version of the TSM was constructed and its performance evaluated during the recently completed

INTELSAT TDMA field trial. The breadboard TSM was installed in conjunction with the field trial equipment at the Andover earth station and used for several months. Experience gained from the evaluation has shown the necessity for a TDMA monitoring capability for burst mode measurements to supplement the existing or planned continuous mode monitoring capability.

This paper examines the theoretical considerations involved in monitoring the selected TDMA network parameters, *i.e.*, the techniques and number of measurements necessary to achieve a desired accuracy. The breadboard field trial implementation of the TSM is described, and the overall performance and recommendations for operational network monitors are discussed. The final sections outline a TSM implementation which can be added to an existing monitoring system such as the CSM.

TDMA network parameters

The objectives of the TDMA monitoring study were to identify parameters that should be monitored to ensure the maintenance of overall TDMA network performance, and to determine techniques for performing the necessary measurements. A total of six network parameters were selected as sufficient to ensure normal operation and minimize interference with other services: burst power level, transmit burst position, down-link frequency, ambient receive noise level, TDMA frame period, and an estimate of the TDMA burst bit-error rates (BER). These parameters, together with implementation and measurement accuracy, are described briefly in the following subsections.

Burst power level

Monitoring burst power levels is probably one of the most important TSM functions. Maintaining the optimum operating point of the satellite traveling wave tube amplifier (TWTA) and minimizing the burst-to-burst variations within the TDMA frame greatly improve overall network performance. Burst mode power measurements require equipment with response times of the order of 10 μ s or less. Since normal rms measuring equipment employing thermal detection techniques has response times of the order of milliseconds, a new method for burst mode power measurement was developed for use in the breadboard TSM. The new technique, using a combination of analog and digital hardware, has a response time of the order of 6 μ s. This allows measurements of single TDMA bursts and simultaneous measurement

of all bursts within a single 750- μ s frame period. Single burst relative power level measurement accuracy is slightly better than ± 0.5 dB. By averaging the measurements over multiple frames, this uncertainty can be typically reduced to ± 0.1 dB. The averaging mode of operation is achieved by using the TSM control software which tracks transmit bursts from one station until measurements are completed.

The power levels measured by the monitor are a combination of received signal plus noise power amplified by the receiving system's gain. In a typical INTELSAT TDMA application, receive carrier-to-noise ratios (C/N) are in excess of 15 dB. For relative power measurements between two or more received signals, the detected signal power level may be compared directly. The requirement to measure absolute power levels entails additional compensation to account for the effects of antenna gain, down-link path loss, absolute noise level, and down-converter gain. The effects of path loss and antenna gain may be assumed to be relatively constant under clear-sky conditions and may be considered separately. The remaining measurement perturbations should be considered in each basic power measurement. A technique has been developed to perform this measurement which requires two additional measurements to be made during the TDMA frame: an ambient noise measurement, P_n , and a reference power level, P_L .

A reference source is located at the TDMA receive antenna and calibrated to a known receive power level in terms of the antenna gain. It is operated in a burst mode compatible with the TDMA frame structure so that it does not affect normal system operation. The actual signal power, P_R , may be determined independently of the receive system gain by combining these measurements with the received signal plus noise power, P_{TR} . The total power measured at the monitor can be expressed as

$$P_{TR} = G(P_n + P_R)$$

where P_n represents the ambient noise level during a 750- μ s TDMA frame and G the receiver system gain. Similarly, the noise level, P_{cn} , measured at the monitor is

$$P_{cn} = GP_n$$

The implementation of a burst power monitor used in the breadboard TSM is similar to that used in automatic level control circuitry (see

Figure 1), except that loop response time and dynamic range are emphasized rather than RF output signal stability. The monitor's input signal from the TDMA receive down-converter is amplitude stabilized using a variable attenuator with an insertion loss which depends on input power level. The attenuator control voltage is derived from a square law power detector which serves as the basic monitor output.

With a closed-loop automatic gain control (AGC) configuration, the power detector always operates near the same operating point, reducing measurement errors caused by detector variations. The analog voltage is sampled and converted to a digital format by a strobe command from the TSM controller. The sampling occurs automatically 6 μ s after the desired TDMA burst is detected. The digital representation of the sampled loop control voltage provides the input to the software TSM control processor. The nonlinearities in the control loop characteristic are offset by the software processing.

The voltage-power relationship is approximated by a polynomial with constant coefficients of the form

$$P_{in} = \sum_{j=1}^N a_j V_c^j \quad (1)$$

where V_c is the loop control voltage and P_{in} the measured power level. Coefficients a_j are contained in the power monitor software and may be easily modified to compensate for circuit aging or realignment. They are computed by entering known signal levels into the monitor and performing a least squares fit to the resulting data points. The calculated coefficients are then used by equation (1) to determine the measured power levels.

The breadboard power monitor was subjected to extensive testing before installation in the TSM. Special attention was given to loop control voltage sensitivity to the form factor of the measured signal. Three types of signals were measured (QPSK, CW carrier, and noise only), and their respective loop responses were plotted. As shown in Figure 2, only small differences of the order of tenths of a decibel were noted for the different signaling formats. Additional testing of the power monitor was performed using the breadboard TSM after installation at Andover. These tests compared the power measurement results of the TSM and the present satellite system monitoring group (SSMG) power measuring equipment for a continuous mode QPSK

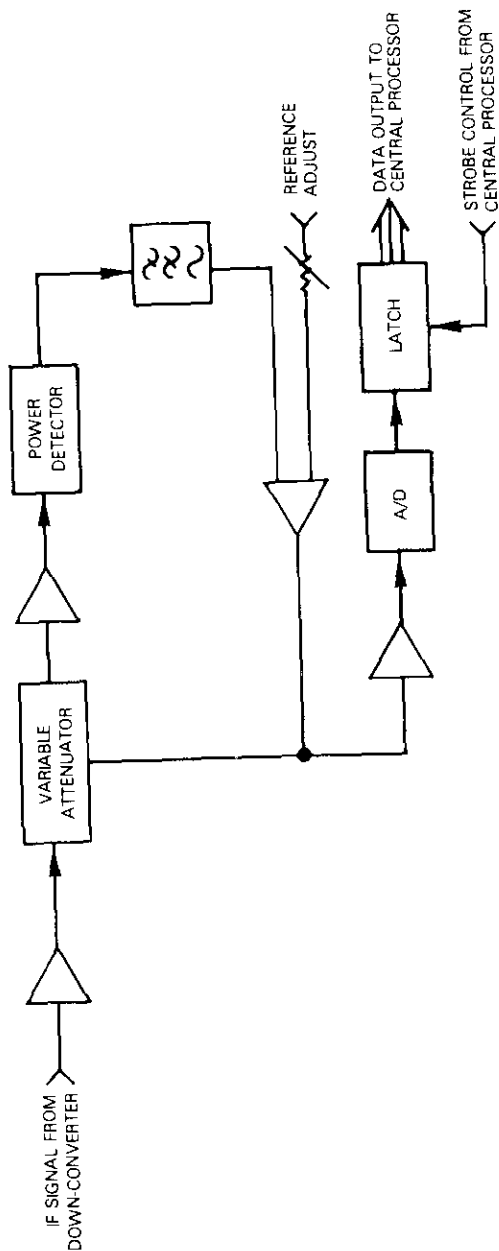


Figure 1. Power Level Monitor

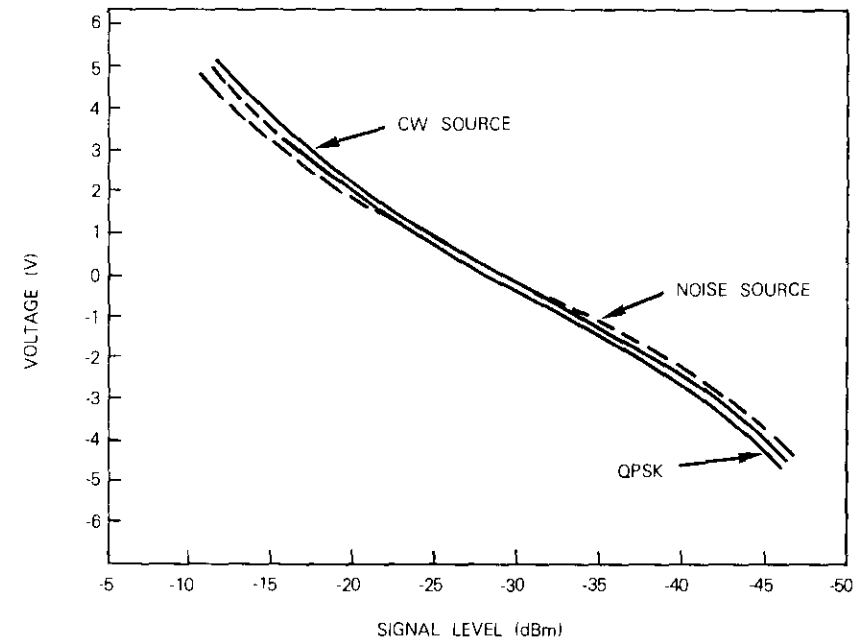


Figure 2. Measurement Voltage vs Signal Power (single measurement)

carrier. With reference to Figure 3, the results of the two techniques are quite similar. For additional comparison, power measurements of the QPSK signal during burst mode operation were made using the same power settings. These indicated approximately 0.2-dB difference between TSM continuous and burst mode measurements. Unfortunately, an SSMG comparison was not possible since the equipment was incapable of performing burst mode measurements.

Burst position monitor

The burst position monitor measures the time interval between reception of the unique word (UW) in the TDMA frame synchronization burst and selected data burst UWs. The time interval is measured in microseconds and then converted by the TSM to symbol intervals for rapid interpretation of the data burst's transmit position.

The burst position monitor is implemented using a high-speed counter operating at 120 MHz. This results in a measurement error corresponding to a ± 1 clock cycle or $\frac{1}{4}$ symbol for the 30-Msymbol/s rate used

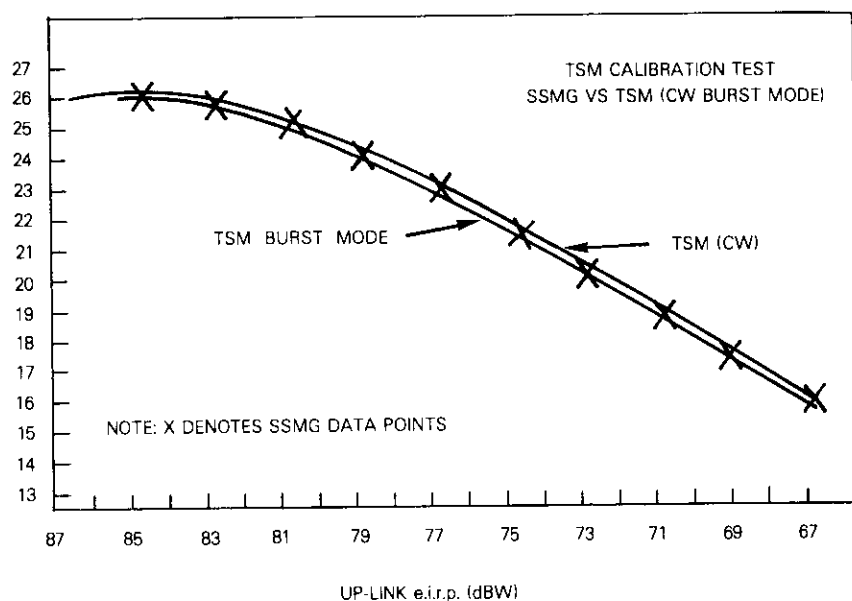


Figure 3. TSM Calibration Test SSMG vs TSM (CW Burst Mode)

in the TDMA field trial equipment. The counter begins when the reference burst UW is decoded by the TDMA terminal and stops when the desired data burst's UW is detected. The value of the counter is then interrogated by the TSM control computer, converted to time and symbol intervals, and output to the teletypewriter (TTY) or data storage equipment. With this type of approach, transmit burst position can be measured in a single TDMA frame period.

Frequency measurement

In a TDMA network employing a QPSK signaling format, down-link frequency monitoring equipment must be capable of synchronizing to the selected TDMA burst and performing a gated frequency measurement of the recovered carrier. Since a QPSK transmission has no transmitted carrier component, the system monitor measures the recovered carrier signal from the TDMA burst modem to determine the actual down-link receive frequency. This measurement is performed at the receive system's intermediate frequency and must be compensated for down-converter frequency deviations.

Measurement accuracies in excess of one part in 10^6 are necessary

for accurate determination of the received burst frequencies. Regardless of the selected frequency measurement technique, the measurement must be averaged over multiple TDMA frame periods to achieve the desired accuracy. Frequency measurements can be classified into two general categories, direct and reciprocal. The direct approach simply counts the number of cycles of the measured signal which occur during a predetermined interval. As suspected, while implementation is very straightforward, the required measurement time increases as higher accuracy is required. For an accuracy of 10^{-5} , a 70-MHz signal would require a continuous measurement time of approximately 1.4 ms.

An alternate technique which determines the period of the received waveform by using a high-frequency reference signal significantly reduces the minimum required measurement time ($200 \mu\text{s}$ for 10^{-5} at 70 MHz). Therefore, measurements were selected as the preferred technique in the TSMS. A selected burst was measured for a $10\text{-}\mu\text{s}$ interval over consecutive TDMA frame intervals. The total number of frames over which the measurement must be averaged to achieve a specific accuracy is a function of the reference clock frequency, count trigger errors due to a finite C/N , and the time interval of the individual measurements. The following relationship holds:

$$M = \left[\frac{1/f_r + \tau}{T_m(\Delta f/f)} \right]^2$$

where M = number of individual measurements

f_r = reference frequency clock in Hz

τ = counter trigger error due to finite C/N

T_m = individual measurement interval in seconds

$\Delta f/f$ = required measurement accuracy.

The total time required to complete a carrier frequency measurement is M times the TDMA frame interval, T_f :

$$T_{\text{meas}} = MT_f$$

The reciprocal counter signal measurement accuracy is limited by the ± 1 count error determined by the choice of reference clock frequency. The ability to resolve time intervals to fractional parts of

the reference clock cycle would improve the overall measurement accuracy by the accuracy to which a fraction of a clock cycle can be measured.

A method for achieving this interpolation capability using a combination of analog and digital techniques has been examined in the TSM. This method employs a standard reciprocal counter technique, as discussed previously, combined with an analog interpolator circuit consisting of two current sources and a capacitor. The two current sources differ in magnitude by a factor Γ . The interpolation is achieved by charging the capacitor for the fractional part of the reference clock cycle corresponding to the ± 1 count error. The capacitor is then discharged at the slower rate, I_2/Γ ; the longer discharge time is measured with a second digital counter using the same reference signal as the previous counter. Improvements in measurement accuracies of up to one part in 10^3 are achievable using this approach. Care must be taken in the design and maintenance of the current sources to maintain overall accuracy improvement.

In addition, the interval between successive measurements must be long enough to allow the completion of the basic integer count and to provide the time, ΓT_{ref} , needed to measure the ± 1 count inaccuracy. Hence, while all the data necessary to perform the measurement are complete in real time, an additional processing time, ΓT_{ref} , is needed before the measurement results are available. Table 1 gives typical measurement times for both the reciprocal counter and interpolation techniques for a 70-MHz recovered carrier signal and a 750- μ s TDMA frame period.

TABLE 1. TSM FREQUENCY MEASUREMENT

Technique	Accuracy	Gate Time (μ s)	No. of Single Measurements	Measurement Time
500-MHz Reciprocal Counter	1×10^{-6}	10	90,000	68 s
Interpolation with 10-MHz Reference	1×10^{-3}	10	900	675 ms
	1×10^{-6}	10	102	77 ms
	1×10^{-3}	10	2	1.5 ms

Frame period

The TDMA frame period and proper transmit burst position relative

to the reference signal are both determined by performing time interval measurements. In the TDMA frame period, the time interval between successive frame synchronization bursts is measured. For frequency measurements, the results of several independent measurements must be averaged to achieve the required accuracy. The same measurement techniques used to determine the receive burst frequency may be employed to measure the TDMA frame period. In this case, the counter input consists of detection pulses from the frame synchronization burst detector. Table 2 summarizes typical accuracies and required measurement times for the TDMA frame period.

A TDMA frame period monitor using an interpolation counter with a 10- μ s reference clock was installed in the breadboard TSM. Each measurement was performed over a total of 200 TDMA frame periods

TABLE 2. TSM FRAME PERIOD

Technique	Accuracy	No. of Single Measurements	Measurement Time
10-MHz Reciprocal Counter	1×10^{-8}	13,460	10.1 s
500-MHz Reciprocal Counter	1×10^{-6}	135	101 ms
	1×10^{-6}	400	300 ms
Interpolation Counter With 10-MHz Reference	1×10^{-8}	4	3 ms
	1×10^{-8}	178	267 ms
	1×10^{-6}	1	750 μ s

and the individual measurement results averaged to obtain a single measurement. Accuracies of the order of 10^{-7} were achieved although the analog interpolation hardware had to be calibrated carefully. Therefore, a digital counter and a high-frequency reference source seem preferable for operational use.

BER

The measurement of burst BER, in addition to the routine burst parameter measurements, provides a method of rapidly assessing overall link performance by using a single monitor. The BER monitor can furnish estimates of TDMA burst BER at the receive modems, which

are demodulated without using special transmission formats and without interrupting the regular traffic flow. This monitor, based on pseudo-error monitoring principles [2]–[5], employs a modified decision threshold in conjunction with the TDMA modem to produce an amplified estimate of the actual burst BER. As described by Gooding [2], the technique has two primary advantages over estimating the error rate by directly counting actual data errors:

a. pseudo-errors obtained by using a modified decision threshold can be determined with good reliability without a true copy of the transmitted data;

b. the pseudo-error rate (PBER) is larger than the actual error rate, so that less measurement time is required to obtain a statistically significant number of errors.

As implemented for use with the QPSK signaling format employed in TDMA, the pseudo-error monitor measures the number of times the received signal vector falls within a region close to a slicer decision threshold at the sampling instant. The basic QPSK signal states and decision thresholds are shown in Figure 4.

The TDMA modem employs two sets of decision boundaries to differentiate between the four possible QPSK signal states. A pseudo-error monitor to estimate burst BER can be implemented by including an additional set of boundaries about each decision threshold. If the received signal vector falls within one of the pseudo-error regions at the received signal sampling time, an error is indicated. The sensitivity of the monitor can be adjusted by varying the width, W° , of the pseudo-error regions.

Performance data for pseudo-error monitors are available for various noise and interference environments [2]–[4]. Research has shown that the monitor technique is a viable method of providing an on-line BER estimation capability without significantly complicating the monitoring hardware.

As configured in the breadboard TSM, the pseudo-error monitor provides an amplified, but uncalibrated, estimate of each TDMA burst BER. The primary goal of the pseudo-error monitor evaluation was to determine its response in a burst mode TDMA environment. For this test, only relative rather than absolute BER data were required. A similar calibrated version of the monitor could be used to provide BER estimates for the low error rates often encountered in TDMA in much less time than normally required by more conventional techniques.

Monitor calibration is easily achieved by performing continuous BER

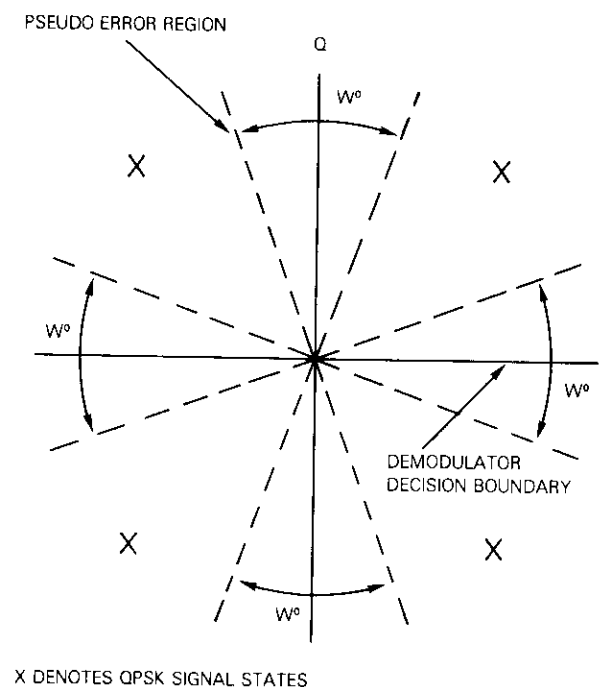


Figure 4. QPSK State Diagram with Pseudo-Error Regions

measurements after installation and by computing a pseudo-error monitor calibration factor corresponding to the ratio of real to pseudo-error rates. This calibration factor will be suitable for normal BER operating ranges better than 10^{-3} and will remain constant as long as the demodulator voltage levels and timing are not changed.

The breadboard TSM's pseudo-error monitor is a form of automated eye pattern monitor operating on the BPSK waveform present in the *P* and *Q* channels of the TDMA receive modem. As indicated in the eye pattern diagram of Figure 5, a pseudo-error region is established about the decision threshold so that a pseudo-error occurs each time the signal vector falls in the region at the signal sampling time. In the breadboard TSM, these errors were accumulated over 200 successive TDMA symbol intervals, and the result averaged over successive frames to determine the actual amplified error rate estimates. The pseudo-error monitor is built using a pair of high-speed comparators to define

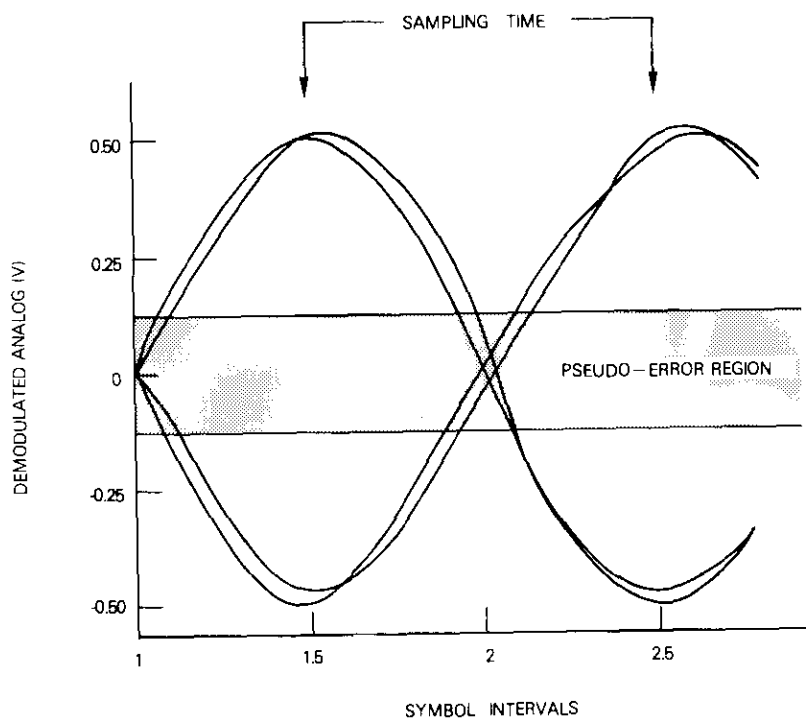


Figure 5. Typical Eye Pattern

the pseudo-error region of Figure 5. The analog signal from the TDMA demodulator and the recovered TDMA symbol provide the input signals to the monitor. The comparators are sampled at instants defined by the symbol clock and the comparator outputs used to drive an error counter. The counter is interrogated by the TSM computer, which calculates BER by processing several blocks of monitor data to achieve the error rate estimate. Examples of processed BER measurements appear later in this paper.

General TSM architecture

Figure 6 is a block diagram showing the five functional components of the TDMA monitor: receive TDMA equipment, specialized monitoring equipment, a hardware controller, a control computer, and data storage

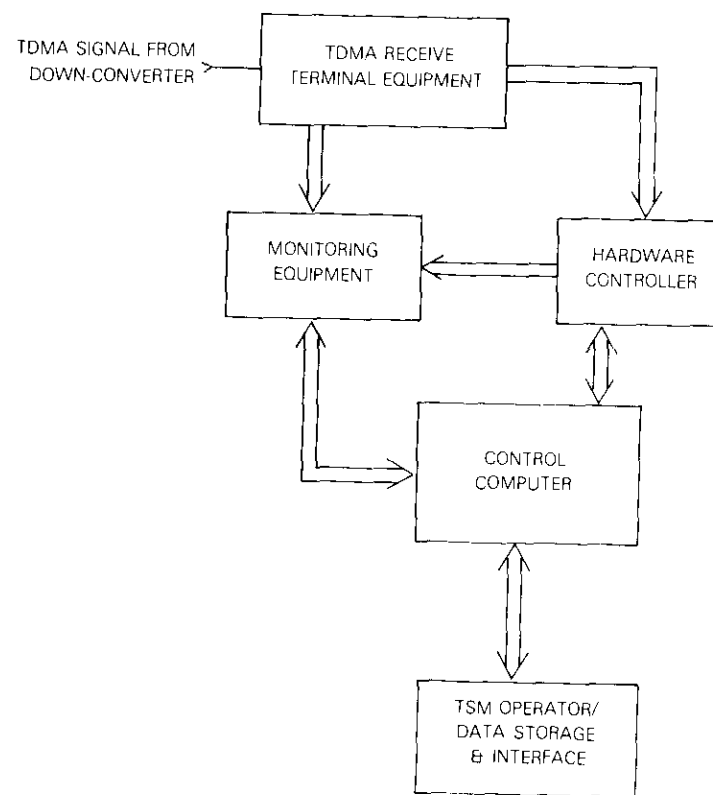


Figure 6. TDMA System Monitor Hardware Architecture

and display devices. The TSM monitoring philosophy is to provide a burst mode monitoring capability which will allow TDMA network measurements to be performed without disturbing normal operation. To achieve this goal, the TSM must be capable of synchronizing itself to the TDMA network, measuring the signal parameters, and displaying the resulting data in real time.

The TDMA receive only equipment enables the TSM to synchronize with the TDMA network and supplies the basic TDMA test signals used by the individual monitoring equipment, which is designed to respond on a burst-to-burst basis under supervision of the TSM's control computer. Since this requires the switching of short-duration high-speed control signals, the real-time monitoring control functions are

performed with the aid of separate hardware control circuitry. The hardware controller is preprogrammed by the control computer at the beginning of each TDMA frame to select a specific burst position and set of individual monitoring functions. The proper timing and test signals are then routed to the individual monitoring equipment and the desired data measured. When the measurement is complete, the individual monitors signal the control computer and the test data are collected and processed.

Using a separate hardware controller to achieve the real-time monitoring control capability significantly reduces the speed requirements of the TSM's central control computer. As a result, an 8-bit microprocessor implementation of the TSM control system is possible, even though a 16-bit HP2116B minicomputer was employed in the breadboard TSM used for the field trial evaluation.

Breadboard TSM design

The design of the breadboard TSM is functionally similar to that described in Figure 6. To minimize the overall cost of the breadboard monitor, the U.S. Andover TDMA terminal equipment provided the necessary synchronization and signal test points to the TSM. Minor modifications to the equipment were made before shipment to Andover to provide buffered test points for traffic burst and reference burst synchronization signals, analog *P* and *Q* data signals, and a modem IF signal together with recovered carrier and TDMA symbol clock. These signals supplied the necessary inputs to the TSM monitoring equipment outlined previously.

Using the U.S. terminal equipment as a source of test signals significantly reduced the breadboard TSM construction cost and eliminated the need for reprogramming the TSM's control system whenever TDMA operating configurations were modified. Although the older HP2116B minicomputer limited the rate at which data could be collected and processed, it offered software compatibility with the computers presently used at the earth stations for satellite system monitoring. The use of this computer indicated the level of difficulty involved in implementing a real-time TDMA monitoring system with the existing monitoring equipment computer facilities.

Figure 7 is a block diagram showing the overall structure of the breadboard TSM. Two types of computer output capability were provided: an ASR-33 model teletype to allow local access to the TSM,

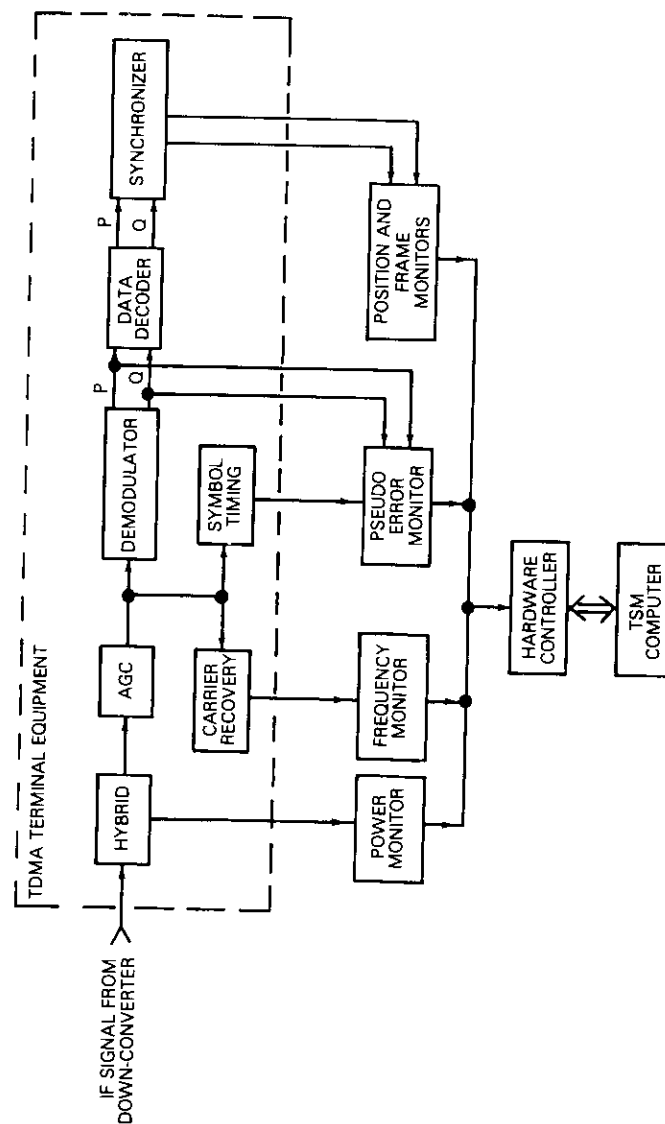


Figure 7. Breadboard TDMA System Monitor Block Diagram

and a magnetic tape system for long-term data collection. The HP2116B computer provided the required data and operator interface to the TSM, and maintained overall control of the data collection hardware. The computer was responsible for controlling the TSM's automated data collection cycle and transferring the test data to magnetic tape.

Although not shown in Figure 7, each monitor is connected directly to the control computer by a common 16-bit data bus that transfers data to the computer from the monitors and programs the TSM's hardware controller. This controller performs the real-time routing of high-speed signals obtained from the TDMA terminal equipment, as well as all sequencing and timing of the frame-by-frame data collection cycles based on instructions from the HP2116B computer. Individual monitor input signals are obtained from the appropriate test points in the TDMA terminal equipment. The hardware controller then sends these control signals to the individual monitors to initiate the selected measurements at the appropriate time in the TDMA frame interval.

Breadboard TSM data processing

Several data collection processing options are possible with the TSM. In its normal unattended mode of operation, TDMA network measurements are performed for a selected portion of each hour throughout the 24-hour interval. The TSM operator selects the parameters to be measured, designated stations, and the measurement start and stop times via the TTY and computer switch register. The test data are recorded onto magnetic tape for later processing on an IBM/360 computer system.

Immediate data measurement results were printed on the TSM's TTY at Andover and were given to the field trial participants upon request. Figure 8 shows a typical TTY printout. The selected TDMA burst is identified in terms of its relative position in the TDMA frame and a 2-letter identifier corresponding to the transmitting earth station's geographic location. The day and time of measurement are also given for easy reference, after which the specific TDMA parameter values are specified.

The example reflects burst power in both absolute and relative forms, transmit position, an estimated BER, frame period, and idle transponder noise measurements. The PBER shown is the amplified error rate for a set of 200 consecutive TDMA frame intervals. The remaining data were also averaged over 200 frames to achieve improved accuracy in

BURST NO. 3 (LR)	
TIME FOR DAY 291	13 hr 8 min 2 sec
POWER	4.391 Volts
	-2.95 dBm
	26.36 dBW
POS	152.63 μ sec
	4581.49 symbols
EBER	0.2971E-02
FRAME:	750.00048 μ sec
NPWR	-0.850 Volts
	-20.28 dBm

Figure 8. *Typical TSM Teletypewriter Output*

the frame period and power measurements. The number of frames over which data are averaged can be selected by the TSM operator and can vary from 1 to 200. The noise power (NPWR) measurement is performed by the burst power monitor. A control signal is synthesized in the hardware controller to allow a power measurement to be performed when no TDMA signal burst is present in the transponder. This measurement is a function of the overall down-link noise level and can be used to obtain a slightly pessimistic estimate of the receive C/N levels by computing the difference in decibels between burst power and noise power measurements. The estimate is conservative because it does not consider small signal suppression effects which occur in the satellite transponder as a result of operating the TDMA burst close to saturation of the satellite TWTA*.

Data are normally collected sequentially for each TDMA burst in the frame beginning with the first. Only one burst is measured per frame; hence, if measurements are averaged over 200 frames, a minimum of 150 ms per station is required. Additional delay in outputting measurement results was encountered with the breadboard TSM because of the slow output rate of the TSM's ASR-33 style teletype. For additional flexibility, a higher speed output mode is included to provide only rapid burst power measurements with reduced TTY printout time. This mode of operation, referred to as the burst profile mode, measures every burst in the TDMA frame in a single 750- μ s frame interval. It is

* In this case the small signal corresponds to up-link noise at the input to the satellite transponder.

particularly useful for evaluating the status of each station in the TDMA frame. Figure 9 contains a typical TTY printout for this mode. The first five burst numbers correspond to the relative down-link power levels of the five TDMA terminals at the time of measurement. Levels of the order of -3 dBm correspond to active stations with the relative noise level approximately -20 dBm. Burst 6 is a locally injected TSM reference burst used for calibration. With reference to Figure 8, bursts 2 through 4 are active with stations 1 and 5 inactive. It should be noted that while this mode of operation enables rapid inspection of TDMA frame status, a power level measurement accuracy of only ± 0.5 dB is possible, since each TDMA burst is measured only once. This does not present a serious difficulty since the normal averaged mode of operation can always be used for more accurate measurements.

Relative Burst Power (No., Level)	
1	-20.88 dBm
2	-3.03 dBm
3	-2.87 dBm
4	-2.92 dBm
5	-19.88 dBm
6	-5.42 dBm
NPWR	-20.11 dBm

Figure 9. *Burst Profile Teletypewriter Output*

TSM experience during field trials

During the TDMA field trials, the TSM proved to be useful in evaluating the performance of the proposed TDMA monitoring techniques and also indicated the need for a monitor capable of operating in a burst mode format. The breadboard TSM was particularly useful during the early phases when considerable time was spent adjusting the up-link e.i.r.p. of the individual earth stations. At first, the satellite monitoring equipment designed to monitor the existing FDMA network was used. Since this equipment could measure in the continuous mode only, each participating station had to transmit in a continuous mode and adjust its power level as indicated by the monitoring equipment. In addition, only one station could be adjusted at a time (others remained inactive), which lengthened the adjustment process.

After installation of the TSM, burst mode power adjustments could be performed in the regular TDMA format. Power level adjustment information was simultaneously given to each earth station so that total power setup time was greatly reduced. It was also interesting to note that measured down-link power variations, before adjustment, of the order of 2 to 3 dB between stations were not uncommon even though each station reported transmitting equivalent e.i.r.p. levels on the up-link. This experience indicates the need for a burst mode measurement capability compatible with the TDMA frame structure.

Another capability associated with the TSM's burst power monitoring features, but not actually employed during the field trials, is its applicability to up-link power control. Since all signals received by the TSM originate from a common down-link, any relative variations between TDMA bursts must be the result of an up-link variation. This information could be automatically transmitted to the individual stations for up-link power control. In a sense, this was accomplished manually during the field trial burst power setups and proved to be quite successful.

An examination of the long-term magnetic tape data provided additional insight into the performance of the TSM's individual parameter monitors. Attempts to measure absolute power for several months indicated the need for reference signal injection at the antenna feed to allow the TSM to automatically compensate for receive system gain changes. During the field trials this was not possible; therefore, a manual recalibration had to be performed after each modification to the earth station receive/down-converter circuitry. Since this imposed a severe burden on the terminal operators, the TSM was relegated to performing only relative power measurements between the participants once the absolute measurement capability was proved.

The burst position and bit-error-rate monitoring approaches proved to be reliable and successful. It was not possible to obtain accurate bit-error-rate calibration information from the TDMA equipment to allow pseudo-error monitor calibration in terms of actual BER rates. It is anticipated that the TSM (after it is returned to COMSAT Laboratories) will undergo more controlled tests to examine the error amplification rates and prediction times.

The monitor hardware implemented in the TSM is useful for a wide range of applications varying from simple data collection and processing to real-time alarm monitoring. This is illustrated by the typical examples of long-term process data plotted in Figures 10 and 11 over a 5-day

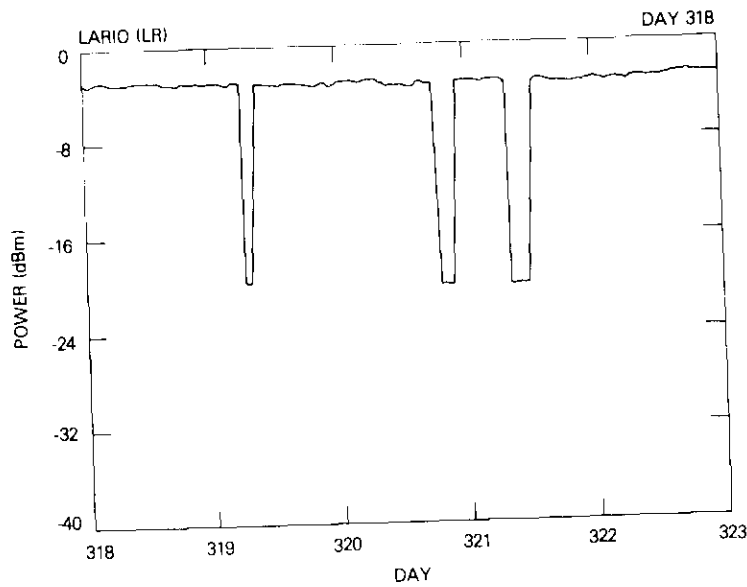


Figure 10. Receive Power Level

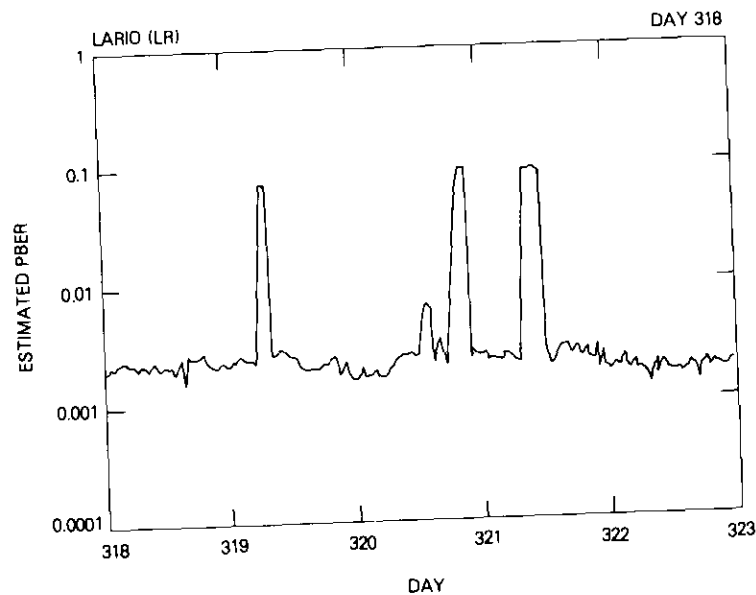


Figure 11. Estimated PBER

interval for a single TDMA station. Figure 10 shows the down-link power level for a particular station measured at the Andover TSM. The normal relative operating point is -3 to -4 dBm with an overall down-link noise level corresponding to -20 dBm. This plot shows that there were three intervals during the 5-day period in which the terminal was not transmitting in the TDMA frame. Similarly, the processed error rate data in Figure 11 indicate a significant change during these intervals. The analysis of such data could be included in the TSM to provide an automatic alarm capability, if desired.

Operational TDMA monitor

The breadboard TSM has shown the usefulness and need for a real-time TDMA network monitoring capability. Since the breadboard version was constructed with surplus equipment where possible, its features had to be limited to the basic monitoring functions. The implementation of an operational version of the TDMA system monitor should consider both the required functions and the need to display monitored data. In this area, various possibilities exist which can be implemented at relatively low cost. For example, replacing the ASR-33 TTY used in the breadboard version with a CRT display that includes a graphics capability would greatly enhance monitoring functions. TDMA network profiles could be plotted to display large amounts of information for rapid review. Similarly, additional software processing could be included to provide an automatic alarm monitoring capability and to maintain short-term historical data which could be made available at the TSM operating console.

An operational TDMA system monitor in the INTELSAT system would complement existing or planned CSM equipment intended for use in the FDM/FM network. The operational TSM can be implemented as a stand-alone system to exploit the serial nature of TDMA operation; however, it must employ existing CSM input/output capabilities to satisfy operator interface and long-term data collection requirements. This would have the advantage of centralizing the monitoring functions without imposing severe restrictions on either system. Figure 12 shows an example of such a system using a microprocessor controller for the TSM. The configuration is similar to that of Figure 6, except for the simplification of the control computer and removal of peripheral input/output devices. In this system, the TSM function is a stand-alone monitor controlled by the microprocessor system which has been operator

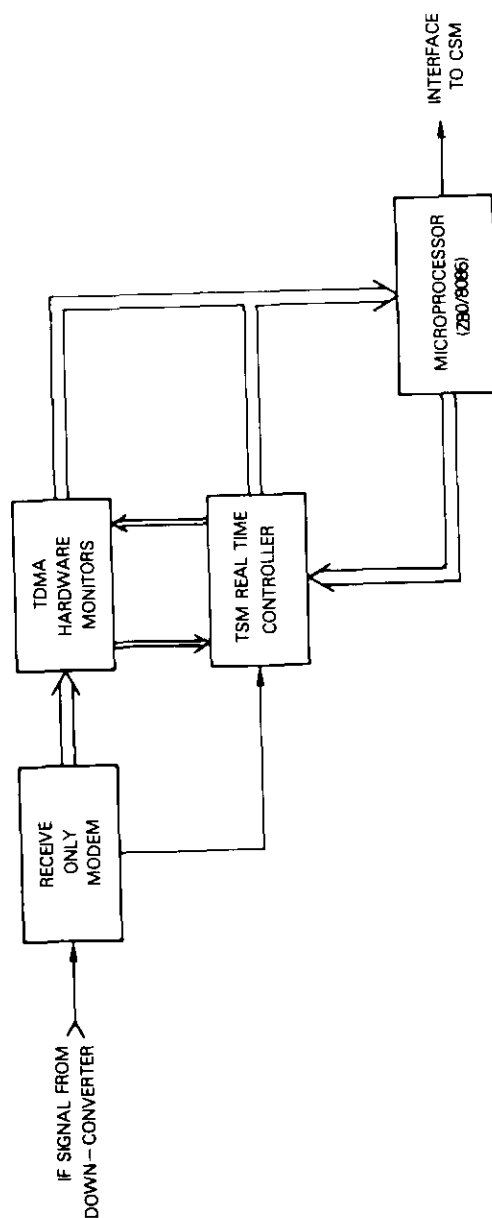


Figure 12. Operational TSM Configuration

programmed via the CSM's computer system. Interface to the CSM is identical to that of any other standard test equipment used by the CSM except that a TSM interrupt capability is included to allow the TSM to control the operating console for alarm monitoring purposes. Sufficient data storage and processing capability are provided in the TSM's microprocessor controller to allow the maintenance of short-term historical data files for use in the event of network difficulties and to perform required individual monitor programming and raw data reduction.

Conclusion

The requirements for monitoring the overall performance of a TDMA network within the INTELSAT system have been examined. Techniques for performing real-time monitoring of critical parameters have been enumerated, and their operational feasibility verified by implementing and testing a breadboard model during recent INTELSAT TDMA field trials. Based on this experience, a TDMA monitor system has been recommended which measures and reports, in real time, data on TDMA frame periods, satellite down-link noise levels, receive frequency, BER, and individual transmit burst positions. Future implementation of TSM equipment can easily provide the necessary monitoring capability using existing technology.

References

- [1] E. E. Steinbrecher and L. F. Gray, "A Computer-Controlled Satellite Signal Monitoring System," *COMSAT Technical Review*, Vol. 1, No. 1, Fall 1971, pp. 79-116.
- [2] D. J. Gooding, "Performance Monitor Techniques for Digital Receivers Based on Extrapolation of Error Rate," *IEEE Transactions on Communications Technology*, COM-16, June 1968, pp. 380-387.
- [3] B. J. Leon et al., "A Bit Error Rate Monitor for Digital PSK Links," *IEEE Transactions on Communications*, COM-23, No. 5, May 1975, pp. 518-525.
- [4] D. J. Schaefer et al., "Simulation and Performance Assessment of a Digital Communications Link by Hybrid Computer," National Telecommunications Conference, Dallas, Texas, November 1976.
- [5] J. L. Hammond et al., "Methods of Monitoring and Fault Isolation for Digital Communication Links," National Telecommunications Conference, Dallas, Texas, November 1976.



Daniel J. Schaefer received a B.S.E.E. degree from Iowa State University in 1966, and M.S.E.E. and Ph.D. degrees from Purdue University in 1969 and 1975, respectively. Before joining COMSAT in 1975, he was with ITT responsible for the development of VHF/UHF communications equipment. Presently, he is Assistant Manager of the Multiple Access and Digital Techniques Department, engaged in the research and development of digital signal processing and multiple-access techniques applied to satellite communications. Dr. Schaefer

is a senior member of IEEE.

Index: phase shift keying, time-division multiple access, modem, design criteria

TDMA modem design criteria

C. J. WOLEJSZA AND D. CHAKRABORTY

(Manuscript received September 5, 1979)

Abstract

This paper summarizes the major aspects of modem design for time-division multiple-access (TDMA) operation. Emphasis is placed on tradeoffs between acquisition speed and performance degradation in the coherence recovery circuits and on methods of achieving efficient spectrum utilization for wideband phase shift keyed (PSK) signals in nonlinear satellite channels. A survey of simulation results is presented, and compromises between the rolloff factor, available bandwidth, and degradations due to the nonlinearity are illustrated.

Filter design, however, is only one of the limiting factors of PSK modem performance. The design of the carrier and clock recovery circuits is also important. Significant losses in the carrier-to-noise ratio arise from channel filtering, nonlinear channel characteristics, and specific methods used for carrier and clock extraction from the modulated signal. Since both carrier and clock recovery networks are adversely affected by the threshold phenomenon known as cycle skipping, high signal-to-noise ratios are usually required to reduce jitter and to provide adequate margin. TDMA frame efficiency requirements dictate that acquisition time be minimized; therefore, critical tradeoffs must be made between the signal-to-noise ratio and response time. Basic equations for carrier and clock recovery circuits are presented to illustrate the criteria for selecting specific circuit components. In particular, large offsets introduced by satellite frequency translators frequently require compensation by automatic frequency control (AFC). An AFC technique available for TDMA is described and design equations are presented.

Advanced demodulation techniques are discussed, including the use of biphas preamble, injection oscillators for signal-to-noise ratio improvement, and an optimum joint estimator/detector for carrier and clock phase and data information extraction.

Introduction

The use of time-division multiple-access (TDMA) wideband satellite communications systems introduces a number of system constraints and design tradeoffs which affect the digital modems. In general, a single TDMA carrier is present in a transponder at a given time. Efficiency considerations require maximum available power utilization and hence nonlinear operation of the spacecraft TWTA and possibly the earth station HPA. In addition, adjacent channel interference requires narrowband channel filtering and good spectrum control. Finally, for operation at 12 and 14 GHz, different up-link fades at different sites with large burst-to-burst signal level variations are likely.

Key design criteria for high-speed TDMA modems include the following:

- a. modem transmit/receive filter analysis and optimization for nonlinear operation and adjacent channel interference [1], [2];
- b. carrier acquisition/steady-state tradeoffs with operation at threshold signal-to-noise (S/N) ratio [3];
- c. automatic frequency control in the burst mode [3];
- d. clock acquisition/steady-state tradeoffs at threshold S/N ratio [4], [5];
- e. automatic gain control design considerations in a fading or low-duty-cycle environment.

Each of these items requires considerable analysis and tradeoffs between conflicting requirements. The specific modem design parameters depend on the system configuration and the specified performance goals. The configuration which will be considered is typical of the INTELSAT system. Figure 1 shows the PSK modulator with low-pass transmit modem filters, a typical up-chain with adjacent carrier interference at the spacecraft input. Additional adjacent channel interference may occur due to adjacent transponders, but this contribution is reduced by the spacecraft filters. The down-chain, which is common to all bursts, includes the modem receive filter.

The key factors in the channel which affect modem design and performance are the nonlinear characteristics of the earth station high-power amplifier (HPA) and the satellite traveling wave tube amplifier

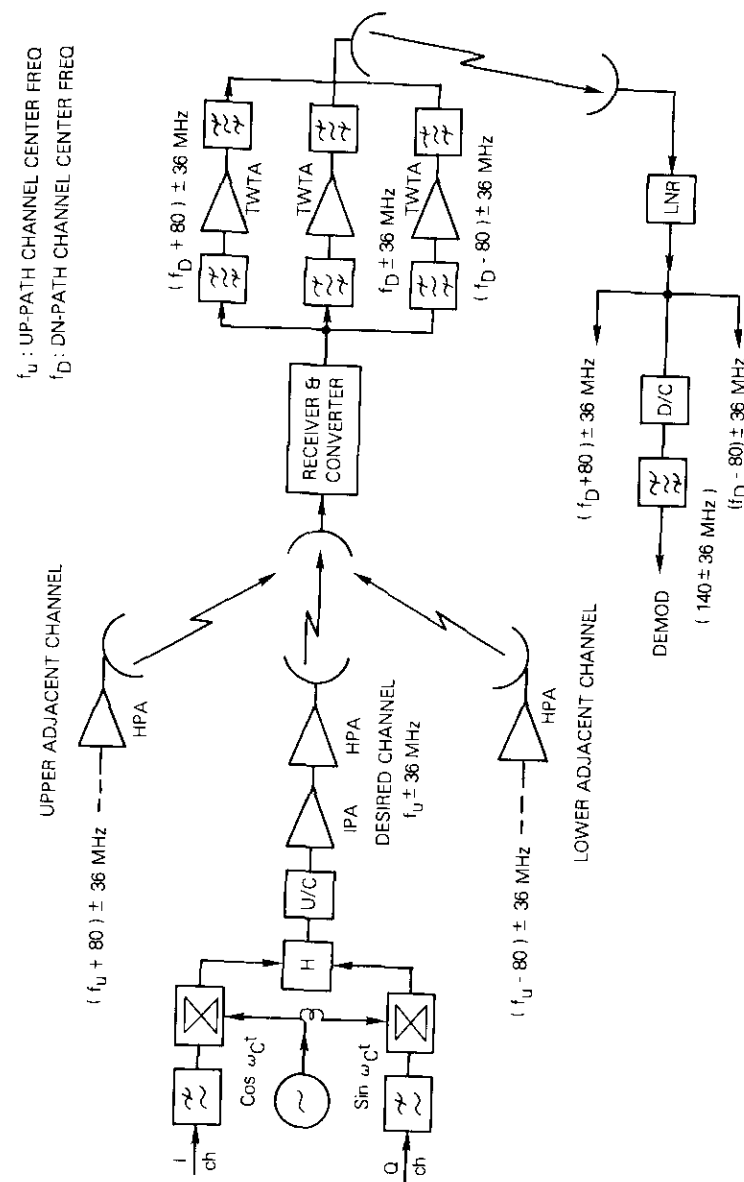


Figure 1. Basic Block Diagram of the Satellite Channel Model

(TWTA). Typical amplitude and phase characteristics of these devices are given in Figure 2. In terms of modem design, the only "designable" elements shown in Figure 1 are transmit and receive modem filters. The following sections consider each design area in more detail and summarize the design issues and methods necessary for complete TDMA modem design.

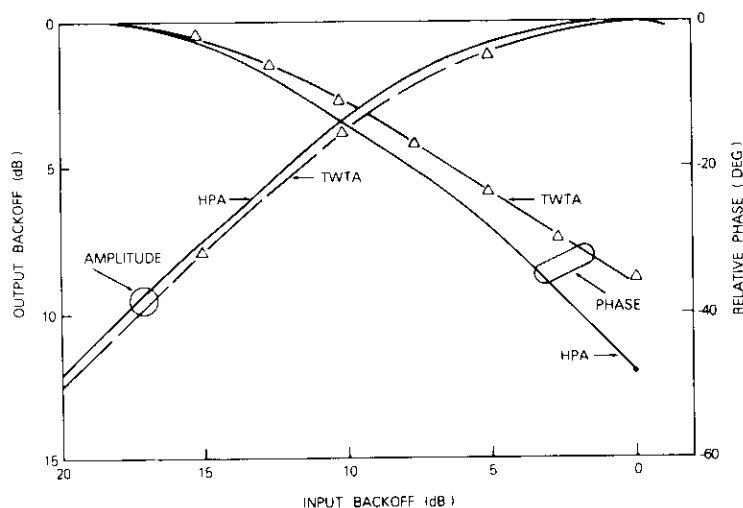


Figure 2. Measured Amplitude and Phase Characteristics of a Typical Earth Station HPA and Transponder TWTA

Channel filter analysis and optimization

When the modem filters for a nonlinear satellite transponder are selected, conflicting factors such as intersymbol interference, out-of-band emission, and thermal noise rejection need to be considered. When the earth station HPA and/or the satellite transponder TWTA is operated at or near saturation, the ensuing PSK spectrum regeneration produces spillover of sidelobe energy in adjacent transponders. Suppression of the regenerated sidelobe from the HPA cannot be controlled by the modem filters (transmit and receive, as shown in Figure 1). Additional filters at the output of the HPA and a sharper filter at the transponder output will eliminate the effect of adjacent channel interference arising from spectral regrowth, but will not be considered in this paper. These factors will now be examined and optimal solutions for the QPSK modem filters will be derived.

Transmit filter optimization

Large values of transmit BT product are preferable in terms of intersymbol interference. However, for a frequency plan which is critically sensitive to adjacent channel interference, specific transmit filter constraints must be considered. These constraints are outlined in INTELSAT specifications and discussed in the following:

a. *Criterion I (excluding bandwidth by the HPA).* The out-of-band emission (energy outside the desired band) must be ≤ 4 dBW/4 kHz beyond the transponder band.

b. *Criterion II (including bandwidth by the HPA).* The out-of-band emission (energy outside the desired band) must be ≤ 24.5 dBW/4 kHz beyond the transponder band.

The earth station installation normally does not provide any filtering at the output of the HPA; consequently, when the HPA is operated close to saturation, out-of-band sidelobes will be generated. Transmit filters at the modulator cannot control the regenerated sidelobe level. The sidelobe level and resulting out-of-band emission are controlled by the operating point of the HPA and the HPA output filter (if provided). In view of these considerations, the modulator transmit filter rolloff should be designed by assuming a 14-dB HPA input backoff whereby the regenerated sidelobe level is negligible. When the HPA must be operated at higher drive levels, an HPA output filter will also be required to suppress the regenerated sidelobes. Operation of the HPA up to saturation (without this filter) will also be discussed in this paper.

The conventional QPSK modem filter combination* in a linear environment is a Nyquist filter at the modulator which introduces spectrum shaping to compensate the input $(\sin x/x)$ spectrum, resulting in a flat spectrum over most of the band of signal energy. A maximally flat amplitude and delay-equalized receive matched filter will then result in smooth, well-defined phase and amplitude variations in the demodulator, thus minimizing intersymbol interference. A typical Nyquist filter combination has the raised cosine filter characteristic:

*In theory, square-root Nyquist and cosine roll-off type filters at the transmitter and the receiver provide zero intersymbol interference at the sampling time. Because of its relative ease of implementation, the Nyquist transmit filter with a maximally flat receiver filter is emphasized in this paper. When phase and timing errors are considered, a special subclass of Nyquist filter provides optimal performance [6], but these filters are difficult to implement in a narrowband channel.

$$\begin{aligned}
 T(\omega)R(\omega)S(\omega) &= 1, & |\omega| < (1 - \gamma)\omega_c \\
 &= \cos^2 \frac{\pi}{4} \frac{\omega - (1 - \gamma)\omega_c}{\gamma\omega_c}, & (1 - \gamma)\omega_c < |\omega| < (1 + \gamma)\omega_c \\
 &= 0, & |\omega| > (1 + \gamma)\omega_c
 \end{aligned} \quad (1)$$

where $T(\omega)$ = amplitude characteristic of the transmit filter
 $R(\omega)$ = amplitude characteristic of the receive filter
 $S(\omega)$ = transmit signal spectrum
 $\omega_c = 2\pi f_c$ = half-symbol angular frequency
 γ = roll-off factor.

In a nonlinear environment, the original spectrum $S(\omega)$ is almost completely regenerated after each nonlinear operation; hence, near Nyquist filters would be required for amplitude compensation after each nonlinearity to maintain the spectral shape given by equation (1). In a real system, if the HPA is operated in a nonlinear region, the regenerated spectrum is deformed by the transponder input filter, and the resulting deformed spectrum is further amplified and distorted by the transponder output multiplexer filter. Thus, a matched filter at the receiver as defined in equation (1) fails to produce the smooth, well-defined phase and amplitude variation needed in the demodulator, and the condition of minimum intersymbol interference is invalidated. Since the principle of superposition is also not applicable in this case, the designer must use computer simulation and analysis to find good near-optimum filter combinations for nonlinear channels [1].

Two categories of filter have been considered for this "optimization": an amplitude-shaping Nyquist type filter with $x/\sin x$ shaping and a maximally passband flat (elliptic) filter. The out-of-band emission characteristics of a QPSK channel using the Nyquist transmit filter are shown in Figure 3, which gives the band edge* radiated power per 4 kHz as a function of the rolloff factor. Similar characteristics for a fifth-order elliptic filter are shown in Figure 4, which gives the band edge out-of-band emission as a function of the BT product. As indicated by Figures 3 and 4, the transmit filter must be very sharp to satisfy both INTELSAT criteria. For example, the BT product of the elliptic function transmit filter must be less than unity to satisfy both criteria. For a BT product less than unity, the channel performance degradation

*For a 120-Mbit/s carrier, band edge is assumed to be at 40 MHz from the center of the carrier.

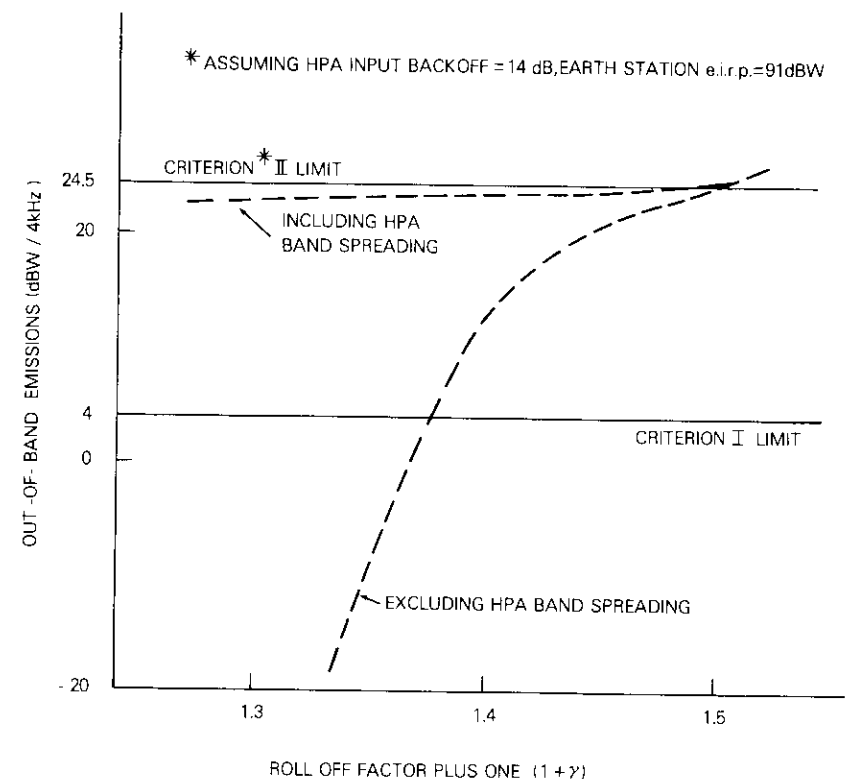


Figure 3. Out-of-Band Emission vs Transmit Filter Rolloff Factor

increases rapidly because of excessive intersymbol interference, and when the BT product exceeds unity, INTELSAT Criterion I is violated.

This problem will be further accentuated in a nonlinear channel in which strict band limitation prior to the nonlinear amplifier is not beneficial. Therefore, it is believed that Criterion I (formulated specifically for FM multicarrier operation) should be relaxed. The present study is based on satisfying only Criterion II, which includes spectrum spreading due to the HPA when operated at 14-dB input backoff. The characteristics of the two classes of transmit filter under consideration are given in Table 1 (from Figures 3 and 4). These parameter limits represent the maximum values which will permit Criterion II to be satisfied.

Spectrum regeneration

Despite initial filtering, nonlinear elements in the channel cause sidelobe regeneration and spectrum distortion. Hence, it is necessary

TABLE 1. TRANSMIT FILTER PARAMETER LIMITS (satisfying Criterion II)

Modulation	Filter Type	Maximum Value of Parameter
PSK	Nyquist Shaping Filter	$\gamma = 0.45$ (rolloff factor)
PSK	Elliptic Filter ($n = 5$)	$BT = 1.04$

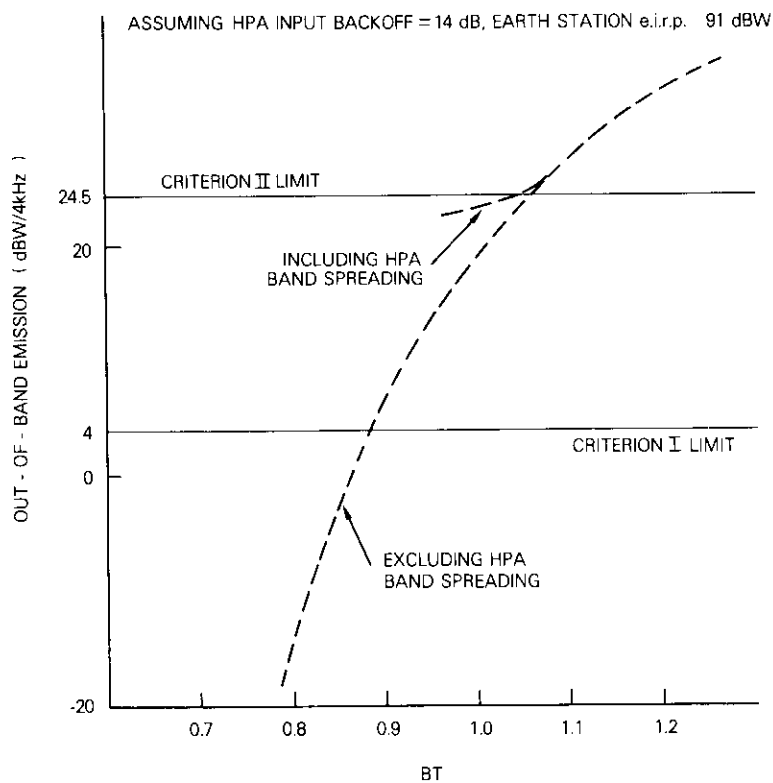


Figure 4. Out-of-Band Emission vs Transmit Filter BT Product

to examine the effect of nonlinearity on band-limited PSK signal power spectra.

The power spectra have been computed by the computer simulation channel program (CHAMP) [7]. Specifically, the computations are performed by averaging modified periodograms obtained by taking the discrete Fourier transform (FFT in this case) of consecutive records of

the signal after weighting by an appropriate data window. The computed power spectra of the 120-Mbit/s QPSK modulation format are shown in Figure 5 for a modulator band-limiting network, namely, a cosine rolloff Nyquist filter with 45-percent rolloff (maximum parameter value) and a nonlinear device (HPA) operating in tandem at different input backoff points, including saturation. The band-limiting network used in this spectrum analysis is based upon an INTELSAT V channel configuration, where an 80-MHz RF slot separation is allocated between center frequencies of two adjacent transponders and the usable channel bandwidth is 72 MHz. Figure 5 indicates that the INTELSAT out-of-band emission Criterion II is satisfied only at 14-dB HPA input backoff. When the HPA is operating at or near saturation, the above criterion is violated, unless an output (HPA) filter is used.

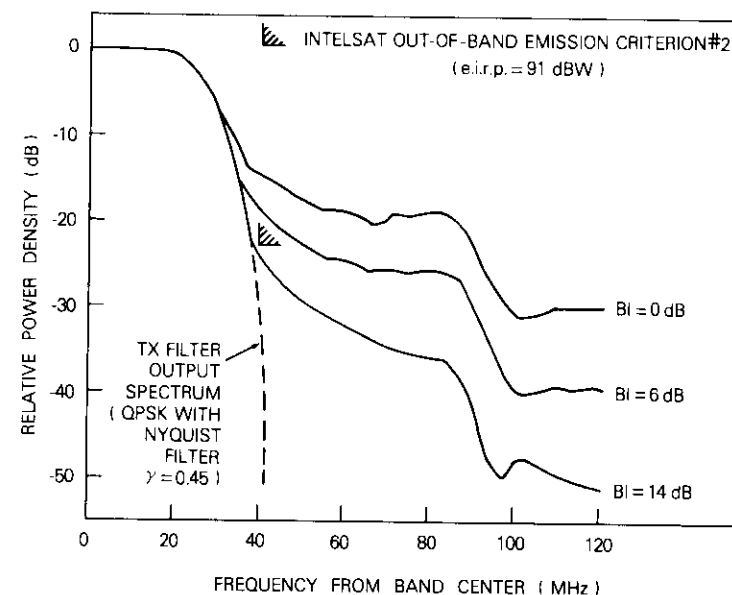


Figure 5. Out-of-Band Emission at HPA Output for Various Input Backoff Levels (optimized channel for QPSK)

Receive filter optimization

Transmit filter parameters must be chosen to satisfy the out-of-band emission criteria and, as noted above, to yield the softest rolloff.

Essentially, the receive filter restricts the excess thermal noise. The receive filter parameter has been optimized for two different types of transmit filters under examination: a Nyquist shaping filter and a flat passband elliptic filter.

This optimization is conducted in the computer simulated channel. The computed equivalent power loss of a QPSK channel (at constant bit-error rate) above ideal channel performance is shown in Figure 6, which gives the power loss as a function of receive BT product of a 5-pole elliptic function filter. The transmit filter is a Nyquist type filter with the maximum parameter value of 45-percent cosine rolloff. In the second case, the transmit filter is of the elliptic function type with a

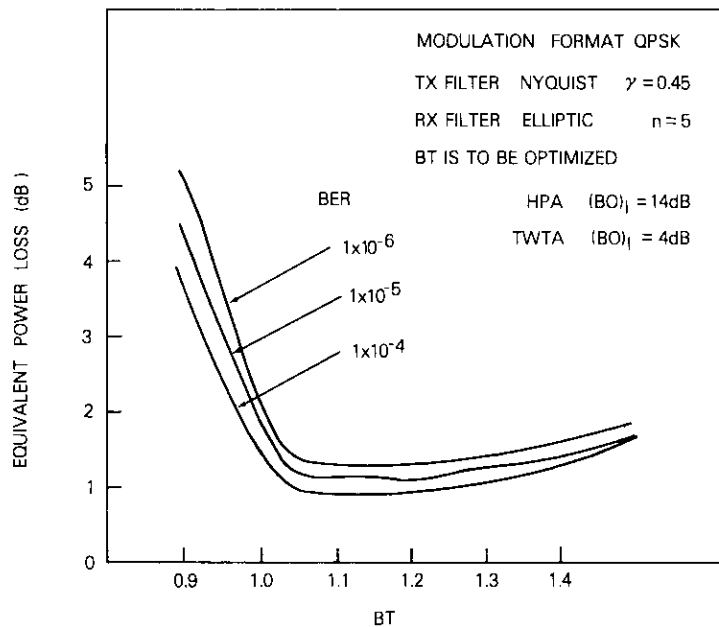


Figure 6. Optimization of Receive Filter BT Product (equivalent power loss above an ideal performance vs BT product)

BT product of 1.04 and $n = 5$ (poles). The equivalent power loss above an ideal channel performance is shown in Figure 7, which plots the power loss as a function of rolloff factor for the Nyquist-type receiver filter. In both cases, the HPA input backoff is set at 14 dB, and that of the transponder TWTA is set at 4 dB using the unmodulated carrier to

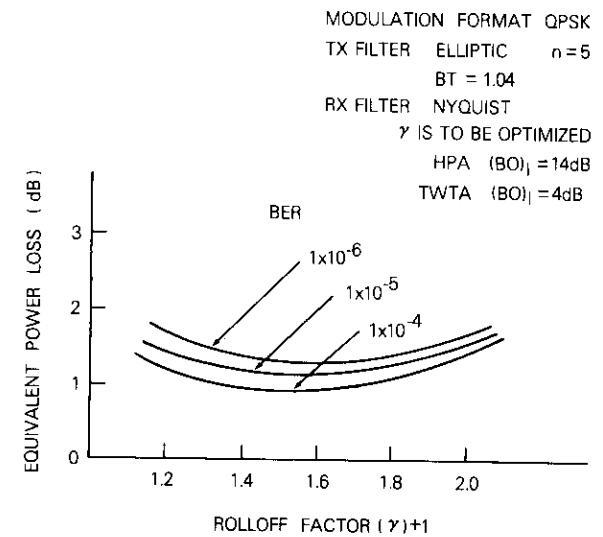


Figure 7. Optimization of Receive Filter Rolloff Factor (equivalent power loss above an ideal performance vs rolloff factor)

set the operating point. The latter operating point was selected on the basis of prior experience [8] as a likely operating point to provide overall system optimization.

The results of Figures 6 and 7 indicate that, in the optimized region of the receive filter, the difference in the channel performance of these two sets of channel filter combinations is insignificant for the operating conditions of the HPA and the TWTA under consideration. Results of other HPA and TWTA operating combinations are discussed subsequently.

Sensitivity of modem performance to operating point

It is difficult, especially in the presence of fading, to maintain the optimum operating point for all conditions; therefore, it is useful to study the performance sensitivity in terms of the selection of the HPA operating point and the setting of the transponder TWTA. Channel performance has been analyzed for different combinations of HPA* and

*It should be noted that, if the HPA is operated nearer to saturation, the INTELSAT specification on out-of-band emission will be violated unless a filter is provided at the output of the HPA.

TWTA input backoff points for the two sets of transmit and receive filter combinations referenced above. The results are shown in Table 2, where the transmit filter is of the Nyquist type and the receive filter is of the elliptic function type optimized for $BT = 1.13$. Similarly, Table 3 shows the results for an elliptic function type transmit filter and a receive Nyquist type filter with an optimized rolloff factor of 0.6. These selections were based upon maintaining an overall Nyquist shape and minimizing the number of computations. The data shown in Tables 2 and 3 are summarized in Figure 8, where the equivalent power loss of the coherent PSK (CPSK) channel above an ideal channel performance at BER of 1×10^{-4} is shown as a function of HPA/TWTA operating point

TABLE 2. EQUIVALENT POWER LOSS AT VARIOUS OPERATING CONDITIONS FOR OPTIMIZED CPSK CHANNEL WITH NYQUIST TRANSMIT FILTER

HPA Input Backoff (dB)	Power Loss (dB)								
	0-dB Transponder TWTA Input Backoff			4-dB Transponder TWTA Input Backoff			14-dB Transponder TWTA Input Backoff		
	1×10^{-4} BER	1×10^{-5} BER	1×10^{-6} BER	1×10^{-4} BER	1×10^{-5} BER	1×10^{-6} BER	1×10^{-4} BER	1×10^{-5} BER	1×10^{-6} BER
0	1.92	2.37	2.71	—	—	—	—	—	—
6	1.11	1.35	1.52	1.02	1.22	1.37	—	—	—
14	0.91	1.09	1.23	0.89	1.09	1.28	0.53	0.62	0.71

TABLE 3. EQUIVALENT POWER LOSS AT VARIOUS OPERATING CONDITIONS FOR OPTIMIZED CPSK CHANNEL WITH ELLIPTIC FUNCTION TRANSMIT FILTER

HPA Input Backoff (dB)	Power Loss (dB)								
	0-dB Transponder TWTA Input Backoff			4-dB Transponder TWTA Input Backoff			14-dB Transponder TWTA Input Backoff		
	1×10^{-4} BER	1×10^{-5} BER	1×10^{-6} BER	1×10^{-4} BER	1×10^{-5} BER	1×10^{-6} BER	1×10^{-4} BER	1×10^{-5} BER	1×10^{-6} BER
0	1.65	1.97	2.24	—	—	—	—	—	—
6	1.10	1.30	1.44	1.01	1.21	1.35	—	—	—
14	0.91	1.07	1.19	0.96	1.15	1.31	0.74	0.88	0.98

(input backoff) for the two categories of transmit and receive filter combinations.

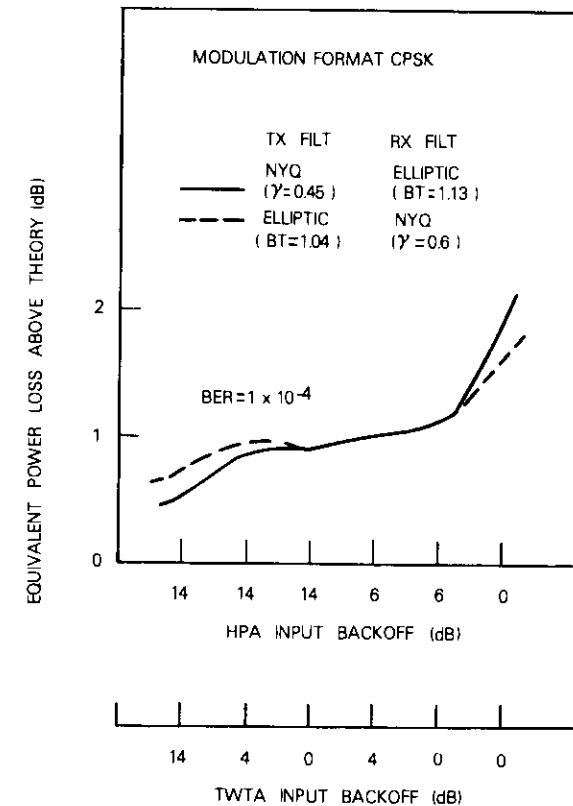


Figure 8. Performance Comparison for Two Different Filter Combinations

Figure 8 shows that, for cascaded amplifier operation at moderate (14- to 4-dB) input backoffs, the Nyquist transmit-elliptic receive filter combination offers a better solution. On the other hand, for cascaded, heavily nonlinear amplifiers, the flat passband, elliptic transmit-Nyquist receive filter combination yields better channel performance. For intermediate cases of cascaded nonlinearities (4- to 6-dB input backoffs), the choice of either filter combination does not result in significant changes in performance.

Coherence recovery design issues

To reduce the number of cases considered, it is assumed that a preamble of the form $0, \pi, 0, \pi, \dots$, is used. This preamble, after filtering and processing, represents the worst possible case in terms of carrier recovery circuit performance. It is also, however, the best possible case for the timing recovery circuit. This case will be used because two common alternatives for timing recovery patterns, $0, 0, \pi, \pi, \dots$, and $0, \pi/2, 0, \pi/2, \dots$, result in at least a 3-dB loss in timing recovery performance. Other preambles may be considered. However, the selected preamble has certain advantages in that the effects of the nonlinearity on its performance can be determined through a relatively straightforward method.

For the carrier recovery circuit (CRC), the technique to be considered, shown in Figure 9, is the classical frequency multiplication by 4 with a bandpass filter followed by division by 4. It is assumed that the carrier recovery circuit has built-in automatic frequency control of the incoming signal and reduces frequency uncertainty by use of frequency feedback [3]. A long time constant (many frames) is assumed for the AFC circuit. For the timing recovery circuit (TRC), the technique shown in Figure 10 is the classical half-symbol delay with binary detection. This is expected to give approximately the best possible signal-to-noise ratio for the assumed preamble although a square law detector has been suggested as an alternative [9]. A bandpass filter and a limiter are used to improve the signal-to-noise ratio and to provide the digital clock signal required by the bit detection circuitry.

Analysis of carrier recovery circuit performance

The carrier recovery circuit noise performance will be analyzed in two parts. The first part will consider the degradation which occurs because of the system components during the preamble portion of the burst; the second part will determine the degradation in carrier S/N ratio during the data portion of the burst. When these limitations are defined, specific calculations of degradation in modem performance will be possible for most sources of degradation.

PREAMBLE PORTION OF THE BURST

For the preamble assumed above, the waveform at the output of the PSK modulator (assuming that filtering is performed after the modulation) can be written in the form

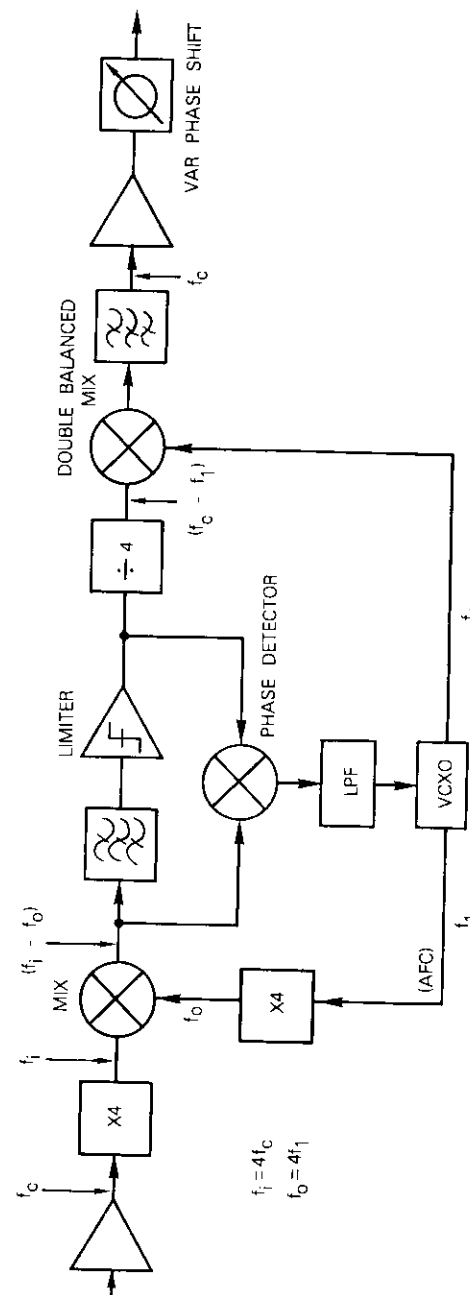


Figure 9. Carrier Recover Circuit Technique

$$m(t) = A d(t) \cos \omega_c t \quad (2)$$

where A = signal amplitude
 $d(t)$ = square wave with amplitude ± 1 and rate $R/4$
 R = bit rate
 ω_c = angular carrier frequency.

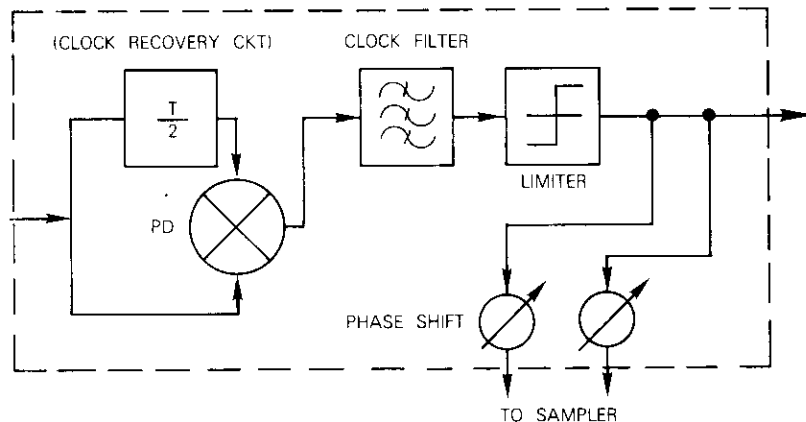


Figure 10. Timing Recovery Circuit Technique

Using a Fourier series expansion for the square wave yields

$$m(t) = A \frac{4}{\pi} \left\{ \cos \Delta\omega t - \frac{1}{3} \cos 3\Delta\omega t + \frac{1}{5} \cos 5\Delta\omega t - \dots \right\} \cdot \cos \omega_c t \quad (3)$$

where $\Delta\omega = \pi R/2$. Thus, the modulated signal during the preamble, before filtering, can be represented as a suppressed carrier amplitude modulated signal with an infinite number of discrete harmonically related components at spacings equal to odd multiples of half the symbol rate. The transmit filter characteristics given earlier indicate that very little attenuation of the principal sidebands is caused by the transmit filter. However, the third harmonic components occur at a point at which the modem transmit filter has an attenuation greater than 26 dB; at the fifth harmonic the attenuation is even greater. Therefore, the input to the earth station HPA consists primarily of the two components closest to the carrier:

$$m(t) \cong \frac{4A}{\pi} \cos \Delta\omega t \cos \omega_c t \quad (4)$$

EFFECTS OF THE NONLINEARITIES

Since the input to the HPA during the preamble is essentially a 2-carrier signal, the 2-carrier characteristic curve of the HPA may be used to determine the magnitude of the components at the output. A typical experimental characteristic is shown in Figure 11 [10]. From this figure, it can be concluded that the loss in aggregate power (referred to the unmodulated level used as the E_b/N_o reference), when the HPA is operating near saturation, will range from 1.2 to 1.8 dB for the preamble portion of the burst for backoffs from 0 to 6 dB. This is because energy in the two components of the modulated signal is partly transformed by the nonlinearity to out-of-band components. These out-of-band components are again rejected by the satellite input filters. Therefore, the input to the satellite TWTA during the preamble also consists of a 2-carrier signal of the form given in equation (4). It may be expected, therefore, that 1.2- to 1.8-dB loss in aggregate power relative to the unmodulated single-carrier power is also introduced by the satellite TWTA. Thus, regardless of the up- and down-path signal-to-noise ratio, a total loss of about 1.2 to 1.8 dB due to nonlinear operation should be assumed during the preamble. It should be noted that, in the 2-carrier case, this suppression of aggregate power occurs in the range of 6- or 7-dB input backoff up to single-carrier saturation. Above single-carrier saturation the loss in aggregate power appears to increase over this previously defined value.

After passing through the satellite TWTA, the 2-carrier components of the preamble with the regenerated sidebands caused by the nonlinearity will pass through the transponder output filter and the modem receive filter again, effectively removing the sidebands from consideration. However, the modem receive filter is narrower than all previous filters in the system; in fact, the principal component present during the preamble can be attenuated by up to 2 dB by the modem receive filter.* Therefore, during the preamble, a reduction of up to 2 dB relative to band center in S/N ratio is introduced by the receive filter in addition to that introduced by the nonlinear distortion mechanism. It should be noted that the receive filter also determines the noise bandwidth of the receiver and therefore the aggregate noise power level seen by the carrier recovery circuits.

*It should be noted that the filter preceding the carrier recovery circuit need not be the Nyquist receive filter discussed previously since the attenuation of this component by a Nyquist filter could be 6 dB.

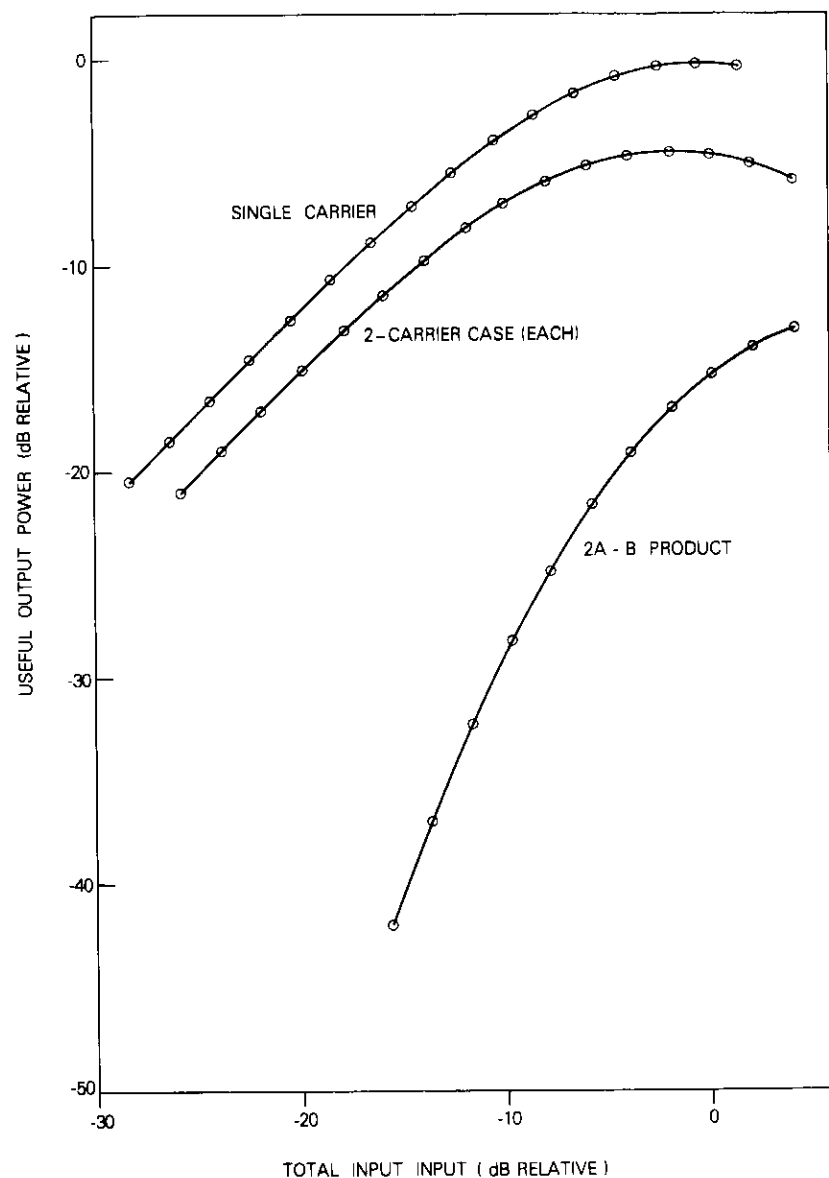


Figure 11. Single-Carrier and 2-Equal-Carrier Transfer Characteristics

EFFECTS OF CARRIER REGENERATION

In the carrier recovery technique shown in Figure 9, the first operation performed on the receive signal to extract the carrier is frequency multiplication by 4, which is usually implemented by cascading two square law devices. It is well known that a loss in S/N ratio occurs in the square law device. This degradation is first determined by the single-carrier method to obtain the effective noise power; then, the 2-carrier case is considered to determine loss in carrier power introduced by the preamble modulation and filtering.

The S/N ratio at the second harmonic frequency at the output of one of the square law devices in the $\times 4$ circuit is given by [11]

$$(S/N)_o = \frac{(S/N)_i^2}{2 + 4(S/N)_i} \approx \frac{(S/N)_i}{4} \quad (5)$$

where $(S/N)_i$ = input signal-to-noise ratio
 $(S/N)_o$ = output signal-to-noise ratio.

For frequency multiplication by 4, this degradation is introduced twice. For large $(S/N)_i$, the total loss is at least 12 dB.

To determine the effects of the square law device on the 2-carrier case, consider the input signal

$$r(t) = \frac{4A_R}{\pi} \cos \Delta\omega t \cos \omega_c t \quad (6)$$

where A_R is the effective receive signal level. At the output of the square law device the signal takes the form

$$r^2(t) = \frac{16A_R^2}{\pi^2} \cos^2 \Delta\omega t \cos^2 \omega_c t \quad (7)$$

Rearranging in terms of trigonometric identities yields

$$r^2(t) = \frac{16A_R^2}{\pi^2} \frac{1 + \cos 2\Delta\omega t}{2} \frac{1 + \cos 2\omega_c t}{2} \quad (8)$$

or

$$r^2(t) = \frac{16A_R^2}{\pi^2} \cdot \left(\frac{1 + \cos 2\Delta\omega t + \cos 2\omega_c t + \cos 2\Delta\omega t \cdot \cos 2\omega_c t}{4} \right) \quad (9)$$

The amplitude of the desired second harmonic term is therefore given by

$$A'_{2H} = \frac{4A_R^2}{\pi^2} \quad (10)$$

By the same procedure, the amplitude of the unmodulated signal which would be produced by the square law device at the second harmonic is given by

$$A_{2H} = \frac{A_R^2}{2} \quad (11)$$

Therefore the ratio of signal amplitude for the 2-component case to that for the unmodulated case is

$$R_L = \frac{8}{\pi^2} \quad (12)$$

Since the second square law device acts on a single component, the total loss in signal-to-noise ratio caused by the first frequency doubling given by equation (12) is approximately 1.8 dB. It should be noted that all of the other components produced by the first frequency doubling fall at points substantially separated from the desired second harmonic.

DATA PORTION OF THE BURST

During the data portion of the burst, it is assumed that the modulation on the carrier consists of completely independent symbols which assume all of the four possible phases in random order with no correlation before or after a particular symbol. Therefore, analysis of the nonlinear system is very difficult, particularly because the modem and satellite filters introduce memory into the system which produces both intersymbol interference and a very complicated envelope structure at the input to the nonlinear amplifiers. Because of these analytical

problems, data from previous modem designs will be used to estimate the degradation in carrier recovery circuit performance during the data portion of the burst.

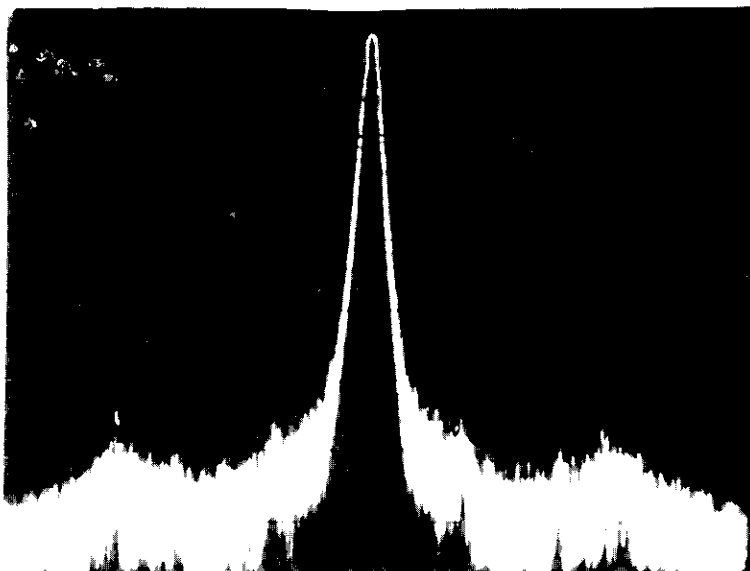
FILTERING AND REGENERATION LOSS

It is well known that filtering alone causes loss in S/N ratio of the regenerated carrier when data are present. Figure 12 shows the actual output of the $\times 4$ frequency multiplier of the carrier recovery circuit of a practical modem operating at 49 Mbit/s. For this modem, a 5-pole Bessel type transmit filter is used with a 6-pole maximally flat receive filter. The bandwidths of these filters are relatively broad compared to the signal spectrum, and have relatively slow rolloffs. These measured results are therefore assumed to be typical for a burst modem operating in a wide bandwidth. For a narrow bandwidth system, more degradation may be expected.

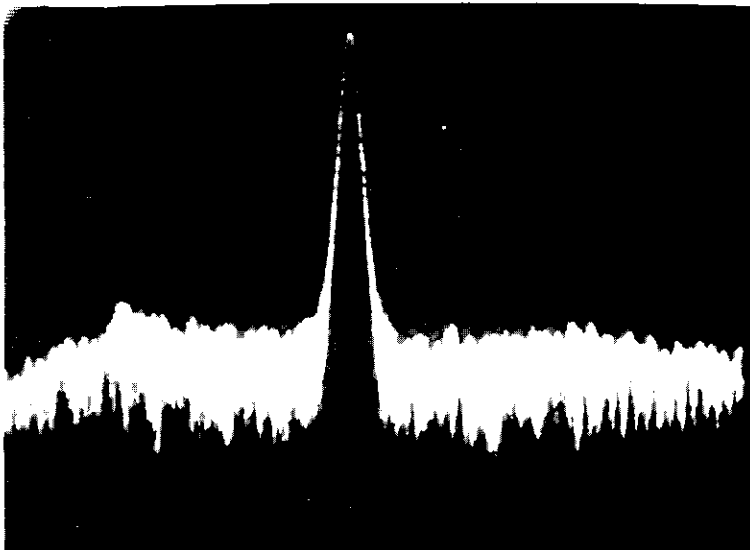
Three cases are shown in Figure 12. Case A is the continuous unmodulated carrier with no noise in the system, case B shows the signal-to-noise density ratio with only modulation present, and case C shows the signal-to-noise density ratio with modulation and noise in the system at a carrier-to-noise (C/N) of 12 dB in 33 MHz. Comparisons of these photographs indicate that the presence of modulation introduces a noise component, called pattern noise, which is, in this case, of the same order of magnitude as the thermal noise component and which is totally independent of the S/N ratio on the channel. This pattern noise will decrease the effective overall S/N ratio of the recovered carrier.

It should also be noted that the presence of modulation on the carrier reduces the recovered carrier component as shown in Figures 12b and 12c by about 2 dB. This reduction in carrier power results in an additional loss of 2 dB in signal-to-thermal noise power.

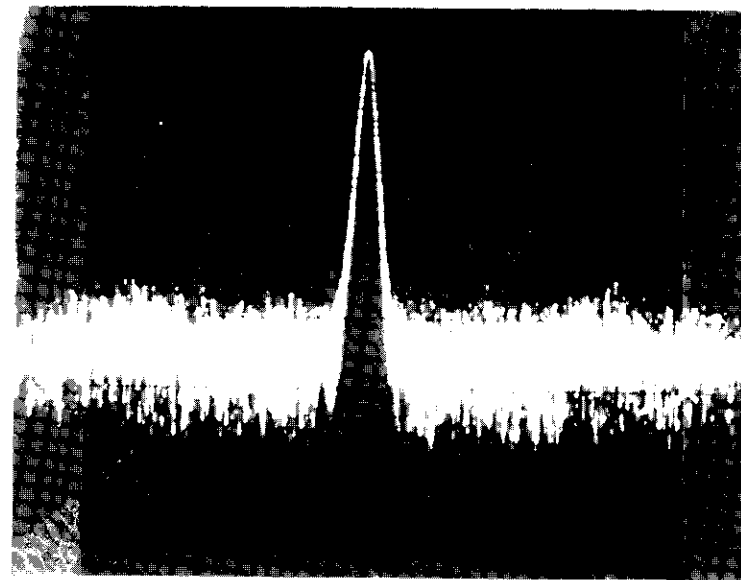
For the general case the actual signal to pattern noise will probably be a function of the filter rolloff. For practical filter bandwidths it is expected to be a significant contributor to the degradation of the overall receive S/N. To estimate this degradation, it will be assumed that the carrier-to-pattern noise ratio shown in Figure 13 is typical of most modems and will be scaled to the input bandwidth. (This is only an equivalent S/N ratio which will be scaled to the bandwidth of the carrier recovery filter, since the pattern noise spectrum is expected to differ significantly from the flat noise spectrum. However, the pattern noise spectrum is flat within the bandwidth of the carrier recovery



a. Unmodulated Carrier (no noise, power level = -10 dBm)



b. Modulated Carrier (no noise, power level = -12 dBm)

Figure 12. Output of $\times 4$ Frequency Multiplierc. Modulated Carrier ($C/N = 12$ dB in 33 MHz, power level = -12 dBm)Figure 12. Output of $\times 4$ Frequency Multiplier

filter.) The net equivalent S/N ratio, as a first-order approximation, is given by

$$S/N_{eq} \approx [(S/N_{th})^{-1} + (S/N_p)^{-1}]^{-1} \quad (13)$$

where N_{th} = thermal noise power
 N_p = pattern noise power
 S = signal power
 N_{eq} = equivalent noise power.

EFFECTS OF THE NONLINEARITIES

The losses incurred in the carrier recovery circuit caused by the passage of the data modulated signal through the channel nonlinearities shown in Figure 1 are much more difficult to analyze. It is expected that, because of envelope variation introduced by the various filters in the system and the AM-PM transfer effect, unwanted phase modulation will be introduced on the carrier component. This will degrade the carrier recovery S/N ratio and may increase the pattern noise component.

No measured data or analytical results are yet available to allow a precise estimation of this degradation. However, in the preamble section above, the degradation in S/N ratio was estimated to be 1.8 dB. Under these conditions, the rate of data transitions is maximum, and consequently the maximum envelope variation occurs. This is the worst-case AM to PM distortion and filter loss. During the data portion of the burst, some symbols will not experience transitions if the following symbol is of the same phase. Further, for QPSK for half the time only 90° transitions will occur with a significantly smaller envelope variation. It will therefore be assumed that the degradation previously calculated for the preamble will also occur during the data portion of the burst. For further calculations it will be assumed that the nonlinearity degradation during the data portion will be 1.8 dB.

Timing recovery circuit (TRC) performance

The analysis of the timing recovery circuit is similar to that of the carrier recovery circuit. In fact, up to the receive filter output, the analysis, including filter and nonlinear losses during the preamble and average power loss during data, are identical to the carrier recovery circuit analysis. The principal difference lies in the clock extraction and filtering circuits. The preamble and data portions of the burst are again considered separately.

PREAMBLE PORTION OF BURST

As discussed earlier, the preamble of the burst essentially consists of two equal components separated by the symbol rate and symmetrically located around the (suppressed) carrier. The losses incurred as the preamble passes through the system up to the receive filter are identical to those already discussed. The form of the signal at the input to the TRC is therefore

$$S(t) = A'_R \cos \Delta\omega t \cos \omega_c t + n_1(t) \cos \omega_c t + n_2(t) \sin \omega_c t \quad (14)$$

where $n_1(t)$ and $n_2(t)$ are zero-mean, narrowband, Gaussian noise processes with $\overline{n_1^2} = \overline{n_2^2} = \sigma_n^2$, and A'_R is the effective received signal level.

The S/N ratio at the input is given by

$$(S/N)_i = \frac{A'_R{}^2/4}{\sigma_n^2} \approx \frac{A'_R{}^2}{2N_o B_{in}} \quad (15)$$

where N_o = power spectral density of the noise
 B_{in} = input noise bandwidth.

Since the timing recovery circuit under discussion uses the half-symbol delay detector and filter technique, the S/N ratio must be determined at the detector output:

$$S(t + T_s/2) = A'_R \cos \Delta\omega \left(t + \frac{T_s}{2}\right) \cos \omega_c \left(t + \frac{T_s}{2}\right) + n_1 \left(t + \frac{T_s}{2}\right) \cos \omega_c \left(t + \frac{T_s}{2}\right) + n_2 \left(t + \frac{T_s}{2}\right) \sin \omega_c \left(t + \frac{T_s}{2}\right) \quad (16)$$

Note that for QPSK

$$\frac{\Delta\omega T_s}{2} = \frac{\pi R T_s}{2} = \frac{\pi}{2}$$

and assume a phase shift (ϕ) such that

$$\cos \left\{ \omega_c \left(t + \frac{T_s}{2}\right) + \phi \right\} = \cos \omega_c t$$

$$\sin \left\{ \omega_c \left(t + \frac{T_s}{2}\right) + \phi \right\} = \sin \omega_c t$$

Assuming that $t' = t + T_s/2$ yields a detector output of the form

$$S(t)S(t') = \{ [A'_R \cos \Delta\omega t \cos \omega_c t + n_1(t) \cos \omega_c t + n_2(t) \sin \omega_c t] \} \{ [A'_R \sin \Delta\omega t \cos \omega_c t + n_1(t') \cos \omega_c t + n_2(t') \sin \omega_c t] \} \quad (17)$$

After multiplying out and collecting terms with only low-frequency components,

$$S(t)S(t') \approx \frac{A'_R{}^2}{4} \sin 2\Delta\omega t + \frac{A'_R n_1(t)}{2} \sin \Delta\omega t + \frac{A'_R n_1(t')}{2} \cos \Delta\omega t + \{ n_1(t)n_1(t') + n_2(t)n_2(t') \} \quad (18)$$

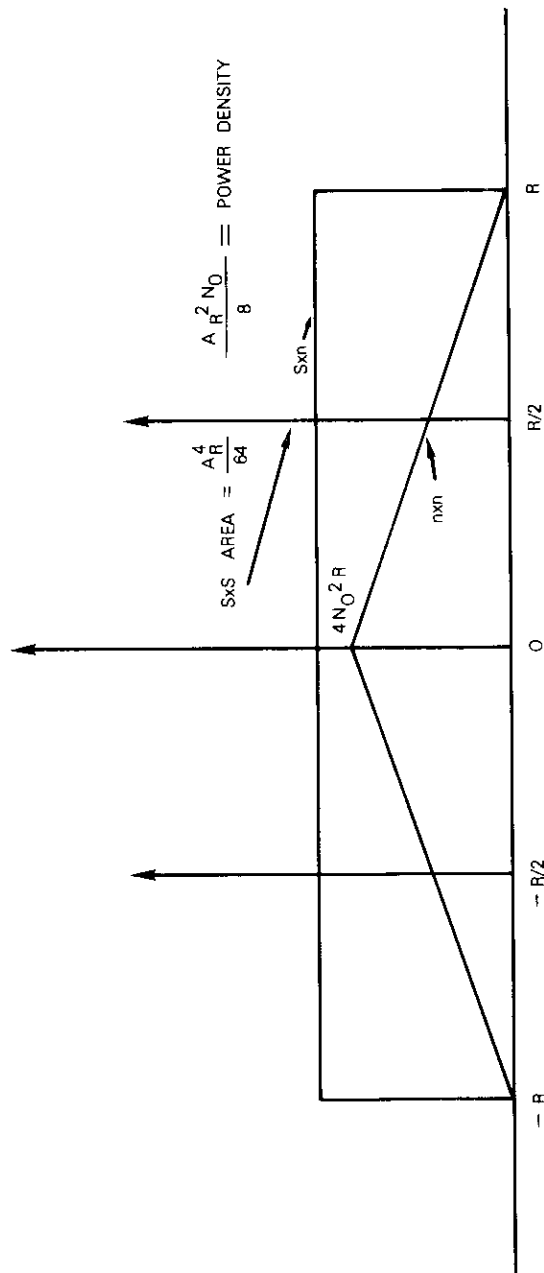


Figure 13. Power Spectrum of Timing Recovery Circuit Output

This signal consists of three parts: the first term represents the signal at the clock frequency, the next two terms represent the signal times noise ($S \times N$) term used in the analysis of square law devices, and the last two terms represent the noise times noise ($N \times N$) terms. The resulting power spectrum then assumes the form shown in Figure 13, assuming that $B_{in} = R$ (biphase psk for example). It can be shown that the S/N ratio of the output clock is of the form

$$(S/N)_o = \frac{(S/N)_i^2}{4(S/N)_i + 32} \quad (19)$$

which is different from that of the square law device. For large $(S/N)_i$, the loss is at least 6 dB. Therefore,

$$(S/N)_F = (S/N)_o \frac{B_{in}}{B_F} \quad (20)$$

where $(S/N)_F$ = final output signal-to-noise ratio at symbol clock
 B_F = timing recovery circuit filter noise bandwidth
 B_{in} = input noise bandwidth.

DATA PORTION OF BURST

During the data portion of the burst, the difficulty of analyzing the clock S/N ratio is compounded by the nonlinear distortion and the randomness of the data transitions. It can be shown that, for an unfiltered psk signal, the clock component during data is 6 dB below the preamble level. Since the previous analysis of the clock S/N ratio during the preamble accounts for the filters and nonlinear amplifier, it will be assumed that the 6-dB loss in power is the only significant additional loss during the data portion of the burst.

Development of design equations for carrier recovery circuit

It is possible to choose a filter bandwidth for the carrier recovery circuit based upon a number of tradeoffs. Once this bandwidth is chosen, it becomes possible to estimate the signal-to-noise ratio in the recovered carrier at the demodulator, the fixed phase shift through this filter introduced by the frequency offset, the errors caused by transients during the acquisition time, and therefore the total degradation in bit-

error performance due to the carrier recovery circuit. The following subsections consider these degradations in some detail.

AFC circuit analysis

In a multiplication-type carrier recovery scheme (Figure 9), the narrowband single-Q bandpass filter located between the mixer and the limiter yields a large phase offset for a small frequency deviation of the incoming signal. This phase offset will perturb the recovered carrier phase, resulting in incorrect decisions. An automatic frequency correction network is therefore essential for high-speed TDMA modems [3].

The phase and amplitude characteristics of a typical single-Q bandpass filter as a function of frequency deviation relative to the center of the band are shown in Figure 14. Figure 15 is an analytical block diagram of the multiplication-type carrier recovery process discussed previously. The design parameters of the AFC loop will now be

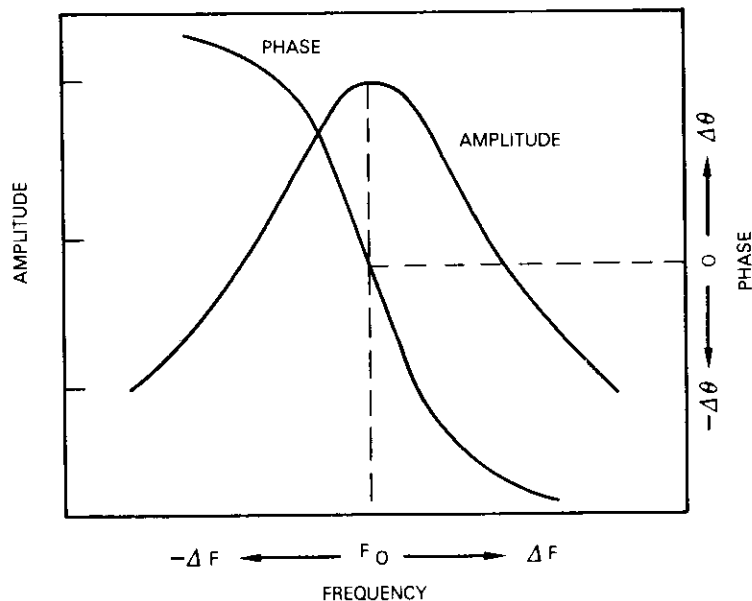
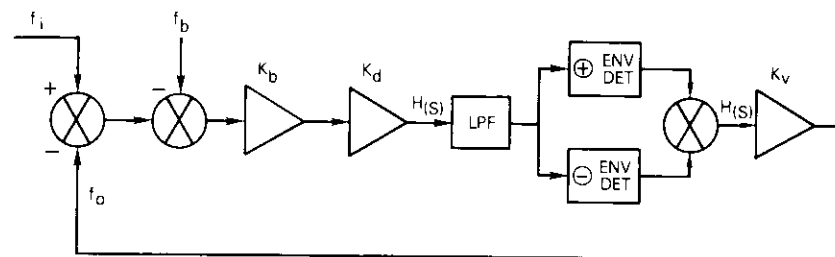


Figure 14. Typical Characteristics of a Single Q Bandpass Filter

established for a given set of specification values. The following set of specification values, typical of an INTELSAT system, is assumed:

burst-to-burst frequency offset:	± 3 kHz
carrier frequency drift:	± 50 kHz
drift in the VCO free-run frequency:	1×10^{-3}
stability of BPF-1 center frequency:	1×10^{-3}
IF:	140 MHz



f_i = INPUT FREQUENCY, f_0 = VCO OUTPUT FREQUENCY
 f_b = BPF CENTER FREQUENCY
 K_b = PHASE SENSITIVITY OF SINGLE-Q-NARROW-BANDPASS-FILTER
 K_d = PHASE DETECTOR SENSITIVITY
 K_v = VCO MODULATION SENSITIVITY

Figure 15. Analytical Block Diagram of the AFC Loop

PARAMETER DERIVATION

When the input signal consists only of the sync burst during initial acquisition, the frequency error, f_e , can be written as

$$f_e = f_i - f_0 - f_b \quad (21)$$

where

$$f_0 = \hat{f}_0 + K_b K_d K_v H(s) f_e \quad (22)$$

Therefore,

$$f_e = \frac{(f_i - f_b - \hat{f}_0)}{1 + K_b K_d K_v H(s)} \quad (23)$$

and the phase error, θ_e , becomes

$$\theta_e = K_b f_e = \frac{K_b}{1 + K_b K_d K_v H(s)} (f_i - f_b - \hat{f}_0) \quad (24)$$

where f_i = input frequency = $4 \times f_c$ (Hz)
 f_0 = VCO output frequency = $4f_1$ (Hz)
 f_b = BPF-1 resonant frequency (Hz)
 \hat{f}_0 = VCO free-running frequency (Hz)
 K_b = phase sensitivity of BPF-1 = $\pi/2B$ (rad/Hz)
 K_d = phase detector sensitivity (V/rad)
 K_v = VCO modulation sensitivity (Hz/V)
 B = 3-dB bandwidth of BPF-1 (single-Q type)
 $H(s)$ = transfer characteristics of the LPF, including the envelope detectors (see Figure 15).

If $H(0) = 1$, the static phase and frequency error can be written as

$$f_{es} = \frac{1}{1 + K_b K_d K_v} (f_i - f_b - \hat{f}_0) \quad (25)$$

$$\approx \frac{(f_i - f_b - \hat{f}_0)}{K_b K_d K_v}, \quad K_b K_d K_v \gg 1$$

$$\theta_{es} = \frac{K_b}{1 + K_b K_d K_v} (f_i - f_b - \hat{f}_0) \quad (26)$$

$$\approx \frac{(f_i - f_b - \hat{f}_0)}{K_d K_v}, \quad K_b K_d K_v \gg 1$$

from equations (23) and (24).

One commonly used AFC circuit has two envelope detectors as shown in Figure 15. The positive polarity envelope detector tracks the maximum carrier frequency in the bursts, and the negative polarity envelope detector tracks the minimum carrier frequency in the bursts. Since the output of the two envelope detectors is given by the sum of the values mentioned above, the average input frequency, \bar{f}_i , should be used instead of f_i . Thus, from equation (25), the average frequency error can be written as

$$\bar{f}_{es} = \frac{(\bar{f}_i - f_b - \hat{f}_0)}{K_b K_d K_v} \quad (27)$$

The frequency difference between bursts will be within 4×3 kHz ($\times 4$ due to multiplication of the carrier); therefore,

$$|f_c - \bar{f}_{es}| \leq 1.2 \times 10^4 \text{ Hz} = |\bar{f}_c| \quad (28)$$

From the discussion above, the loop parameters can be derived for design purposes:

$$|\bar{f}_c| = \frac{1}{K_b K_d K_v} |f_i - f_b - \hat{f}_0| \leq 1.2 \times 10^4 \quad (29)$$

which will be the same when considered in terms of deviation from the nominal frequency value,

$$|\bar{f}_c| = \frac{1}{K_b K_d K_v} \{ \Delta \bar{f}_i - \Delta f_b - \Delta \hat{f}_0 \} \leq 1.2 \times 10^4 \quad (30)$$

Under the worst condition,

$$K_b K_d K_v \geq \frac{1}{1.2 \times 10^4} \{ |\Delta \bar{f}_i| + |\Delta f_b| + |\Delta \hat{f}_0| \} \quad (31)$$

where $|\Delta \bar{f}_i| = 4 \times 50$ kHz = 2×10^5 Hz carrier drift (specification value)

$|\Delta f_b|$ = center frequency drift of BPF₁* = $53.2 \times 10^6 \times 1 \times 10^{-3} = 0.5 \times 10^5$ Hz

$|\Delta \hat{f}_0|$ = drift in VCO free-running frequency* = $126.7 \times 10^6 \times 1 \times 10^{-3} = 1.267 \times 10^5$ Hz.

From equation (31),

$$K_b K_d K_v \geq \frac{3.8 \times 10^5}{1.2 \times 10^4} \approx 32$$

Practical circuits can be built with

$$K_b = 2 \times 10^{-6} \text{ (rad/Hz)}$$

$$K_d \approx 1.6 \text{ (V/rad)}$$

$$K_v = 1 \times 10^7 \text{ (Hz/V)}$$

STABILITY OF AFC LOOP

A feedback circuit can oscillate if its open-loop gain exceeds unity

*Center frequency is chosen to yield the best intermodulation performance.

and simultaneously its open-loop phase shift exceeds 180° . Stability can be analyzed by means of Bode plots [12], one representing phase vs frequency and the other gain vs frequency. The Bode criterion for unconditional stability is that the gain must fall below unity (0 dB) before the phase shift reaches 180° . Figure 16 is an example of a Bode plot for a practical AFC loop. The solid curves represent the gain and phase characteristics of a stable loop and the dashed curves represent those of an unstable loop. An unstable loop can be made stable by appropriate gain and phase compensation using a lag-lead network.

Static phase error degradation

Two factors introduce fixed phase errors in the receiver. The first is the AFC system, which uses frequency feedback and will display a small residual frequency error. The second factor is the burst-to-burst frequency uncertainty caused by up-link deviations. These frequency uncertainties are multiplied, respectively, by 4. The resulting frequency errors are non-negligible when compared with the bandwidth of the carrier recovery filter. This causes phase shift to be introduced at the extremes of the frequency offset (see Figure 14). These phase shifts can be very closely approximated for these ranges of frequency uncertainties by

$$\theta_\epsilon = \frac{1}{M} \tan^{-1} \left\{ \frac{\pi \Delta f}{B_n} \right\} \quad (32)$$

where Δf = frequency uncertainty at the carrier recovery bandpass filter

B_n = noise bandwidth of the carrier recovery filter

M = multiplication factor

θ_ϵ = resulting phase error.

Phase perturbation due to transient effects

For a TDMA burst response, the voltage equation of a tuned circuit yields a steady-state solution and a transient solution. The steady-state phase perturbation effect has already been discussed. The phase perturbation associated with the transient solution can be written as

$$\theta_t = \frac{1}{4} \arctan \left[\frac{\exp\{-(\pi f_b/Q)\} t \sin 2\pi(\Delta f)t}{1 - \exp\{-(\pi f_b/Q)\} t \cos 2\pi(\Delta f)t} \right] \quad (33)$$

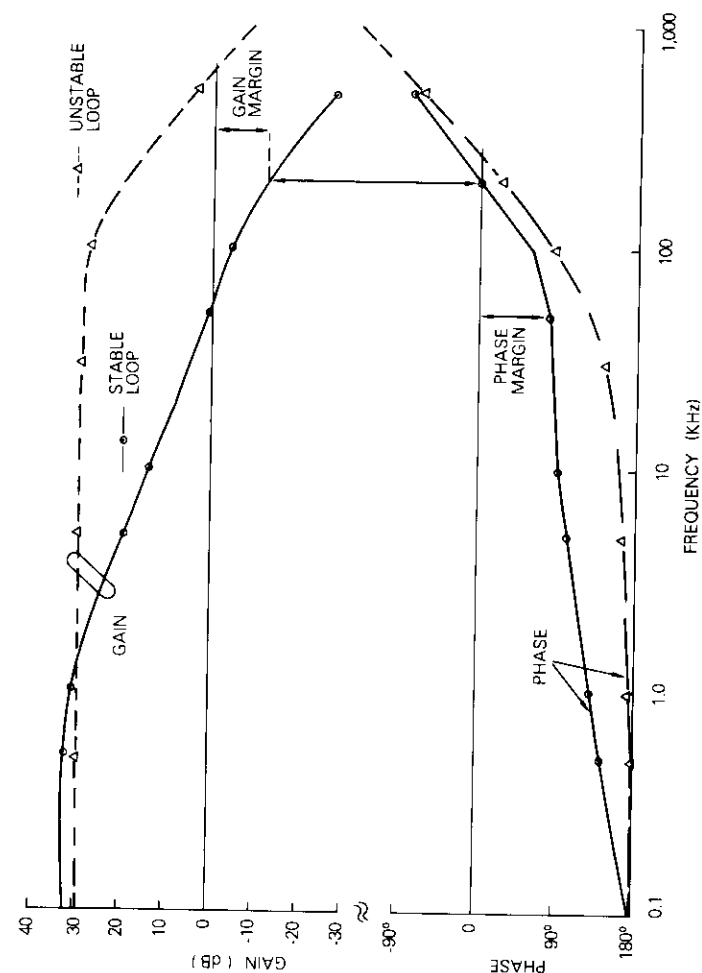


Figure 16. Bode Plot of a Practical Stable AFC Loop

where f_b = BPF center frequency
 f = actual input frequency
 Q = BPF quality factor.

Normally, for reasonable frequency offsets, this component is weaker than the effect introduced by energy from a preceding burst. This effect will be considered subsequently.

Signal-to-noise transients

The final source of degradation in the performance of the carrier recovery circuit is transients introduced during the preamble as the carrier reference changes from one burst to the next. This results in two types of effects. First, signal level at the carrier recovery filter output rises asymptotically, causing the signal-to-noise ratio to rise accordingly. The second effect results from the interaction of the decaying carrier from the previous burst with the increasing carrier in the present burst. The envelope of the increasing carrier caused by the combined effect of one decaying burst and the rise of the burst of interest depends upon the initial phase difference between the carrier of each burst. Since, in general, these transients are not completely settled at the end of the preamble, some degradation in performance is observed in this portion of a burst relative to steady-state.

Geometrically, these effects are illustrated in Figure 17a, which also shows the initial phase and relative amplitude. The envelope of the interfering burst decays exponentially as given by

$$e_i(t) = d_b e^{-2B_n(t+T_g)} e^{j\theta} \quad (33a)$$

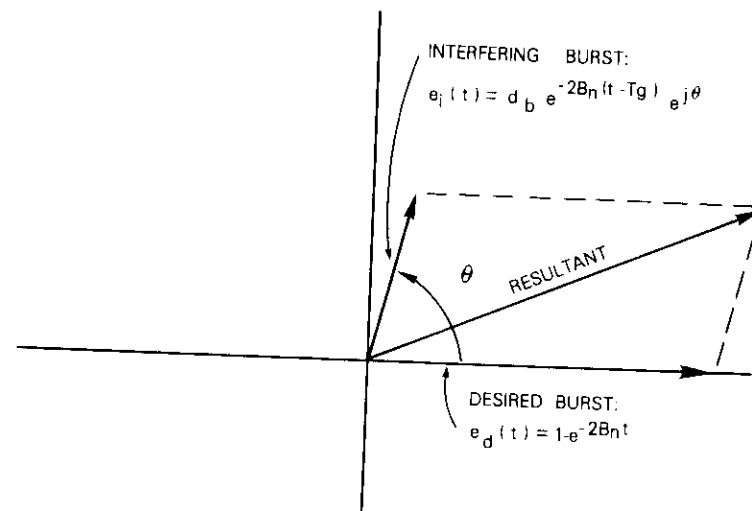
while the desired burst grows asymptotically by the same time constant as shown in normalized form by

$$e_d(t) = [1 - e^{-2B_n t}] \quad (33b)$$

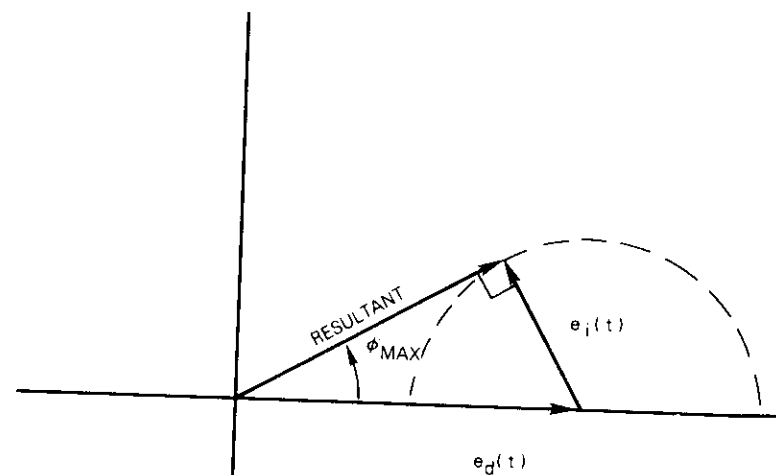
where e_i = interfering waveform envelope
 e_d = desired envelope
 d_b = relative amplitude factor
 B_n = noise bandwidth of carrier recovery circuit filter
 θ = initial phase difference
 T_g = guard time.

The combined signal can then be represented by

$$C_d(t) = 1 - e^{-2B_n t} + d_b \cos \theta e^{-2B_n(t+T_g)} + j d_b \sin \theta e^{-2B_n(t+T_g)} \quad (34)$$



a. Arbitrary Initial Phase



b. Worst-Case Phase Perturbation

Figure 17. Phase Perturbation Phasor Diagram

From equation (34), the total S/N ratio as a function of time is given by

$$(S/N)_{dB} = S/N_{in} + 20 \log \{ [1 - e^{-B_n t} + d_b \cos \theta e^{-2B_n(t+T_p)}]^2 + [d_b \sin \theta e^{-2B_n(t+T_p)}]^2 \} + 10 \log \frac{B_n}{B_{\omega in}} - \delta \quad (35)$$

where S/N_{in} = S/N ratio derived from equation (13)
 δ = loss due to the presence of modulation
 $B_{\omega in}$ = input noise bandwidth.

With this relationship, the S/N ratio at the end of the preamble can be determined from the relative amplitude of the envelope at that time compared to steady-state by inserting the preamble time into the expression in equation (35).

It is instructive to observe the behavior of equation (35) for constant preamble as a function of filter bandwidth and initial phase. As an example, Figure 18 is a plot of equation (35) for the parameters given in Table 4, where filter Q is used as the parameter ($Q = f_0/B_{3dB}$

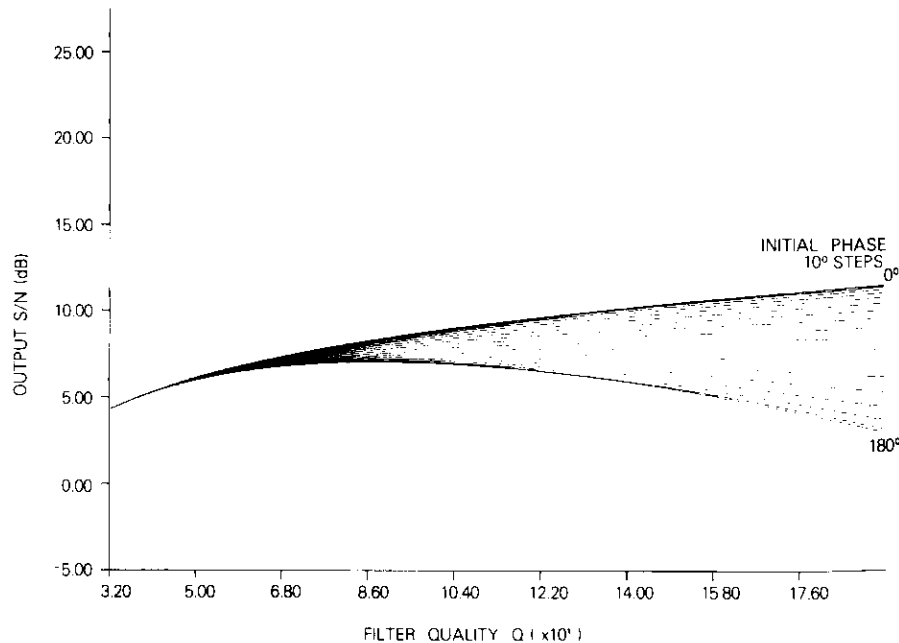


Figure 18. S/N Ratio vs Time for the Parameters of Table 4

= $\pi f_0/2B_n$), and the time is held constant and equal to the preamble length.

TABLE 4. SYSTEM PARAMETERS FOR SELECTION OF OPTIMUM Q

E/N_o	10.5 dB
R	60 Mbit/s
f_0	64 MHz
Preamble Length	30 symbols
Nonlinearity Loss	2.0 dB
Reconstruction Loss (δ)	2.0 dB
Signal-to-Pattern Noise	-0.5 dB
Amplitude Difference	0 dB

For initial phase angles near 180° there is a peak in the S/N ratio vs Q. This peak provides one criterion of optimality in the tradeoff between acquisition time and steady-state performance. For initial phase angles near zero, the S/N ratio is monotonic with Q, and shows approximately steady-state performance. Hence, one criterion of carrier recovery circuit design is the determination of optimum Q vs preamble time and steady-state behavior. For the parameters of Table 4, the optimum Q is approximately between 70 and 100.

Phase perturbation due to interference

The final criterion in the tradeoff between steady-state performance and acquisition time is the phase perturbation produced by the decaying burst. From equation (34), this is given by

$$\phi_e(t) = \frac{1}{M} \tan^{-1} \left\{ \frac{d_B \sin \theta e^{-2B_n(t+T_p)}}{1 - e^{-2B_n t} + d_B \cos \theta e^{-2B_n(t+T_p)}} \right\} \quad (36)$$

Figure 19 shows the transient phase error at the end of the preamble as a function of filter Q factor using the parameters of Table 4. It should be noted that the maximum phase error does not occur for a constant initial phase angle. The maximum phase angle can be obtained by determining from geometric considerations, as shown in Figure 17b, the value of θ for which $d\theta_e/d\theta$ vanishes. The maximum phase angle occurs when the interfering signal and the resultant signal are in quadrature; therefore,

$$\phi_{\max} = \frac{1}{M} \sin^{-1} \left\{ \frac{d_b e^{-2B_b(t+T_0)}}{1 - e^{-2B_b t}} \right\} \quad (37)$$

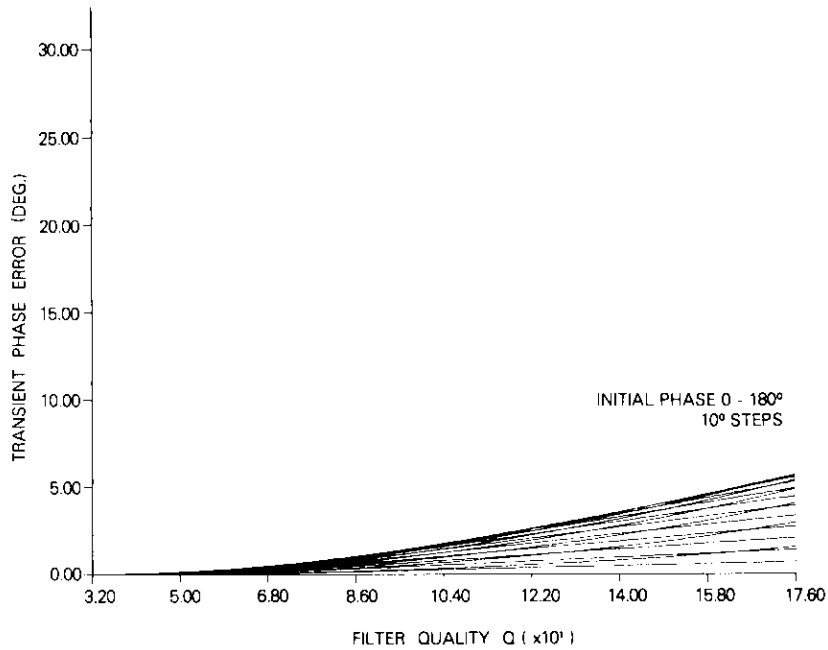


Figure 19. Transient Phase Error at the End of the Preamble vs Q for the Parameters of Table 4

It is of interest to observe the actual transient behavior of the carrier recovery circuit for the optimum value of filter bandwidth. For this case the optimum value is $Q = 100$. Signal-to-noise ratio and phase perturbation as functions of time, with initial phase as a parameter, are shown in Figures 20 and 21, respectively. Note that, at the end of the preamble time, the acquisition transients have nearly settled down, and the S/N ratio is sufficient for good performance of the frequency divider (see Figure 9).

Development of design equations for the timing recovery circuit

The development of the design equations for the transient response

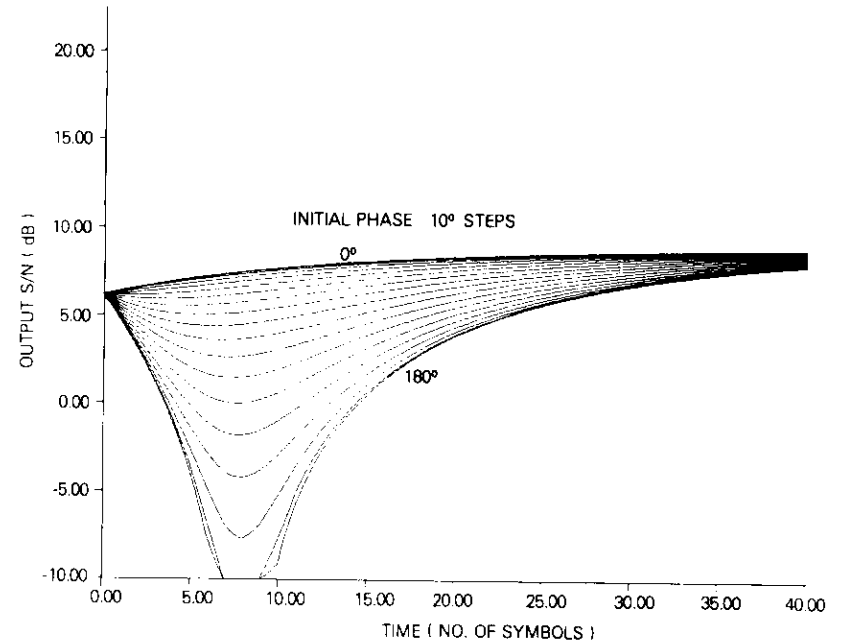


Figure 20. S/N Ratio vs Time with Initial Phase as a Parameter

of the timing recovery circuit follows the same general approach as for the carrier recovery circuit. Since the frequency uncertainty of the received clock is constrained to be small to facilitate stable TDMA frame synchronization, the only concerns with respect to design are S/N ratio vs time and transient phase errors due to interburst interference.

Signal-to-noise transients

The transients in the timing recovery circuit filter are the result of the decay of the interfering burst and the buildup of the desired burst. One difference between the timing and carrier recovery circuit responses is that for the former the signal level during the preamble is 6 dB greater than during data as noted earlier. Consequently, the form of the envelope of the components of the clock is

$$e_i(t) = \frac{1}{2} d_b e^{-2B_b t(t+T_0)} \quad , \quad t > 0 \quad (38)$$

and

$$e_d(t) = \begin{cases} 1 - e^{-2B_T t} & , \quad T_p > t > 0 \\ \frac{1}{2} - e^{-2B_T t} + \frac{1}{2} e^{-2B_T(t-T_p)} & , \quad t > T_p \end{cases} \quad (39)$$

where B_T = noise bandwidth of the clock recovery filter
 T_p = preamble time
 d_b = relative amplitude factor.

For an initial phase angle θ , the complex envelope is therefore

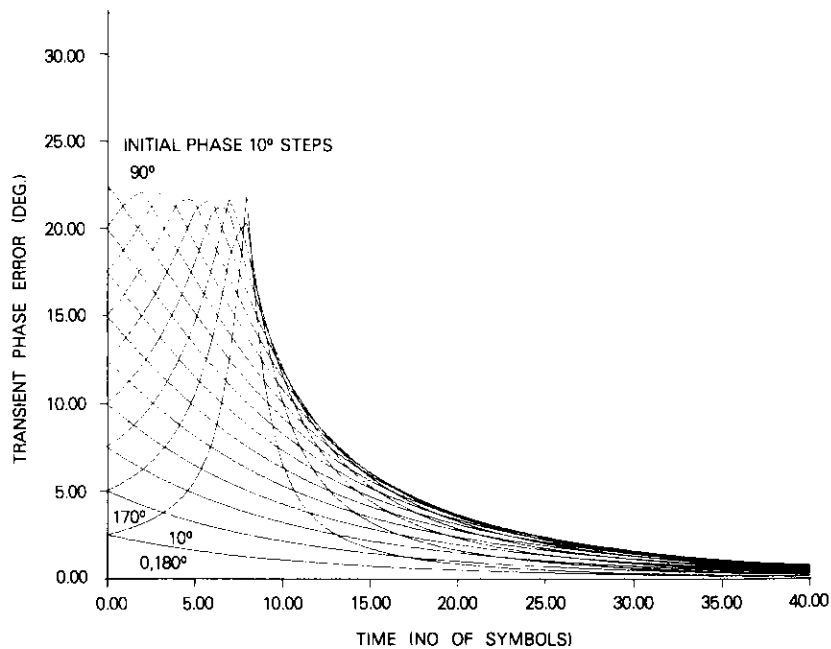


Figure 21. Phase Perturbations vs Time with Initial Phase as a Parameter

$$e_0(t) = \begin{cases} 1 - e^{-2B_T t} + \frac{d_b \cos \theta}{2} e^{-2B_T(t+T_p)} + j \frac{d_b \sin \theta}{2} e^{-2B_T(t-T_p)} ; & 0 < t < T_p \\ \frac{1}{2} - e^{-2B_T t} + \frac{1}{2} e^{-2B_T(t-T_p)} + \frac{d_b \cos \theta}{2} e^{-B_T(t+T_p)} \\ \quad + j \frac{d_b \sin \theta}{2} e^{-2B_T(t+T_p)} ; & t > T_p \end{cases} \quad (40)$$

Because of the different forms of the envelope in two regions, the response must be evaluated both at the end of the preamble and in the steady-state mode. For example, a time equal to twice the preamble was selected as equivalent to steady-state and the envelope S/N ratio vs Q was determined at both the preamble time and the "steady-state" time. The resulting curves, with initial phase angle as the parameter, are given in Figure 22. The system parameters from Table 4 were used for the plots.

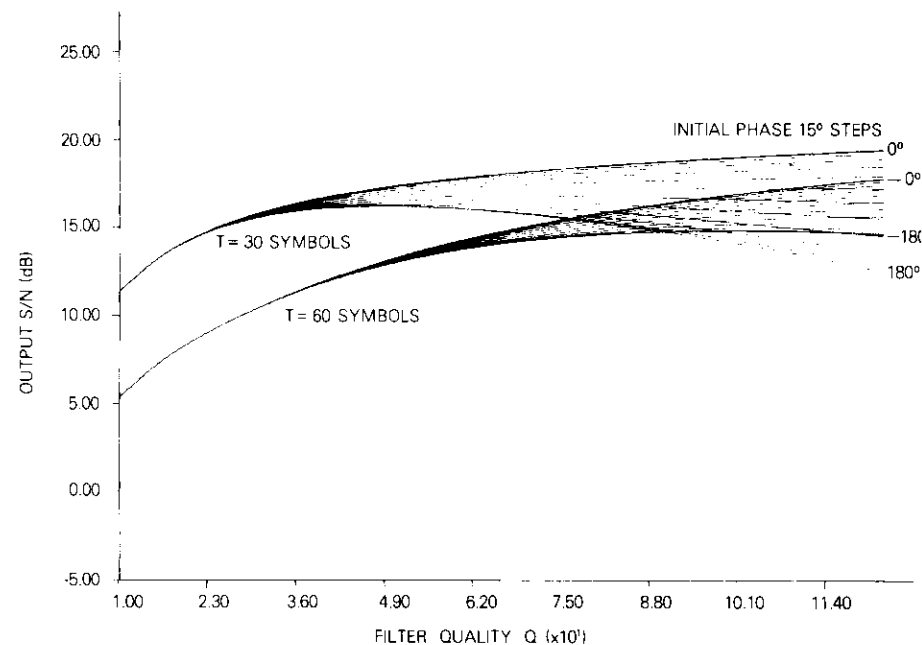


Figure 22. S/N vs Q at Preamble and Steady-State Times with Initial Phase Angle as a Parameter

Phase perturbation due to interference

From equations (38) and (39), the phase error due to interburst interference can be found as follows:

$$\Phi_i(t) = \begin{cases} \tan^{-1} \left[\frac{d_b \sin \theta e^{-2B_T(t+T_g)}}{2(1 - e^{-2B_T t}) + d_b \cos \theta e^{-2B_T(t+T_g)}} \right]; & 0 < t < T_p \\ \tan^{-1} \left[\frac{d_b \sin \theta e^{-2B_T(t+T_g)}}{1 - 2e^{-2B_T t} + e^{-2B_T(t-T_p)} + d_b \cos \theta e^{-2B_T(t+T_g)}} \right]; & t > T_p \end{cases} \quad (41)$$

Figure 23 shows the phase perturbation vs single-tuned circuit Q given by equation (41) for both the end of the preamble and steady-state.

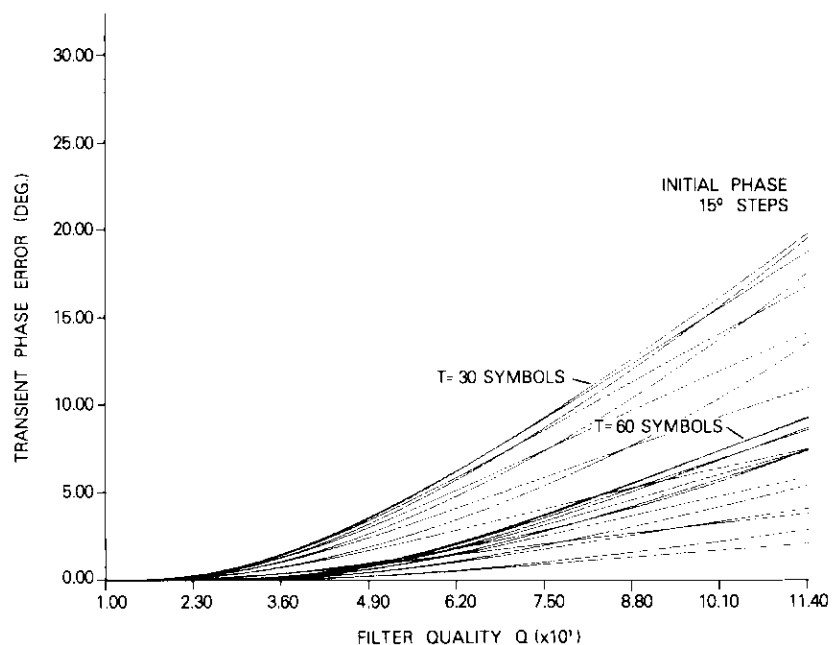


Figure 23. Phase Perturbation vs Single-Tuned Circuit Q for End of Preamble and Steady-State

From Figure 22 it can be seen that the optimum timing recovery filter Q is approximately 45.

The output S/N vs time (symbols) for a Q-factor value of 45 is shown in Figure 24, and its transient phase vs time (symbols) characteristic is shown in Figure 25.

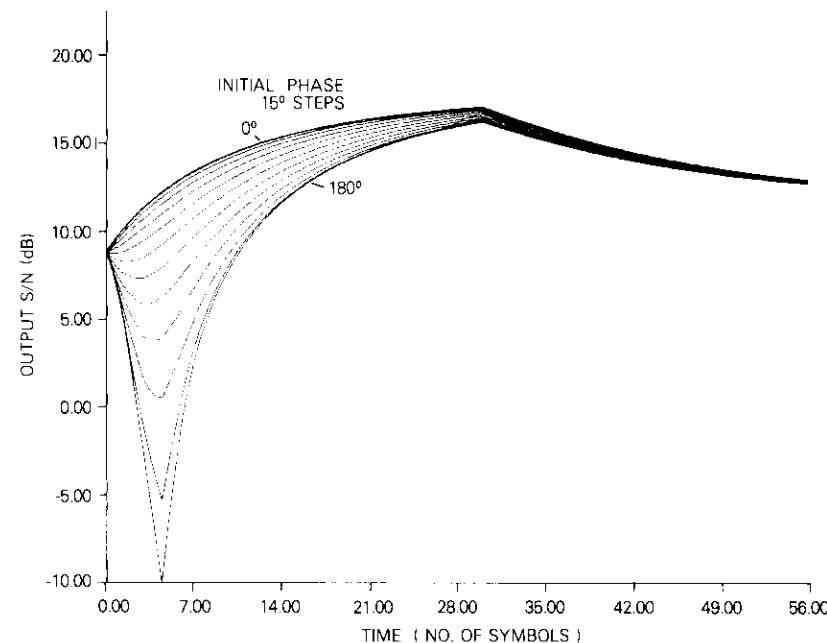


Figure 24. Output S/N vs time for Q = 45

Special problems in AGC for TDMA

In high-speed TDMA applications, the AGC circuit must be able to operate with short burst lengths and to tolerate large burst-to-burst level differences arising from deep fades due to atmospheric and rain attenuation. An AGC loop with a hold circuit is most suitable for such applications. Figures 26a and 26b are typical block diagrams of an AGC loop and the hold circuit, respectively.

The parameters of the hold circuit should be chosen so that the charge time, T_c , is small to realize fast rise and so that the discharge time, T_d , is long to maintain AGC operation over the frame period. That is, for 90-percent charge-up, T_c will be

$$2.2C(r + r_f) < T_{min}$$

where T_{min} = minimum burst length
 C = charging capacitance (see Figure 26b)
 r = series charging resistance
 r_f = diode forward resistance.

Reciprocally, the discharge time, T_d , is

$$2.2CR > T_{max}$$

where T_{max} = maximum frame length
 R = shunt discharge resistance.

With these conditions fulfilled, the AGC circuit will be effective in both continuous and burst modes.

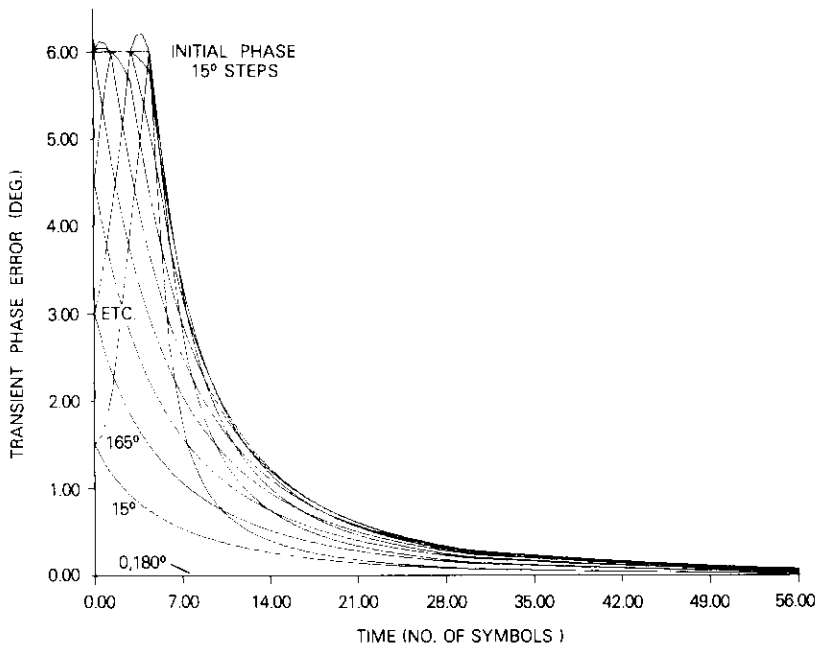


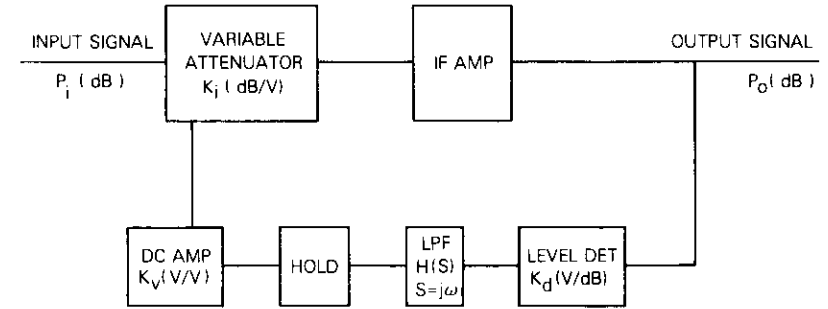
Figure 25. Transient Phase vs Time for $Q = 45$

The input-output characteristics of the AGC loop described in Figure 26a can be described by the following empirical relationship:

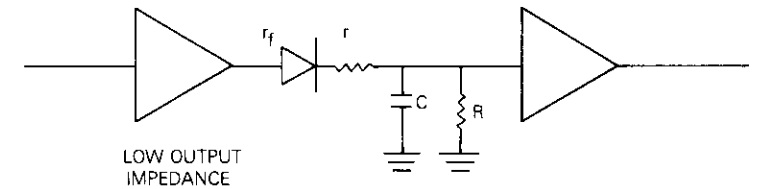
$$\Delta P_o = \frac{1}{1 + K_d K_v K_r H(s)} \Delta P_i \quad (42)$$

where ΔP_o = output signal level variation (dB)
 ΔP_i = input signal level variation (dB)
 K_d = level detector sensitivity (V/dB)
 K_v = DC amplifier gain (V/V)
 K_r = variable attenuator characteristic (dB/V)

and $H(S) = H(j\omega)$ is the transfer characteristics of the LPF, whose rise time for a step input should be selected so that it is almost equal to the minimum burst length, T_{min} .



a. TDMA AGC Block Diagram (high input impedance)



CHARGE TIME CONST = $C(r + r_f)$
 r_f = DIODE FORWARD RESISTANCE
 DISCHARGE TIME CONST = CR

b. Recommended AGC Circuit for TDMA Application

Figure 26. Recommended AGC Circuit for TDMA Application

If it is assumed that $H(o) = 1$ and the maximum burst-to-burst input level variation including deep fading is ± 10 dB, the output level variation is

$$\Delta P_o = \frac{20}{1 + K_d K_v K_\ell} \quad (43)$$

where, by definition, the expression $1 + K_d K_v K_\ell$ is numerical and input and output power variations are in decibels. For an output level variation specification of ± 0.2 dB (considered to be adequate for fast TDMA), then

$$K_d K_v K_\ell = 49 \quad (44)$$

The above value for a practical and stable AGC loop can be designed by selecting the loop parameters as follows:

$$\begin{aligned} K_d &\approx 1.6 \text{ (V/dB)} \\ K_v &= 100 \\ K_\ell &= 0.3 \text{ (dB/V)} \end{aligned}$$

Advanced design concepts

The analyses of the previous subsections show that there are a number of problem areas in the classical TDMA modem design philosophy. These areas, which strongly influence the design tradeoffs and achievable performance, include interburst interference in both carrier recovery circuits and timing recovery circuits. This interference manifests itself in both loss of S/N ratio and in phase transients which reduce modem performance. In addition, the use of classical frequency multiplication by 4 creates a significant degradation in C/N ratio because of the nonlinear operation (multiplication). Finally, there is a significant loss in clock S/N ratio due both to interburst interference and loss of the clock component during the data portion of the burst. Improvements in modem performance are being investigated. In particular, attention is being directed toward two improvements in circuit performance: reduction of interburst interference and improvement in S/N ratio. The following subsections discuss some advanced alternatives.

Reduction of interburst interference

There are two methods which have been studied for reducing

interburst interference. In the first method, called "quenching," a signal from the TDMA control subsystem is used to quench or otherwise dissipate the energy in the bandpass filter of the carrier and timing recovery circuits [13]. This allows each burst to start fresh at the beginning of each preamble and to grow asymptotically without interference or degradation from the preceding burst; thus, the S/N ratio as a function of time grows faster than in the worst-case situation with interburst interference, and there is no phase perturbation from the prior burst. The curve in Figure 27 shows the typical S/N ratio characteristic response for the same conditions given in Figure 20 but with the interburst interference removed. Comparison with Figure 20 indicates that the S/N ratio improves significantly faster than in the

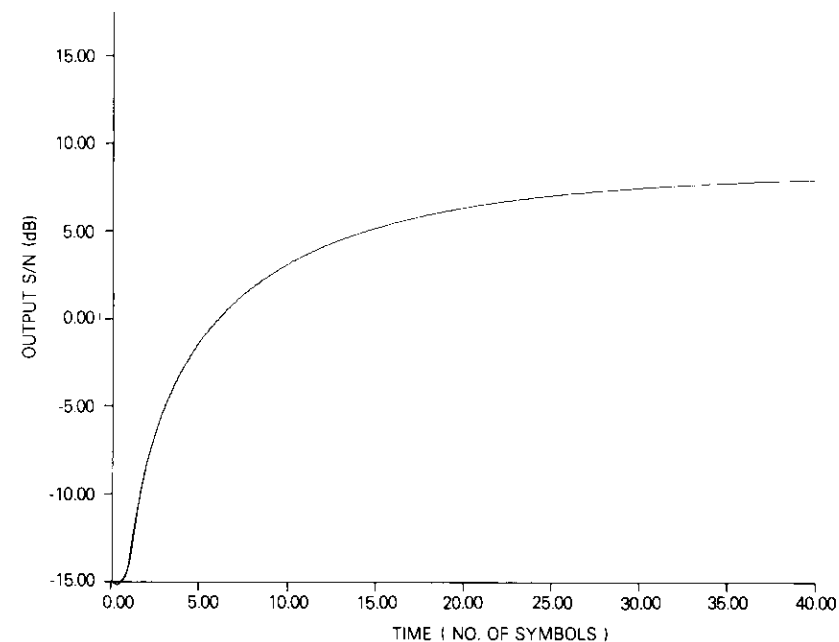


Figure 27. *S/N Ratio vs Time without Intersymbol Interference*

worst case in Figure 20. If the circuit Q is increased, as shown in Figure 28, an even greater steady-state S/N ratio can be achieved without much loss in response time.

The second method of reducing interburst interference is also effective in dealing with the variation in clock level noted previously.

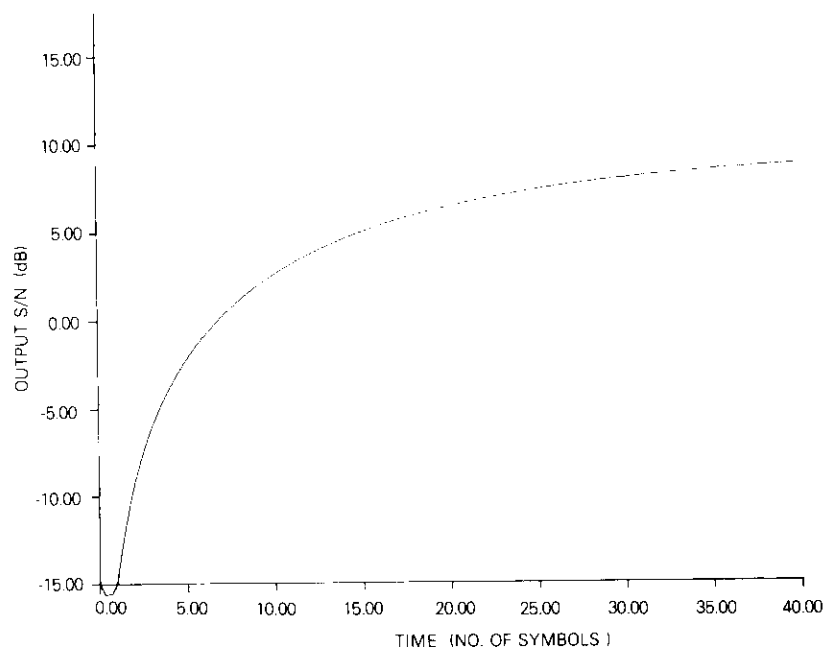


Figure 28. *S/N Ratio vs Time without Intersymbol Interference and Increased Circuit Q*

This method uses a variable quality factor tuned circuit to improve the S/N ratio. Figure 29 is a sample circuit diagram for such a variable Q circuit. The diode shown on the circuit is selected with a minimum forward voltage. If the incoming signal is in phase with the oscillations in the tank circuit, the diode is not driven into conduction and hence has a high impedance. Thus, the tuned circuit is not loaded by the

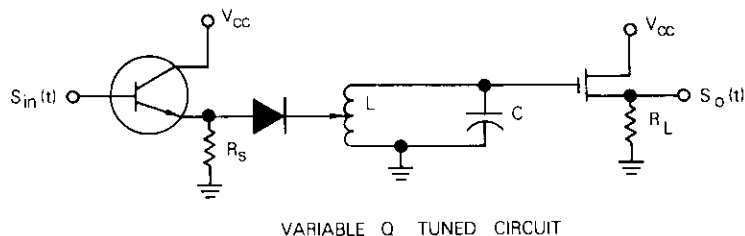


Figure 29. *Variable-Q Tuned Circuit*

drive circuit and the resultant Q is very high. If, however, the incoming waveform is out of phase with the signal in the tank circuit, the diode becomes forward biased and loads the tank with the source impedance. This allows a fast attack characteristic which permits, for example, the clock recovery circuit to respond quickly to a new burst, yet provides a higher Q during steady-state for improvement in the S/N ratio.

A variation of the variable Q circuit, known as the injection oscillator [14], is also being investigated. In the injection oscillator, feedback is used around the tuned circuit to provide a simple oscillator circuit [15]. In addition, a point in the feedback circuit is provided to inject the signal from either the carrier extraction or clock extraction circuit. When such a signal is injected into the oscillator circuit through the source impedance, the oscillator circuit is loaded by the incoming signal and tends to phase lock to the incoming signal. If the incoming signal vanishes or has gaps, as is common in the clock recovery circuit, the feedback in the circuit will cause continued oscillation and provide an output signal at a very high Q. This particular circuit shows excellent promise in terms of providing both fast acquisition and good steady-state signal-to-noise ratio.

Improvement in carrier-to-noise ratio

Other investigations are intended to exploit the characteristics of the typical TDMA signal. In particular, the preamble normally used for present modems consists of biphase modulation with alternating 180° phase shifts. Thus, at least during the preamble, the use of frequency multiplication by 4 produces unnecessary degradation in the C/N ratio. One method of improving carrier recovery circuit performance would be to use frequency multiplication by 2 during the preamble. Although frequency multiplication by 2 will not provide an adequate carrier component for coherence recovery during the data portion of the burst, a carrier component can be generated without the second frequency multiplication by using decision feedback [9]. Multiplication by 2 would be used to provide the carrier reconstruction during the preamble. Decision feedback, which would be derived from the demodulated data, would be used only after the preamble during the data portion of the burst. This technique is expected to have approximately 6 dB better S/N ratio performance than the conventional approach at the frequency divider, which is the principal element determining the threshold S/N ratio.

Another method of carrier-to-noise ratio improvement uses the *a*

priori knowledge of the nature of the preamble, *i.e.*, $0, \pi, 0, \pi, \dots$ pattern. Application of optimum data detection/parameter estimation results in an optimum structure which uses decision feedback and signals derived from the clock recovery circuit [16]. This structure promises to provide the best possible S/N ratio for the carrier recovery circuit and can be used with phase lock technology, bandpass filters, or injection oscillators for S/N ratio improvement.

Conclusions

Several aspects of TDMA modem design have been discussed including an approach to channel filter design, an analysis of conventional carrier and clock recovery circuit transients, an estimate of the effect of modem filtering and channel nonlinearities on carrier and clock recovery S/N ratio, and an analysis of AFC and AGC in a TDMA environment.

Modem filter optimization for an INTELSAT channel requires consideration of the out-of-band emission specification, the effect of the nonlinear amplifiers in the channel, and the need to minimize bit-error rate. The results of computer simulation indicate that a moderate rolloff (40- to 50-percent) raised cosine filter in conjunction with a sharper 5-pole elliptic filter with a BT product of 1.04 can provide good performance over a wide range of operating points for an INTELSAT type channel (120-Mbit/s QPSK carriers on 80-MHz spacing). For moderate nonlinearities the raised cosine filter should be used on the transmit side, while for extreme nonlinearities it should be used as the receive filter.

The analysis of the carrier and clock recovery circuits demonstrated the degradations in S/N ratio introduced by the channel characteristics and the extraction process itself. For the carrier recovery circuit, sources of degradation include the effects of the nonlinearities (2.0 dB), out-of-band losses of the channel filters including the modem filters (~ 2 dB), "pattern" noise (due to the modulation), and frequency multiplication by 4 for carrier extraction (≥ 12 dB). For the clock recovery circuit, sources of degradations are basically the same except that clock extraction by the delay line method introduces only 6-dB loss in S/N ratio. However, during data another 6 dB is lost due to less frequent data transitions. Nevertheless, for INTELSAT satellite channel parameters, the analyses show that good S/N ratios (7.5 dB for carrier and 13 dB for clock) can be achieved with a 30-symbol preamble, even when the effects of the nonlinear HPA and TWTA are considered.

Acknowledgments

Thanks are due to V. Uzunoglu and J. Poklemba for many useful discussions. T. Noguchi and S. Yokoyana of Nippon Electric Company of Japan are also acknowledged for many useful discussions and advice.

References

- [1] D. Chakraborty, T. Noguchi, S. J. Campanella, and C. J. Wolejsza, "Digital Modem Design for Nonlinear Satellite Channels," Fourth International Conference on Digital Satellite Communications, Montreal, Canada, October 1978.
- [2] L. Lundquist, M. Lopriore, and F. M. Gardner, "Transmission of 4ϕ -Phase-Shift-Keyed Time Division Multiple Access over Satellite Channel," *IEEE Transactions on Communications*, September 1974.
- [3] M. Asahora, N. Toyonaga, S. Sasaki, and T. Miyo, "Analysis of Carrier Recovery Adopting a Narrow-Band Passive Filter with AFC Loop," Third International Conference on Digital Satellite Communications, Kyoto, Japan, November 1975.
- [4] Y. Matsuo, S. Sugimoto, and S. Yokoyama, "A Study on Carrier and Bit-Timing Recovery for Ultrahigh-Speed PSK-TDMA System," Second International Conference on Digital Satellite Communications, Paris, France, November 1972.
- [5] S. Yokoyama and T. Noguchi, "Theoretical and Experimental Considerations of the Carrier and the Bit-Timing Recovery in the Burst Mode Operation," INTELSAT/IEE International Conference on Digital Satellite Communication, London, England, November 1969.
- [6] L. E. Franks, "Further Results on Nyquist's Problem in Pulse Transmission," *IEEE Transactions on Communications Technology*, April 1969, pp. 337-340.
- [7] W. L. Cook, "Interactive Computer Simulation of Satellite Transmission Systems," 5th Annual Pittsburgh Conference on Modeling and Simulation, April 1974, *Proc.*, pp. 767-772.
- [8] D. Chakraborty, "Experiments with High-Speed Digital Transmission Via Satellite Links," Third International Conference on Digital Satellite Communications, Kyoto, Japan, November 1975.
- [9] W. C. Lindsey and M. K. Simon, *Telecommunication System Engineering*, Englewood Cliffs, NJ: Prentice-Hall, Inc., 1973, pp. 435-440.
- [10] A. L. Berman and E. I. Podraczky, "Experimental Determination of Intermodulation Distortion Produced in a Wideband Communications Repeater," *1967 IEEE International Convention Record*, Vol. 15, Pt. 2, pp. 69-88.

- [11] W. B. Davenport and W. L. Root, *Random Signals and Noise*, New York: McGraw-Hill Book Co., Inc., 1958, pp. 257-267.
- [12] H. W. Bode, *Network Analysis and Feedback Amplifier Design*, Princeton, NJ: D. Van Nostrand Co., Inc., 1964.
- [13] F. M. Gardner, "Carrier and Clock Synchronization for TDMA Digital Communications," ESS Technical Report TM-169 (ESTEC), December 1976, pp. 46-51.
- [14] C. Hayashi, H. Shibayama, and Y. Nishikawa, "Frequency Entrainment in a Self-Oscillatory System with External Force," *IRE Transactions on Circuit Theory*, December 1960, pp. 413-422.
- [15] V. Uzunoglu, Private Communication.
- [16] J. Poklemba, Private Communication.



Chester J. Wolejsza, Jr., received a B.S.E.E. degree from Cooper Union in 1966, and M.S. and E.E. degrees from M.I.T. in 1967. Immediately thereafter, he joined COMSAT Laboratories, where he is currently Manager of the Modulation Techniques Department of the Communications Processing Laboratory. His responsibilities include supervision of the design and development of PSK modulation and coding systems which perform optimally in the band- and power-limited environment of a satellite communications channel. Mr.

Wolejsza has been a member of Tau Beta Pi and Eta Kappa Nu and an associate of Sigma Xi.

Dayamoy Chakraborty received a Ph.D. in physics from the University of Surrey, England, in 1967. Since 1968, he has been employed by COMSAT. From 1968-1971, he was involved with the satellite system optimization study and the analysis of transmission deviations. Dr. Chakraborty transferred to COMSAT Laboratories in 1971 and has been involved in developing high-speed digital satellite communications systems. Currently, as Assistant Manager of the Modulation Techniques Department, he directs research in nonlinear satellite channel model design, maximum likelihood sequence estimation, and application of advanced modulation methods in satellite communications. Prior to joining COMSAT, he was employed by the British Post Office, Research Department, Dollis Hill, London.

Dr. Chakraborty is the author of numerous publications on microwave techniques and communications technology and is a senior member of IEEE and a Corporate member of IEE.



Index: filter, nonlinearity, hardware simulation, quaternary phase shift keying

Optimum filtering for QPSK in bandwidth-limited nonlinear satellite channels

M. E. JONES AND M. R. WACHS

(Manuscript received May 31, 1979)

Abstract

This paper reports on the results of hardware simulation experiments concerning optimum pulse shaping filter characteristics and configurations for conventional quaternary phase shift keyed (QPSK) transmissions in nonlinear channels. It is shown that QPSK transmission performance through a channel comprising two nonlinear traveling wave tube amplifiers (TWTAs) can be significantly improved by replacing the normally employed sharp rolloff (Nyquist) pulse shaping filters with filters characterized by either a more gentle rolloff (Nyquist) or a wider bandwidth (non-Nyquist). The study considers bit-error rate as a function of nonlinearities, adjacent channel interference caused by high-power amplifier (HPA) spectrum regeneration, dual-path transmission degradation, and co-channel interference.

Several filter characteristics and configurations are investigated and comparative performance results are presented. Emphasis is placed on the tradeoff between nonlinear channel bit-error-rate degradation and adjacent channel interference resulting from HPA spectrum regeneration. Dual-path transmission and co-channel interference degradation for selected configurations are also

This paper is based on work performed at COMSAT Laboratories under the sponsorship of the Communications Satellite Corporation (COMSAT) and the International Telecommunications Satellite Organization (INTELSAT).

discussed. Finally, demodulation synchronization losses as a function of channel filtering are presented for a particular modem design.

The best filter configuration tested consists of a wider bandwidth, non-Nyquist (30-percent-rolloff Nyquist for 1.13 times the transmission rate) transmit filter and a 50-percent-rolloff Nyquist demodulator filter placed after carrier demodulation and ahead of the sampling function.

Introduction

Considerable effort has been focused on characterization and optimization of wideband digital transmission performance in bandwidth-limited, nonlinear satellite channels [1]–[12]. Investigations have included mathematical analysis, computer simulation and hardware simulation approaches. Computer time-domain simulation in conjunction with hardware simulation has been especially useful. Until recently the design of TDMA transmission systems has relied heavily on the use of Nyquist pulse-shaping filtering and demodulator sampling as applied to a linear channel.

In this paper the results of a hardware simulation study of transmission characteristics intended to minimize the impairments experienced by wideband QPSK transmission are reported. Previous measurements [12] have shown that, when sharp rolloff (30-percent) Nyquist transmit filters are used, considerable impairment results from the nonlinear elements of the channel. Thus, means of reducing the nonlinear loss impairment by modifying the pulse-shaping filter design were investigated. Initial work had shown that a small increase in filter bandwidth (10 percent) would reduce the impairment loss in the case of a single TWTA nonlinearity.

This paper confirms these results and extends them to include the evaluation of several pulse-shaping filter configurations in a channel which comprises two nonlinear TWTA's. The effects of adjacent channel interference caused by earth station HPA spectrum spreading, transponder dual-path transmission, and up-link co-channel interference are also examined. A study of demodulator carrier and bit-timing effects as a function of filtering has provided a better understanding of the contribution of non-ideal synchronization to the nonlinear channel bit-error-rate impairment.

Background

Current communications satellites employ repeaters with 40-MHz-wide contiguous channels. Practical filter design and adjacent channel

isolation requirements result in a usable bandwidth of about 36 MHz. INTELSAT IV and IV-A satellites can support up to 60-Mbit/s phase shift keyed (PSK) transmission with a margin based on appropriate up- and down-link assumptions. Future INTELSAT V satellites will be capable of supporting 120 Mbit/s with 72-MHz channel bandwidth. Thus, a bandwidth occupancy of just under 1.7 bit/s/Hz is achieved with 4-phase PSK and filters which comply with Nyquist's criterion for signaling in a linear minimum bandwidth channel. Filtering can occur at the modulator or the demodulator, or it can be apportioned between the two. In present INTELSAT applications all of the pulse-shaping filter function occurs at the modulator. At the demodulator a receive bandpass filter limits thermal noise and adjacent channel interference. It contributes negligible signal distortion because its noise bandwidth is slightly wider than the symbol rate, and because it is well group-delay equalized. After filtering, the signal is demodulated using carrier reference multiplication, sampling, and decision functions. The carrier recovery function is implemented using $\times 4$ multiplication followed by bandpass filtering. The bit-timing recovery function employs half-symbol delay and multiplication followed by bandpass filtering.

Performance of the presently specified INTELSAT modem using 30-percent-rolloff Nyquist transmit filtering in a channel consisting of a satellite repeater alone and in a channel consisting of a satellite repeater and earth station HPA in cascade has been reported [12]. Bit-error rate as a function of received carrier-to-noise (C/N) ratio is presented in Figure 1 for the transponder alone (0- and 14-dB input backoff), the transponder (0-dB input backoff) in cascade with an 8-kW earth station HPA (0- and 14-dB input backoff), and the modem alone. The effects of adjacent channel, dual path, and co-channel interference are excluded. These results clearly indicate that the addition of nonlinear elements to the channel results in severe impairments.

Hardware simulation approach

The optimum filter for a linear, additive Gaussian noise channel is the "Nyquist" filter, which can ideally result in no intersymbol interference, provide equal time between symbol transition values, and preserve the pulse areas [13]. However, a communications satellite transmission link involves a cascade of linear, additive Gaussian noise channel segments isolated by nonlinear elements. The filter which is optimum for a linear channel is not necessarily optimum for the satellite link. Considerations for the satellite link pulse-shaping-filter optimi-

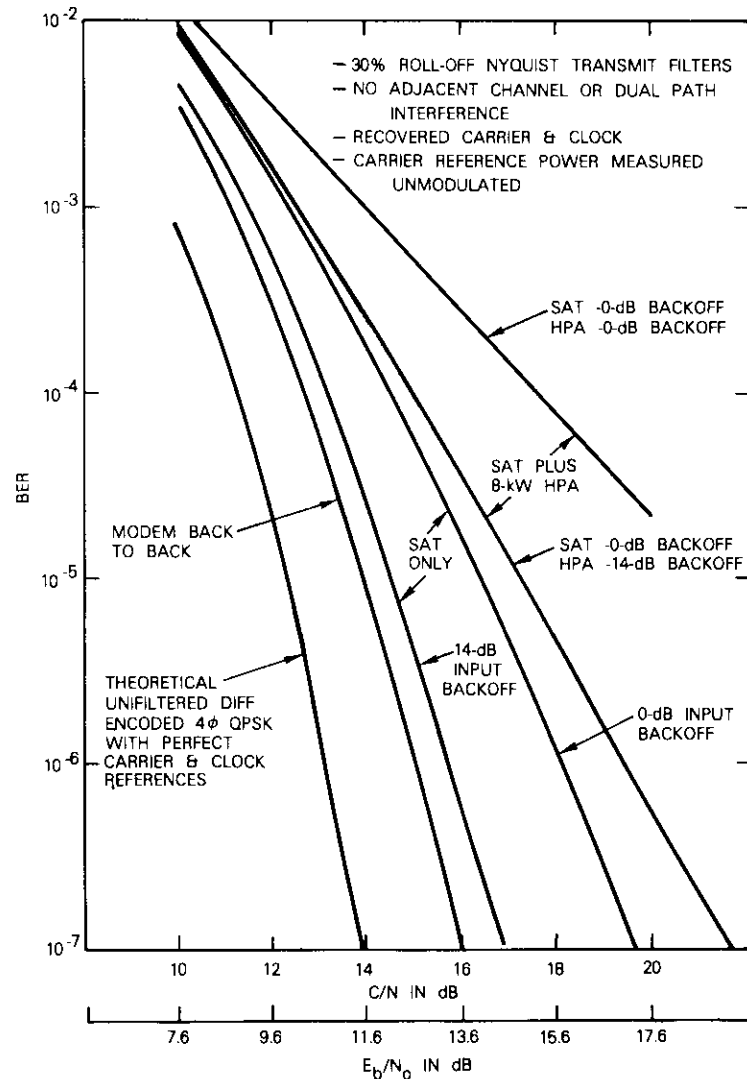


Figure 1. Typical INTELSAT Specified Modem Performance in a Satellite Channel

zation tradeoff will include the following;

a. *Spectrum spreading.* A regrowth of energy outside of the

filtered modulator signal spectrum is due to HPA amplitude and phase nonlinearities which produce adjacent channel interference. Filtering after the HPA nonlinearity is usually impractical because of power level, filter insertion loss, weight limitations, and the requirement in some cases for frequency agility.

b. *AM to PM and AM to AM conversion effects due to filtering.* The filtered modulated signal exhibits considerable amplitude variation. When this amplitude variation interacts with the phase and amplitude transfer function of the nonlinear device, multiplicative noise components are introduced which effectively add intersymbol interference at the demodulator sampling instants. Performance of the carrier and bit timing recovery circuits is also degraded.

c. *Dual-path transmission.* The overlap in the filter skirt regions of adjacent transponders allows portions of the signal to propagate through more than one transponder. The amplitude and group delay responses of the transmission channel suffer perturbations which are severe near the transponder band edge, but which may, in certain cases, extend well into the passband. These perturbations are a function of the time-varying gain and time delay differences between the two transponders and cannot be equalized with conventional fixed equalization.

For this study, the link is divided into two sections. The filtering for each section has been designated to meet separate criteria. The transmit, or up-link, filtering should accomplish spectrum control with a minimum of nonlinearity (AM to PM and AM to AM) induced degradation. Because of the high power levels encountered at earth stations, filtering must be performed prior to the HPA. The HPA nonlinearities widen the input spectrum. The resulting spectrum consists of two components: the desired filtered spectrum shape and an undesired nonlinearity regenerated (wide) spectrum. Widening the filter redistributes the power in the regenerated portion of the spectrum (beyond the main lobe of the input spectrum), but of course increases the width of the filtered spectrum (main lobe). In the limit (no filter) the original $(\sin x/x)^2$ power spectrum will be restored. The wider filter results in reduced nonlinear channel performance impairment. The transmit filter is thus selected to be wide enough to minimize the nonlinear channel impairment, but narrow enough to achieve the desired control in the post-HPA spectrum.

Although these two filter requirements may conflict depending on

the system, it will be shown that they do not conflict for the INTELSAT system. The post-HPA spectrum is evaluated on the basis of the level of spectral components falling into the utilized bandwidth of the adjacent transponders.

The receive, or down-link, filtering should minimize thermal noise and reject spectral components experiencing dual-path transmission without introducing significant intersymbol interference or impairment of the demodulator synchronization functions. The receiver used in the simulation experiments is configured to permit separate demodulator and synchronization function filtering. In the present study the synchronization function filter was fixed, while the demodulator filter was varied for optimum performance.

Test description

Figures 2 through 5 describe the satellite channel and modem configurations used for the major portions of the hardware simulation study. Figure 2 is a simplified functional block diagram of the overall satellite channel consisting of an HPA link and a satellite link. Due to the physical separation of satellite and HPA facilities, it is necessary to interface these elements at 70 MHz. The HPA link detail is shown in Figure 3, which includes the HPA link elements that enable up-conversion of a 70-MHz QPSK signal, transmission through an HPA simulator at a frequency of 6030 MHz, and down-conversion to 70 MHz. Transmit and receive amplitude equalizers are required to compensate for the long cables to and from the HPA simulator. A common local oscillator is used to implement up- and down-conversion functions, thus canceling local oscillator frequency errors.

Two alternative HPA simulators were employed: a 45-W helix TWTA and a Varian 12-kW coupled-cavity TWTA (VTC 6660 C2). Comparison measurements have shown that nonlinear channel bit-error-rate performance and spectrum-spreading characteristics are very similar for both helix and coupled-cavity devices over the signal bandwidth required by these tests. Because of power supply limitations, it was necessary to lower the modulation anode voltage on the VTC 6660 C2 12-kW TWTA to limit the beam current and hence saturation output power to about 7.2 kW.

The satellite link detail is shown in Figure 4. Three channels of an INTELSAT IV transponder simulator are implemented as shown. Transponder channel 3 was used to transmit the QPSK signal. During dual-

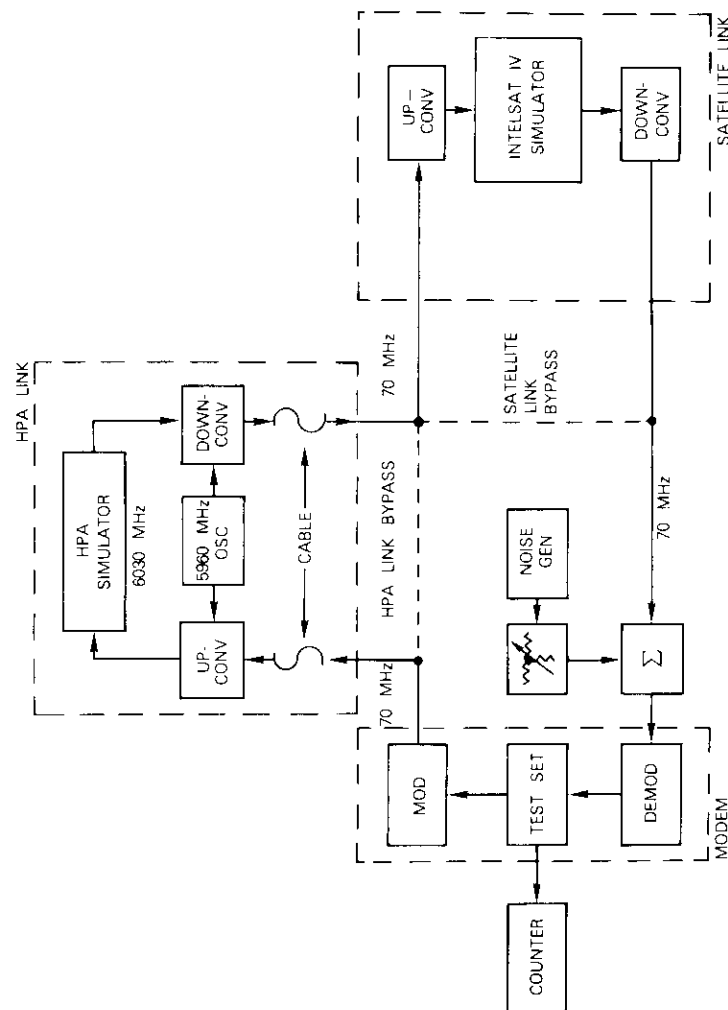


Figure 2. 4-Phase PSK Transmission Test Configuration Functional Block Diagram

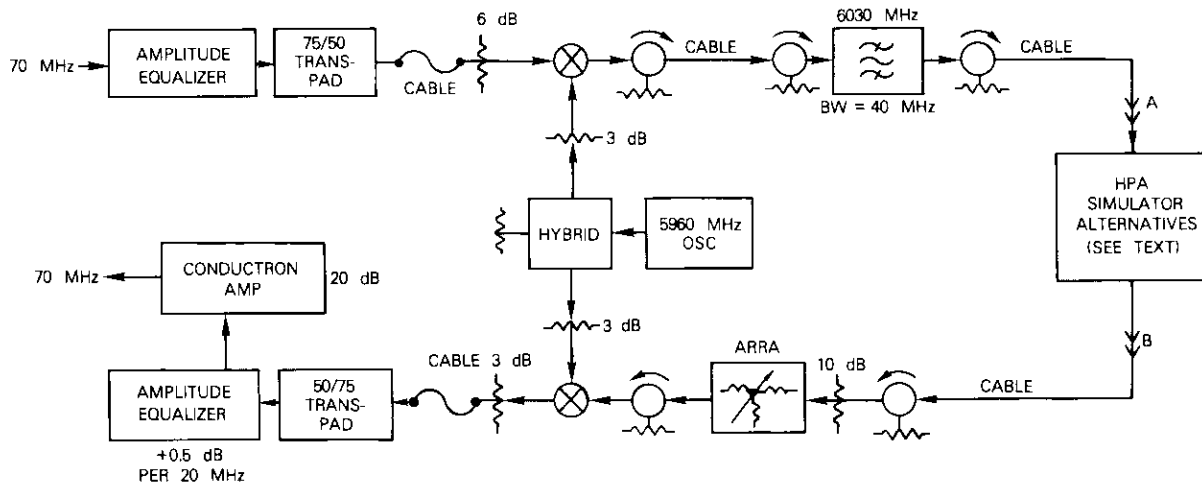


Figure 3. HPA Link Detail

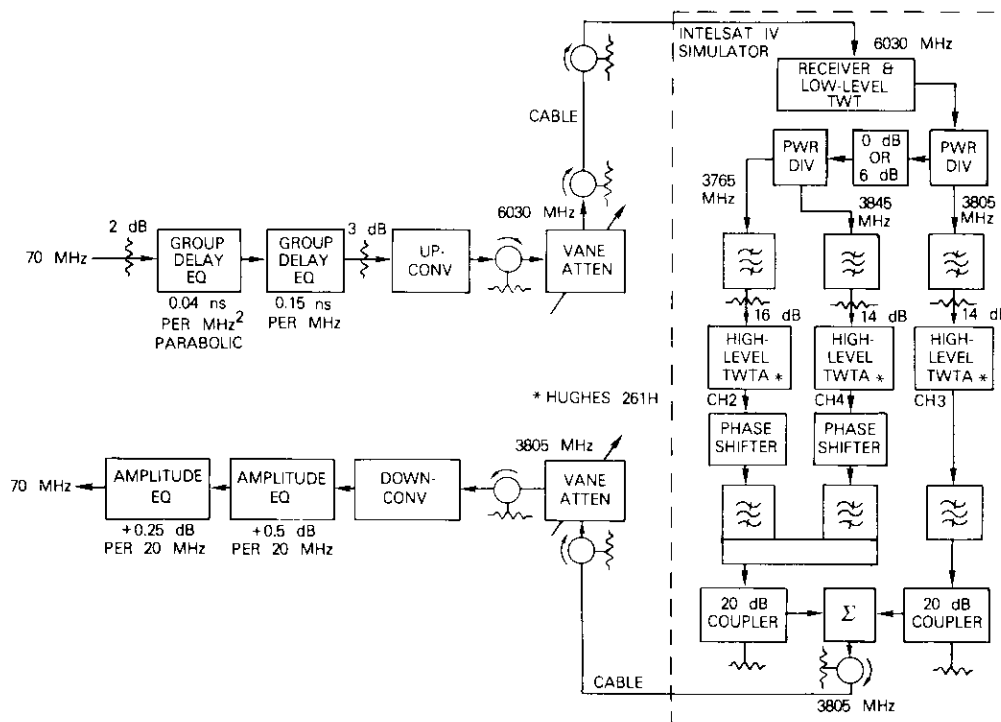


Figure 4. Satellite Link Detail

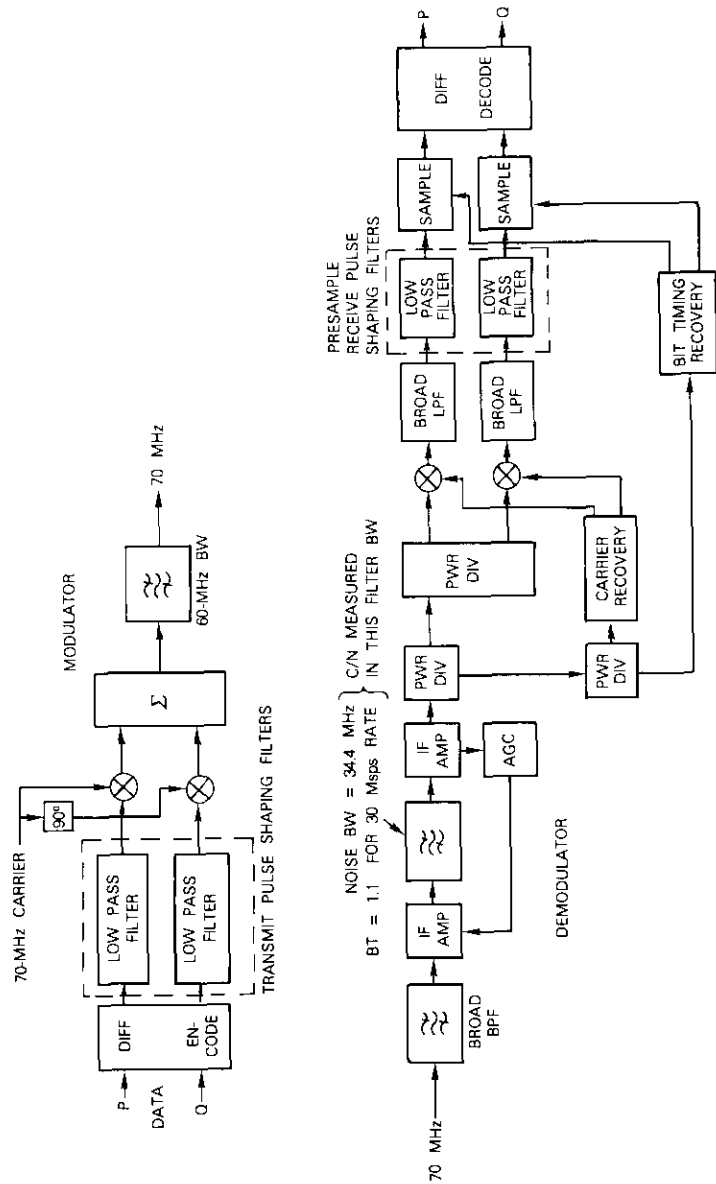


Figure 5. Modem Detail

path tests, channels 2 and 4 were used to provide dual-path transmission.

Figure 5 is a block diagram of the modem configuration. The dashed boxes indicate the location where filter functions were varied. Tables 1 and 2 and Figure 6 define the filter configurations and the corresponding filter element characteristics used in the study.

Finally, Figure 7 describes a satellite link used to perform demodulator synchronization and up-link co-channel interference investigations. The satellite transponder employed the Hughes 261H TWTA, the same device used in the INTELSAT IV simulator.

The characteristics of the 45-W helix TWTA HPA, the 12-kW Varian VTC 6660 C2 coupled-cavity TWTA HPA (including a driver TWTA), and the Hughes 261H satellite transponder TWTA used in these hardware investigations are presented in Figures 8, 9, and 10, respectively. For all performance measurements, the link amplitude and group delay were equalized for the flattest response. Up- and down-link equalization were separately performed. Typical link responses for the cascaded HPA and satellite link, excluding the pulse-shaping filter, are shown in Figure 11.

TABLE 1. PULSE-SHAPING-FILTER CHARACTERISTICS

Filter	Nyquist Rate (Msymbols/s)	Nyquist Rolloff (%)	2-dB Bandwidth (MHz)	Relative BT*
A	30	30	15.0	1.00
B	30	50	15.0	1.00
C	34	30	17.0	1.13
D	N.A.	N.A.	17.5	1.15
E	N.A.	N.A.	31.0	2.07

* B is 2-dB BW; 1/T is 30 Msymbols/s.

TABLE 2. MODEM PULSE-SHAPING-FILTER CONFIGURATION ALTERNATIVES

Configuration	Transmit Filter ^a	Presample Receiver Filter ^{a,b}
1	A: 30% rolloff Nyquist, BT = 1.0 for 30 Msymbols/s	None
2	B: 50% rolloff Nyquist, BT = 1.0 for 30 Msymbols/s	None

TABLE 2. MODEM PULSE-SHAPING-FILTER CONFIGURATION ALTERNATIVES (continued)

Configuration	Transmit Filter ^a	Presample Receiver Filter ^{a, b}
3	C: 30% rolloff Nyquist for 34 Msymbols/s (68 Mbit/s), BT = 1.13 for 30 Msymbols/s	A: 30% rolloff Nyquist, BT = 1.0 for 30 Msymbols/s
4	C: 30% rolloff Nyquist for 34 Msymbols/s (68 Mbit/s), BT = 1.13 for 30 Msymbols/s	B: 50% rolloff Nyquist, BT = 1.0 for 30 Msymbols/s
5	D: 30% rolloff elliptic, BT = 1.15 for 30 Msymbols/s	A: 30% rolloff Nyquist, BT = 1.0 for 30 Msymbols/s
6	E: wide elliptic function, BT = 2.00 for 30 Msymbols/s	B: 50% rolloff Nyquist, BT = 1.0 for 30 Msymbols/s
7	B: 50% rolloff Nyquist, BT = 1.0 for 30 Msymbols/s	A: 30% rolloff Nyquist, BT = 1.0 for 30 Msymbols/s

^a All filters contain an $(x/\sin x)$ spectrum shaping function for the design symbol rate except filters D and E.

^b The receiver has another wider bandpass filter (BT = 1.10) ahead of recovery, demodulating, and sampling functions for all configurations.

Bit-error-rate measurements

Bit-error-rate measurements were conducted with the HPA and satellite links in cascade and both TWTA's operating at saturation (0-dB input backoff) for each filter configuration of Table 2. Initially the 45-W helix TWTA was employed in the HPA simulator. Figures 2-5 indicate the test configurations used. For each measurement, the demodulator carrier phase and bit timing were adjusted to yield a minimum bit-error rate at a received C/N ratio of 13 dB. Following this adjustment, bit-error rate as a function of C/N ratio was measured. In all cases, a modulated carrier was used for the carrier power reference, and the C/N ratio was measured in the demodulator common IF bandpass filter. (The noise bandwidth of this filter is 33.7 MHz.) To compare the cascade link results on the basis of an

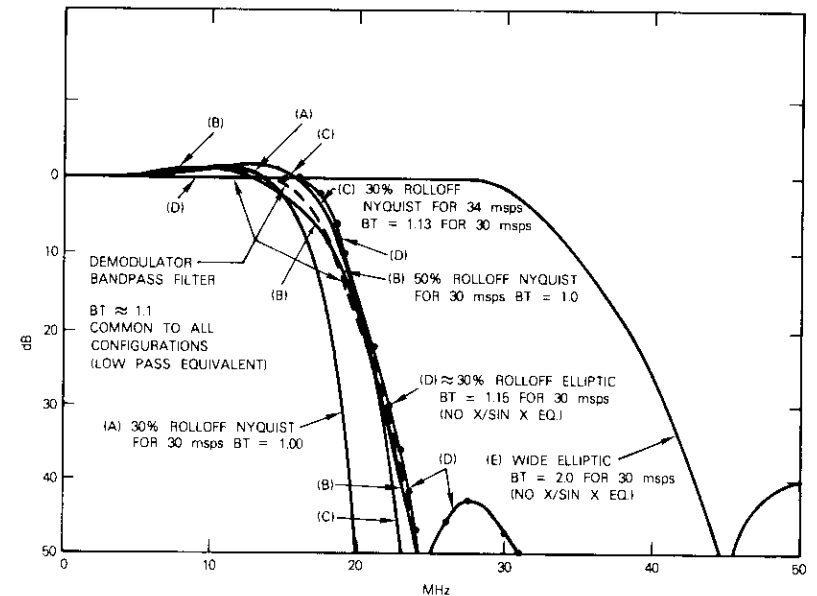
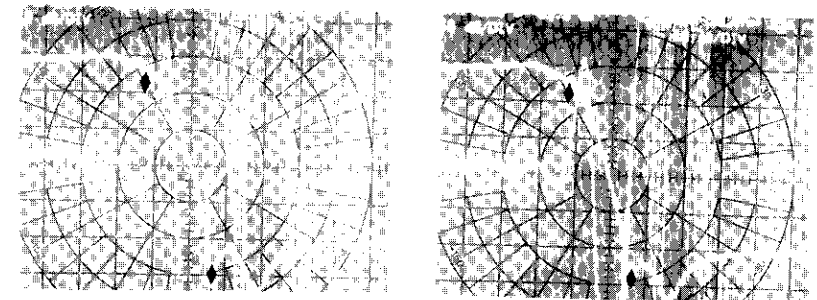


Figure 6a. Filters A, B, C, D, and E and Demodulator Noise Limiting Filter Amplitude Response Comparison

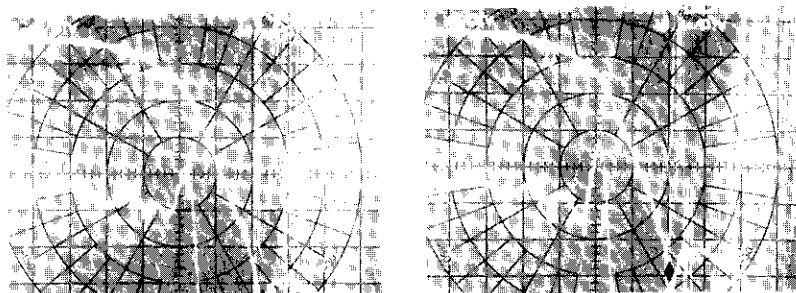


FILTERS (A)

◆ MARKERS AT 15 MHz AND 20.8 MHz

VERTICAL—10 dB AND 10 NANoseconds PER DIVISION
HORIZONTAL—3 MHz PER DIVISION

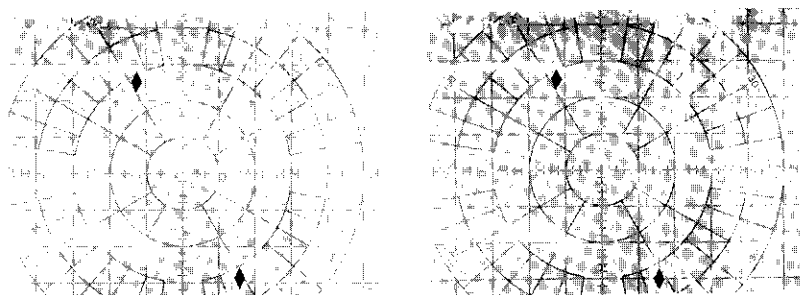
Figure 6b. Filter A Amplitude and Group Delay Responses (matched filter pair)



FILTERS (B)

◆ MARKERS AT 15 MHz AND 25 MHz

Figure 6c. Filter B Amplitude and Group Delay Responses (matched filter pair)

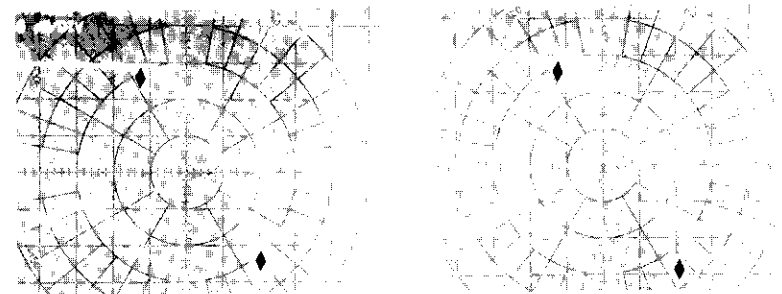


FILTERS (C)

◆ MARKERS AT 15 MHz AND 23.5 MHz

VERTICAL—10 dB AND 10 NANoseconds PER DIVISION
HORIZONTAL—3 MHz PER DIVISION

Figure 6d. Filter C Amplitude and Group Delay Responses (matched filter pair)



FILTERS (D)

◆ MARKERS AT 15 MHz AND 25 MHz

VERTICAL—10 dB AND 10 NANoseconds PER DIVISION
HORIZONTAL—3 MHz PER DIVISION

Figure 6e. Filter D Amplitude and Group Delay Responses (matched filter pair)

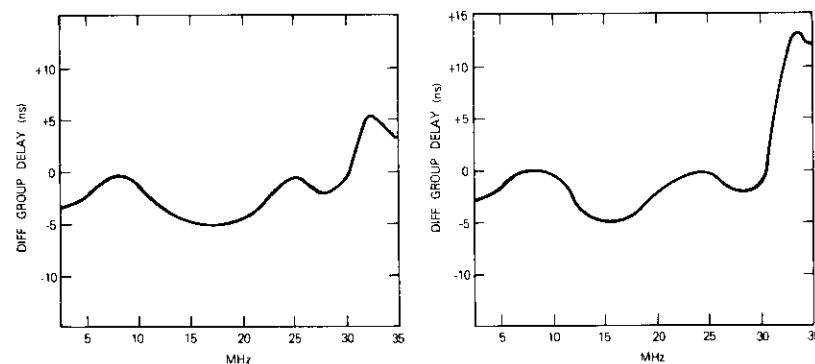
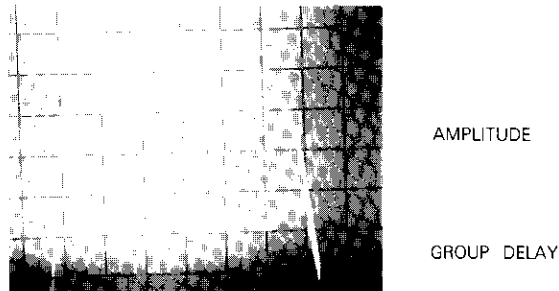


Figure 6f. Filter E Group Delay Responses (matched filter pair)



DEMODULATOR BANDPASS FILTER

VERTICAL—1 dB AND 5 NANoseconds PER DIVISION,
HORIZONTAL—5 MHz PER DIVISION

Figure 6g. Demodulator Bandpass Filter Amplitude and Group Delay Responses

unmodulated carrier reference, a correction factor should be applied as shown by the data in Table 3. (However, this correction factor is not to be applied to modem back-to-back performance data.)

TABLE 3. TANDEM LINK C/N CALIBRATION DATA

Filter Configuration	$C_{unmod}/C_{mod}(\text{dB})$			
	Modulator Output	HPA Output	Demod Input	Demod Rx BPF Output ^a
1	+0.15	+0.23	+0.40	+0.45
2,7	+0.60	+0.30	+0.40	+0.50
3,4	+0.12	+0.25	+0.40	+0.50
5	+1.11 ^b	+0.25	+0.40	+0.55
6	+0.40	+0.10	+0.20	+0.40

^a For link operation at a given BER, in dB: $C_{unmod}/N = C_{mod}/N + (C_{unmod}/C_{mod})$; $C_{unmod}/C_{mod} \sim 0.50$ dB, all cases.

^b For case 5, the HPA input backoff was set on C_{mod} ; in all other cases, it was set on C_{unmod} .

The results of these tests, shown in Figure 12, indicate that the performance of filter configurations 2-5 falls within a 0.3-dB band in the region of 1×10^{-4} to 1×10^{-7} bit-error rate, with configuration 4 producing the best performance. Configuration 6 is included to show

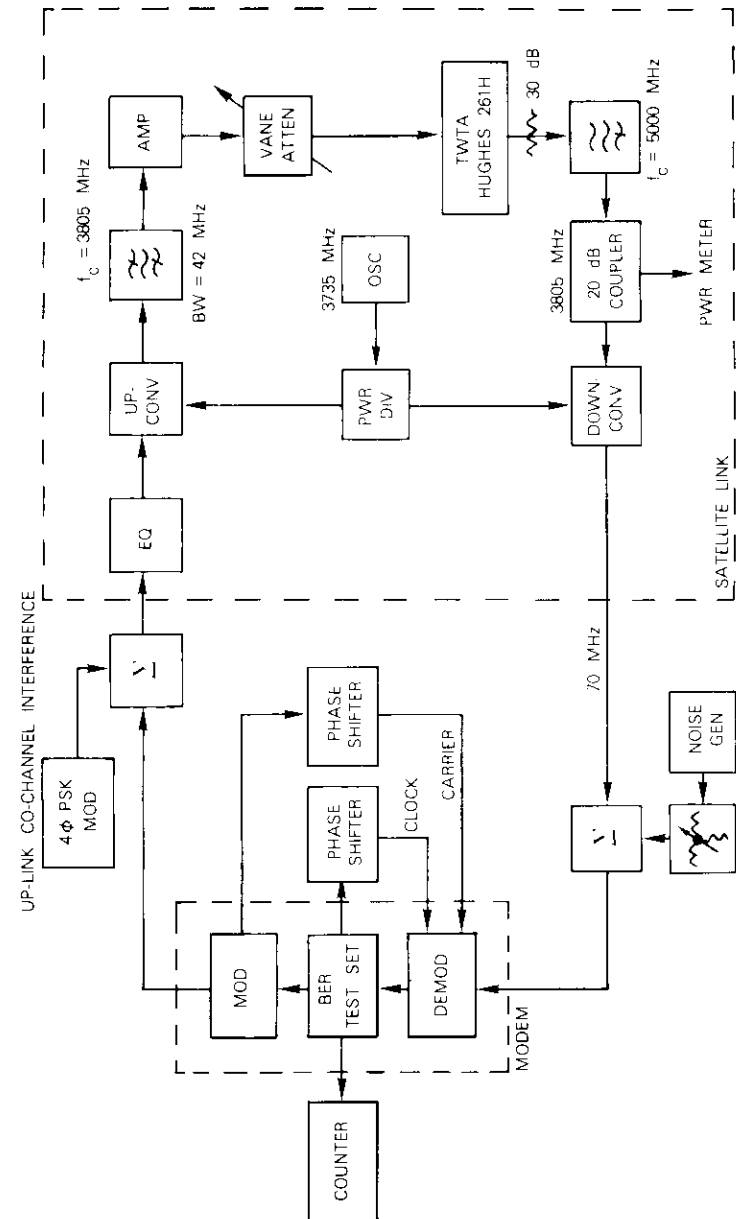


Figure 7. Satellite Link Configured for Hardwired Reference and Co-channel Interference Tests

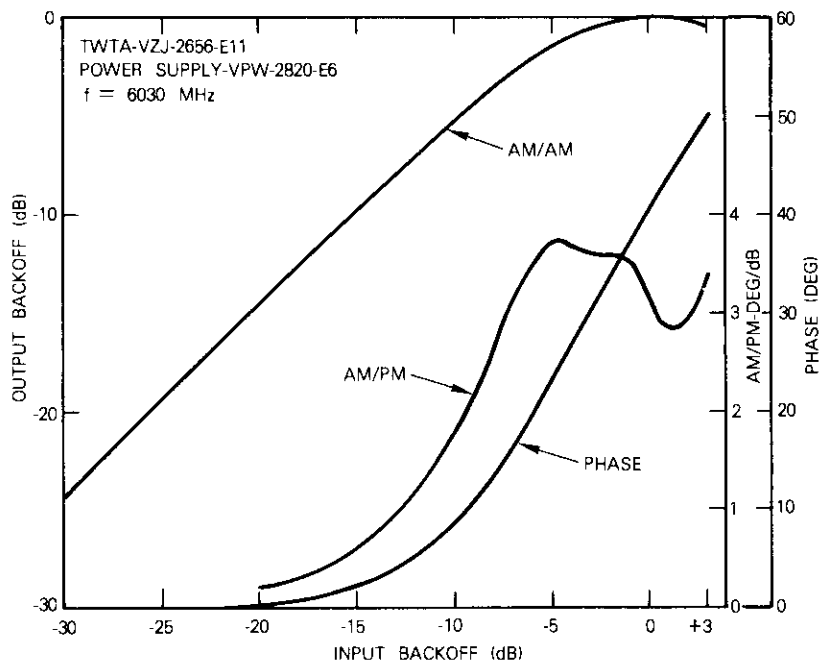


Figure 8. Single-Carrier Transfer Characteristics for Varian 45-W Helix TWTA

the performance possible with a very wideband transmit filter ($BT = 2.0$). Adjacent channel interference and dual-path transmission would preclude its use in actual practice. The performance of configuration 7 is surprisingly good considering that it contains two Nyquist functions, one before and one after the channel nonlinearities.

The inclusion or exclusion of the $(x/\sin x)$ weighting function as part of the transmit filter does not significantly affect the resulting performance. However, including the $(x/\sin x)$ weighting function produces a flat up-link signal-power spectral density across the entire transponder channel, which can benefit systems which employ frequency reuse.

It is interesting to note that, with two TWTA nonlinearities, a considerable variation in filter configurations will result in better than 5-dB gain in performance at 1×10^{-6} bit-error rate with respect to filter configuration 1. Modem back-to-back performance data for the

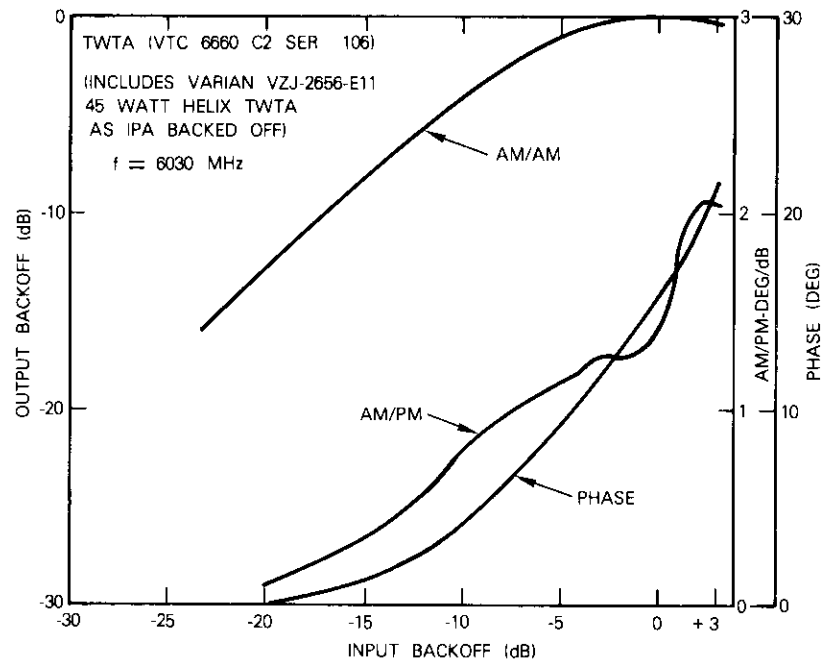


Figure 9. Single-Carrier Transfer Characteristics for Varian Coupled-Cavity TWTA

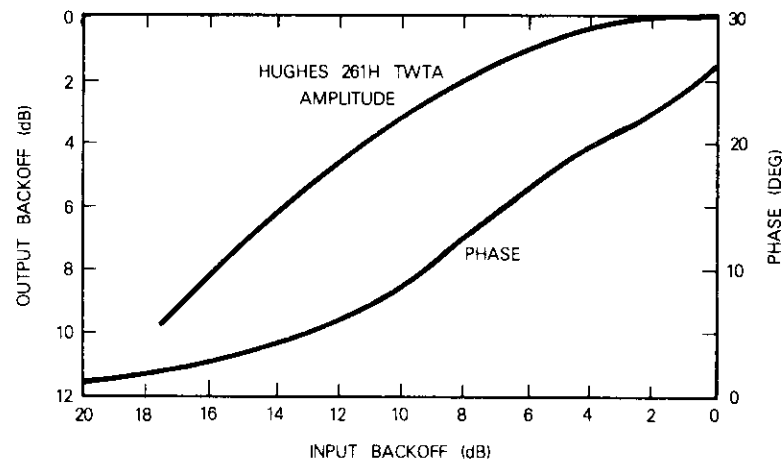


Figure 10. INTELSAT IV Satellite Simulator TWTA Characteristics

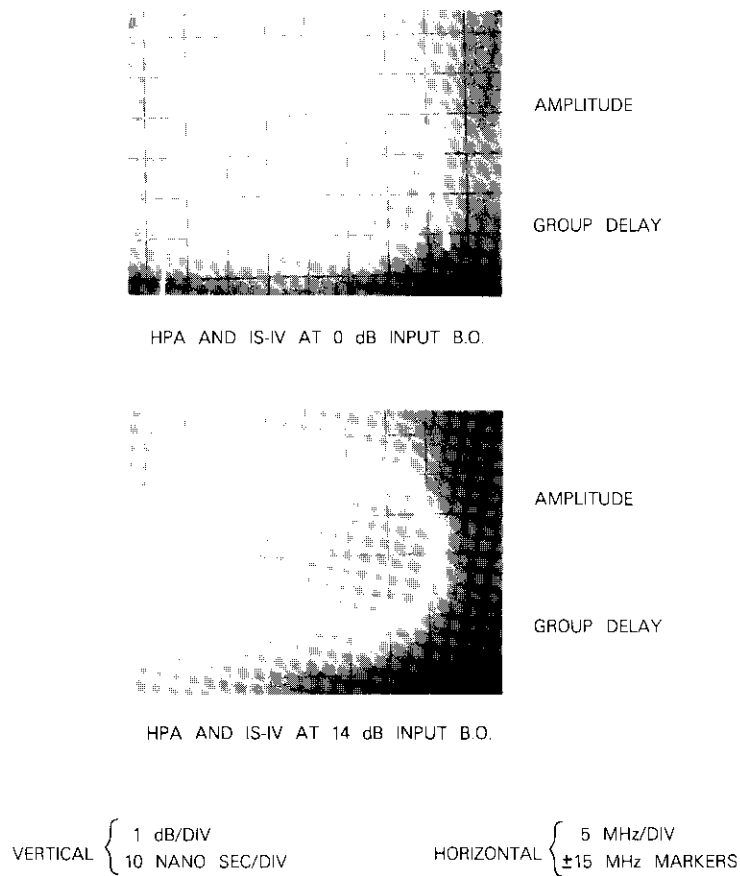


Figure 11. Typical INTELSAT IV and HPA Cascaded Link Responses

filter configurations and theoretical performance for unfiltered differentially encoded QPSK with perfect demodulator carrier and bit timing references are also shown in Figure 12. Finally, bit-error rate was measured for filter configuration 4 with the 12-kW coupled-cavity TWTA employed as the HPA simulator. These results, shown in Figure 13, demonstrate the validity of employing a lower power helix TWTA as an HPA simulator for bit-error-rate measurements.

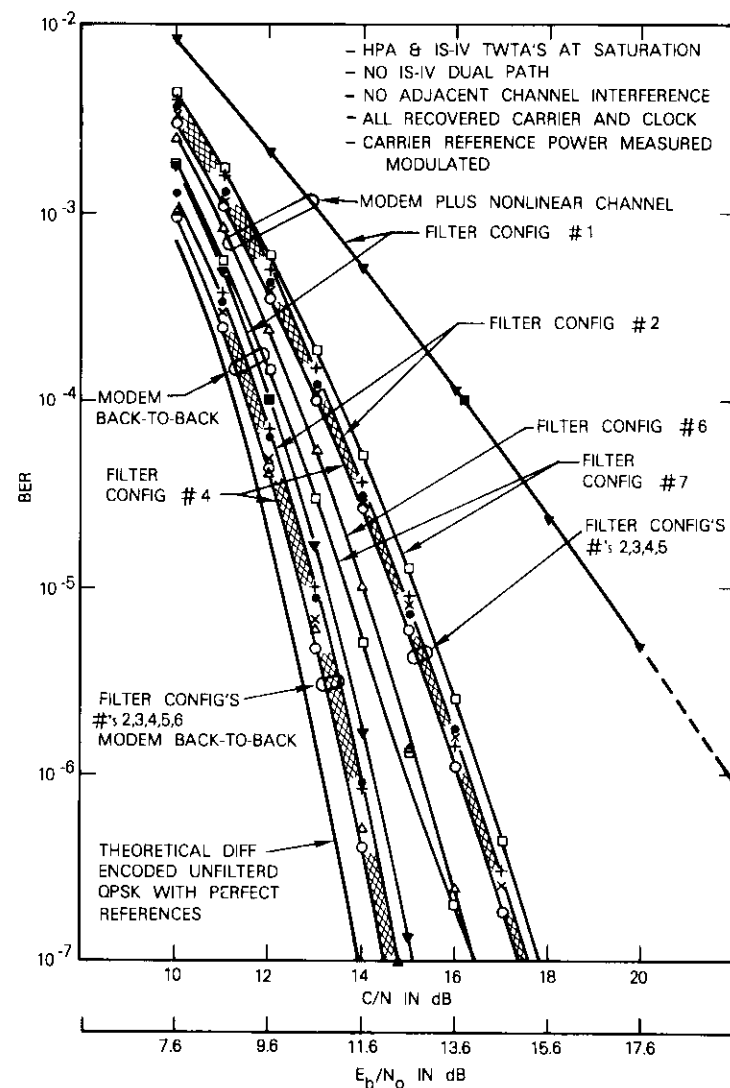


Figure 12. Bit-Error-Rate Performance

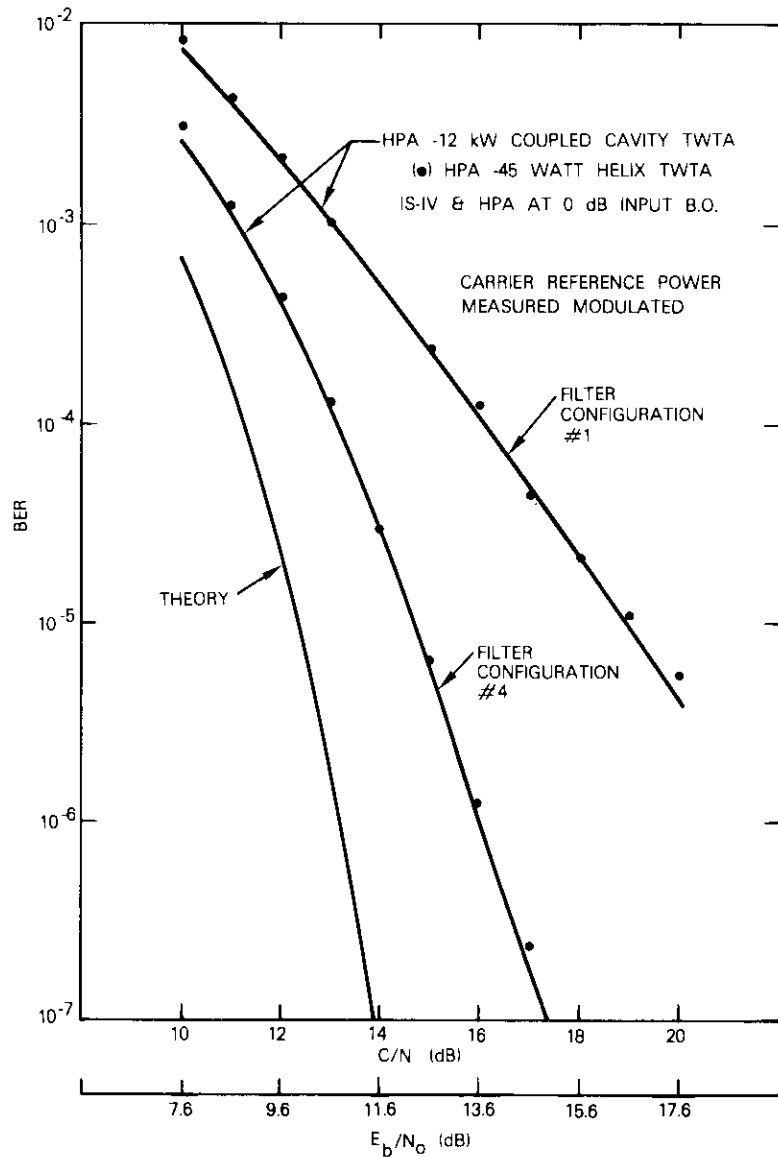


Figure 13. Performance Comparison of Tandem Link HPA and INTELSAT IV Using Different HPA TWTA Types with Filter Configurations 1 and 4

Adjacent channel interference

Adjacent channel interference is an important system consideration. Strict adjacent channel up-link interference criteria are usually specified to preclude impairment of a small FDM-FM carrier positioned at the close edge of an adjacent transponder channel. In effect, the specified transmit modulation pulse-shaping-filter rolloff factor (0.3 for filter A) was selected on this basis for the INTELSAT TDMA system. However, the effect of the earth station HPA nonlinearity, even when the HPA is backed off, can regenerate significant filtered sideband energy.

Power spectral density measurements using the 45-W helix HPA were performed to examine the impact of the various transmit filters on the HPA output spectrum. To ensure that this was a valid representation of an actual earth station HPA (coupled-cavity TWTA), some comparative spectral measurements were made on the coupled-cavity TWTA. Filter A of Table 1 was used in the modulator. HPA output spectra as a function of input backoff were measured for both the helix and coupled-cavity device; the results are given in Figures 14 and 15. It is noted that, except for small differences, the spectral regrowth char-

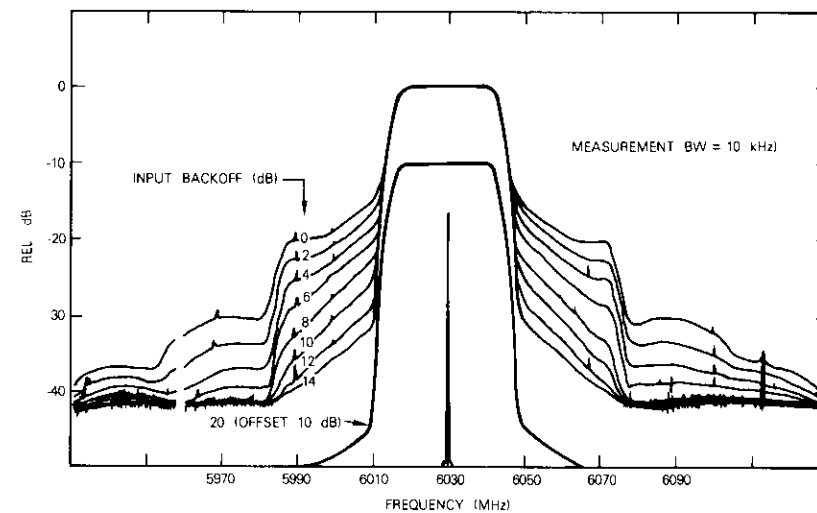


Figure 14. HPA Output Spectra for Filtered QPSK [filter A, 30% rolloff Nyquist (30 Msymbols/s), operated at $BT = 1.00$, 45-W helix TWTA]

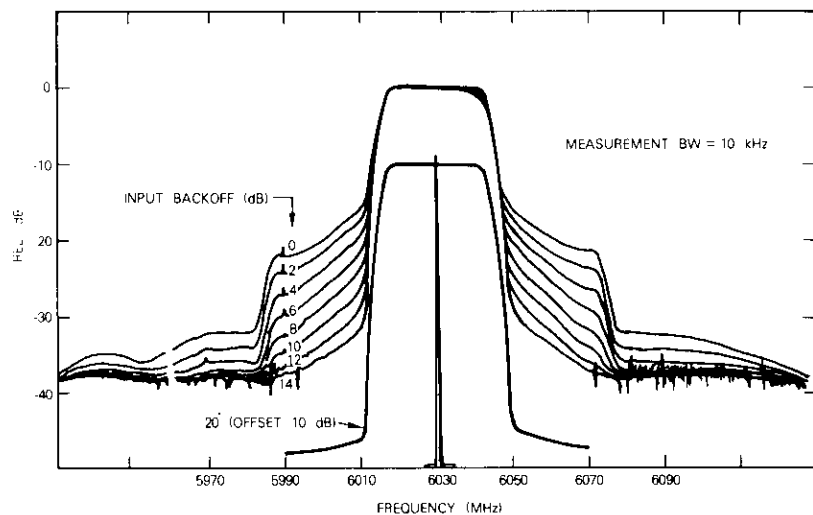


Figure 15. HPA Output Spectra for Filtered QPSK [filter A, 30% rolloff Nyquist (30 Msymbols/s), operated at $BT = 1.00$, Varian 12-kW coupled-cavity TWTA, operated at 7-kW]

acteristics are very similar. The measured characteristics for each TWTA type are given in Figures 8 and 9.

A series of QPSK spectrum regrowth measurements was performed using the 45-W helix TWTA with different pulse-shaping-filter characteristics. In all cases, power spectral density was measured in a 10-kHz bandwidth using a spectrum analyzer in which the normal diode detector was replaced by a true rms detector.

For these measurements, variable filter bandwidth was simulated by varying the modulation clock frequency for a given bandwidth filter. The results were scaled in frequency to permit comparison at the same symbol rate. Filter A spectral regrowth data were measured at different QPSK modulation clock rates corresponding to $1.0 \leq BT \leq 1.2$. Figures 14 and 16 show representative results for BT products of 1.00 and 1.15. From these data the relative spectral densities in the adjacent satellite channel for 0- and 6-dB HPA input backoffs were derived and are plotted in Figure 17 as a function of filter BT product. It is interesting to note that, as the filter bandwidth is increased from $BT = 1.0$, the relative power spectral density in the usable area of the nearest edge of the adjacent channel (23.75 MHz from the desired

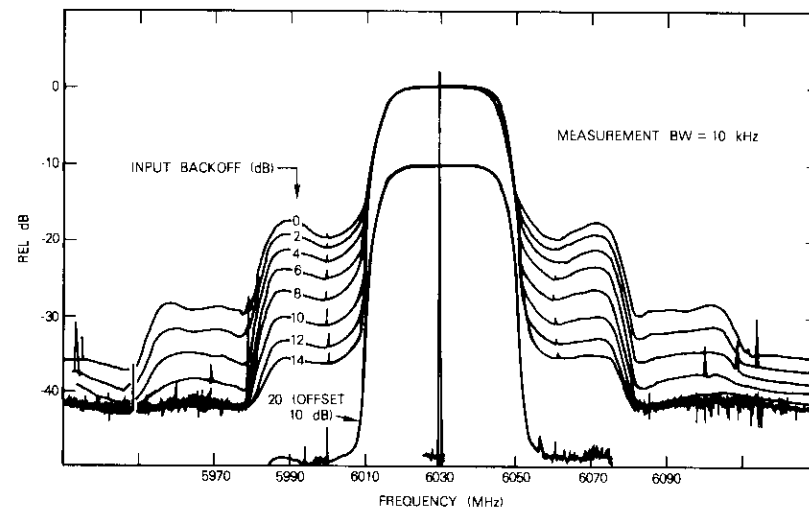


Figure 16. HPA Output Spectra for Filtered QPSK [filter A, 30% rolloff Nyquist (30 Msymbols/s), operated at $BT = 1.15$]

channel frequency) actually decreases. At the same time the level at 40 MHz removed from the desired channel center frequency (center of the adjacent channel) increases. The spectral density at these two frequencies becomes equal at about $1.15 \leq BT \leq 1.2$ depending on HPA input backoff.

Measured power spectral data for filters B and D are shown in Figures 18, 19, and 20. Figures 21-23 compare measured adjacent channel power spectral densities for filters A and B at BT products of 1.00 and 1.15 and filter D at $BT = 1.15$ derived from data in Figures 14, 16, 18, 19, and 20. Nearly the same power spectral density levels at 23.75 MHz removed from the center of the desired channel can be obtained with any of these filters operated at $BT = 1.15$. The level at 40 MHz tends to be equalized to the level at 23.75 MHz for this BT product.

The tolerable power spectral density in the adjacent channel based on interference to an FM signal has been specified as 24.5 dBW/4 kHz for the INTELSAT TDMA system. The foregoing data can be related to a possible TDMA operational scenario. If it is assumed that the required e.i.r.p. from an earth station transmitting 60-Mbit/s QPSK TDMA is 90 dBW, the power spectral density at the signal center frequency can be

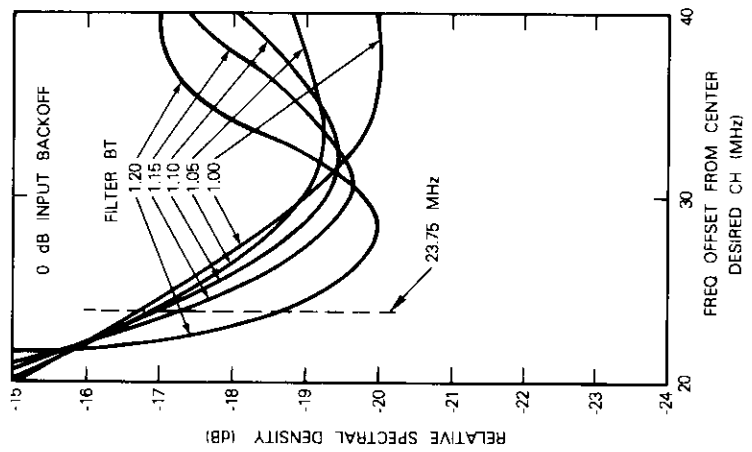
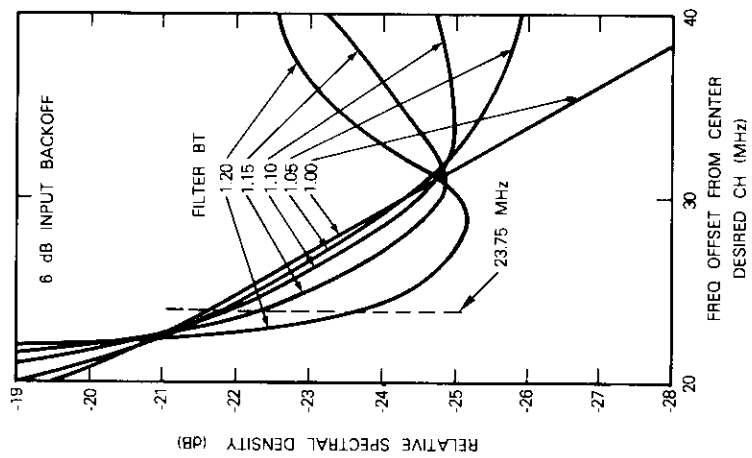


Figure 17. Summarized HPA Regrowth Spectra for Filtered QPSK [Filter A, 30% rolloff Nyquist (30 Msymbols/s)]

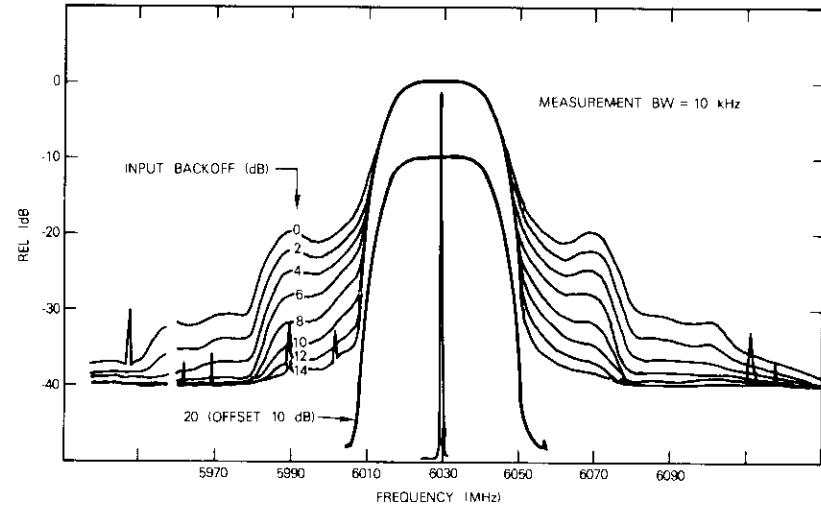


Figure 18. HPA Output Spectra for Filtered QPSK [filter B, 50% rolloff Nyquist (30 Msymbols/s), operated at BT = 1.00]

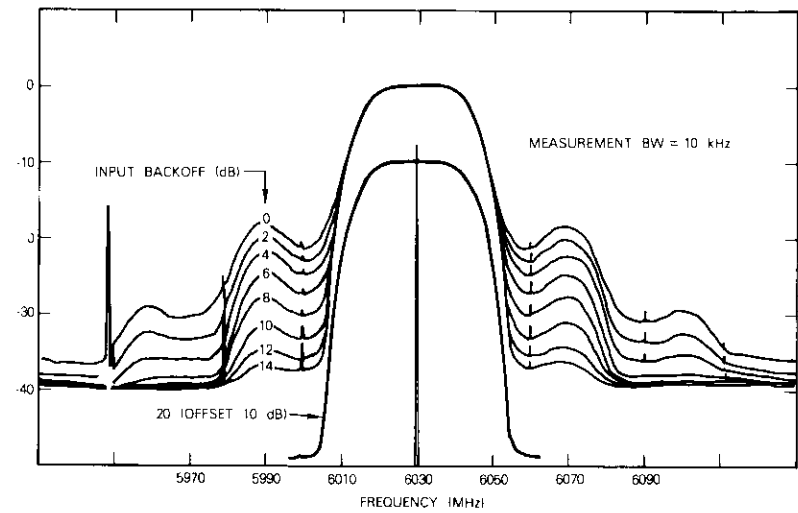


Figure 19. HPA Output Spectra for Filtered QPSK [filter B, 50% rolloff Nyquist (30 Msymbols/s), operated at BT = 1.15]

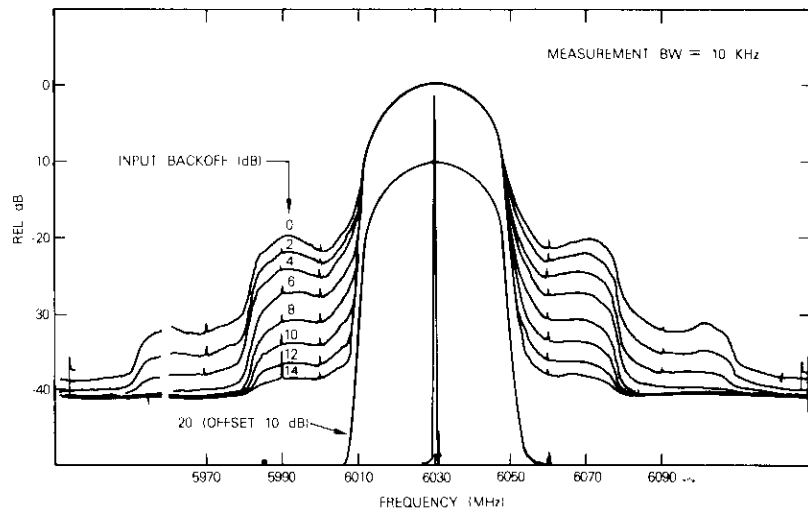


Figure 20. HPA Output Spectra for Filtered QPSK [filter D, 30% rolloff elliptic, no $(x/\sin x)$ equalization, operated at $BT = 1.15$, (30 Msymbols/s)]

calculated. Specifically, for a symbol rate of 30×10^6 MHz and an e.i.r.p. of 90 dBW, the power spectral density is 51.2 dBW/4 kHz. The relative power spectral density of the regrown spectrum must be reduced by $51.2 - 24.5 = 26.7$ dB to meet the interference criteria at 23 MHz from the center of the desired carrier. This can be achieved by operating the HPA at an input backoff of 6–10 dB with filters A, B, or D at $BT = 1.15$; filters B and D give slightly better performance in this respect.

More detailed data have been plotted in Figure 24 to enable accurate determination of operating input backoff for filter B at a BT product of 1.15. In this case an input backoff of 9 dB will ensure compliance with the 24.5-dBW/4-kHz interference criterion anywhere in the adjacent channel for offset frequencies equal to or greater than 23.75 MHz. It should be noted that the steepness of the spectrum in the region of 23.00 to 23.75 MHz removed from the center of the desired channel could introduce problems in maintaining the predicted level. Figure 24 was obtained by averaging the upper and lower sideband levels of Figure 19 as required by the slight asymmetry of the measured spectrum.

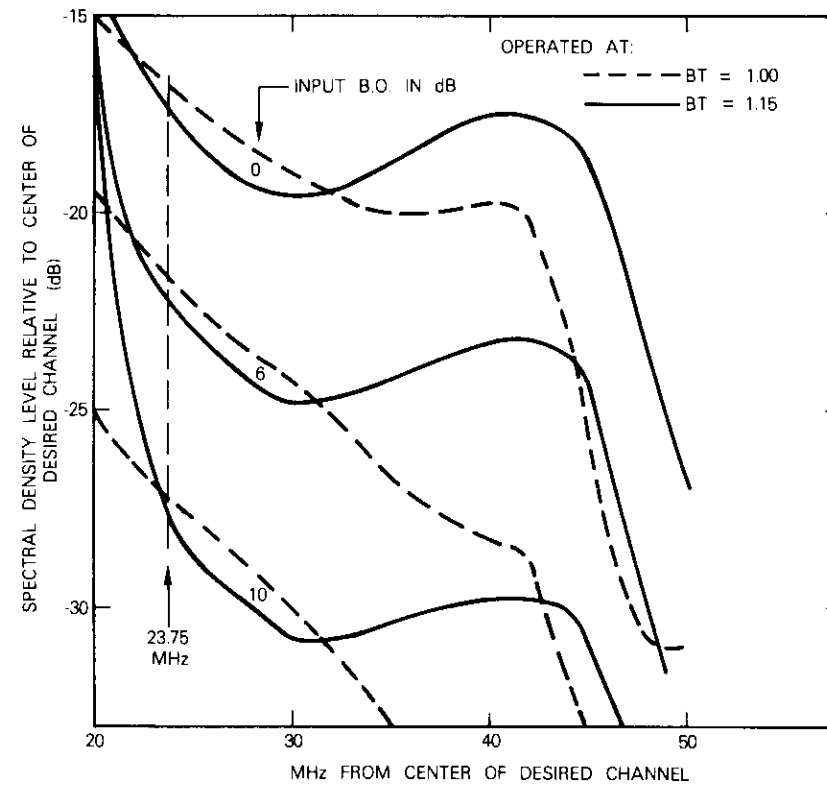


Figure 21. HPA Regrowth Spectra Detail Comparison for Filtered QPSK [filter A, 30% rolloff Nyquist (30 Msymbols/s)]

Dual-path degradation

Degradation resulting from parallel transmission through the filter skirt region of adjacent transponders must be considered when specifying the channel pulse-shaping filters. Dual-path transmission leads to ripples in the amplitude and group delay responses. The magnitude of these ripples increases at the transponder band edges. Narrowing the demodulator predetection filter thus tends to reduce dual-path degradation. Dual-path tests were conducted using the INTELSAT IV transponder simulator.

Dual-path transmission tests were performed with filter configurations 1, 2, 3, 4, and 6 of Table 2. The INTELSAT IV simulator was

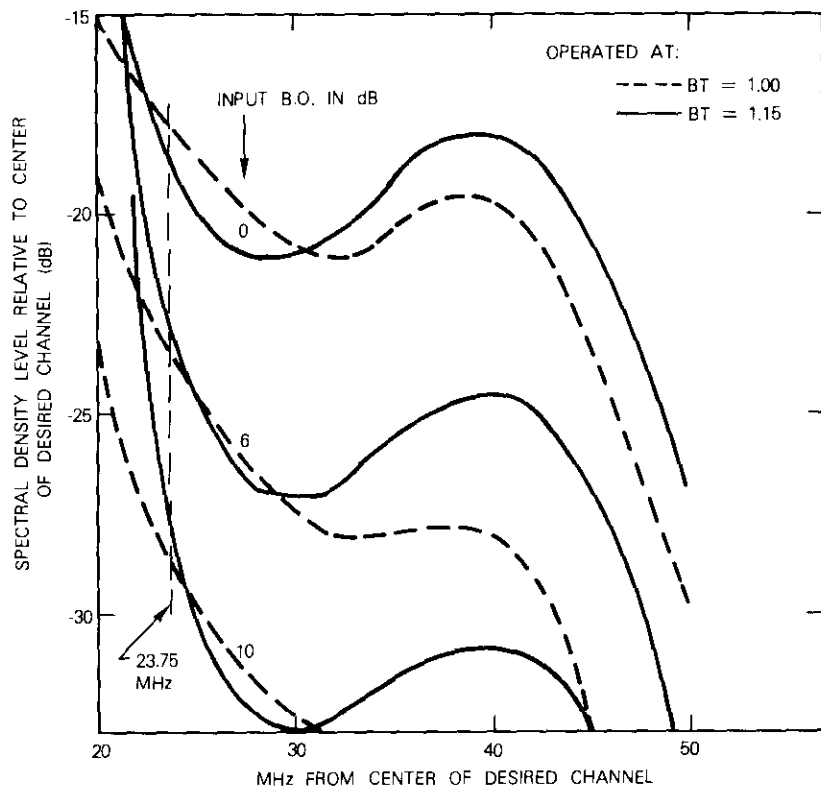


Figure 22. HPA Regrowth Spectra Detail Comparison for Filtered QPSK [filter B, 50% rolloff Nyquist (30 Msymbols/s)]

configured as in Figure 4 with the small signal gains of transponder channels 2, 3, and 4 adjusted to be equal. Phase shifters were placed at the output of channel 2 and 4 TWTAs. Initially channels 2 and 4 were turned off and bit-error-rate data were taken with HPA and INTELSAT IV channel 3 TWTAs at saturation. Channels 2 and 4 were then turned on and the phase shifters adjusted for maximum bit-error rate. Since channels 2 and 4 were unloaded, adjacent channel gain was high and therefore large dual-path effects occurred. The test was repeated with the small signal gain of channels 2 and 4 reduced by 6 dB. This condition is equivalent to nominal dual path, representing the case in which adjacent channels are loaded with one or more signals.

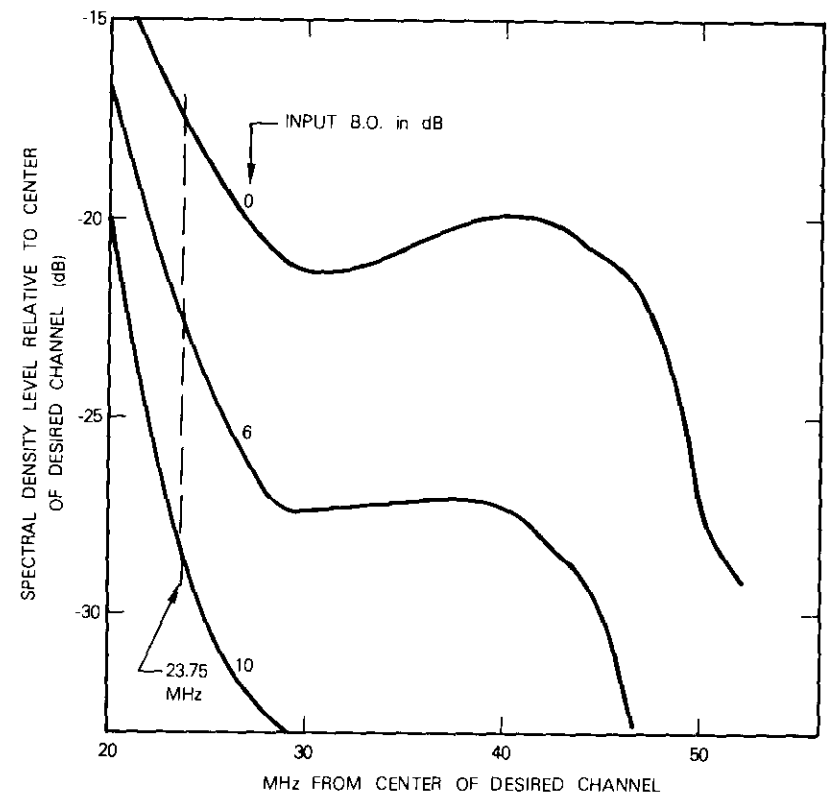


Figure 23. HPA Regrowth Spectra Detail Comparison for Filtered QPSK [filter D, 30% rolloff elliptic, $BT = 1.15$ for 30 Msymbols/s)]

Test results are presented in Figures 25, 26, and 27. Configuration 1 performance appears on each figure for comparison with that of each of the other configurations. As indicated in Figure 25, using a very wide ($BT = 2.0$ of configuration 6) rather than a narrower ($BT = 1.0$ to 1.13) transmit filter results in more dual-path loss. However, of the two narrow transmit filter configurations tested (configurations 3 and 4, where Nyquist filters are employed at the demodulator), the configuration using the wider, more gentle rolloff Nyquist filter gave less dual-path loss (Figure 26). This suggests that, for these filter configurations, the dual-path transmission may have a greater effect on the recovery circuits than on the data decision circuits.

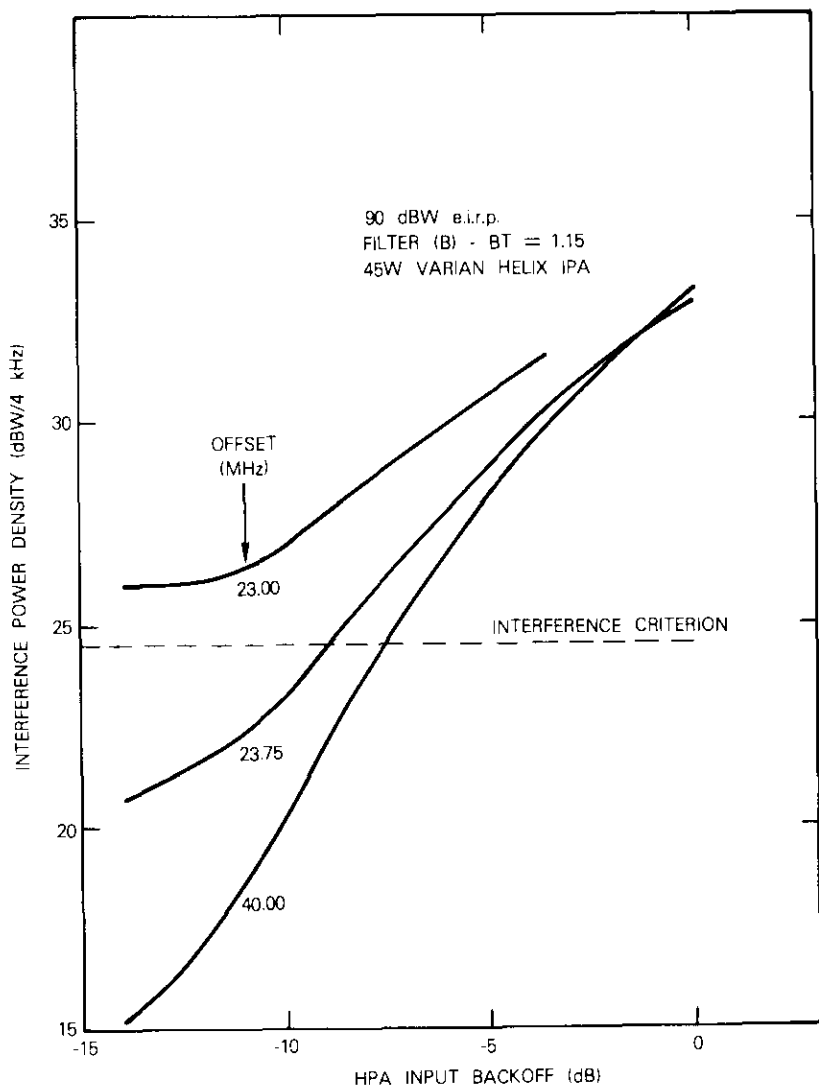


Figure 24. Earth Station Transmitted Adjacent Channel Interference Power Spectral Density with Filter B at $BT = 1.15$ (90-dBW Earth Station e.i.r.p.)

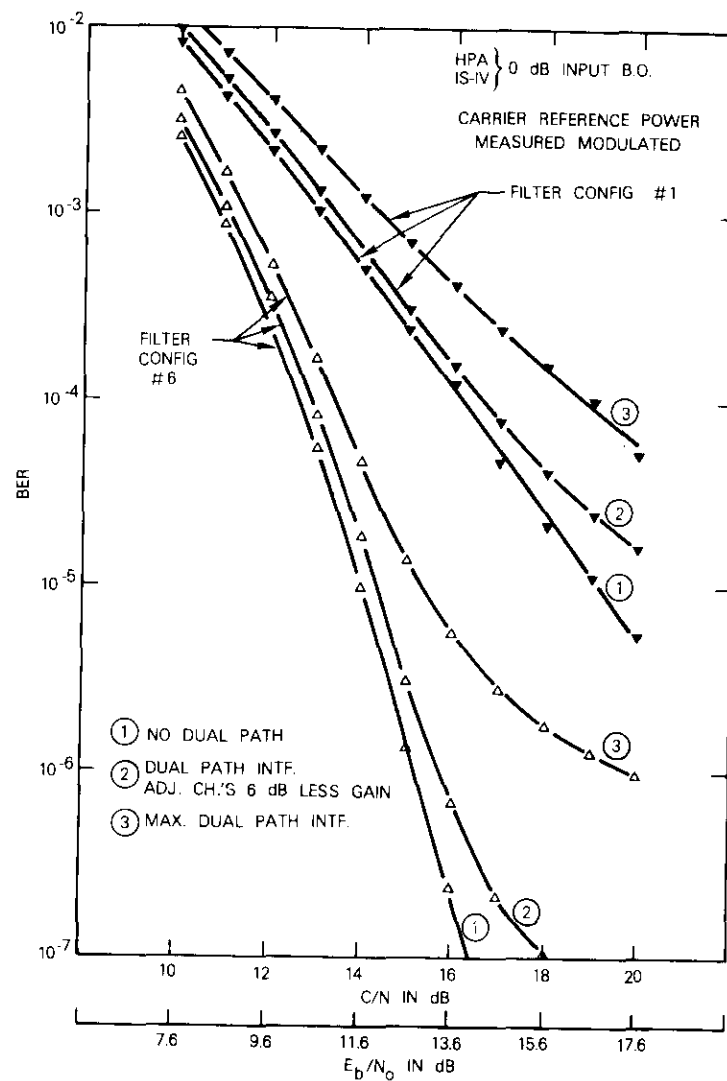


Figure 25. Performance Comparison with and without Dual-Path Transmission for Configurations 1 and 6

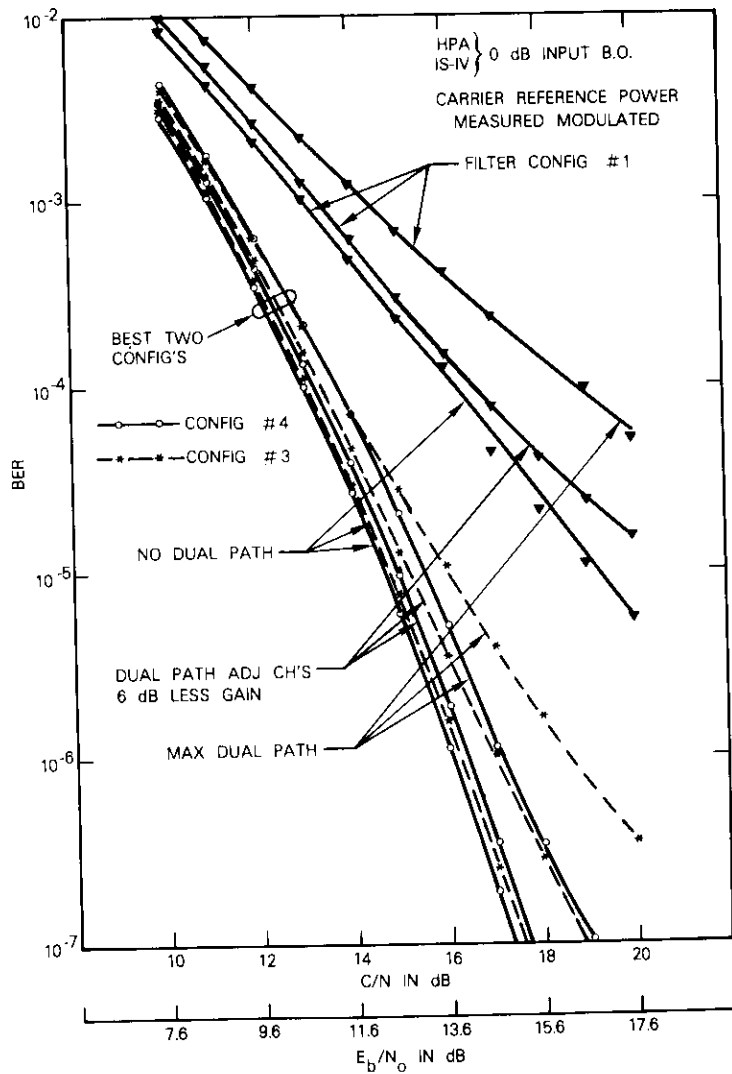


Figure 26. Performance Comparison with and without Dual-Path Transmission for Configurations 1, 3, and 4

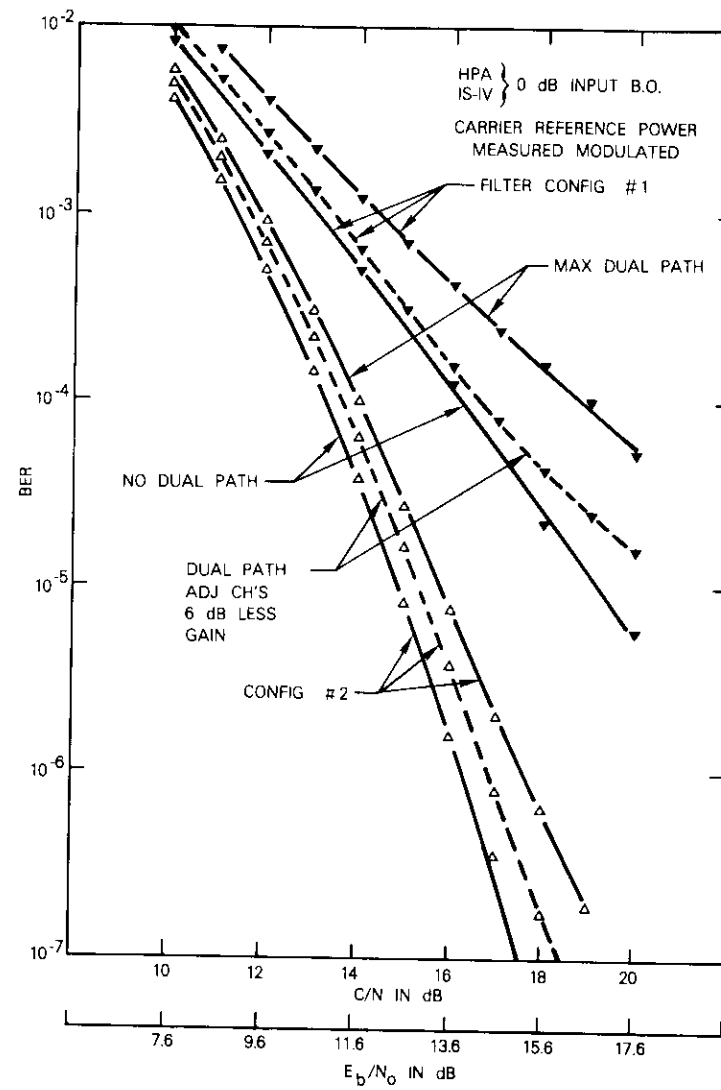


Figure 27. Performance Comparison with and without Dual-Path Transmission for Configurations 1 and 2

Co-channel interference

The initial work which led to the present investigation indicated that for a single channel nonlinearity the effects of up-link co-channel interference were less severe when wider transmit bandwidth pulse shaping filters were used. Figure 7 shows the co-channel interference measurement configuration using a satellite transponder with a single QPSK modulated interference source added on the up-link at the carrier frequency. Bit-error-rate performance was measured with the satellite TWTA at saturation and at 14-dB input backoff using filter configuration 3. An up-link desired signal-to-interference ratio of 20 dB was implemented for these tests. The results are plotted in Figure 28, which also gives comparison results for configuration 1.

Demodulator synchronization reference investigation

Measurements were conducted to investigate the contribution of the demodulator carrier and bit-timing recovery circuits to the overall nonlinear channel bit-error-rate performance impairment. Bit-error rate was measured as a function of the transmit pulse-shaping filter bandwidth for recovered carrier and recovered clock, hardwired carrier and recovered clock, and hardwired carrier and hardwired clock. The investigation was performed using a single satellite TWTA nonlinearity configured with the modem as shown in Figure 7. The satellite TWTA was operated at 0- and 14-dB input backoffs. Figure 29 summarizes these data for a 1×10^{-5} bit-error rate.

These results indicate that for Nyquist transmit filtering (filter A, $BT = 1.00$) a significant portion of the impairment loss in the nonlinear channel is contributed by the carrier and bit-timing synchronization circuits. In the case of a quasi-linear channel (14-dB input backoff) with the same filtering, the contribution due to the synchronization circuits is less. As the transmit filter bandwidth departs from the Nyquist condition by increasing the bandwidth ($BT > 1.0$), the impairment loss in the quasi-linear channel increases as expected because the non-Nyquist filter now introduces some intersymbol distortion at the demodulator sampling instants. However, the contribution of the synchronization circuit to the total impairment remains about the same for $BT = 1.07$, becomes slightly less at $BT = 1.13$, and appears to approach zero at wide bandwidths ($BT \rightarrow 2.0$). The total

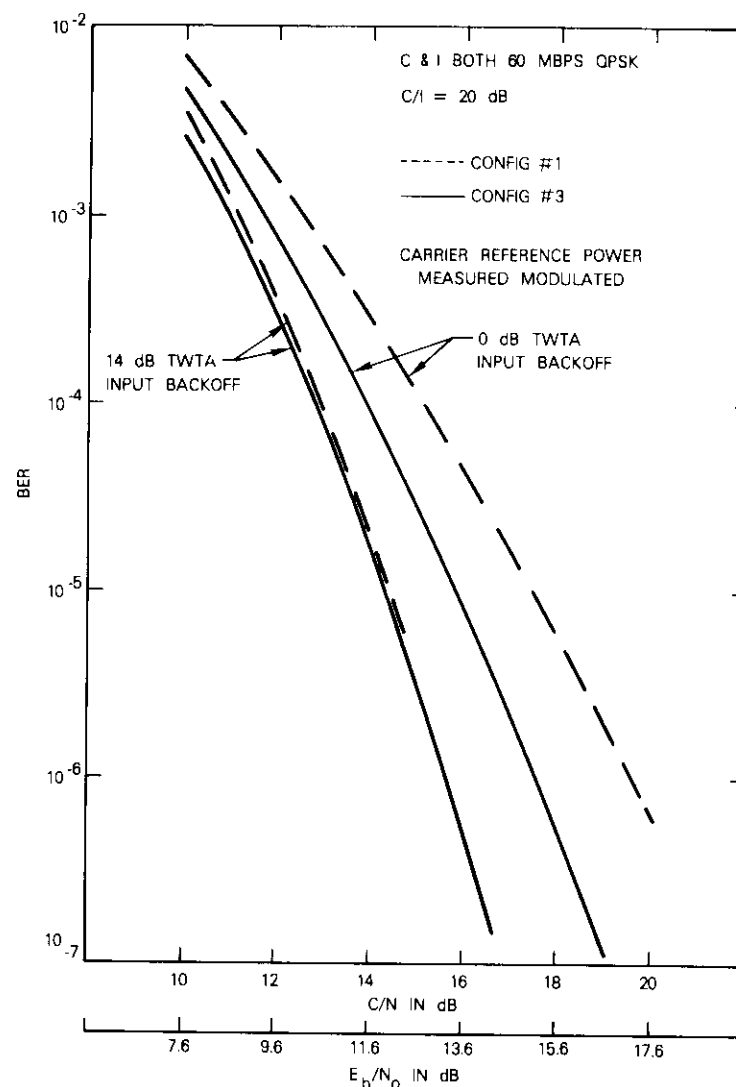


Figure 28. Co-Channel Interference Performance in a Satellite Simulator for Filter Configuration 3

loss slowly builds up to an asymptotic value in the quasi-linear channel as the transmit bandwidth is increased.

In the nonlinear channel case, as the total impairment loss drops

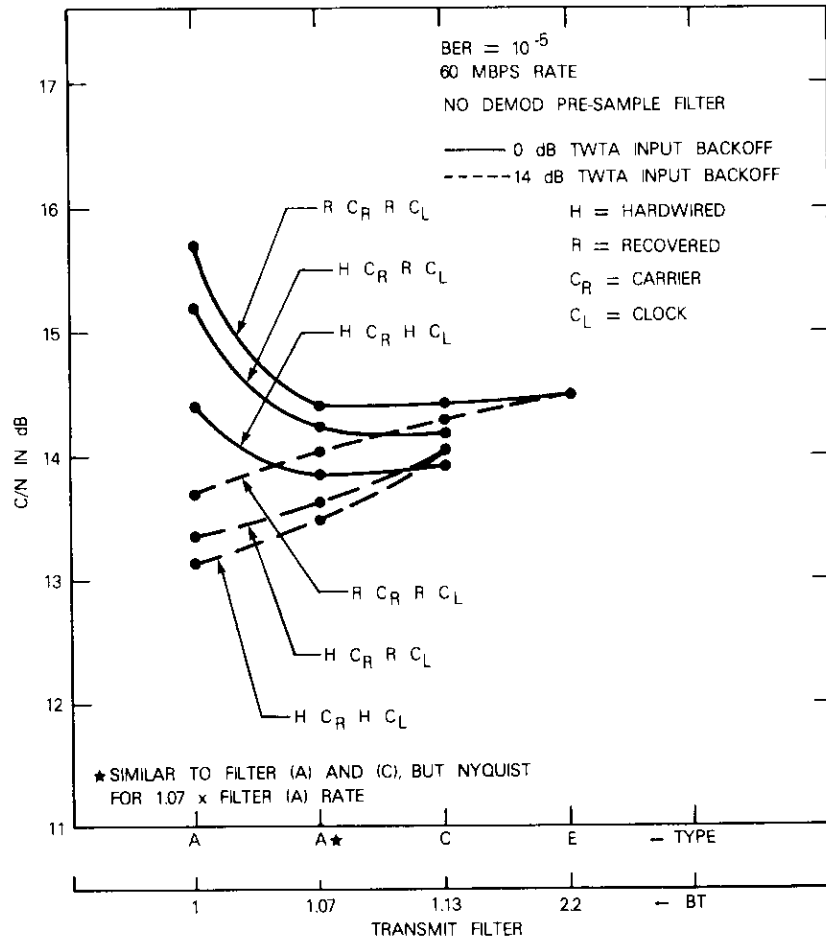


Figure 29. Constant BER Performance Summary of Synchronization Measurements for a Single Nonlinearity with Variable Transmit Filter Bandwidth

dramatically with slightly increasing transmit-filter BT (even with BT = 1.07), the contribution of the synchronization circuits gradually decreases with increasing filter BT product. The demodulator noise limiting bandpass filter (BT = 1.1) affects the total loss. It becomes the limiting filter for wide bandwidth transmit filters and therefore

limits the degree of synchronization circuit loss reduction with increasing transmit filter bandwidth.

Figure 30 shows measurements for the nonlinear channel case only (satellite TWTA at saturation) extended to show the effect of including the demodulator presample Nyquist filter. This result shows more clearly the gradual reduction of the loss contribution from synchroni-

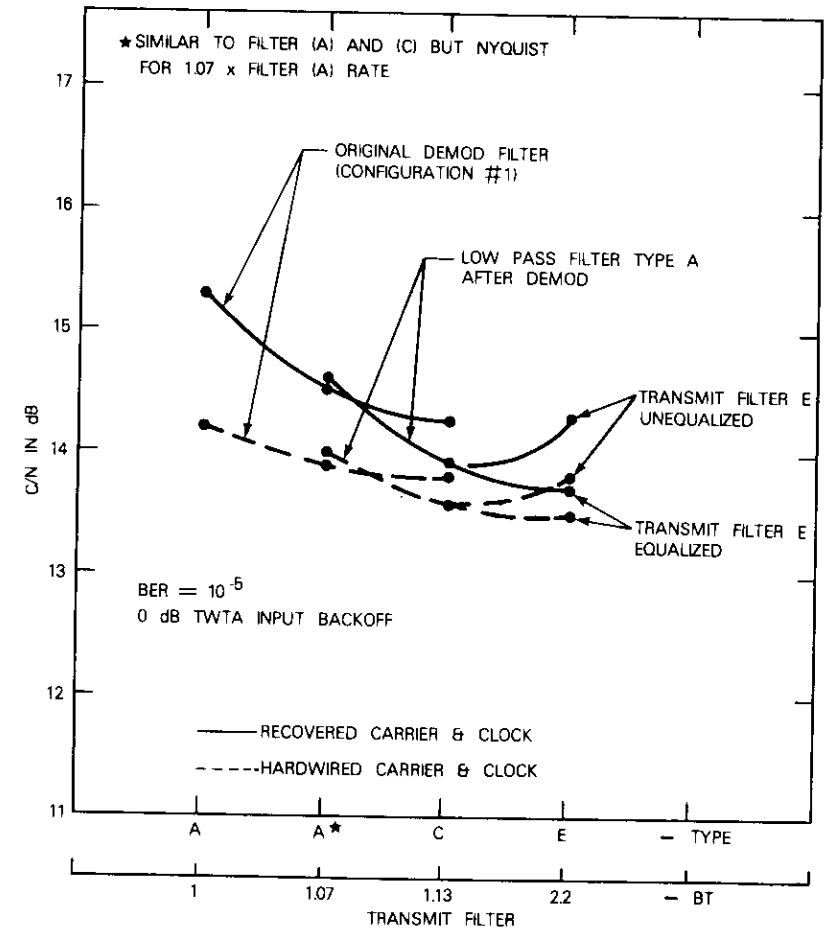


Figure 30. Performance Comparisons of Modem Filter Configuration and Filter Bandwidth for a Single Nonlinearity

zation circuits as the transmit filter bandwidth is increased. For transmit filter $BT > 1.13$, the additional total impairment reduction as well as the contribution of the synchronization circuits is small.

These results indicate that a slight increase in the bandwidth ($BT \sim 1.13$) of the transmit pulse-shaping filter significantly reduces the recovery circuit degradation. This corresponds to an increase in the transmission bandwidth as viewed by the recovery circuits, since the "tight" Nyquist filters are now following the demodulator phase detectors. Again, however, the receive noise limiting bandpass filter ($BT = 1.1$) will limit the improvement possible in recovery circuit performance for the particular modem implementation employed in this study.

For the modem design employed in this study, the synchronization circuit's contribution to the impairment is reduced by the improved transmit pulse shaping filters. Filter configuration 1 shows a 1.5-dB improvement in performance when the demodulator employs hardwired carrier and clock references in a channel composed of a single TWTA nonlinearity. Filter configuration 3 shows a corresponding 0.3-dB improvement. Although it may be possible to modify the synchronization circuits to reduce the 0.3-dB loss for configuration 3 when recovered carrier and clock references are employed, the effort may not be cost effective.

Conclusions

This study has demonstrated that, for nonlinear channels, modification of the sharp rolloff (30-percent) Nyquist pulse-shaping filter that precedes the channel nonlinearities can significantly reduce the AM/PM and AM/AM induced transmission impairment. Acceptable modifications of this filter include a soft rolloff (50-percent) Nyquist structure or a sharp rolloff (30-percent) non-Nyquist structure with a bandwidth 1.13 to 1.15 times the Nyquist bandwidth.

For the non-Nyquist transmit filter cases, additional improvement in transmission performance can be realized by adding a 30- to 50-percent-rolloff Nyquist filter at the demodulator following the carrier demodulation function and preceding the sampling function. This location avoids any detrimental influence on the carrier and bit timing synchronization functions.

In a channel consisting of two TWTA nonlinearities, the filter configurations which include these types of modifications (configura-

tions 2, 3, 4, and 5) exhibit performance that falls within 0.3 dB. Although the best performance was exhibited by configuration 4, the performance of all four configurations was significantly better than that of configuration 1, which employs a sharp rolloff Nyquist transmit filter (conservatively 5 dB better for 1×10^{-6} bit-error rate). The trends of the study indicate that employing a 50-percent-rolloff 34.5-Msymbol/s Nyquist transmit filter ($BT = 1.15$ for 30 Msymbol/s) combined with the 50-percent-rolloff Nyquist presample filter will further improve performance.

The study of HPA spectrum spreading shows that any of the transmit filters recommended for improved bit-error-rate performance will meet the specified INTELSAT interference requirements if an HPA input backoff of at least 10 dB is employed. The sensitivity of the regenerated spectrum interference level near the edge of the adjacent channel as a function of offset frequency may require a larger HPA backoff to ensure compliance with the interference criteria.

Dual-path transmission tests with an INTELSAT IV laboratory simulator indicate that the filter configurations exhibiting improved performance also exhibit better dual-path performance than configuration 1. The incorporation of improved filter configurations also reduces the impairment effects of up-link co-channel interference.

Finally, the demodulator synchronization investigation has provided a better understanding of synchronization circuit contributions to transmission impairment. For the improved pulse-shaping filter configurations employed in this study, further reduction in nonlinear channel impairment by synchronization circuit redesign will not be significant.

Acknowledgment

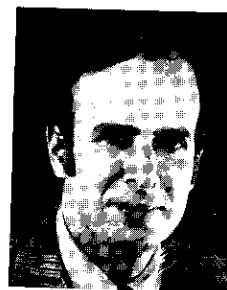
The authors wish to thank D. Lee for setting up the transmission links and making spectrum and bit-error-rate measurements and J. Elsbach for constructing and testing the new pulse-shaping filters.

References

- [1] D. L. Hedderly and L. Lundquist, "Computer Simulation of a Digital Satellite Communication Link," *IEEE Transactions on Communications*, April 1973, pp. 321-325.

- [2] L. Lundquist, M. Lopriore, and F. M. Gardner, "Transmission of 4 ϕ -Phase Shift Keyed Time Division Multiple Access over Satellite Channels," *IEEE Transactions on Communications*, September 1974, pp. 1354-1360.
- [3] L. Lundquist, "Optimizing a TDMA Channel Including Synchronization," International Conference on Communications, Minneapolis, Minnesota, June 1974.
- [4] L. Lundquist, M. Shum, and S. Fredricsson, "Pulse Shaping in Bandwidth Limited Design Satellite System," *IEEE Transactions on Communications*, April 1978, pp. 478-484.
- [5] R. A. Harris and R. A. Gough, "Factors Influencing the Choice of Pulse Shaping Filters for the ECS System," ESA/Swiss PTT Colloquium, Berne, Switzerland, June 24-25, 1976.
- [6] S. A. Fredricsson, "Optimum Receiver Filters in Digital Quadrature Phase Shift Keyed Systems with a Nonlinear Repeater," *IEEE Transactions on Communications*, December 1975.
- [7] S. Fredricsson, "Analysis of Bandlimited Nonlinear QPSK Channels," Final Report, ESRO/ESTEC Contract 1855/73 SW, Technical Report 78, September 1978, pp. 1389-1399.
- [8] L. Campbell, P. McLane, and M. Mesiza, "Optimum Receiver Filters for BPSK Transmission Over Bandlimited Nonlinear Channel," National Telecommunications Conference, Dallas, Texas, November-December 1976.
- [9] S. Murakami, Y. Furuya, Y. Matso, and M. Sugiyama, "Modulation Scheme Comparative Study for Nonlinear Satellite Channels," International Conference on Communications, 1978.
- [10] C. Devieux, Jr., "QPSK Bit Error Rate Performance as Affected by Cascaded Linear and Nonlinear Elements," *COMSAT Technical Review*, Vol. 8, No. 1, Spring 1978, pp. 205-218.
- [11] D. Chakraborty, T. Noguchi, S. J. Campanella, and C. J. Wolejsza, "Digital Modem Design for Nonlinear Satellite Channels," 4th International Conference on Digital Satellite Communications, Montreal, Canada, October 23-25, 1978.
- [12] M. E. Jones and M. R. Wachs, "Measured 60 Mbit/s 4-Phase PSK Signal Impairments through Earth Station HPA and Satellite Transponder," National Telecommunications Conference, Dallas, Texas, November-December 1976.
- [13] W. R. Bennett and J. R. Davey, *Data Transmission*, New York: McGraw-Hill Book Company.

Milton E. Jones received a B.S.E.E. in 1951 and an M.S.E.E. in 1956 from Newark College of Engineering (now New Jersey Institute of Technology). He worked for International Telephone and Telegraph Federal Laboratories where he was involved in missile guidance communications systems. While employed by Computer Sciences Corporation, he performed system studies for the U.S. Defense Satellite Communication System development. In 1975 he joined COMSAT Laboratories as a member of the Systems Applications and Simulation department where he has been engaged principally in hardware simulation studies for the evaluation of satellite link transmission impairments. He is a member of IEEE and Tau Beta Pi.



Marvin R. Wachs received a B.E. (E.E.) degree from the City College of New York in 1965 and an M.S. degree in electrical engineering from George Washington University in 1969. From April 1974 to May 1979, he was Manager of the System Application and Simulation Department at COMSAT Laboratories. In this capacity, he was responsible for supervising hardware simulation of various communications satellite transmission systems, including INTELSAT IV, INTELSAT IV-A, and MARISAT. Prior to April 1974, Mr. Wachs was a member of the technical staff specializing in RF transmission as applied to satellite transponders. Mr. Wachs is a member of Tau Beta Pi and Eta Kappa Nu. Currently, he is Program Manager at Hughes Aircraft.

Translations of Abstracts in this issue

Essai pratique du système AMRT d'INTELSAT

S. CAMPANELLA, R. COLBY, B. PONTANO,
H. SUYDERHOUD ET M. ONUFRY

Sommaire

INTELSAT a organisé dans la région Atlantique un essai pratique de terminaux AMRT munis d'un équipement de concentration numérique des conversations, en vue surtout de mesurer et évaluer le fonctionnement de l'équipement AMRT dans une station terrienne type, et d'évaluer la qualité du service dans des conditions réelles. La France, la République fédérale d'Allemagne, l'Italie, les Etats-Unis et le Royaume-Uni ont participé à cet essai. L'équipement avait été mis au point suivant les spécifications d'INTELSAT par deux groupes différents de fabricants. Le présent article explique comment l'essai pratique a été organisé; il décrit en détail les paramètres des secteurs terrien et spatial et présente les résultats des essais effectués. Il traite également de l'expérience opérationnelle ainsi acquise et suggère certaines modifications et améliorations que l'on pourrait apporter aux spécifications actuelles de l'équipement AMRT.

Acquisition et synchronisation de trames AMRT en boucle ouverte

S. CAMPANELLA ET K. HODSON

Sommaire

La position de paquets AMRT peut être réglée par des méthodes à boucle fermée ou à boucle ouverte. La boucle fermée employée jusqu'à présent dans la plupart des systèmes AMRT n'est pratique que lorsqu'une station peut recevoir son propre paquet de trafic réémis par le satellite, encore que